INVESTIGATION OF THE MULTI-DOMAIN AGGREGATION MECHANISM OF ATAXIN-3

A thesis submitted for the degree of Doctor of Philosophy

Helen Michelle Saunders

B.Sc.(Hons), B.Com., Dip.Lang(Chi)

Department of Biochemistry and Molecular Biology

Monash University

May 2010

Notice 1

Under the Copyright Act 1968, this thesis must be used only under the normal conditions of scholarly fair dealing. In particular no results or conclusions should be extracted from it, nor should it be copied or closely paraphrased in whole or in part without the written consent of the author. Proper written acknowledgement should be made for any assistance obtained from this thesis.

Notice 2

I certify that I have made all reasonable efforts to secure copyright permissions for third-party content included in this thesis and have not knowingly added copyright content to my work without the owner's permission.

ERRATA

p 2, section 1.1.2, line 2: “hereditary and transmissible” for “hereditary as and transmissible”

p 2, section 1.1.2, line 4: “include” for “includes”

p 34, last line: “protein-containing” for “protein containing”

p 57, line 2: “investigation of the aggregation” for “investigation the aggregation”

p 73, 2nd paragraph, line 6: “proportion” for “proportions”

p 92, last paragraph, line 1: “Although HX is commonly” for “Although commonly”

p 93, 2nd paragraph, line 1: “sequence-specific” for “sequence specific”

p 93, 2nd paragraph, line 2: “side chains” for “side chain”

p 121, 2nd paragraph, line 4: “have been characterized” for “has been characterized”

ADDENDUM

p 23, 2nd paragraph, line 5, ‘can cause’ for ‘causes’

p 23, 2nd paragraph, add to end ‘However in a recent transgenic mouse model, it has been demonstrated that wild type ataxin-3 does not abrogate the effects of pathogenic-length ataxin-3 (300).’

p 40, 2.1.3, add the following to the oligonucleotide list:

L169Qfwd	(5’ – 3’)	GTTAAGGGTGATCAGCCAGATTGCGAA	60 ºC
L169Qrev	(5’ – 3’)	TTCGCAATCTGGGTCATCACCCTTAAC	60 ºC
L169Ifwd	(5’ – 3’)	GTTAAGGGTGATATCCCAGATTGCGAA	58 ºC
L169Irev	(5’ – 3’)	TTCGCAATCTGGGATATCACCCTTAAC	58 ºC
L169Tfwd	(5’ – 3’)	GTTAAGGGTGATACCCCAGATTGCGAA	60 ºC
L169Trev	(5’ – 3’)	TTCGCAATCTGGGGTATCACCCTTAAC	60 ºC
Q24Gfwd	(5’ – 3’)	AATAACTTATTGGGAGGAGAATATTTT	51 ºC
Q24Grev	(5’ – 3’)	AAAATATTCTCCTCCCAATAAGTTATT	51 ºC

p 68, line 2, add ‘In the representative membrane shown (Fig 4 A), ataxin-3(Q64) showed a lower signal at 65 hrs compared to 48 hrs. This may be due to the sample dropping out of solution, however as observed in Fig 4 B, was not the norm over the 3 independent experiments.’

p 70, 2nd paragraph, line 3, ‘are separable’ for ‘are not independent’

p 70, 2nd paragraph, line 4, ‘wherein’ for ‘whereby’

p 70, 3rd paragraph, line 3, ‘higher’ for ‘lower’

p 71, sentence 2, add ‘and that aggregation is not necessarily impacted by changes in stability.’

p 73, 4th paragraph, line 3, add to end ‘In addition, the catalytic activity of the Josephin domain may contribute to the resistance of aggregation within the cell, as demonstrated in *Drosophila* (Warrick et al., 2005).’

p 81, Figure 2 legend, line 3, change “Representative traces are” to “Representative traces of three independent experiments”

p 81, Figure 3 legend, add to end ‘Traces are shown until a timepoint where they reach plateau, up to 150 hrs.’

p 81, Figure 4 legend, add to end, ‘Error bars represent SEM.’

p 82, Table 2, row 1, change ‘(°C)’ to ‘(°C ± SEM)’ and ‘(hrs)’ to ‘(hrs ± SEM)’

p 93, Figure 4.1 legend line 5: change “carbonyl” to “aliphatic”

p 101, 2nd paragraph, after sentence 4, insert ‘This suggests that Josephin is folded in 50 % acetonitrile, pH 2.0. This is unexpected considering that for several ataxin-3 variants, low pH was previously found to unfold the protein (69), and highlights the different properties of the Josephin domain when independent of the full length protein.'

p 111, 2nd paragraph, add to end 'Previously, Masino et al. have determined that Josephin unfolding is reversible, thus allowing ΔG to be calculated (208).′

p 112, Figure 4.12 legend, add to end 'Error bars for both A and B represent SEM from three independent experiments.'

p 132, line 6, 'aggregate' for 'fibril'

p 142, Figure 3 legend, add to end 'Error bars represent SEM.'

p 143, Figure 6 legend, part (A), line 3, add 'The numbers beside the membranes correspond to different lipids as follows: 1-Lysophosphatidic acid, 2-Lysophosphatidlycholine, 3-Phosphatidylinositol (PtdIns), 4-PtdIns(3)P, 5-PtdIns(4)P, 6-PtdIns(5)P, 7-Phosphatidylethanolamine, 8-Phosphatidylcholine, 9-Sphingosine 1-phosphate, 10-PtdIns(3,4)P_2, 11-PtdIns(3,5)P_2, 12-PtdIns(4,5)P_2, 13- PtdIns(3,4,5)P_3, 14-Phosphatidic acid, 15-Phosphatidylserine, 16-blank.'

p 157, 1st paragraph, sentence 5, add 'and that SDS may be pushing aggregation down an alternative pathway.'

p 167, reference 33, '(2010) for (2009)' and add to end '**395**, 717-27'

p 185, add to end '300. Hubener J. and Riess O. (2010) Polyglutamine-induced neurodegeneration in SCA3 is not mitigated by non-expanded ataxin-3: conclusions from double transgenic mouse models *Neurobiol dis.* **38(1)**, 116-24.'

CONTENTS

Table of Contents……………………………………………………………………….i
Acknowledgements …..………………………………………………………………iv
General Declaration ……………………………………………………………...v
Declaration for Chapter 3 ……………………………………………………..vi
Declaration for Chapter 5 ……………………………………………………vii
Abbreviations ……………….………………………………………………...…..viii
Abstract ………………………………………………………………………………x

CHAPTER 1

INTRODUCTION 1

1.1 INTRODUCTION TO AMYLOID DISEASE 1
  1.1.1 Conformational Disorders... 1
  1.1.2 Amyloid Disease 2
  1.1.3 Amyloid Fibril Structure... 4
  1.1.4 Species Formed Along the Aggregation Pathway............... 8
  1.1.5 Kinetics of Aggregation..10
  1.1.6 Initial Misfolding Events 11

1.2 POLYGLUTAMINE DISEASE 15
  1.2.1 General Characteristics of PolyQ disease.........................15
  1.2.2 Localization of Inclusions in PolyQ disease......................17
  1.2.3 Role of Proteolysis in PolyQ Disease...............................18
  1.2.4 Identification of Toxic Species in PolyQ Disease...............19

1.3 SPINOCEREBELLAR ATAXIA TYPE 3 (SCA3) 21
  1.3.1 General Characteristics of SCA3 21
  1.3.3 Ataxin-3 Structure and Function.....................................22
  1.3.2 Molecular Characteristics of SCA3...................................25

1.4 POLYGLUTAMINE AGGREGATION..27
  1.4.1 Introduction to the PolyQ Aggregation Pathway 27
  1.4.2 PolyQ Aggregation and Protein Context 28
  1.4.3 Interplay Between the PolyQ Domain and the Stability of Adjacent Regions....30
  1.4.4 Multi-domain Misfolding and Aggregation...........................31

1.5 AIMS OF THIS STUDY 37

CHAPTER 2
MATERIALS AND METHODS 39

2.1 DNA CLONING AND MICROBIAL TECHNIQUES 39
  2.1.1 Reagents and Enzymes 39
  2.1.2 2xTY Growth Medium 39
  2.1.3 Oligonucleotide Design 40
  2.1.4 QuikChange Site-Directed Mutagenesis.. 40
  2.1.5 Agarose Gel Electrophoresis.. 41
  2.1.6 Plasmid Purification 42
  2.1.7 Preparation of Competent Cells 42
  2.1.8 Bacterial Transformations for Expression 43

2.2 PROTEIN TECHNIQUES 43
  2.2.1 Reagents.. 43
  2.2.2 Expression of Ataxin-3 Variants 44
  2.2.3 Protein Purification.. 45
    2.2.3.1 Concentration Determination 46
  2.2.4 Protein Pre-Analysis Techniques 47
    2.2.4.1 SDS Polyacrylamide Gel Electrophoresis (SDS-PAGE)........................... 47
    2.2.4.2 Western Blot.. 48
    2.2.4.3 Size Exclusion Chromatography 49
    2.2.4.4 Ubiquitin Protease Activity Assay.. 49
  2.2.5 Protein Analysis Techniques.. 50
    2.2.5.1 Circular Dichroism (CD).. 50
    2.2.5.2 Equilibrium Denaturation.. 51
    2.2.5.3 Mass spectrometry (MS).. 52
  2.2.6 Aggregation Assays.. 53
    2.2.6.1 ThioflavinT Fluorescence 53
    2.2.6.2 Filter Trap Assay 54
    2.2.6.3 Transmission Electron Microscopy 55
  2.2.7 Phospholipid Overlay Assay 55

CHAPTER 3
THE IMPACT OF FLANKING DOMAIN STABILITY ON AGGREGATION KINETICS OF A POLYQ PROTEIN.. 57

CHAPTER 4
CONFORMATIONAL DYNAMICS OF THE JOSEPHIN DOMAIN OF ATAXIN-3 89

4.1 INTRODUCTION 89
  4.1.1 Protein Aggregation and Dynamics.. 89
  4.1.2 Ataxin-3 Aggregation and Dynamics.. 90
  4.1.3 Theory of Hydrogen Exchange Mass Spectrometry 92

4.2 RESULTS 96
  4.2.1 Josephin MS under Native Conditions 96
  4.2.2 Josephin Exists in Multiple Conformations in Solution 98
    4.2.2.1 Multiple Charge State Envelopes are Not Linked to Parameters on the MS 98
    4.2.2.2 Denaturing Conditions Shift the Charge State Envelope 101
    4.2.2.3 The Partially Unfolded Conformations are Not Linked to Aggregation 102
  4.2.3 Josephin HX MS 104
    4.2.3.1 Deuteration of Josephin 104
    4.2.3.2 D→H Exchange 106
    4.2.3.3 H→D Exchange using NanoESI-MS Demonstrates the Multiple Conformations of Josephin Exist in Equilibrium 108
    4.2.3.4 Analysis of Josephin HX Kinetics 110

4.3 DISCUSSION 113
  4.3.1 Implications of the Conformational Heterogeneity of Josephin 113
  4.3.2 The Dynamic Nature of the Josephin domain 115

CHAPTER 5
AGGREGATION OF ATAXIN-3 IN SDS: EVIDENCE FOR ALTERNATIVE AGGREGRATION PATHWAYS 117

CHAPTER 6
GENERAL DISCUSSION & CONCLUSIONS 155

6.1 ROLE OF FLANKING DOMAINS IN POLYQ AGGREGATION 155

6.2 RELATIONSHIP BETWEEN FOLDING AND AGGREGATION PATHWAYS OF ATAXIN-3 159

6.3 MULTI-DOMAIN MISFOLDING AND POLYQ DISEASE 162

6.4 GENERAL CONCLUSIONS 163

CHAPTER 7
REFERENCE LIST 165

APPENDICES 187

APPENDIX 1: SMALL HEAT-SHOCK PROTEINS INTERACT WITH A FLANKING DOMAIN TO SUPPRESS POLYGLUTAMINE AGGREGATION 188

APPENDIX 2: MULTI-DOMAIN MISFOLDING: UNDERSTANDING THE AGGREGATION PATHWAYS OF POLYGLUTAMINE PROTEINS 194

ACKNOWLEDGEMENTS

Firstly, I would like to thank my supervisor Steve for his support and encouragement over the last four years. In particular, I would like to thank him for giving me the freedom to work on the projects which really interested me whilst keeping me realistic as to how many projects I could fit into four years! In addition, I thank my co-supervisor Roberto for making the trip to Monash numerous times in order to stay up to date with my project and provide advice.

The Bottomley lab has been a great place to work, and I would like to thank everyone who went out of their way to help me in some way or share their knowledge. In particular I would like to thank the polyQ people – Andy, Michelle, Bronwen, Amy, SuLing, Glyn and Victoria - for the many useful discussions. I would like to thank all my collaborators at Monash – Phil and Cathy Bird, Wei Wen Dai, Andy and Amy – for their assistance with various projects.

I spent a fantastic 5 months at Leeds University, and I would like to thank Sheena for making me so welcome in her lab, Johnny and David for sharing their mass spec knowledge, and Carol, Wei-Feng and Jenny for some great weekend trips away.

My family and friends have all been a great support to me over the years and I thank them for their understanding all those times I had to run away to take a sample at the lab.

Lastly, I have to thank my partner Jonathon for his support during the last four years - I appreciated your company on the many late night and weekend trips to the lab and couldn't have done it without you.

GENERAL DECLARATION

In accordance with Monash University Doctorate Regulation 17/Doctor of Philosophy (PhD) and Master of Philosophy (MPhil) regulations the following declarations are made:

I hereby declare that this thesis contains no material which has been accepted for the award of any other degree or diploma at any university or equivalent institution and that, to the best of my knowledge and belief, this thesis contains no material previously published or written by another person, except where appropriate reference is made in the text of the thesis.

This thesis contains two unpublished publications. The core theme of the thesis is the characterization of the aggregation pathway of ataxin-3. The ideas, development and writing up of all the papers in the thesis was the principal responsibility of myself, the candidate, working within the Department of Biochemistry and Molecular Biology under the supervision of Professor Stephen Bottomley.

The inclusion of co-authors reflects the fact that the work came from active collaborations between researchers and acknowledges input into team-based research.

In the case of Chapters 3 and 5, my contribution to the work involved the following:

Thesis Chapter	Publication Title	Publication Status	Nature and Extent of My Contribution
3	The impact of flanking domain stability on aggregation kinetics of a polyQ protein.	Submitted to Protein Science	Mutagenesis, protein purification, experimentation, data analysis and manuscript preparation
5	Aggregation of ataxin-3 in SDS: evidence for alternative aggregation pathways	Submitted to Journal of Molecular Biology	Protein purification, experimentation, data analysis and manuscript preparation

I have renumbered sections of submitted or published papers in order to generate a consistent presentation within the thesis.

Helen Saunders
21 May 2010

DECLARATION BY CO-AUTHORS FOR CHAPTER 3

In the case of Chapter 3, the following co-authors contributed to the work:

Name	Nature of Contribution	Extent of Contribution (%)
Helen M Saunders	Mutagenesis, protein purification, experimentation, data analysis and manuscript preparation	80%
Amy L Robertson	General advice and refinements to the manuscript	5%
Dimitri Giles	PoPMuSiC analysis and refinements to the manuscript	
Marianne Rooman	PoPMuSiC analysis	
Yves Dehouck	PoPMuSiC analysis	
Stephen P Bottomley	General advice, supervision and refinements to the manuscript	

Candidate's Signature: ..[redacted].. **Date:** 21/5/2010

The undersigned hereby certify that:

(1) the above declaration correctly reflects the nature and extent of the candidate's contribution to this work, and the nature of the contribution of each of the co-authors

(2) they meet the criteria for authorship in that they have participated in the conception, execution, or interpretation, of at least that part of the publication in their field of expertise;

(3) they take public responsibility for their part of the publication, except for the responsible author who accepts overall responsibility for the publication;

(4) there are no other authors of the publication according to these criteria;

(5) potential conflicts of interest have been disclosed to (a) granting bodies, (b) the editor or publisher of journals or other publications, and (c) the head of the responsible academic unit; and

(6) the original data are stored at the following location and will be held for at least five years from the date indicated below:

Location: Monash University, Department of Biochemistry and Molecular Biology, Clayton Campus

Signature: ......[redacted]......... **Date:** 21/5/10
Amy L Robertson

Signature: ....[redacted]................... **Date:** 21/5/2010
Dimitri Giles

Signature: ....[redacted].......... **Date:** 21/5/2010
Marianne Rooman

Signature: ....[redacted]............... **Date:** 21/5/2010
Yves Dehouck

Signature: ....[redacted]..................... **Date:** 21/5/10
Stephen P Bottomley

DECLARATION BY CO-AUTHORS FOR CHAPTER 5

In the case of Chapter 5, the following co-authors contributed to the work:

Name	Nature of Contribution	Extent of Contribution (%)
Helen M Saunders	Mutagenesis, protein purification, experimentation, data analysis and manuscript preparation	80%
Andrew M Ellisdon	General advice and refinements to the manuscript	5%
Roberto Cappai	General advice and refinements to the manuscript	
Stephen P Bottomley	General advice, supervision and refinements to the manuscript	

Candidate's Signature: ..[redacted]... **Date:** 21/5/2010

The undersigned hereby certify that:

(1) the above declaration correctly reflects the nature and extent of the candidate's contribution to this work, and the nature of the contribution of each of the co-authors
(2) they meet the criteria for authorship in that they have participated in the conception, execution, or interpretation, of at least that part of the publication in their field of expertise;
(3) they take public responsibility for their part of the publication, except for the responsible author who accepts overall responsibility for the publication;
(4) there are no other authors of the publication according to these criteria;
(5) potential conflicts of interest have been disclosed to (a) granting bodies, (b) the editor or publisher of journals or other publications, and (c) the head of the responsible academic unit; and
(6) the original data are stored at the following location and will be held for at least five years from the date indicated below:

Location: Monash University, Department of Biochemistry and Molecular Biology, Clayton Campus

Signature: ....[redacted]....... **Date:** 21/5/2010
Andrew M Ellisdon

Signature: ....[redacted]........ **Date:** 19/5/10
Roberto Cappai

Signature: .....[redacted]...... **Date:** 21/5/10
Stephen P Bottomley

ABBREVIATIONS

AFM	Atomic Force Microscopy
ANS	Anilinonaphthalene Sulfonate
APS	Ammonium Persulfate
AR	Androgen Receptor
A-β	Amyloid-β
β-me	β-mercaptoethanol
BCA	Bicinchoninic Acid
BSA	Bovine Serum Albumin
CACNA1A	Alpha 1A-voltage-dependent Calcium Channel
CBP	Creb-Binding Protein
CD	Circular Dichroism
CMC	Critical Micelle Concentration
CRABP I	Cellular Retinoic Acid-binding Protein I
CSE	Charge State Envelope
CV	Column Volumes
DNA	Deoxyribonucleic Acid
DNaseI	Deoxyribonuclease I
DRPLA	Dentatorubral-Pallidoluysian Atrophy
DTT	Dithiothreitol
DUB	De-ubiquitinating Enzyme
ε	Extinction Co-efficient
ECL	Enymatic Chemiluminescence
EDTA	Ethylenediaminetetraacetic Acid
EGCG	(-)-Epi-Gallocatechine Gallate
EPR	Electron Paramagnetic Resonance
ESI-MS	Electrospray Mass Spectrometry
FPLC	Fast Protein Liquid Chromatography
ΔG	Free Energy of Unfolding
$\ddot{A}G_{ex}^{app}$	Apparent Free Energy of Exchange
GdnHCl	Guanidine Hydrochloride
HD	Huntington's Disease
His6	Hexa-histidine
HX	Hydrogen Exchange
IAPP	Islet Amyloid Polypeptide
IPTG	Isopropyl-β-D-Thiogalactopyranoside
k_{acid}	Acid Catalyzed Second Order Rate Constant
k_{base}	Base Catalyzed Second Order Rate Constant
k_{int}	Intrinsic Exchange Rate

k_{obs}	Observed Rate of Exchange
k_w	Water Catalyzed Second Order Rate Constant
m/z	Mass to Charge Ratio
MS	Mass Spectrometry
NII	Neuronal Intranuclear Inclusions
NMR	Nuclear Magnetic Resonance
$\mathbf{OD_{600\ nm}}$	Optical Density at 600 nm
PABPN1	PolyA Binding Protein Nuclear 1
PAGE	Polyacrylamide Gel Electrophoresis
PBS	Phosphate Buffered Saline
PCR	Polymerase Chain Reaction
PD	Parkinson's Disease
PMSF	Phenylmethyl Sulphonyl Fluoride
polyA	Polyalanine
polyQ	Polyglutamine
PoPMuSiC	Prediction of Proteins Mutations Stability Changes
PPII	Proline Type II Helix
PtdIns	Phosphotidylinositols
PUF	Partially Unfolded Forms
QBP1	PolyQ Binding Peptide 1
R	Gas Constant
SBMA	Spinal and Bulbar Muscular Atrophy
SCA	Spinocerebellar Ataxia
SDS	Sodium Dodecyl Sulfate
SEC	Size Exclusion Chromatography
SpA	Staphylococcus Protein A
T	Absolute Temperature
TAE	Tris acetate - EDTA buffer
TBP	TATA-Box-Binding Protein
TBSG	Tris Buffered Saline with Glycerol
TEM	Transmission Electron Microscopy
TEMED	N,N,N',N'-tetramethylethylenediamine
TFA	Tri-fluoro Acetate
thioT	Thioflavin T
Tris	Tris(hydroxymethyl)aminomethane
UIM	Ubiquitin Interaction Motif
UPS	Ubiquitin Proteosomal System
VCP	Valosin-Containing protein

ABSTRACT

Spinocerebellar Ataxia Type 3 (SCA3) is one of nine polyglutamine (polyQ) diseases which are all characterized by progressive neuronal dysfunction. A hallmark of these diseases is the presence of neuronal inclusions which contain aggregated polyQ protein, implicating protein misfolding as a key part of this disease. The only sequence homology which exists between the polyQ proteins is the polyQ tract, thus suggesting that protein context is responsible for dictating the specific characteristics of each disease. Increasingly, flanking domains to the polyQ tract have been demonstrated to modulate the aggregation of polyQ proteins. Fibrillogenesis of ataxin-3, the causative protein of SCA3, occurs via a multi-stage pathway when studied *in vitro*. The isolated Josephin domain of ataxin-3 has the intrinsic ability to aggregate under native conditions and thus the multi-stage model of ataxin-3 aggregation has proposed the first stage of aggregation is mediated by interactions of the Josephin domain. This thesis has further characterized the multi-stage aggregation pathway of ataxin-3, with a focus on the role of the Josephin domain during misfolding and aggregation.

This thesis initially determined that changing the stability of the flanking Josephin domain dramatically impacts upon ataxin-3 fibrillogenesis *in vitro*. Mutations within the Josephin domain that increased stability led to decreased aggregation rates and vice versa. This provided support to the hypothesis that Josephin domain interactions are involved in the first stage of ataxin-3 aggregation. The stability mutants also distinguished between two previously proposed models of misfolding to demonstrate that ataxin-3 aggregates from an intermediate which is on the folding pathway. Defining the conformational landscape of ataxin-3 is one mechanism which may provide insights into the initial misfolding events involved in aggregation. As Josephin domain interactions were demonstrated to mediate the first stage of aggregation, hydrogen exchange mass spectrometry was used investigate the dynamics of this folded domain. The Josephin domain was found to be highly dynamic, and under native conditions exists in rapid equilibrium with several partially unfolded conformations. From these data it is proposed the unfolded conformations are not involved in the fibrillogenic pathway, as mutants with either increased or decreased aggregation rates do not change the proportions of the partially unfolded conformations. In addition, the proportion of the partially unfolded conformations was unaffected by several protein interaction partners of ataxin-3. Therefore native ataxin-3 exists within a more complex conformational landscape than previously thought, which is potentially linked to the normal function of the protein. In a further exploration of the conformational landscape of ataxin-3, addition of the membrane mimetic sodium dodecyl sulfate resulted in a number of alternative aggregation pathways. Ataxin-3 was found to bind several phospholipids only when in a fibrillar conformation, which may be linked to the mechanism of toxicity, as has been reported for other amyloidogenic proteins.

Together, these studies have demonstrated that native ataxin-3 exists within a complex conformational landscape, and provided evidence for a multi-domain aggregation mechanism for ataxin-3. This thesis has added to the growing body of evidence that suggests flanking domains influence the misfolding and aggregation of polyQ disease proteins.

CHAPTER 1

INTRODUCTION

1.1 INTRODUCTION TO AMYLOID DISEASE

1.1.1 Conformational Disorders

The correct folding of proteins within the cell is a complex process requiring a significant number of accessory proteins such as chaperones and folding catalysts (1). However even after a protein has obtained its native structural state, subsequent inappropriate conformational changes can occur which may result in disease. In these diseases (termed the conformational disorders), functional proteins undergo a change which results in their self association and irreversible tissue deposition (2). The mechanism of toxicity for these diseases can be due to both a gain-of-function and loss-of-function. Deposition of protein can cause toxicity via the uptake of cellular components into the deposits, resulting in cellular dysfunction and death, whilst there can also be a loss-of-function of the aggregating protein due to its adoption of inactive conformations. There are a wide range of diseases which are grouped as conformational diseases, and all typically involve a late and gradual onset of pathology.

1.1.2 Amyloid Disease

The amyloidoses are a subset of the conformational disorders, and include sporadic, hereditary as and transmissible diseases (Table 1.1). Amyloid diseases can be systemic, such as light chain and dialysis-related amyloidoses, or localized as for type II diabetes, and includes a number of neurodegenerative diseases such as Alzheimer's, Parkinson's (PD) and prion diseases. The pathological hallmark of these neurodegenerative diseases is the presence of insoluble, ordered proteinaceous deposits or 'amyloid fibrils' within the brain (Fig 1.1). The presence of these deposits has implicated a role for protein misfolding in disease, which has led to much interest in characterizing both the deposited amyloid fibrils and the mechanism via which fibrils form. Although these deposits predominantly consist of amyloid fibrils formed by a specific protein, a number of other proteins and carbohydrates also form part of the deposits (3).

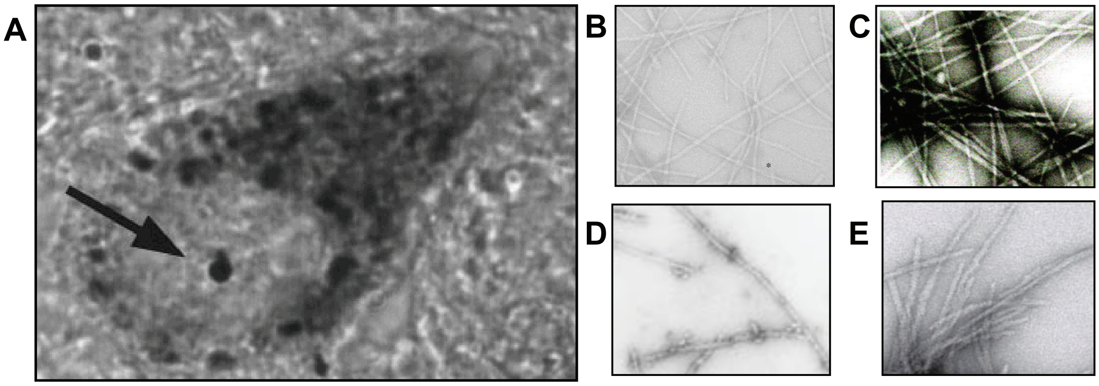

Figure 1.1 Morphology of Proteinaceous Deposits and Amyloid Fibrils. (A) Proteinaceous deposits within the brain, as highlighted by the arrow, are a characteristic of a number of neurodegenerative amyloid diseases. The arrow highlights a nuclear inclusion formed in Spinocerebellar Type 3 (SCA3) (4). Within the deposits, the aggregated protein is present in ordered, fibrillar species as shown in the TEM images of fibrils formed from (B) islet amyloid polypeptide (IAPP) (5), (C) amyloid-β (6), (D) α-synuclein (7) and (E) huntingtin exon-1 (8).

Table 1.1 Amyloid Diseases

Disease	Aggregating Protein	Nature of Deposits	Main Location of Deposits	Nature of Inheritance
Alzheimer's Disease	Amyloid-β	Localized	Brain - Hippocampus, cerebral cortex	Sporadic; Acquired
Parkinson Disease	α-synuclein	Localized	Brain - Substantia nigra, hypothalamus	Sporadic; Hereditary
Huntington Disease	Huntingtin	Localized	Brain - Striatum, cerebral cortex	Hereditary
Creutzfeld-Jacob Disease and other prionopathies	Prion protein	Localized	Central nervous system, brain	Sporadic; Transmissible; Hereditary
Dialysis-related amyloidoses	β-2-microglobulin	Systemic	Musculoskeletal tissues	Acquired
Hereditary systemic amyloidosis	Lysozyme	Systemic	Kidney, liver, spleen	Hereditary
Familial amyloid polyneuropathy	Transthyretin	Systemic	Most organs and tissues - heart, vessels	Hereditary; Acquired

Despite the formation of fibrillar aggregates with similar properties in these diseases, protein deposition and neuronal loss occurs in different brain regions for each particular disease (Table 1.1). The reasons for this are not fully understood, however it may be due to factors such as local changes in protein expression, different concentrations or activity of chaperones or differences in clearance pathways such as autophagy, which is known to ameliorate toxicity associated with protein aggregation (9). Amyloid was traditionally defined as the extracellular deposition of protein fibrils (3), however this definition has now been expanded to include protein fibrils which are deposited intracellularly (10).

Regardless of whether formed by a peptide, unstructured polypeptide or natively globular protein, the end point of the aggregation pathway, the amyloid fibril, displays a number of key defining characteristics. As determined by transmission electron microscopy (TEM) (Fig 1.1), amyloid fibrils have a long, straight morphology, with a typical diameter of 7-13 nm (11). In addition to this, amyloid fibrils show a number of tinctoral properties. Under polarized light fibrils show green birefringence upon binding to congo red, and thioflavin S and thioflavin T both hyperfluoresce upon binding to fibrils (12). These characteristic features of amyloid fibrils are well established and recent advances in high resolution techniques such as solid state NMR (ssNMR) and X-ray crystallography are also providing new insights into the structure of fibrils at a molecular level.

1.1.3 Amyloid Fibril Structure

Two main models of fibril structure have been proposed; the traditional cross β-sheet model and the β-helix model (Fig 1.2). X-ray diffraction data has played a key role in determining these models, as have a multitude of lower resolution techniques, such as TEM, atomic force microscopy (AFM), electron paramagnetic resonance (EPR), scanning TEM, hydrogen deuterium exchange and limited proteolysis. These techniques provide important constraints to the modeling of the fibril at a molecular level from the higher resolution techniques. At a supramolecular level, cryoelectron microscopy has been used to characterize the structure of fibrils. For example, using this technique insulin fibrils have been found to be a heterogeneous mix of fibrils containing either 2, 4, or 6 protofilaments twisted together (13).

Evidence for the traditional cross-β sheet model comes from X-ray diffraction studies which have shown that fibrils have a common structure whereby the β-strands are positioned 4.8 Å apart and perpendicular to the long axis of the fibril. β-sheets also exist parallel to the fibril long axis and are 8-11 Å apart depending on the side chains involved (14,15). There is no sequence or structural homology between amyloid forming proteins, and thus typically it is main-chain interactions that stabilize the core of the fibril. This supports the hypothesis that under suitable conditions, all polypeptides have an inherent ability to form fibrils (16,17).

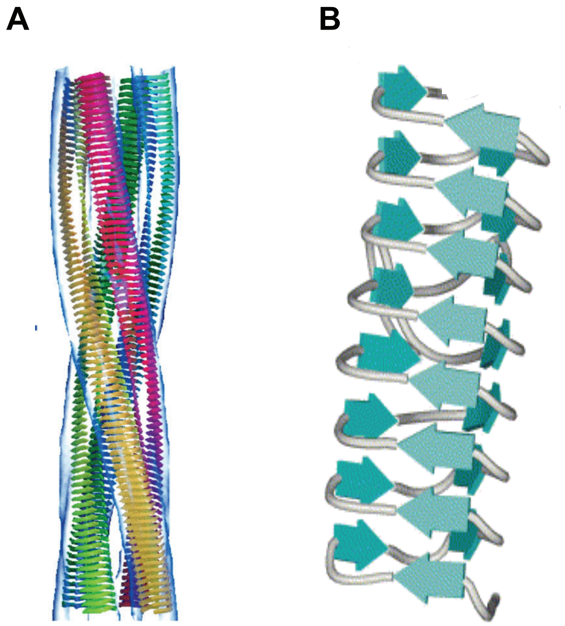

Figure 1.2 Cross-β and β-helix Fibril Models. The two main models of fibril structure are (A) the cross-β and (B) the β-helix model. Both models have β-strands which are 4.8 Å apart and perpendicular to the long axis of the fibril, however only the cross β-sheet model has an intersheet distance of 8 – 11 Å. Images are adapted from (13,18) respectively.

Whilst the cross-β structure is generic to amyloid fibrils, the ultrastructure of the fibril differs between different disease proteins. The recent advances in ssNMR have led to the characterization of protofilament structure at a molecular level, and have provided support for the cross-β structure proposed through X-ray diffraction studies. Although not identical, several proteins including amyloid-β (A-β), HET-s prion(218-289), and transthyretin(105-115) have been shown to have a similar protofilament structure consisting of two layers of parallel β-sheets (Fig 1.3) (6,19,20). However, demonstrating the differences which exist between disease fibrils, the fibril structure of the α-synuclein(30-110) fragment has five layers of parallel in-register β-sheets (21). In many cases only fragments of disease proteins have been used for ssNMR due to technical difficulties, however for A-β, studies have shown that smaller fragments of this peptide results in anti-parallel β-sheets, whilst full length A-β results in parallel β-sheets (6,22-24).

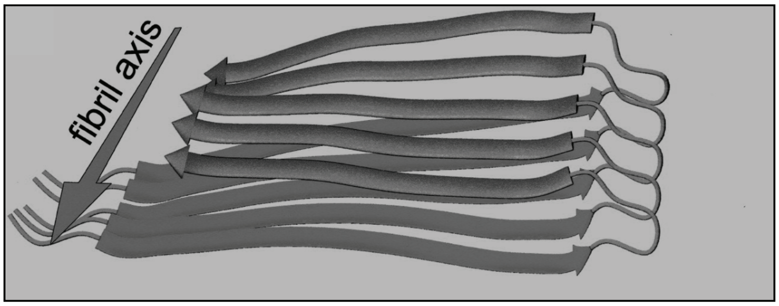

Figure 1.3 A-β(1-40) Fibril Model. Structure of an A-β(1-40) fibril modeled using ssNMR data. Looking down the long axis of the fibril shows each molecule forms a β-strand – turn – β-strand motif which forms a parallel β-sheet, (adapted from (6)) and two such parallel β-sheets form a protofilament.

Mature fibrils are not amenable to structure determination using X-ray crystallography. Microcrystals have however been formed from small fibrillogenic peptides which have similar diffraction patterns to, and which are able to seed, fibrils and thus provide insight into the side-chain interactions and packing of strands in the fibril at a molecular level (25-27). For example, using a specifically designed peptide, Serpell and coworkers found that beyond the inherent H-bonded network of the cross-β motif, aromatic residue sidechain stacking and charge interactions were important for stabilizing fibrils (25).

The second main fibril model is the β-helix model (Fig 1.2B) where fibrils have parallel β-strands 4.8 Å apart and perpendicular to the fibril axis, which form a helix with a hollow centre (18,28). A β-helix structure has been proposed for several disease fibrils, including polyglutamine (polyQ), prion and β_2-microglobulin fibrils (29-31). Perutz and coworkers have proposed that the structure of polyQ fibrils are a water-filled nanotubule, based on X-ray diffraction data whereby the equatorial diffraction signal was smaller than is typically observed for amyloid fibrils and thus excluded from analysis (31). However, these data have been reanalyzed by others who propose that it is consistent with a cross-β structure whereby the polar polyQ sidechains hydrogen bond with the main-chain and thus allow dense packing (32). The second analysis of the data is also supported by molecular modeling of X-ray diffraction data, and it is thought that the different diffraction pattern may have resulted from an atypical data collection method, whereby the sample had a film texture, as opposed to the typical fiber structures generally used (33).

Amyloid fibrils exhibit a common core cross-β structure, however there are a number of differences between different fibrils, such as the inter sheet differences seen in the X-ray diffraction equatorial reflection which ranges from 8-11 Å (15), due to factors such as the steric bulk of side chains (34). In addition to this, the proportion of the polypeptide chain which is incorporated into the fibril core varies greatly, ranging from 100 % of fibrillogenic 7mer peptides to approximately 50 % of A-β and 13 % of HET-s prion protein (6,20,27). The question of whether the β-sheets are arranged parallel or anti-parallel within the fibril differs for each protein, with both having been observed. Margittai and Langen suggest that it depends upon the number of amino acids within the fibril core, with less than 20 amino acids leading to anti-parallel β-sheets and more than 20 resulting in parallel β-sheets, due to the stereochemistry involved (35). Therefore it appears that although fibril formation may be a generic property of all proteins, the type of fibril formed will differ depending on the protein sequence and size.

1.1.4 Species Formed Along the Aggregation Pathway

A poor correlation exists between the mass of fibrillar material deposited in the tissue and the presentation of clinical features (36,37). This implicates a role for other factors in pathogenesis, and one aspect into which there has been considerable interest is the species formed along the aggregation pathway. To fully understand the aggregation pathway requires determination of the thermodynamic and kinetic properties of the species populated during aggregation, a number of which are common to amyloidogenic proteins (38). The pre-fibrillar species common to most amyloid pathways include the oligomer, protofibril and protofilament.

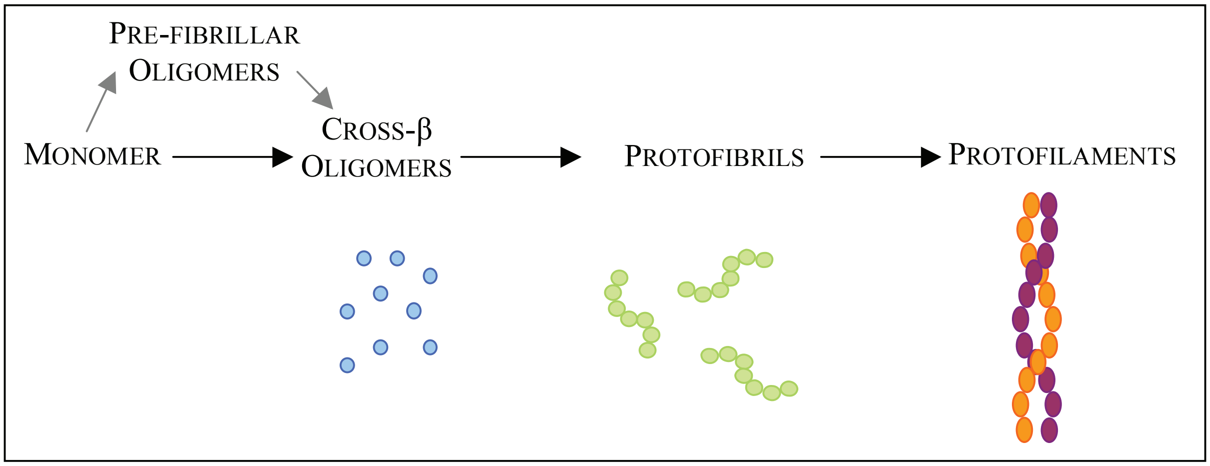

Figure 1.4 Structural Species Formed During Aggregation. The conformational species formed during the process of fibril formation include the oligomer, protofibril and protofilament. All these species typically contain β-sheet rich structures. Pre-fibrillar oligomers are also formed by some amyloidogenic proteins.

The initial species formed in the aggregation pathway for most proteins is the oligomer (Fig 1.4). Some proteins such as A-β, Ure2p and insulin form soluble pre-fibrillar oligomers which retain native structure, before forming an oligomer bearing cross-β-like structure (39-41). The pre-fibrillar oligomer has not, however, been observed for all proteins, and other proteins progress directly to a cross-β oligomer, which typically has a diameter of 2-5 nm (38). The transient nature of the cross-β oligomer limits structural analysis, however, oligomers from numerous amyloid proteins – both disease and non-disease related – form a common structure which is distinct to the mature fibril. This is evidenced by the ability of oligomers to bind the A11 antibody (42). Although the epitope of this antibody remains unknown, it has been demonstrated to bind to oligomers but not fibrils (42). Depending on the protein, oligomers may be a heterogeneous mix of structures, or can be more defined such as the distinct 'donut' shaped species formed by several proteins, although not all oligomers progress to form fibrils (43).

Elongation of the on-pathway oligomers results in short, thin curvilinear protofibrils, as visualized using TEM and AFM, which typically have a similar diameter of 3-5 nm but have increased lengths of 20-100 nm (44,45). These protofibrils then form larger protofilaments which are the units of the mature fibril, with 2-6 protofilaments per fibril which generally form a long-range twist (13,46). Aside from the pre-fibrillar oligomer, the pre-fibrillar species are all characterized by a cross-β structure, and the ability to bind the dye thioflavin T. In the process of forming these species, internal structural rearrangements can occur (47), thus explaining the ability of oligomers but not protofibrils to bind to the A11 antibody (42).

In accordance with the lack of correlation between the fibril load and toxicity, increasing evidence suggests that the pre-fibrillar species are responsible for toxicity in a number of cell and animal models of disease. Both A-β transgenic mice and drosophila models show symptoms before the accumulation of amyloid plaques (48,49), whilst non-native transthyretin oligomers have been identified as the toxic species in a cellular model (50). Genetic support for this mechanism of toxicity comes from juvenile PD, where early neurodegeneration occurs without the formation of the intracellular deposits or Lewy bodies typically seen in late onset PD (51,52). The key pre-fibrillar species involved in toxicity has been demonstrated *in vitro* to be the oligomer, and this appears to be a generic mechanism of toxicity as both disease and non-disease proteins form oligomers which are toxic to cultured neurons (53,54). Kayed *et al.* suggest that the oligomers may be cytotoxic due to their recruitment of cellular components into aggregates, their disruption of membranes and resultant depolarization events, and their exacerbation of oxidative stress (42).

1.1.5 Kinetics of Aggregation

The aggregation pathway can be modeled kinetically as a nucleated polymerization mechanism (Fig 1.5) (55). This is characterized by an initial lag phase, in which formation of a critical nucleus occurs. Formation of this nucleus is a rate-limiting step in the pathway, and the number of molecules within the critical nucleus varies depending on the protein involved (56,57). Following the lag phase, the elongation phase then involves rapid extension of the initial critical nucleus, through the pre-fibrillar species, to form the mature fibril. Kinetic modeling suggests that the mechanism of association can occur through monomer addition or association of oligomers (58,59).

In support of the nucleated growth mechanism, the addition of pre-formed species as ‘seed’ eliminates the lag phase as it removes the need for the formation of the thermodynamically unfavourable critical nucleus before extension can occur (60).

Interestingly, the efficiency of seeding varies greatly for different proteins (61-63). Although the ability to form amyloid fibrils is considered an inherent ability of all proteins, their propensity to do so differs greatly, as evidenced by differences in their aggregation kinetics Kinetic modeling provides an important quantitative tool for determining the impact of other factors, from solution conditions to binding partners to potential drugs, on the modulation of the aggregation pathway.

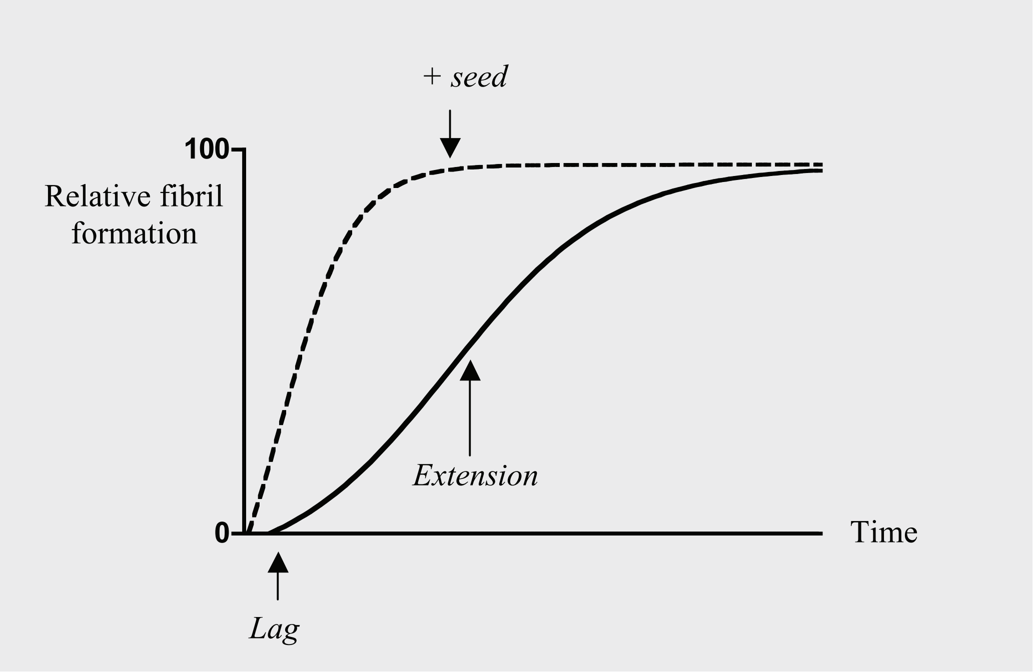

Figure 1.5 Nucleated Polymerization Aggregation Kinetics. The aggregation curve shows nucleated polymerization kinetics with a lag phase in which the rate-limiting nucleus is formed, followed by a rapid extension phase. The dotted line shows the elimination of the lag phase upon the addition of seed.

1.1.6 Initial misfolding events

For fibril formation to occur, proteins must undergo a conformational change from their native state. All potential conformations formed by a protein, whether during folding or misfolding, can be described in terms of their free energy. The heterogeneity of unfolded and partially folded conformations formed by a protein, due to inherent fluctuations of the polypeptide chain, has led to protein conformations being described within an energy landscape (64). Although all conformations are represented on the energy landscape, for most proteins the transition from conformations populated in folding to those of aggregation has not been clearly defined. A number of factors may play a role, such as the cellular environment, factors that affect the global thermodynamic or kinetic stability, or local fluctuations of the protein.

As described by Anfinsen, the typically rapid timeframe for folding indicates that proteins spontaneously fold to their native structures without searching the entirety of conformational space (65). When a protein approaches its native state, the favourable enthalpy earned from forming native-like interactions offsets the decrease in entropy paid for adopting an ordered structure. This results in protein molecules folding correctly within a short timeframe due to native-like interactions being more stable than non-native interactions (66). Therefore, during folding the free energy available to the protein decreases and thus the energy landscape of folding is represented as a funnel.

The initial events of aggregation vary depending on whether or not the protein is natively folded. Analysis of primary sequence can be very informative when predicting amyloidogenic regions in unstructured proteins, where the initial misfolding event involves formation of a partially folded amyloidogenic intermediate (67). For natively folded proteins, the conformational change hypothesis of aggregation proposes they must undergo either partial or global unfolding in order to initiate aggregation (Fig 1.6) (68). Alternatively, some proteins have been proposed to aggregate via an intermediate which is off the folding pathway (69,70). Evolution selects for burial of hydrophobic amyloidogenic regions, and so predicted amyloidogenic regions may be buried in a stable fold and shielded from forming the interactions required for aggregation (71). For folded proteins, two mechanisms exist via which change can result in increased formation of partially unfolded intermediates and thus aggregation; these are protein destabilization and increased protein dynamics (72).

Many disease proteins have destabilizing mutations when compared to wild type non-disease causing proteins. The destabilizing mutations result in a decreased free energy of unfolding and thus a higher population of amyloidogenic intermediates. For example, mutations in α-synuclein which destabilize the protein result in increased aggregation propensity and therefore early onset of disease (73). Therefore determining the thermodynamic stability can provide insight into the mechanism of aggregation of a protein.

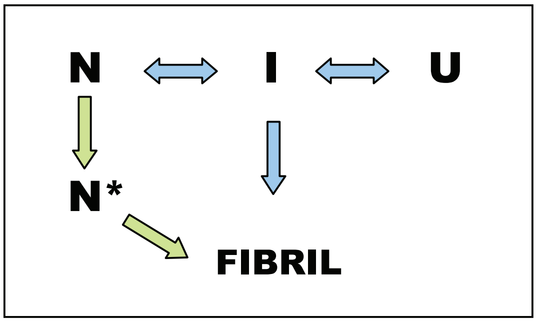

Figure 1.6 Conformational Change Hypothesis of Aggregation. Under this hypothesis, folded proteins unfold to form an amyloidogenic partially unfolded intermediate on the folding pathway which is an initiator of aggregation (blue arrows). Alternatively, some proteins aggregate from an intermediate which is independent of the folding pathway (green arrows).

Local or global fluctuations are another mechanism via which some natively folded proteins sample amyloidogenic conformations. This can occur when a low energy barrier exists to forming amyloidogenic intermediates which results in them being frequently sampled but transiently populated (68). Alternatively, some proteins populate transient amyloidogenic native-like states without crossing the free energy barrier of unfolding (74). It has been demonstrated that the residues which are key for folding can be distinct to those important for aggregation, and therefore protein conformational fluctuations may allow sampling of conformations where these residues are more exposed (71). When factors such as mutation increase the conformational dynamics this can then result in a greater proportion of the transient intermediate and thus faster aggregation kinetics. This is demonstrated by both lysozyme and transthyretin, which both can have amyloidogenic mutations which increase protein dynamics, as determined using hydrogen deuterium exchange mass spectroscopy and NMR (75-77).

In many cases, amyloidogenic intermediates necessary for aggregation form from partially unfolded intermediates which are on the folding pathway. Therefore full characterization of both folding and the transition to aggregation is important in understanding the aggregation mechanism.

1.2 POLYGLUTAMINE DISEASE

1.2.1 General Characteristics of PolyQ Disease

A subset of the amyloid disorders, the polyQ diseases are an inherited group of nine neurodegenerative disorders (Table 1.2) whereby mutation, in the form of a CAG repeat expansion, results in disease. The pathologic hallmark of the polyQ diseases is the presence of neuronal intranuclear inclusions (NII) which contain fibrillar protein (78). As for amyloid disorders in general, formation of NII is now considered to be a protective mechanism which acts by sequestering misfolded polyQ proteins from the cell (79). The NII also sequester a number of other cellular factors, including components of the ubiquitin-proteasome pathway, chaperones and transcription factors which may disturb the homeostasis of the cell (80-82).

The only homology between the nine proteins associated with polyQ disease is the expanded polyQ tract, however the characteristics of the diseases themselves show substantial similarity. With the exception of the X-linked SBMA, all the polyQ proteins show autosomal dominant inheritance (83). An inverse exponential correlation exists between repeat length and both age of disease onset and disease severity (84). Due to repeat instability, anticipation occurs in several polyQ diseases, whereby subsequent generations have an increased repeat length and thus earlier onset and increased disease severity (85-87). Each protein has a threshold glutamine repeat length, with polyQ repeat lengths of over 40 generally leading to disease. The same polyQ tract length does not result in the same age of onset between different disease proteins, suggesting disease characteristics are not solely due to the expanded polyQ tract, but are modulated by protein context. In addition to this, the polyQ diseases all show loss of different subsets of neurons, despite most of the polyQ proteins showing widespread expression throughout the brain (88).

Table 1.2 Characteristics of PolyQ Disease Proteins

Disease	**Protein**	**PolyQ Tract Location (Black) & Relative Size** 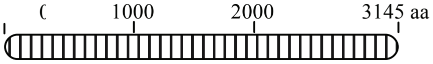	**Pathogenic Q Length**	**Refs**
HD	Huntingtin	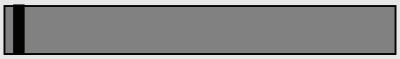	36 - 121	(89,90)
SCA1	Ataxin-1	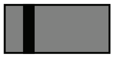	40 - 83	(91,92)
SCA2	Ataxin-2	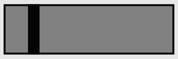	35 - 59	(93)
SCA3	Ataxin-3	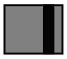	45-84	(94,95)
SCA6	CACNA1A	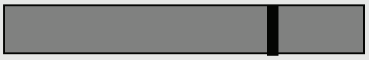	21 - 29	(96)
SCA7	Ataxin-7	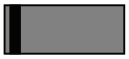	37 - 306	(97,98)
SCA17	TBP	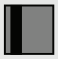	47 - 63	(99,100)
DRPLA	Atrophin 1	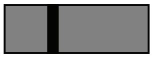	49 - 88	(101)
SBMA	Androgen Receptor	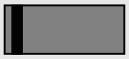	40 - 62	(102)

Abbreviations: DRPLA-Dentatorubral and Pallidoluysian Atrophy, *HD*-Huntington's Disease, *SCA*-Spinocerebellar Ataxia, SBMA-Spinal and Bulbar Muscular Atrophy, CACNA1A-alpha 1A-voltage-dependent calcium channel, *TBP*-TATA-box-binding protein

The functions of the polyQ proteins are unrelated, ranging from a calcium channel protein to a deubiquitinating enzyme, and a focus of recent research has been characterizing the functions of these proteins. Targeting the function of the native protein, as opposed to trying to target a conformational change involved in aggregation, has had some success as a therapeutic approach. In the polyQ disease SBMA, targeting the substrate of the causative protein was demonstrated to inhibit aggregation within a mouse model of disease (103).

1.2.2 Localization of Inclusions in PolyQ Disease

In disease, a redistribution of protein occurs, and for most polyQ diseases the location of aggregates has been demonstrated to be important for toxicity (104-106). Aside from SCA2 and SCA6, nuclear localization and formation of nuclear inclusions is a common characteristic of polyQ disease. Within a recent SCA3 mouse model, the presence of a nuclear export signal alleviated the disease phenotype whilst addition of a nuclear localization signal accelerated aggregation of pathogenic length ataxin-3 (104). This has also been demonstrated in a number of other polyQ proteins, with ataxin-1, huntingtin and DRPLA all showing increased toxicity when targeted to the nucleus (105-108).

Aggregates are predominantly found within the nucleus as NII, but smaller soluble cytoplasmic inclusions are also observed in cell and animal models (109,110). A drosophila model for HD has suggested that soluble cytoplasmic aggregates may also play a role in disease progression, through the trapping of polyQ proteins and blocking of axonal transport (111). The increased toxicity when aggregates are localized to the nucleus as opposed to the cytoplasm may be due to the ameliorating effects of autophagy. Autophagy, or lysosome-mediated protein degradation is a cytoplasmic process which clears polyQ aggregates from the cytoplasm but not the nucleus (112,113). Upregulation of autophagy has been demonstrated to decrease aggregation and toxicity of ataxin-3, huntingtin and the androgen receptor (AR) in a number of cell and animal models (113-115).

During the redistribution of protein which occurs in disease, polyQ proteins may also interact with cellular membranes. The impact of an expanded polyQ tract has been predominantly studied for huntingtin, and it has been shown that expanded huntingtin inserts into synthetic lipid bilayers more than non-expanded, and also alters the specific phospholipids with which huntingtin interacts (116-118). Similarly to a number of other amyloidogenic proteins, a channel hypothesis has been proposed for HD, whereby expanded polyQ tracts are able to form ion channels in membranes that contribute to cellular disruption and death (119,120). This theory is supported by a study of ataxin-3 which demonstrated that expanded ataxin-3 altered the electrophysiological properties of the cell (121).

1.2.3 Role of Proteolysis in PolyQ Disease

There has been much debate over the role of proteolysis as an initiator of aggregation within polyQ disease. The polyQ tract is the only similarity between the disease proteins, and expansion of the polyQ tract is linked to disease severity both in patients and model systems (104,122). The key involvement of the polyQ tract has led to the ‘toxic fragment hypothesis’ which proposes disease pathogenesis is caused by release of a polyQ containing fragment through cleavage (123-125). In support of this, simple polyQ peptides have been demonstrated to form fibrils *in vitro* and these fibrils are toxic when introduced into mammalian cells (126,127).

The only polyQ disease where there is a general consensus for the involvement of proteolysis is huntingtin, whereby huntingtin exon-1 is released and subsequently aggregates (128-131). However a number of other polyQ proteins have been shown to be highly susceptible to proteolysis *in vitro.* The mechanism of cleavage has been investigated by several groups, and ataxin-3, huntingtin, AR and atrophin-1 are all targets for caspases (123,132). In addition to this, huntingtin and ataxin-3 are cleaved by calpains *in vitro* (124,133).

1.2.4 Identification of Toxic Species in PolyQ Disease

To date, it has been proposed that soluble polyQ oligomers are the species within the aggregation pathway responsible for toxicity, however some uncertainty remains as to the mechanism of toxicity (42,53,79). Within the polyQ diseases, substantial evidence suggests that NII are not linked to toxicity. In fact in a number of both cell and animal models, as well as disease brain slices, the formation of NII has been demonstrated to be inversely correlated with disease (134-138). In a convincing experiment, Arrasate et al. used 4D fluorescent microscopy to follow expression of huntingtin exon-1 in single neurons over time, and found that the bigger the inclusions, the fewer cells died in the primary neuronal cultures (139). In a polyQ model system, a toxic monomeric conformation was shown to be responsible for toxicity, however this has not been observed for polyQ disease causing proteins (140). Most evidence suggests toxicity of the proteins is linked to early aggregates within the pathway, and thus defining the initial steps involved in aggregation may be key to understanding toxicity in the polyQ diseases.

There is evidence that polyQ containing fragments are more toxic than full length proteins with a number of studies demonstrating both faster aggregation rates *in vitro*, and increased toxicity in cell studies overexpressing truncated ataxin-3, the AR and huntingtin (124,141-143). There is general agreement that huntingtin exon-1 is cleaved from full length huntingtin before disease progression, and therefore the toxicity of polyQ fragments must be considered (130,131). Although expression of huntingtin exon-1 in mice leads to aggregation, NII formation and disease, the mice do not show all the characteristics of HD

(131). Aggregation and disease progression have been shown to be slower when full length huntingtin is expressed in mice, however a closer model of HD results, which suggests that full-length huntingtin modulates disease (144). Therefore, there is currently evidence for the role of both full length and truncated polyQ proteins in disease and it appears that the involvement of cleavage may differ between the polyQ proteins.

1.3 SPINOCEREBELLAR ATAXIA TYPE 3 (SCA3)

1.3.1 General Characteristics of SCA3

SCA3, also known as Machado-Joseph Disease, is an autosomal dominant disease and is the most common dominantly inherited ataxia (145-147). SCA3 was originally described in families native to the Portuguese Azores islands (148,149). It has since been reported in other populations of non-Portuguese descent, including in America, Europe, Asia, South America, Africa and Australia (150,151).

Although a relatively rare disease, SCA3 is prevalent in specific populations such as in the Portuguese islands of Sao Miguel and Flores, and in an Australian aboriginal community from Groote Eylandt (150,152). There is still debate as to whether SCA3 has evolved from several independent mutations worldwide, or there has been a founder mutation originally occurring in Portugal, which has been spread worldwide via Portugese explorers (151,153,154).

SCA3 is characterized clinically by progressive cerebellar ataxia, and can be distinguished from other dominant cerebellar ataxias by the presence of ophtalmoplegia, a weakness of the muscles that control eye movement (152). SCA3 shows significant phenotypic variation, with ataxia of gait and stance, cerebellar dysarthria, severe peripheral neuropathy and defective temperature discrimination all being seen (145,155).

The gene responsible for SCA3, *ATXN3* maps to chromosome 14q32.1, with the CAG repeat expansion responsible for disease located within the tenth exon (156,157). Individuals homozygous for expanded repeat alleles are not common, however in a few cases homozygotes have presented with more severe phenotypes than heterozygous individuals with the same length CAG expansion (158). The smallest observed polyQ repeat length that has resulted in a disease phenotype is 45 glutamines (95).

In SCA3, although the encoded protein ataxin-3 is ubiquitously expressed throughout the brain, only specific subsets of neurons undergo degeneration. Degeneration is observed within the cerebellum and thoracic cord in most patients, with varying degeneration of the striatum, substantia nigra, basis pons, oculomotor nuclei and peripheral nerves (159). Recently, new imaging techniques have shown more widespread degeneration to the cerebellum, thalamus, midbrain, pons, medulla oblongata and spinal cord (160).

1.3.3 Ataxin-3 Structure and Function

Ataxin-3 is one of the smaller polyQ proteins. It consists of a folded N-terminal Josephin domain, and a predominantly unfolded C-terminal tail which contains two ubiquitin interaction motifs (UIM) in addition to the polyglutamine tract (Fig 1.7). There are two major isoforms of ataxin-3 found in disease, the first containing just two UIMs between the Josephin domain and the polyQ tract, and the second containing a third UIM C-terminal to the polyQ tract (161). Both ataxin-3 isoforms show similar polyubiquitin binding properties and aggregation (162-164). The NMR structure of Josephin was solved in 2005 and consists of two subdomains separated by a cleft, and a mixed α/β fold (Fig 1.8) (165,166). NMR experiments suggest that it is a predominantly rigid structure, however it also possesses a flexible helical hairpin consisting of the α_2 and α_3 helices (Fig 1.8) (166). Ataxin-3 belongs to the family of papain-like cysteine proteases, and has the catalytic triad Cys-14, His-119 and Asp-134 within the Josephin domain (Fig 1.8) (165,166).

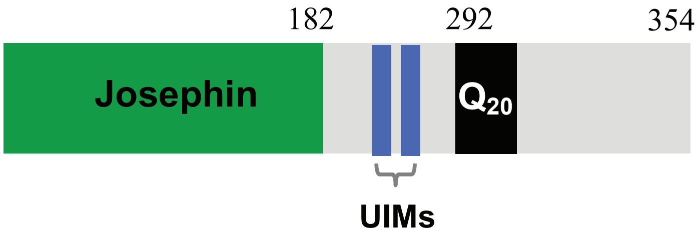

Figure 1.7 Ataxin-3 Structure. Ataxin-3 consists of an N-terminal Josephin domain, two ubiquitin interacting motifs (UIM) and the polyQ tract. A non-expanded tract of 20 glutamine results in an ataxin-3 molecule of 354 amino acids.

Ataxin-3 functions as a de-ubiquitinating enzyme (DUB) as part of the ubiquitin proteosomal system (UPS). The expansion of the polyglutamine tract does not affect either the ability of monomeric ataxin-3 to bind Lys^{48}-linked tetra-ubiquitin, nor change the rate of degradation (162,167). This suggests that it is not a change in function of the monomeric expanded ataxin-3 which is responsible for toxicity.

The UIMs also play an important role in ataxin-3 function, through the binding of ubiquitin chains and also conferring specificity of cleavage (168). If the UIMs are mutated such that they do not bind ubiquitin, this results in the ubiquitination of ataxin-3 being greatly inhibited (162). In addition to binding ubiquitin via the UIMs, ataxin-3 also has two ubiquitin binding sites within the Josephin domain (169). Ataxin-3 causes lower toxicity when the full length protein is present in a native and active conformation. This has been demonstrated within a *Drosophila melanogaster* model system whereby the DUB function of Josephin, in combination with the UIMs, abrogates the level of toxicity in comparison to cleaved C-terminal fragments (170).

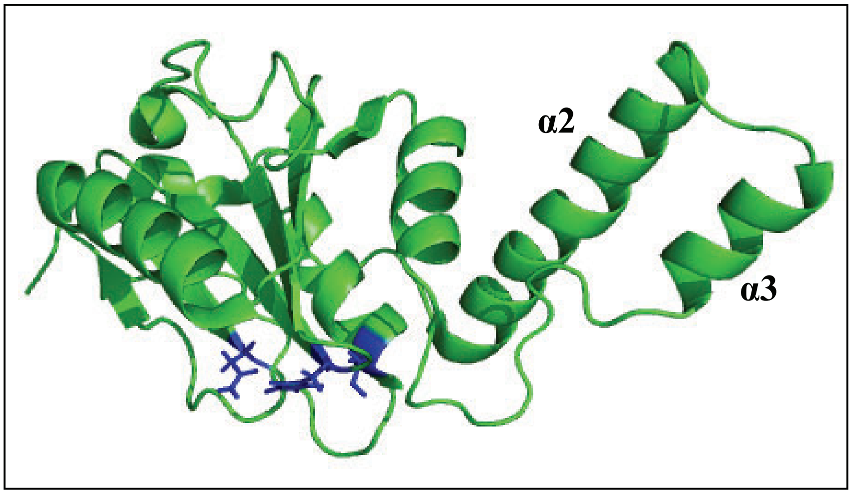

Figure 1.8 Josephin Domain NMR Structure. The Josephin domain structure (PDB: 1YZB) highlighting the active site catalytic triad (blue) and the α2 and α3 helices which form the helical hairpin (166).

Unlike most DUBs which only cleave polyubiquitin chains with a specific linkage, ataxin-3 is currently thought to be unique in its ability to cleave mixed-linkage chains. Winborn *et al*. showed that ataxin-3 cleaves both Lys^{48} and Lys^{63} linkages even when both are present in mixed linkage chains (168). This suggests that ataxin-3 has more conformational flexibility than the other proteins in this family, which may be linked to its high propensity to aggregate under native conditions.

As part of its normal cellular function, ataxin-3 interacts with a number of proteins including HHR23A and B, and valosin-containing protein (VCP). The proteins HHR23A and B, which are homologs of yeast DNA repair proteins, have been demonstrated to interact with ataxin-3 via a ubiquitin-like domain (171). In addition to this, via modulation of the molecular chaperone VCP (also known as p97), ataxin-3 mediates endoplasmic reticulum associated degradation (172,173). VCP interacts with ataxin-3 via an arginine/lysine rich motif located between the second UIM and polyQ tract of ataxin-3. Neither the interactions with HHR23A or VCP are altered by pathogenic length ataxin-3, however both proteins co-localize with ataxin-3 in NII (171,173).

1.3.2 Molecular Characteristics of SCA3

A number of studies have investigated the role of proteolytic cleavage of ataxin-3 in SCA3. Goti *et al.* have identified a fragment in some regions of disease brain from a SCA3 patient (141). However in contrast to this, a number of other studies have not observed any fragments in either disease brain or a mouse model (174-176). It should be noted, however, that aggregation of fragment and full length ataxin-3 are not mutually exclusive. Haake *et al.* have shown that fragments accelerate the rate of full length ataxin-3 aggregation *in vitro* (124), thus providing a possible mechanism for the involvement of both full length protein and fragments in disease.

Ataxin-3 is highly susceptible to cleavage by both caspases and calpains *in vitro,* and a number of cleavage sites have been identified in ataxin-3 which release the polyQ containing C-terminal region from the folded Josephin domain (132,174,177). Although studies show cleaved fragments to have increased aggregation kinetics (178), full length ataxin-3 also forms aggregates and NII in cell models (179). The question remains as to whether it is full length or cleaved ataxin-3 which is the initiator of aggregation.

Pathogenic length ataxin-3 forms NII which also contain non-expanded ataxin-3 (4). In addition to this, a number of other cellular proteins are sequestered, including ubiquitin, components of the proteosome, molecular chaperones and transcription factors such as TATA-binding protein (TBP) (81,178,180). Interestingly NII are found in both affected and unaffected brain regions (178,181), and as for a number of other polyQ diseases their formation does not correlate strongly with toxicity (180). However, even if NII are not directly toxic, studies suggest that sequestration of the cellular proteins may contribute to pathogenesis (182).

NII are heavily ubiquitinated, and contain major components of the UPS such as the 20S and 19S proteosomal complexes (81). Within the cell, the UPS functions as a quality control system via the degradation of misfolded or damaged proteins (183). Whilst the UPS has been demonstrated to degrade flanking domains of polyQ proteins, the ability of the UPS to degrade polyQ tracts remains under debate. It has been suggested that polyQ peptides may block the UPS system and thus result in increased ataxin-3 aggregation or alternatively that polyQ peptides may be degraded in the cytoplasm by amino peptidases (81,184-186). Chaperones are another component of SCA3 NII which indicate the involvement of misfolded proteins. The chaperones HSP40 and HSP70 are upregulated upon expression of pathogenic length ataxin-3, thus suggesting that expanded ataxin-3 induces a stress response within the cell (80).

Transcription factors are another element commonly sequestered by SCA3 NII. This corresponds with the widespread transcriptional dysregulation often seen in cellular models of polyQ disease (187). An example of this is creb binding protein (CBP) which is a co-activator for many different transcription factors, and found in NII of ataxin-3 (179). Therefore although formation of NII is considered a protective mechanism for the sequestration of misfolded and fibrillar polyQ proteins, they may play a role in the later stages of toxicity through the sequestration of multiple cellular factors.

1.4 POLYGLUTAMINE AGGREGATION

1.4.1 Introduction to the PolyQ Aggregation Pathway

The aggregation pathways of several polyQ proteins have been well characterized *in vitro* both structurally and kinetically. Within these proteins, the regions flanking the polyQ tract have been shown to play a role in determining the molecular species formed during aggregation (Fig 1.9). Pathogenic length pure polyQ peptides form two significantly populated species during aggregation, monomer and fibril (Fig 1.9) (188). In the context of the disease protein additional intermediate species such as spherical oligomers and curvilinear protofibrils are also formed (164,189). As discussed previously, polyQ oligomers have also been shown to be toxic (53,79,190), highlighting the importance of flanking domains within the context of disease.

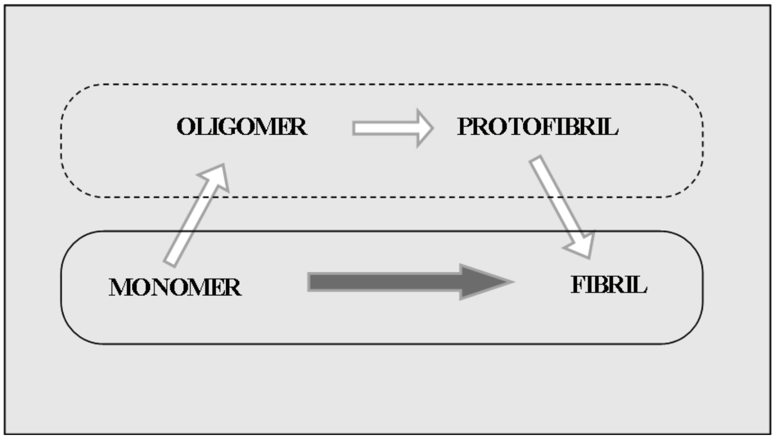

Figure 1.9 Structural Species in Pathological PolyQ Aggregation. The common structural species which are formed during aggregation of pathological length polyQ proteins, with the dotted region indicating species mediated by the flanking domains and the solid region indicating species specifically formed as a result of the pathogenic length polyQ tract.

Use of oligomer-specific antibodies has shown that polyQ proteins and peptides form oligomers with a fold common to well characterized amyloid proteins such as A-β and α-synuclein (42,164). However the endpoint polyQ disease fibrils, generally characterized by resistance to breakdown by detergents, do not form the typical long straight amyloid fibrils, but instead are more heterogeneous and irregular in appearance (191). This is not the case for polyQ peptides, which form long straight fibrils and show the similar cross-β diffraction pattern typical of amyloid fibrils (31,127). No X-ray diffraction data of polyQ disease proteins exists, which in combination with the morphological data, suggests that the flanking domains prevent formation of typical well-ordered endpoint fibrils.

The polyQ fibrillogenic pathway has been characterized kinetically as nucleation-dependent polymerization (127,192). A kinetic analysis has been completed for polyQ peptides and ataxin-3 and in both cases the size of the critical nucleus is one molecule, thus implying a single rarely populated misfolded monomer is sufficient to initiate aggregation (127,192). For ataxin-3, this partially folded intermediate has been proposed to form off the folding pathway, unlike the general paradigm for misfolding and subsequent aggregation (69).

1.4.2 PolyQ Aggregation and Protein Context

In different contexts the same length polyQ expansion results in varying toxicity and disease pathology, and thus many studies have investigated the role that protein context plays in modulating the extrinsic toxicity of the polyQ sequence. The ability of polyQ flanking sequences to modulate aggregation was clearly demonstrated by Nozaki and colleagues who saw differing aggregation rates when the surrounding 17 amino acids of ataxin-2, ataxin-3, huntingtin and atrophin 1 were added to the same length polyQ tract (193). In addition to this, they found that mutating four hydrophobic residues in the upstream flanking sequence of ataxin-2 to charged amino acids decreased the aggregation rate, further highlighting the impact of sequence specificity upon aggregation.

Subsequently, a number of studies have investigated the flanking regions to the polyQ tract within huntingtin exon-1. Through the use of peptide studies, the poly proline (polyP) region immediately C-terminal to the polyQ tract in huntingtin (Fig 1.10), has been shown to slow aggregation and decrease the stability of aggregates compared to a polyQ peptide alone (194). This study also found that the protective effects of the polyP region are directional, having no impact on aggregation when N-terminal to the polyQ tract. The mechanism of inhibition was investigated by Darnell *et al.* (195) who show that the polyP region exists as a PPII helix (proline type II helix), inducing a PPII-like structure in the polyQ tract that opposed the aggregation prone β-sheet conformation formed by this region. In addition to the *in vitro* study using polyQ peptides, it was shown that the polyP sequence decreases toxicity in a yeast huntingtin exon-1 model system (196). Duennwald and colleagues also investigated the impact of two commonly used tags and show the soluble GST domain prevents toxicity whilst the negatively charged FLAG tag increases toxicity. Therefore the polyQ surrounding sequence within huntingtin exon-1 has a significant modulating effect on huntingtin exon-1 aggregation kinetics.

The sequence specific effects of the flanking domain are unsurprising, given that primary protein sequences vary in their amyloidogenicity (197). Aggregation is known to depend on factors determined by the primary sequence such as hydrophobicity, charge and propensity to form secondary structure (197), with certain amino acids having specific effects upon aggregation propensity. In keeping with its inhibitory effect on huntingtin exon-1 aggregation, proline is considered to be a 'β-breaker' as it is structurally incompatible with β-sheet formation (198). There is also a group of 'gatekeeper' residues which are commonly found flanking aggregation prone regions. These include proline, lysine, arginine, glutamate and aspartate, and all have low hydrophobicity, are charged, and show a low propensity to form β-sheet structures (199) as demonstrated in the mutagenesis study on ataxin-2 (193).

In addition to having a direct impact upon the polyQ tract, the flanking sequences allow for varying protein-protein interactions which also modulate aggregation. Ubiquitin is one protein present in the NII of most polyQ diseases, however typically the subset of proteins sequestered within the NII are specific to each disease. The importance of the flanking domain in determining interactions is seen in ataxin-3, where differences between components of NII have been shown between full length versus truncated ataxin-3 (179). In addition to this, huntingtin has over 100 interaction partners within the cell, all of which could potentially affect aggregation (200). Therefore flanking sequences and domains, although not the key cause of toxicity in polyQ proteins, can have a modifying effect on polyQ aggregation through their interaction partners.

1.4.3 The Interplay Between the PolyQ Domain and the Stability of Adjacent Regions

The interplay between the polyQ tract and flanking domains clearly depends upon the characteristics of the domains. The stability of the flanking domain is known to play an important modulatory role in aggregation. In accordance with the general amyloid aggregation theory, an early hypothesis proposed that the expanded polyQ tract destabilized the protein, leading to an increased propensity to aggregate (201). Ataxin-3 is the only disease protein for which kinetic and thermodynamic stability has been determined. Contrary to the initial hypothesis Chow *et al*. have shown that the addition of a non-pathogenic length polyQ tract leads to a destabilization of the protein in comparison to the Josephin domain alone, yet expanding the polyQ tract into the pathogenic length has no further effect on stability (69,163).

The complexity of the effect of the polyQ tract on protein stability is demonstrated by a number of polyQ model systems. On the one hand the addition and subsequent expansion of a polyQ tract did not result in a change in the thermodynamic stability of a *Staphylococcus aureus* protein A domain (202). However this domain is one of the most stable of the model proteins used, so it is unsurprising that the addition of a pathogenic length polyQ tract was not sufficient to disrupt the fold. The CRABP I domain has a similar stability to the Josephin domain of ataxin-3, however the addition of a non-expanded polyQ tract does not impact upon stability, and it is only when the polyQ tract is expanded that there is a corresponding decrease in the stability of the protein. Furthermore, although in a GST-polyQ model the stability was not determined, aggregation could only be induced above 50 ºC, suggesting the stability and/or solubility of the GST domain overrides any effects of the polyQ tract at physiological temperatures (203). Therefore these model systems demonstrate the complexity of the relationship between the polyQ tract and the flanking domains and show that whilst in some situations a polyQ tract can decrease the global stability of a protein, it is not necessary in order to induce aggregation.

1.4.4 Multi-domain Misfolding and Aggregation

It is well established that protein domains can fold independently and recently it has been shown that within a protein multiple domains can misfold in separate steps (191,204). Due to the technical difficulties involved in producing these proteins *in vitro,* the aggregation kinetics and pathways of only three of the nine polyQ proteins have been characterized. Ataxin-1, ataxin-3 and huntingtin exon-1 all contain a flanking region which is able to aggregate independently of the polyQ tract, albeit with slower kinetics (Fig 1.10). A key tool in the identification of these polyQ-independent aggregation regions has been the polyQ binding peptide QBP1, which inhibits aggregation of the polyQ tract (205). The ability of flanking regions to aggregate independently accounts for the aggregation seen by non-expanded ataxin-1 and ataxin-3 *in vitro* (164,206-208).

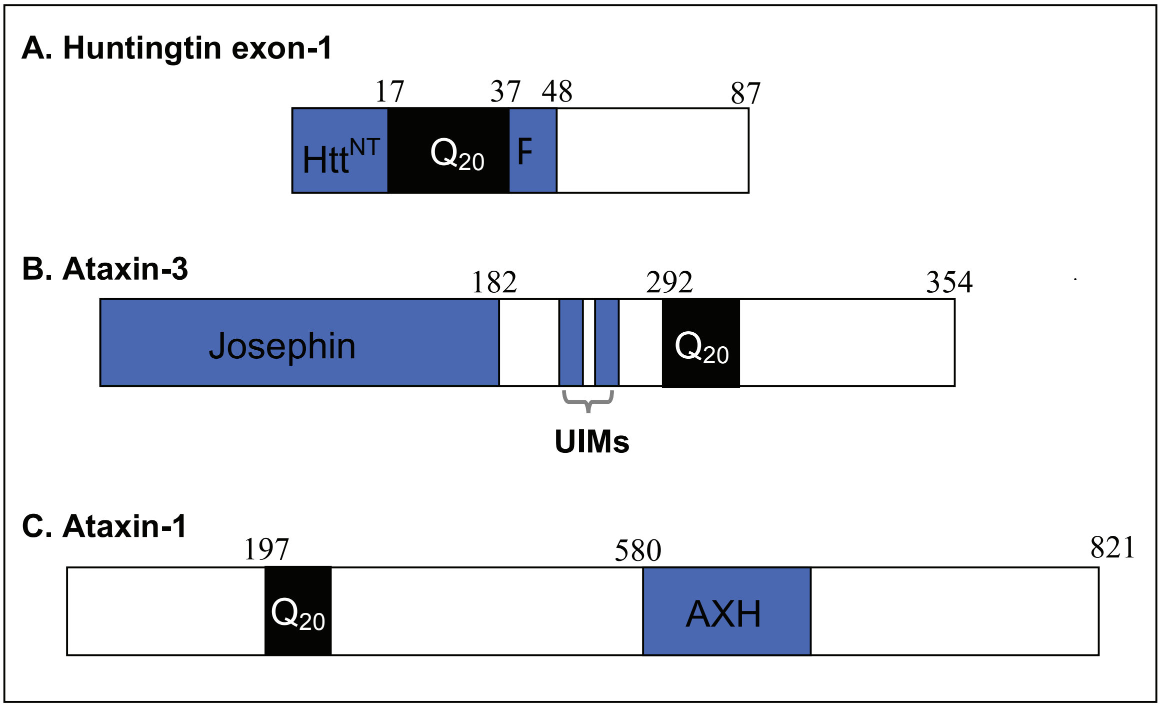

Figure 1.10 Domain Architecture of Huntingtin exon-1, Ataxin-3 and Ataxin-1. The three polyQ proteins huntingtin exon-1 (A), ataxin-3 (B) and ataxin-1 (C) are shown with an arbitrarily chosen polyQ tract length of 20 glutamines, highlighting their flanking domains. The proteins are not illustrated to scale. Huntingtin exon-1 consists of the Htt^{NT} domain which comprises the first 17 amino acids of the protein, the polyQ tract (Q_{20}) and the polyP region (P). Ataxin-3 contains the Josephin domain, the polyQ tract and ubiquitin interacting motifs (UIMs). Ataxin-1 contains the AXH domain and the polyQ tract.

The aggregation pathway of ataxin-3 has been well defined *in vitro* and it has been shown that the 24 kDa Josephin domain of ataxin-3 aggregates when isolated (206,208). The Bottomley group has shown that full length ataxin-3 aggregates with a two-stage mechanism (191). The first stage of aggregation involves interactions of the Josephin domain and results in formation of soluble protofibrils. Both pathogenic and non-pathogenic length ataxin-3, in addition to the Josephin domain, form morphologically similar stage 1 protofibrils (191,206,208). The addition of QBP1 demonstrates that the polyQ tract is not directly involved in the first step, however the expanded ataxin-3 has the fastest aggregation kinetics, suggesting it still impacts the Josephin domain in some way. The second stage in the polyQ aggregation mechanism is only undertaken by pathogenic length ataxin-3 and mediated by interactions of the polyQ tract, it involves a subsequent remodeling to form an SDS-insoluble fibril (191). Thus the two domains in ataxin-3, both with an intrinsic ability to misfold, aggregate sequentially (Fig 1.11).

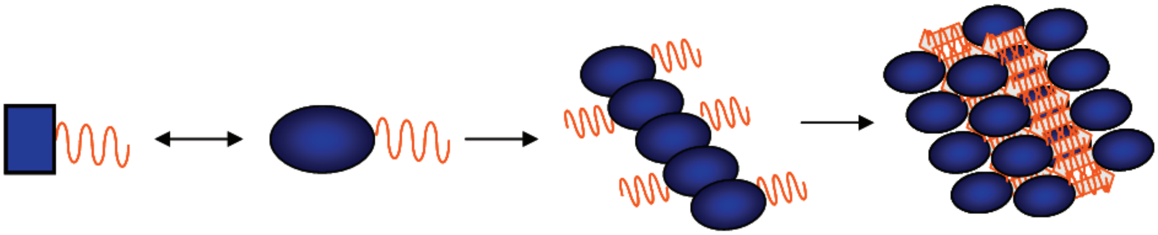

Figure 1.11 PolyQ Multi-domain Aggregation Mechanism. A schematic representation of the multi-stage polyQ aggregation mechanism. In this pathway an initial misfolding event occurs in the polyQ flanking folded domain (square), followed by the formation of soluble species mediated by flanking domain interactions. There is then a conformational rearrangement of the polyQ tract which results in formation of end stage SDS-insoluble fibrils.

Although a complete kinetic analysis has not been completed for ataxin-1 due to the limitations caused by its size, the AXH domain of ataxin-1 has similarly been found to aggregate when isolated (207). Within the context of ataxin-1, the AXH domain has a pro-aggregation effect, as replacement with a homologous non-aggregation-prone sequence decreases the formation of nuclear inclusions within a cell model (207). The formation of detergent insoluble aggregates, commonly attributed to polyQ tract aggregation has not been investigated, nor has the use of QBP1 to ascertain whether the polyQ tract misfolds and aggregates subsequently to the AXH domain.

A recent study by the Wetzel group has shown that huntingtin exon-1 also undergoes multi-domain misfolding during aggregation (189). This study found the 17 amino acids N-terminal of the polyQ tract accelerated aggregation, whether N- or C-terminal to the polyQ tract. This differs from ataxin-1 and ataxin-3 in that the 17 amino acids are not a globular structured domain, but instead exist in a collapsed state, which can be induced into a more aggregation competent extended conformation by the presence of an expanded polyQ tract.

Intriguingly, a kinetic analysis of the huntingtin peptide with the N-terminal sequence resulted in a critical nucleus of minus one. This suggests there is no kinetic barrier to aggregation, and spontaneous aggregation of oligomers occurs in a ‘downhill’ fashion (189). They also found that amorphous aggregates formed in the initial step of aggregation had an exposed polyQ tract that could still bind antibodies. Later aggregates masked the polyQ epitope thus suggesting an additional misfolding event and conformational rearrangement of the polyQ tract to become involved in the fibrils (189). Computer simulations of this region have suggested that the 17 amino acids mirror the conformation of the polyQ tract as opposed to acting independently (209). Thus early studies suggest that huntingtin exon-1 may involve two different misfolding events which each result in formation of different species along the pathway.

With the presence of an amyloidogenic flanking domain being common to polyQ disease proteins, model polyQ protein containing flanking domains with an intrinsic ability to aggregate provide the most representative insight into the aggregation mechanism of polyQ proteins. One model polyQ system involving the cellular retinoic acid-binding protein I (CRABP I) domain fused to huntingtin exon-1 has proved to have an aggregation pathway which is analogous to ataxin-3. The CRABP I domain aggregates independently and when fused to huntingtin exon-1 the aggregation pathway is characterized by an initial step involving CRABP I, followed by a second step mediated by polyQ tract interactions (204). Using proteolysis, this study also observed the two-stage aggregation pathway in an *E. coli* cell model, which is the first evidence of the multi-domain mechanism within a cell.

Multi-domain misfolding is not exclusive to polyQ proteins, having also been observed in several other aggregating proteins such as the poly alanine (polyA) protein Poly A Binding Protein Nuclear 1 (PABPN1) and the yeast prion protein Ure2p (210,211). Expansion of the polyA tract occurs at the N-terminal of PABPN1, with an increase from 10 to 17 alanines leading to disease. Similarly to ataxin-1 and ataxin-3, aggregation still occurs in the absence of the homo-sequence domain, resulting in aggregates which are smaller and more numerous than full length PABPN1 (210). A second example, Ure2p, consists of a highly amyloidogenic unstructured N-terminal domain which is responsible for the prion phenotype, and a compactly folded C-terminal catalytic domain (211). Dimerization of the protein occurs through the C-terminal domain, which is also able to aggregate independently, forming high molecular weight insoluble oligomers, that do not progress to fibrillar aggregates (212). Interestingly, the presence of the amyloidogenic N-terminal domain has no impact upon the stability of the full length protein (212).

The second stage of the multi-domain misfolding pathway involves a conformational change within the polyQ tract. A number of studies, both *in vitro* and *in* *silico* have suggested to date that polyQ peptides have a collapsed structure which is conformationally dynamic (213,214). Using simulations, Leitgeb *et al.* found that a non-pathogenic length polyQ peptide forms unordered structures in addition to a heterogeneous ensemble of conformations containing various secondary structures (215). Molecular dynamics simulations also suggest that above 30 glutamines, there is a stabilization of structure which may allow time for amyloidogenic interactions to form (216).

The three characterized polyQ proteins all show domain-independent misfolding which translates into multi-step aggregation pathways, whereby the different domains aggregate sequentially. Common to all three cases is the role of a non-polyQ containing domain in forming the initial interactions, thus suggesting a mechanism where these domains initially self-associate, increasing the local concentration of the polyQ tract before the polyQ tract plays a significant role in fibril formation.

The aggregation pathways of polyQ proteins characterized to date have all involved multiple domains. With the variation seen between polyQ diseases, it is unsurprising that their specific flanking domains have the ability to independently misfold and modulate the fibrillogenic mechanism of the full length polyQ protein *in vitro*. In these studies, the importance of using a number of complementary techniques to follow the multiple aggregation steps has been highlighted. The mechanism via which an expanded polyQ tract results in accelerated aggregation remains unknown, with no clear relationship between the effects of the expanded polyQ tract and global stability of the protein. Further investigation into polyQ protein dynamics and the effects of the expanded polyQ tract upon local stability will therefore be important for determining the early aggregation events.

1.5 AIMS OF THIS STUDY

The flanking domains of polyQ proteins have increasingly been shown to modulate aggregation (193,207). In particular, ataxin-3 has been proposed to form aggregates initially mediated by interactions of the flanking Josephin domain (164,191). Therefore the overall aim of this study is to characterize the aggregation pathway of ataxin-3, with a focus on the role of the Josephin domain.

This study will begin by testing the two-stage aggregation pathway hypothesis that the Josephin domain mediates the initial stages of aggregation. Following on from this the initial steps of aggregation will be investigated through the characterization of the conformational dynamics of the Josephin domain. Lastly, having further defined the aggregation pathway of ataxin-3, the effects of the membrane mimetic sodium dodecyl sulfate (SDS) on aggregation are determined. With very few of the polyglutamine disease proteins able to be produced recombinantly, the further characterization of the aggregation pathway of ataxin-3 may provide insight into the aggregation of the nine disease proteins. Therefore in summary, the aims of this study are to -

1. *Probe the effects of changing the stability of the flanking Josephin domain and thus test the two-stage aggregation hypothesis of ataxin-3*
2. *Determine the conformational dynamics of the Josephin domain of ataxin-3*
3. *Characterize the effects of the membrane mimetic SDS on the ataxin-3 aggregation pathway*

CHAPTER 2

MATERIALS AND METHODS

2.1 DNA CLONING AND MICROBIAL TECHNIQUES

2.1.1 Reagents and Enzymes

The restriction enzyme *Dpn*I and pfu DNA polymerase was purchased from Promega. Agarose I, biotech grade, was purchased from Amresco and SYBR Green was purchased from Applied Biosystems.

2.1.2 2xTY Growth Medium

For 1L medium: To 900 mL of double deionised water (ddH2O) were added:

Bacto-tryptone	16 g
Bacto-yeast	10 g
NaCl	5 g

The medium was stirred until all solutes had dissolved and the volume then adjusted to 1 L. The medium and all other materials for molecular biology and microbial purposed were sterilized by autoclaving at 120 ºC for 20 min.

Agar plates were prepared by the addition of 1.5 % (w/v) agar to 2xTY medium prior to autoclaving. 10 cm diameter plates were poured to a depth of approximately 1 cm and set at room temperature. Where appropriate, antibiotics were added once the media had cooled to below 50 ºC following sterilization. Antibiotics were added at final concentrations of 0.1 mg/mL for ampicillin and 0.025 mg/mL for kanamycin.

2.1.3 Oligonucleotide Design

All oligonucleotides were purchased from Geneworks (Australia). 40 nmol of lyophilized PCR/Sequencing grade oligonucleotides were obtained, reconstituted in sterile ddH_2O to a final concentration of 100 µM and stored at -20 ºC.

Oligonucleotides:

Name	**Direction**	**Sequence**	**Melting Temperature**
R103Gfwd	(5’ – 3’)	TATCAGAGGCTCGGAATCGATCCTATA	58 ºC
R103Grev	(5’ – 3’)	TATAGGATCGATTCCGAGCCTCTGATA	58 ºC
S81Afwd	(5’ – 3’)	ATTCAGGTTATAGCAAATGCCTTGAAA	54 ºC
S81Arev	(5’ – 3’)	TTTCAAGGCATTTGCTATAACCTGAAT	54 ºC
L169Hfwd	(5’ – 3’)	GTTAAGGGTGATCACCCAGATTGCGAA	60 ºC
L169Hrev	(5’ – 3’)	TTCGCAATCTGGGTGATCACCCTTAAC	60 ºC

2.1.4 QuikChange Site-Directed Mutagenesis

A number of variants were created in pExp_lic_his_ataxin3(Q64), ataxin3(Q15) and Josephin using the QuikChange site-directed mutagenesis method. Using the relevant gene as a template, PCR was performed to produce double–stranded circular DNA. The primers used for PCR each contained a single base substitution as described in 2.1.4. Each PCR mixture contained 100 μM dNTPs, 125 ng of each primer, 25 ng purified vector, 1.5 units pfu DNA polymerase, enzyme buffer and sterile water to a final volume of 25 μL. Five samples were set up to use the gradient function of the Corbett Research Palm Cycler. The following program was run:

Initial denaturation	95 ºC	1 min	
Denaturation	95 ºC	1 min	18 cycles
Annealing	X ºC	1 min	
Extension	72 ºC	13 min	
Final Extension	72 ºC	13 min	
Hold	25 ºC	-	

X = A gradient ranging from 10 ºC to 2 ºC below the melting temperature of the primers.

Following amplification, the non-mutated, methylated parental strain DNA was digested by incubation with *Dpn*I for 3 hr at 37 ºC. 5 μL of the remaining single-stranded vector was then transformed into 50 μL of NovaBlue^{TM} (Novagen) competent cells and incubated overnight. Resulting colonies were sequenced by PCR amplification using the BigDye Terminator reagent according to the manufacturer’s instructions, and then sequenced at the Micromon sequencing facility at Monash University.

2.1.5 Agarose Gel Electrophoresis

For preparation of 1 % agarose gels, 0.25 g of agarose I was added to 25 mL Tris acetate buffer (TAE, 0.04 M Tris acetate, 0.001 M ethylene diaminetetra-acetic acid (EDTA), pH 8.0). The agarose was dissolved by heating, and when it had cooled slightly but was still in liquid form, the solution was poured into a previously prepared gel tray taped firmly at both ends. The tape was removed once the gel had set. A Pharmacia Biotech mini-gel system was used to run gels, with TAE buffer used as tank buffer. Loading buffer and SYBR green was added to DNA samples and gels were run at a constant voltage of 110 V for approximately 30 min. The DNA sample was visualized using fluorescent light.

2.1.6 Plasmid Purification

All expression plasmids used carried a gene conferring ampicillin resistance to the host cells. 5 mL of 2xTY medium containing 0.1 mg/mL ampicillin was inoculated with *E. coli* JM107 cells containing the relevant plasmid and grown overnight at 37 ºC with shaking. Following overnight amplification, the plasmid was extracted and purified from the cells using a Wizard Plus SV Minipreps DNA Purification System (Promega) according to the manufacturer's instructions.

2.1.7 Preparation of Competent Cells

Competent cells were prepared using the rubidium chloride method (217).

Transformation buffer 1: 100 mM Rubidium Chloride, 50 mM Manganese Chloride, 10 mM Calcium Chloride, 30 mM Potassium Acetate, 15 % (w/v) Glycerol, pH 5.8
Transformation buffer 2: 10 mM Rubidium Chloride, 75 mM Calcium Chloride, 10 mM MOPS, 15 % (w/v) Glycerol, pH 6.8

Solutions were filter sterilized and stored at 4 ºC.

A scraping of JM107 cells from a glycerol stock was added to 5 mL 2xTY media and grown overnight at 37 ºC. 500 μL of the starter culture was used to inoculate 50 mL of

2xYT media in a 250 mL flask, and incubated at 37 ºC under shaking conditions until an $OD_{600\ nm}$ of 0.5 was reached. The culture was chilled on ice for 10 min, and then centrifuged for 10 min at 3000 rpm. The supernatant was discarded, and the pelleted cells were resuspended in 15 mL of transformation buffer 1. The cells were incubated on ice for 15 – 30 min then centrifuged again. The cell pellet was then resuspended in 4 mL of transformation buffer 2 and incubated on ice for 15 min. Cells were aliquoted into 100 µL volumes, snap frozen in a dry ice/ethanol bath and immediately transferred to -80 ºC for storage.

2.1.8 Bacterial Transformations for Expression

2 µL of the desired plasmid was added to 100 µL of previously prepared competent *E. coli* BL21(DE3) cells and left on ice for 30 min. Cells were heat-shocked at 42 ºC for 90 sec and placed on ice for 2 min to recover, before being plated on 2xTY agar (1.5 % agar) containing 0.1 mg/mL of antibiotics as dictated by the transformed plasmid.

2.2 PROTEIN TECHNIQUES

2.2.1 Reagents

Thioflavin T (ThioT), guanidine hydrochloride (GdnHCl), lysozyme, β-mercaptoethanol (β-me), ethylenediaminetetraacetic acid (EDTA), phenylmethyl sulphonyl fluoride (PMSF), ubiquitin, Proteinase K, mass spectrometry grade cesium iodide, ultrapure grade ammonium acetate and ultrapure grade ammonium bicarbonate were purchased from Sigma Aldrich Co. ThioflavinT (ThioT) and ultrapure grade guanidine (GdnHCl) were prepared analytically by weight and passed through a 0.22 µm filter. The concentration of guanidine was determined from the refractive index of the prepared sample (218).

Isopropyl-β-D-thiogalactopyranoside (IPTG), which was purchased from Astral Scientific, was prepared analytically by weight and passed through a 0.22 µm filter. N,N,N',N'-Tetramethylethylenediamine (TEMED) and ammonium persulfate (APS) were obtained from ICN and dithiothreitol (DTT) and mass spectrometry grade Trypsin Gold were purchased from Promega. Benzenesulfonyl fluoride hydrochloride (AEBSF), under the trade name Pefabloc, in addition to deoxyribonuclease I (DNaseI) were obtained from Roche. Enzymatic chemiluminescence reagents (ECL) were obtained from Amersham. All quartz cuvettes were purchased from Starna.

2.2.2 Expression of Ataxin-3 Variants

BL21(DE3) *E.coli* cells containing the appropriate expression vector (pExp_Lic_His) were used to inoculate a starter culture of 2xTY medium containing 0.1 mg/mL ampicillen, and this was grown overnight in a shaking incubator at 37 ºC. The following morning, this culture was added to 2xTY medium at 1 % (v/v) and incubated at 37 ºC and 190 rpm until the $OD_{600\ nm}$ was between 0.6-0.8. Subsequently, the incubation temperature was reduced to 28 ºC and protein expression was induced by the addition of 0.5 mM IPTG. The cells were incubated for a further 4 hr and harvested by centrifugation at 5000 rpm for 10 min at 4 ºC. The harvested cells were resuspended in Lysis buffer (2.2.3), snap frozen and stored at –80 ºC.

2.2.3 Protein Purification

Ataxin-3 and variants

Solutions:

Lysis Buffer: 50 mM NaH2PO4, 300 mM NaCl, 1 mM β-me, 0.1 % (v/v) Triton X-100, 10 % (v/v) glycerol, pH 8.0

Wash Buffer: Lysis buffer + 20 mM Imidazole

Elution Buffer: Lysis buffer + 250 mM Imidazole

Tris(hydroxymethyl)aminomethane (Tris) buffered saline (TBSG): 100 mM TrisHCl, 80 mM NaCl, 10 % Glycerol, pH 7.4 (at the required temperature)

The cell lysate was incubated with lysozyme (1.4 mM), DNaseI (0.1 mg/mL) and pefabloc (0.5 mg/mL) for 20 min at 4 ºC. The cells were lysed by sonication and after the addition of pefabloc (0.5 mg/mL) the cell lysate was centrifuged for 30 min at 20,000 rpm at 4 ºC. The pellet was subsequently discarded, and the supernatant was filtered through a 0.45 µm syringe filter then added to 10 % (v/v) p-aminobenzamidine agarose and incubated on a rotary orbitor for 1 hr at 4 ºC.

Pefabloc and imidazole were added to the collected flow-through at concentrations of 0.5 mg/mL and 10 mM respectively. The solution was then loaded at a flow rate of 4 mL/min onto a 5 mL HisTrap high performance (HP) column (Amersham), which had been pre-equilibrated with wash buffer. The column was then washed with 20 column volumes (CV) of wash buffer using an Amersham Äkta fast protein liquid chromatography (FPLC) system. The protein was eluted from the HisTrap HP column with a 10 CV gradient from wash buffer to elution buffer. 1 mL fractions were collected and run on SDS-PAGE (2.2.4.1) to determine those containing ataxin-3. The appropriate fractions were pooled and pefabloc added to a final concentration of 0.5 mg/mL.

The chosen fractions were loaded onto a Hiload Superdex^{TM} 200 (16/60) prep grade column which had been pre-equilibrated with TBSG. 1 mL fractions from this column were collected and again analyzed by SDS-PAGE. The purist fractions were pooled and concentrated using an Amicon Ultra (Millipore) centrifuge device. The protein was filtered with a 0.45 µm syringe filter, divided into 50 – 100 µL aliquots and stored at – 80 ºC.

Proteins other than Ataxin-3

The proteins HHR23A, HHR23B and valosin-containing protein(VCP)/p97 were a gift from Wei Wen Dai.

2.2.3.1 Concentration Determination

The concentration of ataxin-3 following purification was determined by absorbance at 280 nm and also using a bicinchoninic acid (BCA) assay (Pierce). Extinction coefficients (ε) for all ataxin-3 variants were calculated using equation 2.1 (Gill and von Hippel, 1989, Pace *et al.*, 1995):

$$\varepsilon = \text{Number(Tyrosine)} \times \text{Ext(Tyrosine)} + \text{Number(Tryptophan)} \times \text{Ext(Tryptophan)} + \text{Number(Cysteine)} \times \text{Ext(Cysteine)} \qquad \textbf{Equation 2.1}$$

where Ext(Tyrosine) = 1490, Ext(Tryptophan) = 5500, Ext(Cysteine) = 125. BCA assays were completed according to the manufacturer's guidelines, using bovine serum albumin (BSA) as a protein standard. The values derived from both methods correlated well for all ataxin-3 variants.

2.2.4 Protein Pre-Analysis Techniques

2.2.4.1 SDS Polyacrylamide Gel Electrophoresis (SDS-PAGE)

Stock solutions:

4 x Running gel buffer:	1.5 M TrisHCl, pH 8.8
4 x Stacking gel buffer:	0.5 M TrisHCl, pH 6.8
2 x Loading buffer:	0.125 M TrisHCl, 4 % SDS, 20 % glycerol, 0.2 M DTT, 0.02 % bromophenol blue, pH 6.8

10 % (w/v) sodium dodecyl sulphate (SDS) solution

25 % ammonium persulfate (APS) solution

Tank buffer: 0.025 M TrisHCl, 0.192 M glycine, 0.1 % SDS, pH8.3

Table 2.2: Preparation of two SDS polyacrylamide gels, with concentrations (% v/v) of acrylamide as indicated

	Running Gel		**Stacking Gel**
	10 %	12.5 %	
30 % Bis-acrylamide (monomer) (mL)	3.30	4.12	0.44
4 x Running buffer (mL)	2.50	2.50	-
4 x Stacking buffer (mL)	-	-	0.83
ddH_2O (mL)	4.10	3.18	2.36
25 % w/v APS (µL)	60.0	60.0	20.0
TEMED (µL)	8.0	8.0	3.0

SDS gels were prepared according to Table 2.2 and run using a Biorad minigel system. Samples were diluted in 2 x loading buffer and boiled at over 90 ºC for 5 min before being applied to the stacking gel. A constant current of 45 mA was run for 1 hr. The gels were then stained in Coomassie blue staining solution (0.025 % w/v Coomassie brilliant blue

R250, 40 % v/v methanol, 7 % v/v acetic acid) for 1 hr and destained in 40 % v/v methanol, 7 % v/v acetic acid for 12 hr.

2.2.4.2 Western Blot

Transfer Buffer:	50 mM TrisHCl, 20 mM glycine, 20 % (v/v) methanol, 0.01 % (v/v) SDS.
Tris-Buffered Saline (TBS):	20 mM TrisHCl, 0.2 M NaCl, pH 7.4
Tween Tris-Buffered Saline (TTBS):	0.5% Tween in TBS
Blocking Buffer:	5 % (w/v) low fat milk powder in TBS

Primary antibody:

Mouse anti-histidine tag (Serotec), 1:5000 dilution

Secondary antibody:

Horseradish peroxidase (HRP) - conjugated anti-mouse (Amersham), 1:6000 dilution

Western blots were performed using a Mini Trans-Blot Cell (Biorad). SDS-PAGE gels were run as described in Section 2.2.2.1, using pre-stained molecular weight markers (Biorad). Following the completion of the gel run, the gel was transferred to a cassette against a nitrocellulose membrane pre-soaked in transfer buffer. The gel and membrane, sandwiched between two pieces of filter paper and two sponges, were placed in the cassette which was placed in the Mini Trans-Blot Cell kit. The protein was transferred from the gel to the membrane by running a constant voltage of 250 V for 1 hr. Following the transfer, the nitrocellulose was removed from the cassette and soaked in blocking buffer for one hr.

After blocking, the nitrocellulose was washed in TTBS for 3 x 10 min washes. The membrane was then soaked in a solution of the chosen primary antibody in TBS with 0.05 % (w/v) bovine serum albumin (BSA) for two hr. Following another round of washing in TTBS (3 x 10 min), the secondary antibody, again in TBS with 0.05 % (w/v) BSA, was applied to the membrane for 1 hr. The membrane was then washed again with TTBS (3 x 10 min). The blot was treated with ECL reagents (GE Healthcare) for 1 min, and then exposed onto film in a Hypercassette^{TM} (Amersham) which was then developed in a Fuji Processor FPM-100A.

2.2.4.3 Size Exclusion Chromatography

Prior to experimentation, purified proteins were analyzed by size exclusion chromatography (SEC) to confirm they were in their native monomeric state. A pre-calibrated Amersham Biosciences Superose 12 HR 10/300 column was used in conjunction with an Amersham Äkta FPLC system and the associated Unicorn program. The equilibration and elution buffer was TBSG, and 20 – 200 μg of purified protein was injected onto the column. The flow rate was maintained at the recommended rate and the absorbance monitored at a wavelength of either 214 nm or 280 nm.

2.2.4.4 Ubiquitin Protease Activity Assay

To confirm the protein was active, the ubiquitin protease activity of protein was determined. Ataxin-3 variants and the linear substrate GST-Ub52 were incubated at a ratio of 1:4 (enzyme:substrate) at 37 ºC for 1 hr in a reaction buffer containing 100 mM Tris, 1 mM DTT, pH 8.0. The activity was assessed by coomassie-stained SDS-PAGE (2.2.4.1).

The pGEX-Ub52 vector was kindly donated by Roger Everett at the MRC Virology Unit, Glasgow, Scotland. The fusion protein was expressed and purified as described previously (219).

2.2.5 Protein Analysis Techniques

2.2.5.1 Circular Dichroism (CD)

Secondary Structure Analysis

CD spectra were obtained either on a Jasco 810 or a Jasco J-815 spectropolarimeter, both thermostatted by a Jasco peltier. Far-UV CD measurements were obtained using a 0.1 mm path length quartz cuvette with a protein concentration of 20 – 30 μM. Spectra were obtained from 190 – 260 nm using a scanning speed of 50 nm/min, and three scans were accumulated for each sample. The CD measurements were converted to molar ellipticity (θ) using equation 2.2:

$$\theta = \frac{\theta_{obs}}{10 x l x C}$$

Equation 2.2

θ_{obs} is the CD signal in millidegrees, l is the path length in cm and C is the protein concentration (M). The units for molar ellipticity are mdeg.cm^2.dmol^{-1}. Secondary structure content of proteins was estimated by deconvolution of the far-UV CD spectra using the CONTINLL algorithm (220,221) available at the online DICHROWEB facility (222,223).

Tertiary Structure Analysis

Near-UV CD spectra were obtained using a 1 cm path length quartz cuvette. Spectra were obtained from 260 – 350 nm at a scanning speed of 50 nm/min, and three accumulations were averaged for each scan.

Thermal Denaturation

Thermal denaturation was performed in a 1 cm path length stoppered quartz cuvette. The temperature was increased from 20 ºC to 80 ºC at a rate of 1 ºC/min. Each protein was at a concentration of 1 mg/mL in PBS (137 mM NaCl, 10.1 mM NaH_2PO_4, 2.68 mM KCl, 1.76 KH_2PO_4, 10 % Glycerol, pH 7.4), and the change in CD signal at 280 nm was monitored.

2.2.5.2 Equilibrium Denaturation

Equilibrium unfolding was completed using the chemical denaturant GdnHCl. Stock solutions of GdnHCl were prepared in TBSG or 50 mM ammonium acetate, 50 mM ammonium bicarbonate, pH 7.4 buffer. Equilibrium unfolding samples were set up with GdnHCl concentrations ranging from 0 M to 6 M, with a constant protein concentration of 1 μM and the presence of 5 mM EDTA and 15 mM β-me. Samples were left to equilibrate for 3 hr at 4 ºC before CD analysis at 222 nm was completed. Unfolding data was fit to a two-state unfolding model as previously described (224):

$$I = \frac{(I_f + m_f[U]) + (I_U + m_U[U])\exp(-(\Delta G^\circ - m[U])/(RT)}{1 + \exp(-(\Delta G^\circ - m[U])/(RT)} \qquad \textbf{Equation 2.3}$$

where I is the measured signal, $[U]$ is the GdnHCl concentration, T is the temperature in degrees Kelvin and R is the gas constant (1.98 cal/mol/K). I_f and I_U are the values of the native and unfolded states respectively, and m_f and m_U are the respective gradients of the pre- and post- unfolding base lines. ΔGº is the change in free energy between the native and unfolded states at 0 M GdnHCl and *m* is the dependence of the free energy of unfolding on denaturant concentration.

2.2.5.3 Mass spectrometry (MS)

Native Conditions

Spectra under native conditions were obtained using a LCT Premier (Waters) connected to a NanoMate (Advion Biosciences, USA) nanoESI interface and sample delivery system. A capillary voltage of 1.8 kV and a nitrogen nebulizing gas pressure of 0.7 psi were used, together with the following instrument parameters for the LCT premier: sample cone 70 V, ion guide 1 70 V, aperture 1 10 V and ion energy 100 V. Mass accuracy was ensured by calibration with a separate introduction of cesium iodide. Mass spectra were analyzed using MassLynx v4.1 software (Waters UK Ltd.). Spectra were baseline corrected, mildly smoothed using a Sovitzy-Golay algorithm, and then peak centered by peak area.

Denaturing Conditions

Spectra of Josephin in acetonitrile (pH 2.0) were obtained using a Micro Q-Tof (Bruker). Samples were infused using a syringe pump (KD Scientific, USA) at 10 μL min^{-1} and the following instrument parameters were set: gas temperature 325 K, drying gas 5 L min^{-1}, nebulizer gas pressure 20 psi, capillary voltage 5000 V, fragmenter voltage 350 V and skimmer voltage 65 V.

Hydrogen Exchange MS

Josephin in protonated buffer A (50 mM ammonium acetate, 50 mM ammonium bicarbonate, pH 7.4) was diluted 25 fold into deuterated buffer A to initiate exchange. The sample was incubated in a 20 ºC water bath and 10 μL samples were removed over 6 hrs and analyzed using positive nanoESI-MS under native conditions as described above.

In order to eliminate back exchange and determine that Josephin reached the theoretical exchangeable mass during HX, exchange was followed using a closed electrospray source attached to the LCT Premier. In these experiments the sample was infused at 10 μL min^{-1} using a syringe pump (Harvard Apparatus, MA).

2.2.6 Aggregation Assays

Ataxin-3 variants were incubated at a concentration of 30 μM in TBSG (pH 7.4) buffer containing 5 mM EDTA, 15 mM β-me and 2 mM PMSF. Samples were incubated at 37 ºC under non-shaking conditions in air-tight containers to eliminate evaporation. At various time points, samples were removed and assayed as described in the relevant methods section.

2.2.6.1 ThioflavinT Fluorescence

Discontinuous Analysis

A 10 μL sample was taken from the aggregation assay (2.2.6) and diluted into 500 μL buffer containing 30 μM thioT. Samples were placed in a quartz fluorescence cuvette (Starna), and using an excitation wavelength of 440 nm, the emission intensity at 480 nm was monitored on a FluoroMax-4 fluorimeter (Horiba Jobin Yvon).

Continuous Analysis

ThioT fluorescence was monitored using a Fluostar Optima fluorescence platereader (BMG laboratories). Continuous assays were set up as described in section 2.2.6, but with the addition of 30 μM thioT. Excitation and emission filters of 450 nm and 490 nm were used respectively. The reactions were performed in black 384 well clear bottom plates (Corning) with the top of the plate sealed to prevent evaporation. All reactions were incubated at 37 ºC without shaking, and excitation and emission read from the bottom of the plate. The aggregation kinetics obtained from continuous plate reader assays and thus performed in the presence of thioT, were comparable to kinetic data from discontinous thioT measurements.

2.2.6.2 Filter Trap Assay

Solutions:

Stability Buffer:	4 % (w/v) SDS, 100 mM DTT
TBS:	20 mM TrisHCl, 0.2 M NaCl, pH 7.4
TTBS:	20 mM TrisHCl, 0.2 M NaCl, 0.5 % (w/v) Tween, pH 7.4
Blocking Buffer:	3 % (w/v) skim milk powder in TBS
Primary Antibody:	Mouse anti-histidine tag (Serotec), 1:5000 dilution in TBS containing 0.5 % (w/v) BSA
Secondary Antibody:	HRP-conjugated anti-mouse (Amersham), 1:6000 dilution in TBS containing 0.5 % (w/v) BSA

Protein aliquots were diluted into stability buffer at a 1:1 ratio. The samples were heated for 5 min at 100 ºC and then diluted with 200 μL of 2 % (w/v) SDS. 70 μL of each sample was filtered through a pre-equilibrated 0.2 μm cellulose acetate membrane (Schleicher and Schuell) using a Bio-Dot SF microfiltration unit (Biorad). The membrane was washed twice with 0.1 % (w/v) SDS. The membrane was soaked in blocking buffer for 1.5 hr, and rinsed briefly with TTBS. The membrane was then soaked for 1 hr in the primary antibody solution. The membrane was washed in TTBS (3 x 10 min) and then incubated for 2 hr in the secondary antibody solution. The membrane was again washed with TTBS (3 x 10 min). The blot was analyzed using the ECL reagents as described previously in section 2.2.4.2.

2.2.6.3 Transmission Electron Microscopy

Samples were adsorbed onto a carbon grid and negatively stained with 1 % (w/v) aqueous uranyl acetate (pH 8.0). Samples were analyzed by transmission electron microscopy on a Hitachi H7500 electron microscope using an acceleration voltage of 80 kV.

2.2.7 Phospholipid Overlay Assay

Samples taken from an aggregation assay set up as described in section 2.2.6 were incubated with the phospholipids on the PIP strip membrane (Molecular Probes) overnight at 4 ºC. Each lipid dot contained 100 pmol of phospholipids. The membrane was then blotted using the antibodies described in section 2.2.6.2 using the method described previously (225).

CHAPTER 3

THE IMPACT OF FLANKING DOMAIN STABILITY ON AGGREGATION KINETICS OF A POLYQ PROTEIN

PREFACE

Ataxin-3 aggregation was proposed in 2006 to occur via a multi-stage mechanism in a key study which first detailed investigation the aggregation of a pathogenic length polyQ protein *in vitro* (191). This study used ataxin-3 variants with polyQ tract lengths of 1, 15 and 64 to demonstrate that all the variants form SDS-soluble fibrils with a curvilinear morphology, termed stage 1 fibrils. However, only pathogenic length ataxin-3(Q64) fibrils formed SDS-insoluble or stage 2 fibrils with a larger and more filamentous morphology (Fig 3.1).

The study proposed that the fibrils formed in stage 1 were mediated by interactions of the Josephin domain based upon two main sets of evidence (191). Firstly, cross-seeding experiments demonstrated that variants could seed the stage 1 aggregation pathways of each other, suggesting the stage 1 aggregates were structurally similar, whilst ataxin-

3(Q64) stage 2 fibrils could only seed the formation of stage 2 fibrils in ataxin-3(Q64). Secondly, the polyQ binding peptide QBP1, which inhibits polyQ mediated aggregation (205), did not affect the formation of stage 1 aggregates yet inhibited the formation of stage 2 aggregates. Therefore based upon these results, in combination with the similar morphology of stage 1 fibrils formed by all variants, Ellisdon *et al.* concluded that the stage 1 fibrils were mediated by interactions of the Josephin domain (191).

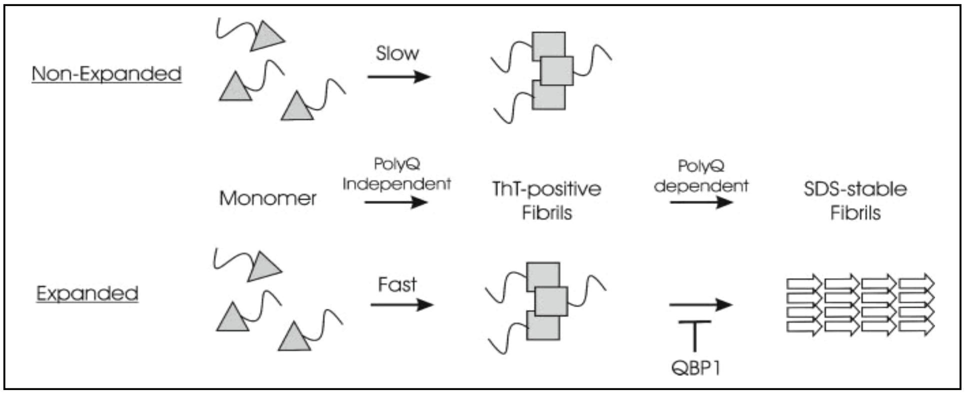

Figure 3.1 Ataxin-3 Multi-stage Aggregation Pathway The two-stage mechanism of ataxin-3 aggregation involves formation of stage 1 fibrils by all variants, and stage 2 fibrils by only pathogenic length ataxin-3. Adapted from (191).

The Josephin domain is approximately half the size of ataxin-3, and has been previously isolated, characterized and demonstrated to be intrinsically fibrillogenic (206,208). Although Ellisdon *et al.* clearly demonstrated that the polyQ tract was not involved in the formation of stage 1 fibrils, they did not consider whether as an alternative to Josephin interactions mediating stage 1 aggregation, interactions in the remainder of the C-terminal region were involved in this pathway. Therefore this study was designed to test the proposed mechanism whereby Josephin interactions mediate the first stage of ataxin-3 aggregation.

The Impact of Flanking Domain Stability on Aggregation Kinetics of a PolyQ Protein

Helen M. Saunders*, Dimitri Gilis#, Marianne Rooman#, Yves Dehouck#, Amy L. Robertson* & Stephen P. Bottomley*

*Department of Biochemistry and Molecular Biology, Monash University, Clayton, VIC 3800, Australia.

#Genomic and Structural Bioinformatics, CP 165/61, Université Libre de Bruxelles, 1050 Brussels, Belgium

Correspondence should be addressed to: Stephen P. Bottomley, Department of Biochemistry and Molecular Biology, Monash University, Clayton, VIC 3800, Australia.
Tel: 61-3-9902; Fax. 61-3-9902; Email: steve.bottomley@med.monash.edu.au

Running title: Josephin domain stability modulates ataxin-3 aggregation

Abstract

Spinocerebellar Ataxia Type 3 (SCA3) is one of nine polyglutamine (polyQ) diseases which are all characterized by progressive neuronal dysfunction. A hallmark of these diseases is the presence of neuronal inclusions which contain aggregated polyQ protein, thus suggesting that protein misfolding is a key part of this disease. Ataxin-3, the causative protein of SCA3, contains a globular, highly structured N-terminal domain (the Josephin domain) and a flexible polyQ containing C-terminal tail whose length modulates pathogenicity. The fibrillogenesis pathway of ataxin-3 has been characterized *in vitro* and proposed to have a non-polyQ dependent step mediated by Josephin domain interactions, followed by a polyQ dependent step.

In order to test the involvement of the Josephin domain in ataxin-3 fibrillogenesis, we have created both pathogenic and non-pathogenic length ataxin-3 variants with a stabilized Josephin domain, and have both stabilized and destabilized the isolated Josephin domain. We show that changing the stability of the Josephin domain dramatically impacts upon ataxin-3 fibrillogenesis *in vitro*. These data support the hypothesis that the first stage of ataxin-3 fibrillogenesis observed *in vitro* is caused by interactions involving the non-polyQ containing Josephin domain and that the stability of this domain is linked to the ataxin-3 aggregation propensity.

Introduction

The polyglutamine (polyQ) diseases are a group of nine inherited neurodegenerative diseases, whereby the expansion of a polyglutamine tract above a specific threshold leads to disease. These diseases are characterized by the presence of neuronal nuclear inclusions which contain fibrillar protein aggregates (Diaz-Hernandez et al. 2004). Thus characterization of the pathway from the natively folded protein to the misfolded fibrillar aggregate is important for understanding the role of these misfolded structures in disease initiation, progression and toxicity.

Of the causative polyQ proteins, aside from their expanded polyQ tract, there is no homology between the host proteins. The importance of protein context is increasingly being recognized in the modulation of aggregation for both polyQ proteins and peptides. Studies have reported that flanking domains affect both aggregation rates and the species formed by polyQ proteins (Nozaki et al. 2001; Chen et al. 2002; Duennwald et al. 2006; Thakur et al. 2009).

Recent studies have demonstrated that a number of the polyQ proteins contain domains which have an intrinsic ability to aggregate (Chow et al. 2004b; Masino et al. 2004; de Chiara et al. 2005b; Thakur et al. 2009). Whilst one theory suggests that under the right conditions, the ability to fibrillise is a generic property of all proteins (Dobson 1999; Fändrich et al. 2001), it is significant that a number of polyQ flanking domains are highly aggregation prone. The Josephin domain of ataxin-3, AXH domain of ataxin-1 and first 17 amino acids of huntingtin all have a propensity to aggregate under physiological conditions (Chow et al. 2004b; Masino et al. 2004; de Chiara et al. 2005b; Thakur et al. 2009). In addition to their intrinsic ability to aggregate when isolated, these domains also play a key role during aggregation when in the context of the full length protein. In a cellular environment, the load of aggregates formed by ataxin-1 is decreased when the AXH domain is substituted with a non-fibrillogenic homologue (de Chiara et al. 2005a; de Chiara et al. 2005b). Similarly, when the Josephin domain of ataxin-3 is substituted with a similarly sized domain, the formation of large aggregates is inhibited (Menon and Pastore 2006). These studies highlight the importance of the flanking domains in the aggregation of polyQ proteins.

An early study suggested that the expansion of the polyQ tract led to protein destabilization and subsequent aggregation (Bevivino and Loll 2001), however a number of recent studies using both disease and model proteins have investigated the effects of expanding the polyQ tract on overall protein stability, with mixed results. The model system CRABP I-huntingtin exon-1 only showed a decrease in global stability with an expanded polyQ tract, whereas no change in stability was observed in a SpA-polyQ model system with various length polyQ tracts (Ignatova et al. 2007; Robertson et al. 2008). In the disease protein ataxin-3, the addition of a polyQ tract destabilized the protein, yet expansion into the pathogenic range had no further effect (Chow et al. 2004a; Chow et al. 2004c). A comprehensive study into the relationship between flanking domain stability and polyQ aggregation has not however been undertaken.

One of the most extensively characterized of the polyQ proteins, ataxin-3 shows a two-stage aggregation mechanism. It has been proposed that the first stage is characterized by interactions involving the flanking Josephin domain, and the second step involves the polyQ tract (Ellisdon et al. 2006). This two-stage mechanism appears to be similar for ataxin-1 and huntingtin, which are the only other disease proteins with well characterized aggregation mechanisms (de Chiara et al. 2005b; Thakur et al. 2009). Thus, we hypothesize that intramolecular interactions between Josephin domains are the key first step responsible for initiating the ataxin-3 aggregation process, and that the stability of this domain modulates polyQ aggregation kinetics. Therefore if this hypothesis is correct, changing the Josephin domain stability will correspondingly affect ataxin-3 aggregation kinetics. We have rationally designed both stabilizing and destabilizing mutations within the Josephin domain of pathogenic and non-pathogenic length ataxin-3 using the PoPMuSiC algorithm, and show that in support of our hypothesis, the corresponding aggregation kinetics of these mutants are modulated *in vitro*.

Results

Prediction of mutations with changed stability using PoPMuSiC

The PoPMuSiC algorithm was used in order to assist with the identification of mutations that would result in a changed stability of the Josephin domain. We introduced successively, with the PoPMuSiC program, all the single-site mutations in the Josephin domain (PDB code 1YZB (Nicastro et al. 2005)) and computed the resulting change in folding free energy ($\Delta\Delta G_{computed}$). To reduce the error on the computed $\Delta\Delta G$ values due to dataset limitations, we used two different datasets, *i.e.* $\mathcal{DB}_1$ and $\mathcal{DB}_2$ (see Experimental Procedures), to evaluate two $\Delta\Delta G$ values: $\Delta\Delta G_{\mathcal{DB}1}$ and $\Delta\Delta G_{\mathcal{DB}2}$. The $\Delta\Delta G_{computed}$'s presented in this paper refer to the average of these two values.

We excluded from our analysis mutations involving prolines, as they are likely to provoke backbone structural rearrangements which are not modeled by the PoPMuSiC program. We also excluded mutations close to the catalytic triad (Cys14, His119, Asn134) to avoid alteration of the biological activity of the protein. We selected the stabilizing mutations that present a $\Delta\Delta G_{computed}$ value lower than -1.0 kcal/mol and the destabilizing mutations with a $\Delta\Delta G_{computed}$ value larger than +2.0 kcal/mol. This resulted in a short list of five potentially stabilizing mutations (Q24G, Q24Y, S81A, R103G, Q129I) and 232 potentially destabilizing mutations.

We chose two of the most stabilizing mutations (Table 1), and four destabilizing mutations which were predicted to have varying stabilities. Of the destabilizing mutations, only the L169H mutation resulted in soluble expression and was used for this study. The lack of expression of the destabilized recombinant proteins suggests protein stability is strongly linked to solubility and/or aggregation.

In the Josephin domain, ataxin-3(Q15) and ataxin-3(Q64) variants, three potentially stabilizing mutations were constructed, R103G, S81A and the double mutant R103G S81A, in addition to the destabilizing mutation L169H (Fig 1). Soluble expression was not achieved for L169H in either ataxin-3(Q15) or ataxin-3(Q64). Purification of Josephin L169H resulted in a yield ten fold lower than that typically achieved for wild type Josephin, however this was sufficient for use throughout this study. For all mutants, ubiquitin-protease activity was confirmed as previously described (Chow et al. 2004b), and the secondary structure and intrinsic fluorescence was determined to be unchanged from wild type (data not shown).

Stability mutations in Josephin correspond as predicted in silico

This study then went on to characterize the stability of these mutants *in vitro*. To determine whether the mutations resulted in a changed thermodynamic stability of Josephin, we used thermal denaturation (Fig 2). Thermal stability was determined by heating the sample 1 ºC per minute, and following the near-UV CD signal at 280 nm. Although a significant loss of tertiary structure occurred upon thermal denaturation, the negative signal observed at high temperatures (data not shown) suggests that some tertiary structure is retained as previously described (Masino et al. 2004). For wild type Josephin the midpoint of the transition was calculated to be 51.3 ± 0.6 ºC (Fig 2A). The two stabilizing mutants Josephin R103G and Josephin S81A both showed an increase in stability with a shift in the transition to midpoints of 55.9 ± 0.2 ºC and 54.1 ± 0.4 ºC respectively, whilst the destabilizing mutant Josephin L169H showed a decrease in stability to a midpoint of 47.5 ºC (Table 2), in agreement with the PoPMuSiC predictions.

Interestingly, the double mutant Josephin R103G S81A showed the same thermal stability as the single mutation Josephin S81A, with a midpoint of 55.4 ± 0.2 ºC. This trend was also observed for ataxin-3(Q15) (Fig 2B) and ataxin-3(Q64) (Fig 2C, Table 2). We have produced a set of stabilizing mutations in all the ataxin-3 variants, in addition to a destabilizing mutation in Josephin, with which to test the hypothesis that Josephin interactions are involved in the two-stage aggregation pathway of ataxin-3.

Stage 1 aggregation kinetics are modulated by the stability mutations in Josephin

In the first stage of ataxin-3 aggregation there is the formation of SDS-soluble curvilinear protofibrils, which are detectable using thioT fluorescence. As demonstrated previously, the aggregation kinetics of the ataxin-3 variants differed, with ataxin-3(Q64) showing the fastest kinetics, followed by ataxin-3(Q15) and lastly the Josephin domain (Chow et al. 2004b; Ellisdon et al. 2006). All of the ataxin-3 variants including the stabilized mutants showed a sigmoidal aggregation curve, consisting of a lag phase followed by rapid elongation, which is indicative of nucleated polymerization kinetics (Fig 3).

In Josephin, ataxin-3(Q15) and ataxin-3(Q64), both of the single stabilizing mutations result in a decreased rate of aggregation in comparison to wild type (Fig 3, Table 2). The aggregation rates of the R103G variants are slower than those of the S81A variants and this fits with the slightly greater degree of stabilization of the R103G mutants (Fig 2). Of the stabilizing mutants, the double mutant R103G S81A slowed the aggregation rates of all three proteins to the greatest extent. This was unexpected considering that it had the same thermal stability as the R103G mutant, and highlights the complex nature of the aggregation mechanism in polyQ proteins.

The destabilized mutant Josephin L169H showed a dramatic change in aggregation kinetics, with the near elimination of the lag phase and a midpoint of aggregation of 4.0 ± 0.9 hours (Fig 3C). Considering that the change in the midpoint of thermal denaturation is similar in magnitude for both the stabilized Josephin R103G and destabilized Josephin L169H, for this set of mutants it appears that destabilizing the Josephin domain has a greater impact on aggregation.

Stage 2 SDS-insoluble aggregation is correspondingly slowed by the stabilizing mutations

The SDS-insoluble aggregates formed by pathogenic length ataxin-3 during the second stage of the aggregation process were monitored by a filter trap assay. Through the use of QBP1, the stage 1 protofibrils have been demonstrated to form independently of the polyQ tract, whereas the stage 2 fibrils form through interactions of the polyQ tract (Ellisdon et al. 2006). In this study, the stabilized ataxin-3(Q64) mutants showed slower aggregation kinetics of SDS-insoluble fibrils.

During stage 1 aggregation, there was a 2-4 fold decrease in the aggregation rates of the stabilizing mutants compared to wild type ataxin-3(Q64) (Fig 3C). The differences in aggregation kinetics were much less for SDS-insoluble aggregation. In the stage 2 aggregation pathway, the aggregation midpoints of the stabilized ataxin-3(Q64) mutants only increased by 20-40 % compared to wildtype ataxin-3(Q64). The midpoints of both stage 1 and stage 2 aggregation were very similar for ataxin-3(Q64) R103G S81A. This implies that stage 2 aggregation is not dependent on the rate of formation of the stage 1 curvilinear aggregates.

Morphology of end-point fibrils of the ataxin-3(Q64) stabilizing mutants is unchanged

The morphology of end point ataxin-3(Q64) fibrils was observed using TEM, in order to determine that the mutants formed typical stage 2 fibrils. The aggregates were analyzed after 90 hours of incubation. The diameters of the fibrils ranged from 45 - 90 nm, with average lengths of 2 to 4 μm (Fig 5). Thus all of the stabilized ataxin-3(Q64) mutants showed the formation of the large, filamentous stage 2 aggregates.

Discussion

Confirmation of a multi-stage aggregation pathway for ataxin-3

There is growing evidence that the flanking domain affects the aggregation of a number of polyQ disease proteins, and this study provides further support for the involvement of the Josephin domain in the ataxin-3 aggregation pathway. The role of the flanking domain in aggregation may contribute to the significant variation in the polyQ tract length threshold which leads to disease, from 21 glutamines in SCA6 to 49 glutamines in Dentatorubral-pallidoluysian atrophy (DRPLA), and the differences in disease severity between polyQ proteins with the same length polyQ tract (Komure et al. 1995; Zhuchenko et al. 1997).

The results of this study support our initial hypothesis that Josephin interactions are involved in the first step of the ataxin-3 aggregation pathway, as suggested by the multi-stage aggregation model (Gales et al. 2005; Ellisdon et al. 2006). Specifically, increasing the thermodynamic stability of the Josephin domain slowed down the rate of stage 1 ataxin-3 fibrillogenesis and vice versa (Fig 3). The destabilized Josephin mutant showed the greatest change in aggregation kinetics, with the elimination of the lag phase and an aggregation midpoint of 4 hours (Fig 3C). Thus in the aggregation pathway of the Josephin domain, changing the stability of the protein significantly affects the kinetics of aggregation. Although only stabilizing mutations were studied for ataxin-3(Q15) and ataxin-3(Q64), in both cases the stabilizing mutations slowed the aggregation rate. This suggests that in the context of full length ataxin-3, the Josephin domain is involved in the initial interactions of stage 1 aggregation.

The mechanism via which stage 1 aggregates transition to stage 2 aggregates has not been determined. If this pathway is linear in nature, and stage 1 fibrils must be formed prior to stage 2, then it assumes there is a rearrangement of the stage 1 fibril to form a stage 2 fibril which is mediated by interactions of the polyQ tract. Whether this transition occurs once a critical concentration of stage 1 fibrils is formed, or from a specific point in the formation of the stage 1 fibril is unknown. Alternatively this pathway could be non-linear in nature, and the two types of fibrils formed independently, albeit with different kinetics. Whilst this may be the case, at the endpoint of aggregation there are only stage 2 type fibrils, suggesting that stage 1 fibrils ultimately form or extend into stage 2 aggregates in ataxin-3(Q64).

This study demonstrated that stabilizing mutations located within the Josephin domain of ataxin-3(Q64) had a greater effect on stage 1 aggregation than on stage 2. These data suggest that the two stages of aggregation are not independent and that it is not a linear pathway whereby there must be completion of stage 1 aggregation before stage 2 occurs. Mutations within the Josephin domain had the same impact on aggregation of both isolated Josephin domain and full length ataxin-3, and therefore this study also supports the hypothesis that both proteins form SDS-soluble fibrils via the same pathway.

Although mutants with changed thermodynamic stability were identified in this study, there were also some unexpected results which highlight the complex nature of ataxin-3. Ataxin-3(Q64) had a lower thermal stability than ataxin-3(Q15) (Table 2), which was unexpected considering previous studies have shown that different length polyQ tracts do not change the stability of ataxin-3 (Chow et al. 2004a). This difference may result from the different measures of stability used, as Chow *et al.* (2004a) followed changes in intrinsic fluorescence and far-UV CD using acid-induced denaturation. Thermal denaturation is irreversible and ultimately results in aggregation of the sample, however it has been previously demonstrated that aggregation occurs subsequent to the loss of tertiary structure, and thus thermal denaturation can be used as a measure of the stability of the protein (Masino et al. 2004). In addition to this, even though both of the single stability mutations resulted in increased stability in all ataxin-3 variants, the double mutant R103G S81A only showed an increase in stability that was equal to the most stabilized single mutation, R103G. This non-additive effect on stability is somewhat surprising since the residues S81 and R103 are located far away from each other in the native structure of the Josephin domain (Fig 1).

There are a number of factors which impact upon aggregation even in an *in vitro* system where the interactions which occur within the cell are lacking. The lack of increase in stability when both of the stabilizing mutations were present in ataxin-3, compared to the single-site mutations, demonstrates the complex nature of the aggregation process. This may be because in addition to changing the thermodynamic stability of the proteins, the mutations may also affect the dynamics, solubility and amyloidogenicity of the protein which is impacting upon aggregation. Further study is needed to investigate the role of local dynamics and aggregation, as hydrogen exchange NMR of the mutants would indicate if there was a change in local dynamics resulting from the mutations.

Aggregation occurs from an intermediate state within the folding pathway

Two distinct mechanisms have been proposed for the initiation of ataxin-3 aggregation. Firstly, that the aggregation pathway is distinct to that of folding, and secondly that aggregation is initiated from an intermediate within the folding pathway (Bevivino and Loll 2001; Chow et al. 2004a). The data presented in this study allow us to distinguish between these two mechanisms. If folding and aggregation occurred through different pathways which both initiate from the native conformation of ataxin-3, then the stability mutations would not be expected to affect the aggregation rate. Therefore the change in aggregation kinetics of the ataxin-3 stability mutants suggests these pathways are not independent, and supports the model whereby aggregation occurs off an intermediate in the folding pathway. This is in keeping with the conformational change hypothesis of aggregation (Kelly 1998). There are examples of proteins which undergo both these mechanisms of aggregation, however the conformational change mechanism is the most common for amyloid proteins. As seen in this study, a mutation which decreases the thermodynamic stability of the protein often results in the increased population of an aggregation prone intermediate conformation which exists on the folding pathway, and thus increased aggregation rates (Horwich 2002).

Determinants of ataxin-3 aggregation in the cell

The presence of numerous competing interactions and more complex environment of the cell make the aggregation rates difficult to compare with *in vitro* studies. Warrick *et al.* suggest that within a *Drosophila* model of ataxin-3, the full length ataxin-3 is less toxic than a truncated C-terminal region which does not contain the Josephin domain (ataxin-3(tr)) (Warrick et al. 2005). The two-stage mechanism identified *in vitro* suggests that the initial stages of aggregation are characterized by interactions of the Josephin domain, which conflicts with the amelioration of toxicity when the Josephin domain is present in

Drosophila. This difference may be attributed to the Josephin interaction partners present within the cell, some of which have been demonstrated to also modulate aggregation *in vitro* (Boeddrich et al. 2006; Robertson et al. 2010).

In a screen for interactors in *Drosophila*, ataxin-3 bound to chaperones such as the small heat shock protein αB-crystallin (Bilen and Bonini 2007). This chaperone has subsequently been demonstrated *in vitro* to transiently interact with the Josephin domain to inhibit Josephin-mediated aggregation, but has no effect upon aggregation caused through polyQ interactions (Robertson et al. 2010). This highlights how the impact of external interactions *in vivo* can dramatically affect the aggregation rates, and also the complementary nature of *in vitro* characterization to determine the effect of extrinsic modifiers on ataxin-3 aggregation.

The involvement of cleavage within the polyQ diseases raises the relevance of studying the impact of the Josephin domain in ataxin-3 aggregation. As opposed to various other polyQ diseases, in SCA3, there is conflicting evidence as to the presence of ataxin-3(tr) fragments, with only one of several studies reporting the presence of fragments (Paulson et al. 1997; Cemal et al. 2002; Berke et al. 2004; Goti et al. 2004). Even within the study which identified ataxin-3(tr) within a patient brain, there was an equal proportions of full length ataxin-3 (Goti et al. 2004). Thus the question still remains as to whether full length or cleaved ataxin-3 is the initiator of aggregation.

Although interactions in the Josephin domain mediate ataxin-3 aggregation *in vitro*, the binding of interaction partners to Josephin *in vivo* may cause the slowed aggregation of full length ataxin-3 in comparison to truncated ataxin-3 which lacks the Josephin domain. Therefore, the characterization of the *in vitro* aggregation pathway provides a means to investigate the effects of cellular factors or therapeutics within a controlled environment. With the flanking domains directly involved in aggregation, targeting these domains as a means to slow the aggregation pathway provides a potential therapeutic strategy.

Experimental Procedures

Materials – Phenylmethylsulfonyl fluoride, β-mercaptoethanol and thioflavin T (ThioT) were all obtained from Sigma.

PoPMuSiC Algorithm – The PoPMuSiC program aims to predict the folding free energy changes ($\Delta\Delta G = \Delta G^{mutant} - \Delta G^{wild\text{-}type}$) that results from single-site mutations in a protein (Gilis and Rooman 2000; Kwasigroch et al. 2002). All the possible point mutations are successively introduced *in silico* in the protein and their ΔΔG's are computed by means of statistical potentials derived from datasets of known protein structures. Two datasets are used here, referred to as $\mathcal{DB}_1$ and $\mathcal{DB}_2$: the first contains 141 well resolved X-ray structures (resolution ≤ 2.5 Å) of protein chains with less than 25 % pairwise sequence identity (Wintjens et al. 1996), and the other 735 high-resolution X-ray structures (resolution ≤ 2.0 Å) of protein chains with no more than 20 % pairwise sequence identity (Hobohm et al. 1992). Two types of potentials are considered. $\Delta G_{torsion}$ is a torsion potential that describes local interactions along the sequence, and is obtained from the frequencies of association between residues or residue pairs and backbone torsion angle domains. $\Delta G_{distance}$ is a distance potential computed from the propensities of residue pairs to be separated by a spatial distance between average side chain centroids C^{μ} (Kocher et al. 1994). These potentials take implicitly the solvent into account as they are derived from solution structures. The folding free energy changes ΔΔG's are evaluated by linear combinations of torsion and distance potentials:

$$\Delta\Delta G_{computed} = \alpha\ \Delta\Delta G_{torsion} + \beta\ \Delta\Delta G_{distance} + \gamma$$

where α, β and γ are weighting factors depending on the solvent accessibility of the mutated residue (Gilis and Rooman 2000).

The PoPMuSiC program requires as input the structure of the target protein in PDB format (Berman et al. 2000) and uses a simplified representation of protein structures consisting of the backbone atoms and the pseudo-atom C^{μ}. The backbone structure is assumed to be unchanged upon mutation.

Mutagenesis – Using the QuickChange mutagenesis method, the following mutations were introduced into Josephin, ataxin-3(Q15) and ataxin-3(Q64): L169H, S81A, R103G.

Expression and Purification of Ataxin-3 variants – All ataxin-3 variants were expressed and purified as previously described (Chow et al. 2004c), and the proteins were stored at -80 °C. Following purification the deubiquitinating activity of the proteins was measured (Chow et al. 2004b) and before use all were analyzed using gel filtration to ensure that no multimeric species were present.

Thermal Denaturation – Thermal unfolding was monitored on a thermostatted Jasco-810 spectropolarimeter and performed by increasing the temperature by 1 ºC per min from 20 ºC to 80 ºC. Changes in the near-UV CD signal were monitored at 280 nm, using a stoppered quartz cuvette with a path length of 1 cm. Protein samples were measured at a concentration of 1 mg/ml.

Fibrillogenesis Time Course Assays – Ataxin-3 variants (30 µM) were incubated in TBSG (80 mM Tris, 100 mM NaCl, 10 % (v/v) glycerol, pH 7.4) containing 5 mM EDTA, 15 mM β-mercaptoethanol and 2 mM phenylmethylsulfonyl fluoride. Samples were incubated without shaking at 37 ºC in air-tight containers to prevent evaporation.

ThioT Fluorescence – ThioT fluorescence measurements were recorded on a BMG Fluorostar plate reader, using the buffering conditions described previously with the addition of 30 µM thioT. Excitation and emission wavelengths of 430 nm and 480 nm with a cut off filter of 455 nm were used, and both excitation and emission were read from the underneath of a black clear bottom plate. All reactions were completed at 37 ºC with no shaking.

Membrane Filter Trap Assay – Aliquots containing 7.4 µg of protein were taken from the fibrillogenesis reaction, diluted 1:1 with a 4 % (w/v) SDS / 100 mM DTT solution and then boiled for 5 minutes at 100 ºC. 200 µl of 2 % (w/v) SDS was then added to each of the samples, and 2.5 µg of protein was filtered through a 0.2 µm cellulose acetate membrane (Schleicher and Schuell) using a Bio-Rad Bio-Dot SF microfiltration unit. The membrane was then washed twice by filtering 200 µl of 0.1 % (w/v) SDS, and blotted with a hexahistidine (His6) antibody (Serotec). Densitometry was completed using the program ImageQuant.

Transmission Electron Microscopy (TEM) – TEM images were obtained using a Hitachi TEM with an accelerating voltage of 80 kV. Samples were adsorbed onto a carbon-coated grid, and stained with 1 % (w/v) uranyl acetate.

Acknowledgements

SPB is a Senior Research Fellow of the NHMRC and the work was supported by both the ARC and NHMRC of Australia.

References

Berke, S.J., Schmied, F.A., Brunt, E.R., Ellerby, L.M., and Paulson, H.L. 2004. Caspase-mediated proteolysis of the polyglutamine disease protein ataxin-3. *J Neurochem* **89**(4): 908-918.

Bevivino, A.E. and Loll, P.J. 2001. An expanded glutamine repeat destabilizes native ataxin-3 structure and mediates formation of parallel beta -fibrils. *Proc Natl Acad Sci U S A* **98**(21): 11955-11960.

Bilen, J. and Bonini, N.M. 2007. Genome-wide screen for modifiers of ataxin-3 neurodegeneration in Drosophila. *PLoS Genet* **3**(10): 1950-1964.

Boeddrich, A., Gaumer, S., Haacke, A., Tzvetkov, N., Albrecht, M., Evert, B.O., Muller, E.C., Lurz, R., Breuer, P., Schugardt, N. et al. 2006. An arginine/lysine-rich motif is crucial for VCP/p97-mediated modulation of ataxin-3 fibrillogenesis. *Embo J* **25**(7): 1547-1558.

Cemal, C.K., Carroll, C.J., Lawrence, L., Lowrie, M.B., Ruddle, P., Al-Mahdawi, S., King, R.H.M., Pook, M.A., Huxley, C., and Chamberlain, S. 2002. YAC transgenic mice carrying pathological alleles of the MJD1 locus exhibit a mild and slowly progressive cerebellar deficit. *Hum Mol Genet* **11**(9): 1075-1094.

Chen, S., Ferrone, F.A., and Wetzel, R. 2002. Huntington's disease age-of-onset linked to polyglutamine aggregation nucleation. *Proc Natl Acad Sci U S A* **99**(18): 11884-11889.

Chow, M.K., Ellisdon, A.M., Cabrita, L.D., and Bottomley, S.P. 2004a. Polyglutamine expansion in ataxin3 does not affect protein stability. *Journal of Biological Chemistry* **279**(46): 47643-47651.

Chow, M.K., Mackay, J.P., Whisstock, J.C., Scanlon, M.J., and Bottomley, S.P. 2004b. Structural and functional analysis of the Josephin domain of the polyglutamine protein ataxin-3. *Biochem Biophys Res Commun* **322**(2): 387-394.

Chow, M.K., Paulson, H.L., and Bottomley, S.P. 2004c. Destabilization of a non-pathological variant of ataxin-3 results in fibrillogenesis via a partially folded intermediate: a model for misfolding in polyglutamine disease. *J Mol Biol* **335**(1): 333-341.

de Chiara, C., Menon, R.P., Adinolfi, S., de Boer, J., Ktistaki, E., Kelly, G., Calder, L., Kioussis, D., and Pastore, A. 2005a. The AXH domain adopts alternative folds the solution structure of HBP1 AXH. *Structure* **13**(5): 743-753.

de Chiara, C., Menon, R.P., Dal Piaz, F., Calder, L., and Pastore, A. 2005b. Polyglutamine is not all: the functional role of the AXH domain in the ataxin-1 protein. *J Mol Biol* **354**(4): 883-893.

Diaz-Hernandez, M., Moreno-Herrero, F., Gomez-Ramos, P., Moran, M.A., Ferrer, I., Baro, A.M., Avila, J., Hernandez, F., and Lucas, J.J. 2004. Biochemical, ultrastructural, and reversibility studies on huntingtin filaments isolated from mouse and human brain. *J Neurosci* **24**(42): 9361-9371.

Dobson, C.M. 1999. Protein misfolding, evolution and disease. *Trends Biochem Sci* **24**(9): 329-332.

Duennwald, M.L., Jagadish, S., Muchowski, P.J., and Lindquist, S. 2006. Flanking sequences profoundly alter polyglutamine toxicity in yeast. *Proc Natl Acad Sci U S A* **103**(29): 11045-11050.

Ellisdon, A.M., Thomas, B., and Bottomley, S.P. 2006. The two-stage pathway of ataxin-3 fibrillogenesis involves a polyglutamine-independent step. *J Biol Chem* **281**(25): 16888-16896.

Fändrich, M., Fletcher, M.A., and Dobson, C.M. 2001. Amyloid fibrils from muscle myoglobin. *Nature* **410**(6825): 165-166.

Gales, L., Cortes, L., Almeida, C., Melo, C.V., do Carmo Costa, M., Maciel, P., Clarke, D.T., Damas, A.M., and Macedo-Ribeiro, S. 2005. Towards a structural understanding of the fibrillization pathway in Machado-Joseph's disease: trapping early oligomers of non-expanded ataxin-3. *J Mol Biol* **353**(3): 642-654.

Goti, D., Katzen, S.M., Mez, J., Kurtis, N., Kiluk, J., Ben-Haiem, L., Jenkins, N.A., Copeland, N.G., Kakizuka, A., Sharp, A.H. et al. 2004. A mutant ataxin-3 putative-cleavage fragment in brains of Machado-Joseph disease patients and transgenic mice is cytotoxic above a critical concentration. *J Neurosci* **24**(45): 10266-10279.

Horwich, A. 2002. Protein aggregation in disease: a role for folding intermediates forming specific multimeric interactions. *J Clin Invest* **110**(9): 1221-1232.

Ignatova, Z., Thakur, A.K., Wetzel, R., and Gierasch, L.M. 2007. In-cell aggregation of a polyglutamine-containing chimera is a multistep process initiated by the flanking sequence. *J Biol Chem* **282**(50): 36736-36743.

Kelly, J.W. 1998. The alternative conformations of amyloidogenic proteins and their multi-step assembly pathways. *Curr Opin Struct Biol* **8**(1): 101-106.

Komure, O., Sano, A., Nishino, N., Yamauchi, N., Ueno, S., Kondoh, K., Sano, N., Takahashi, M., Murayama, N., Kondo, I. et al. 1995. DNA analysis in hereditary dentatorubral-pallidoluysian atrophy: correlation between CAG repeat length and phenotypic variation and the molecular basis of anticipation. *Neurology* **45**(1): 143-149.

Masino, L., Nicastro, G., Menon, R.P., Piaz, F.D., Calder, L., and Pastore, A. 2004. Characterization of the structure and the amyloidogenic properties of the Josephin domain of the polyglutamine-containing protein ataxin-3. *J Mol Biol* **344**(4): 1021-1035.

Menon, R.P. and Pastore, A. 2006. Expansion of amino acid homo-sequences in proteins: insights into the role of amino acid homo-polymers and of the protein context in aggregation. *Cell Mol Life Sci* **63**(14): 1677-1685.

Nozaki, K., Onodera, O., Takano, H., and Tsuji, S. 2001. Amino acid sequences flanking polyglutamine stretches influence their potential for aggregate formation. *Neuroreport* **12**(15): 3357-3364.

Paulson, H.L., Das, S.S., Crino, P.B., Perez, M.K., Patel, S.C., Gotsdiner, D., Fischbeck, K.H., and Pittman, R.N. 1997. Machado-Joseph disease gene product is a cytoplasmic protein widely expressed in brain. *Ann Neurol* **41**(4): 453-462.

Robertson, A.L., Headey, S.J., Saunders, H.M., Ecroyd, H., Scanlon, M.J., and Bottomley, S.P. 2010. Small heat-shock proteins interact with a flanking domain to suppress polyglutamine aggregation *Proc Natl Acad Sci U S A* **Published ahead of print** May 19, 2010, doi:2010.1073.

Robertson, A.L., Horne, J., Ellisdon, A.M., Thomas, B., Scanlon, M.J., and Bottomley, S.P. 2008. The structural impact of a polyglutamine tract is location-dependent. *Biophys J* **95**(12): 5922-5930.

Thakur, A.K., Jayaraman, M., Mishra, R., Thakur, M., Chellgren, V.M., IJ, L.B., Anjum, D.H., Kodali, R., Creamer, T.P., Conway, J.F. et al. 2009. Polyglutamine disruption of the huntingtin exon 1 N terminus triggers a complex aggregation mechanism. *Nat Struct Mol Biol* **16**(4): 380-389.

Warrick, J.M., Morabito, L.M., Bilen, J., Gordesky-Gold, B., Faust, L.Z., Paulson, H.L., and Bonini, N.M. 2005. Ataxin-3 suppresses polyglutamine neurodegeneration in Drosophila by a ubiquitin-associated mechanism. *Mol Cell* **18**(1): 37-48.

Zhuchenko, O., Bailey, J., Bonnen, P., Ashizawa, T., Stockton, D.W., Amos, C., Dobyns, W.B., Subramony, S.H., Zoghbi, H.Y., and Lee, C.C. 1997. Autosomal dominant cerebellar ataxia (SCA6) associated with small polyglutamine expansions in the alpha 1A-voltage-dependent calcium channel. *Nat Genet* **15**(1): 62-69.

Figure Legends

Figure 1 Predicted stability mutations in the Josephin domain. The two stabilizing mutations R103G and S81A and the destabilizing mutation L169H are highlighted on the 1YZB Josephin structure.

Figure 2 Thermal denaturation of Josephin stability mutants. Thermal denaturation was followed at 280 nm using near-UV CD. The temperature was increased by 1 ºC min^{-1} in a stoppered cuvette with a sample concentration of 1 mg ml^{-1}. Representative traces are shown for (A) Josephin (B) ataxin-3(Q15) and (C) ataxin-3(Q64) with wild type (black), R103G (blue), S81A (green), R103G S81A (purple) and L169H (red).

Figure 3 Ataxin-3 stage 1 aggregation kinetics are changed by the Josephin mutants. Stage 1 aggregation was monitored using thioT fluorescence at 30 μM and pH 7.4 with a fluorescence plate reader. Wild type (black), R103G (blue), S81A (green), R103G S81A (purple) and L169H (red) are shown in (A) ataxin-3(Q64), (B) ataxin-3(Q15) and (C) Josephin.

Figure 4 SDS-insoluble aggregation is slowed by a stabilized Josephin domain to a lesser extent. Formation of SDS-insoluble aggregates was analyzed over time, taking aliquots from an aggregation assay at 30 μM and pH 7.4. (A) A representative filter trap membrane shows the formation of SDS-insoluble aggregates formed from ataxin-3(Q64) and the stabilizing ataxin-3(Q64) mutants. (B) Densitometry is shown for ataxin-3(Q64) (black), ataxin-3(Q64) R103G (blue), ataxin-3(Q64) S81A (green) and ataxin-3(Q64) R103G S81A (purple). Analysis of the membrane by densitometry was completed on 3 independent experiments and fit to a sigmoidal curve.

Figure 5 Morphology of endpoint aggregates is unchanged. Transmission Electron Microscopy of (A) ataxin-3(Q64), (B) ataxin-3(Q64) R103G, (C) ataxin-3(Q64) S81A and (D) ataxin-3(Q64) R103G S81A. After 90 hr of aggregation, samples were negatively stained using 1 % uranyl acetate. Scale bar represents 200 nm.

Table 1 PoPMuSiC Predicted Changes in Josephin Stability

Predicted Changes in Josephin Stability		
Mutation Type	**Mutation**	**$\Delta\Delta G_{computed}$ (kcal/mol)**
Stabilizing	R103G	- 1.37
Stabilizing	S81A	- 1.10
Destabilizing	L169H	3.00

Table 2 Thermal Denaturation and Aggregation Midpoints

	Thermal Denaturation Midpoint (ºC)	ThioT Midpoint (hrs)	SDS-Stability Midpoint (hrs)
Josephin	51.3 ± 0.6	79.4 ± 6.7	
Josephin R103G	55.9 ± 0.2	147.5 ± 7.3	
Josephin S81A	54.1 ± 0.4	115.2 ± 6.9	
Josephin R103G S81A	55.4 ± 0.2	>150 hr	
Josephin L169H	47.5 ± 0.1	4.0 ± 0.9	
Ataxin-3(Q15)	49.2 ± 0.1	24.0 ± 1.3	
Ataxin-3(Q15) R103G	52.9 ± 0.8	48.9 ± 1.8	
Ataxin-3(Q15) S81A	50.6 ± 0.9	32.2 ± 1.9	
Ataxin-3(Q15) R103G S81A	53.4 ± 0.4	50.0 ± 2.8	
Ataxin-3(Q64)	51.0 ± 0.3	11.7 ± 1.2	35.0 ± 2.7
Ataxin-3(Q64) R103G	52.1 ± 0.6	25.3 ± 2.1	42.9 ± 2.6
Ataxin-3(Q64) S81A	50.8 ± 0.2	26.3 ± 4.9	41.0 ± 7.1
Ataxin-3(Q64) R103G S81A	52.4 ± 0.3	40.6 ± 2.2	48.7 ± 1.3

Figure 1

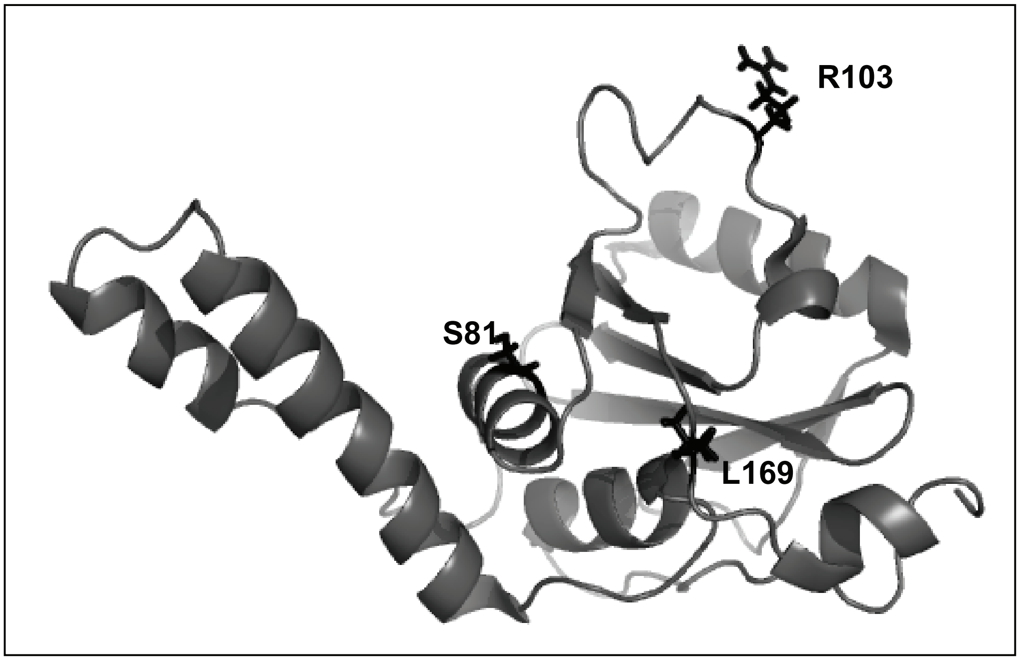
R103
S81
L169

Figure 2

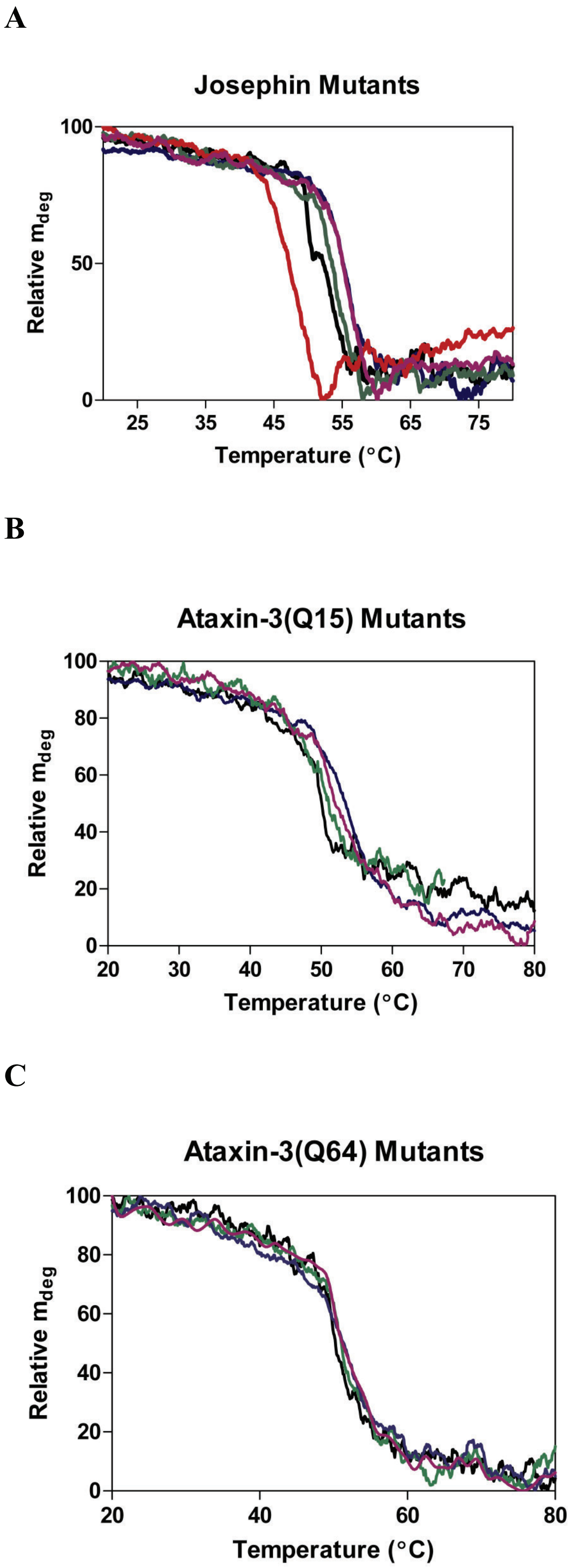
A
Josephin Mutants
100
50
0
Relative m$_{deg}$
25
35
45
55
65
75
Temperature (°C)
B
Ataxin-3(Q15) Mutants
100
80
60
40
20
0
Relative m$_{deg}$
20
30
40
50
60
70
80
Temperature (°C)
C
Ataxin-3(Q64) Mutants
100
80
60
40
20
0
Relative m$_{deg}$
20
40
60
80
Temperature (°C)

Figure 3

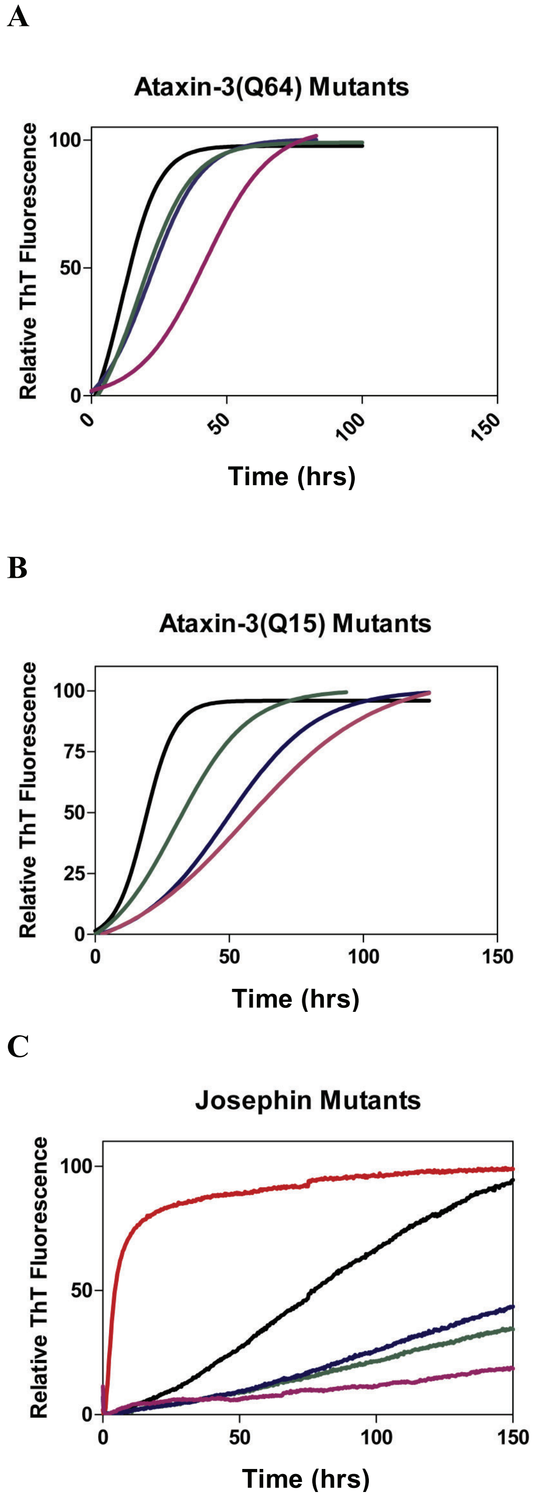
A
Ataxin-3(Q64) Mutants
Relative ThT Fluorescence
100
50
0
0
50
100
150
Time (hrs)
B
Ataxin-3(Q15) Mutants
Relative ThT Fluorescence
100
75
50
25
0
0
50
100
150
Time (hrs)
C
Josephin Mutants
Relative ThT Fluorescence
100
50
0
0
50
100
150
Time (hrs)

Figure 4

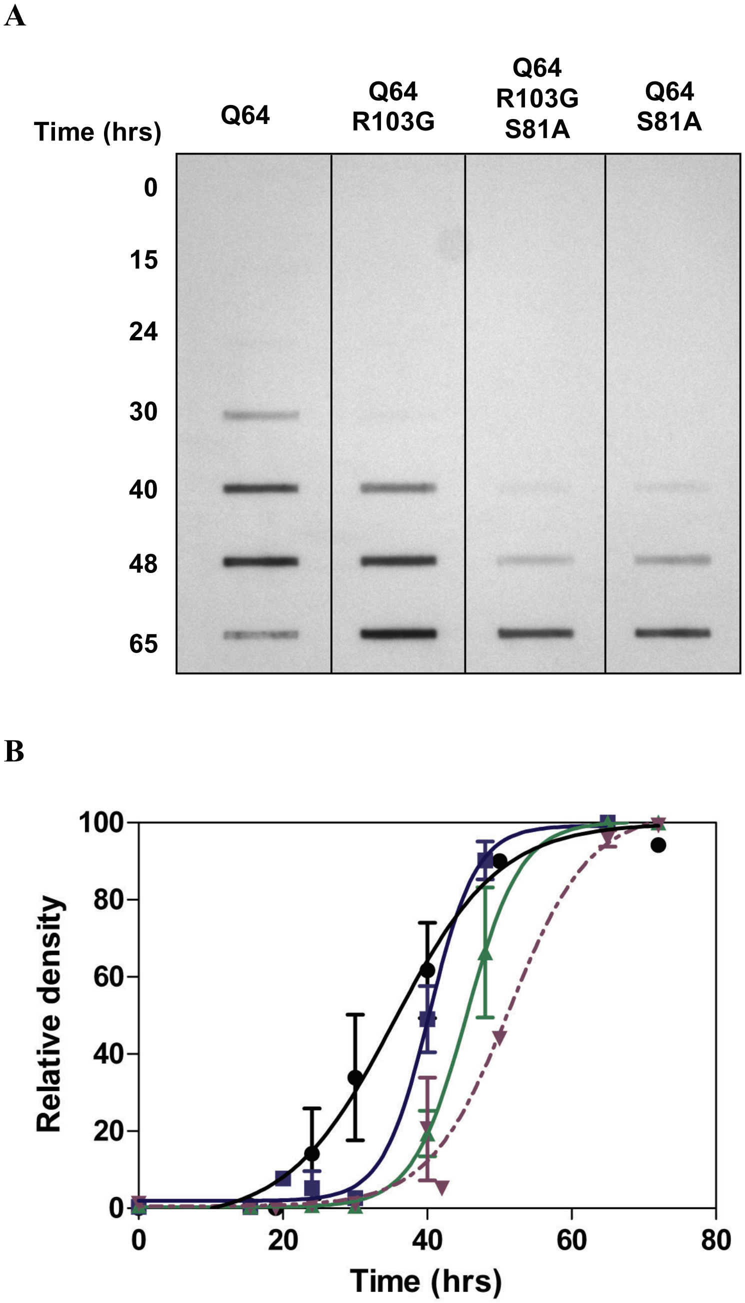
A
Time (hrs)
Q64
Q64
R103G
Q64
R103G
S81A
Q64
S81A
0
15
24
30
40
48
65
B
Relative density
100
80
60
40
20
0
0
20
40
60
80
Time (hrs)

Figure 5

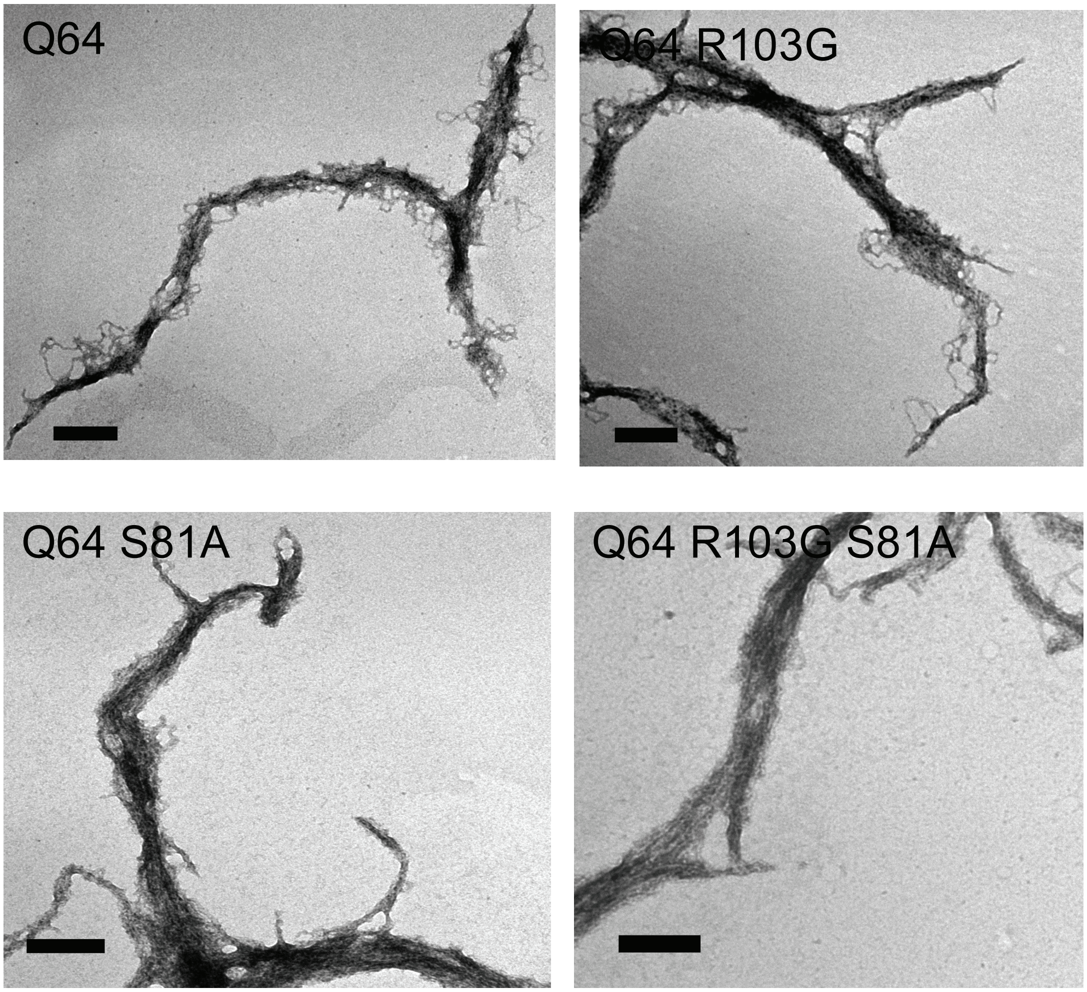
Q64
Q64 R103G
Q64 S81A
Q64 R103G S81A

CHAPTER 4

CONFORMATIONAL DYNAMICS OF THE JOSEPHIN DOMAIN OF ATAXIN-3

4.1 INTRODUCTION

4.1.1 Protein Aggregation and Dynamics

The conformational change hypothesis of aggregation proposes that folded proteins undergo an initial conformational change to adopt a partially unfolded amyloidogenic intermediate (68,226). The propensity to form such an intermediate is linked to the propensity to aggregate (68), and this has been demonstrated for a number of amyloidogenic proteins, including β_2-microglobulin, α-synuclein and lysozyme (77,227,228). For these proteins, mutations or solution conditions that promote aggregation result in an increased population of partially unfolded intermediates (77,227-229).

The proportion of the amyloidogenic intermediate in solution can be affected by both its thermodynamic equilibrium with the native conformation as well as the rate of conversion and conformational dynamics (74). In several amyloid diseases, a destabilizing mutation increases the population of a partially unfolded amyloidogenic intermediate (75,230,231). However in other diseases, mutation leads to an unchanged thermodynamic stability and it is the protein dynamics which are affected. This is observed for both lysozyme and transthyretin, whereby some aggregation prone mutants have increased rates of conformational fluctuations (75-77).

Both global and local dynamic fluctuations can enable a folded protein to momentarily visit partially unfolded conformations, however their influence on aggregation varies for different proteins. Calloni *et al.* suggest that for proteins which form an inherently fluctuating intermediate with non-persistent structure, the region with the highest intrinsic aggregation propensity, as opposed to the most dynamic region, will drive aggregation (229). Conversely, in another study local differences in dynamics between human and mouse α-synuclein were used to explain their altered aggregation propensity (232). Therefore to fully characterize the aggregation pathway of a folded protein, it is important to consider the conformational dynamics.

4.1.2 Ataxin-3 Aggregation and Dynamics

Flanking domains within the polyQ disease proteins have increasingly been shown to modulate polyQ aggregation (189,191,196,207). For example, several studies have shown that both the immediate polyQ flanking sequence in addition to flanking domains change aggregation both *in vitro* and in cell models (189,193,194,196). The dynamics of the flanking domains of polyQ proteins such as the Josephin and AXH domains have not been well characterized. When isolated, the folded Josephin domain is intrinsically fibrillogenic and forms SDS-soluble curvilinear fibrillar species (233,234). In the context of ataxin-3, it is involved in the multi-stage pathway of ataxin-3 aggregation, with the first stage of aggregation being mediated by Josephin domain interactions (Ch 3)(191). Similarly, the AXH domain has also been demonstrated to be intrinsically fibrillogenic when isolated, and shown to increase aggregation in cells in the context of ataxin-1 (207,235). Therefore determining the conformational changes and dynamics of fibrillogenic flanking domains, such as the AXH domain and Josephin, may provide insights into the initial events of aggregation of their respective proteins.

In SCA3, as for many other polyQ diseases, only an expanded polyQ tract with greater than 45 glutamines leads to disease (236). As many amyloid forming proteins contain a mutation which decreases thermodynamic stability, the effect of an expanded polyQ tract on protein stability has been investigated *in vitro*. Mixed results have been obtained with model polyQ systems, with different studies showing either no change in stability or destabilization of the model protein upon polyQ expansion (237,238). Chow *et al.* showed there was no corresponding decrease in kinetic or thermodynamic stability upon expansion of the polyQ tract into the pathological range (69). In contrast to this, there is a difference in aggregation kinetics of ataxin-3 *in vitro*, which suggests that other properties of the protein are affected by the presence of the expanded polyQ tract.

In ataxin-3 the Josephin domain plays a key role in both aggregation and cellular function (165,168,233,234). Ataxin-3 is a de-ubiquitinating protease (DUB), and the Josephin domain contains a papain-like fold (Fig 4.2) (165,166). It contains two ubiquitin binding regions, one of which is within the helical hairpin region, with the second adjacent to it, and the catalytic triad Cys-14, His-119 and Asp-134 (165,166,169). Ataxin-3 is an unusual DUB in that it has the unique ability to cleave multi-linked ubiquitin chains, as opposed to most DUBs which cleave ubiquitin chains of a single linkage (168). This suggests that Josephin may have considerable conformational flexibility and undergo structural changes to function in this manner. Therefore determining the conformation dynamics of the Josephin domain may provide insight into both its activity and aggregation propensity.

4.1.3 Theory of Hydrogen Exchange Mass Spectrometry

Hydrogen Exchange (HX) is a technique used to characterize the structure and dynamics of proteins, as within a folded protein the rate of exchange depends upon factors such as whether a proton is involved in H-bonded secondary structure, or is buried within the core of the protein (239). HX is also used to study the conformational dynamics of proteins as conformational fluctuations allow exchange to occur during the breaking and reforming of H-bonds. Proteins contain a number of protons which exchange on different timescales, and it is the backbone amide protons which exchange over a timeframe amenable to analysis (Fig 4.1).

Although commonly detected by NMR, mass spectrometry (MS) can also be used to analyze HX due to the increase in mass which occurs as amide protons exchange to deuterons. Although MS does not give residue specific information, the advantages of using MS over NMR are that a larger mass range can be analyzed, co-existing populations can be detected and different mechanisms of exchange distinguished (240). The kinetic analysis discussed below has been described previously by a number of groups (239-242).

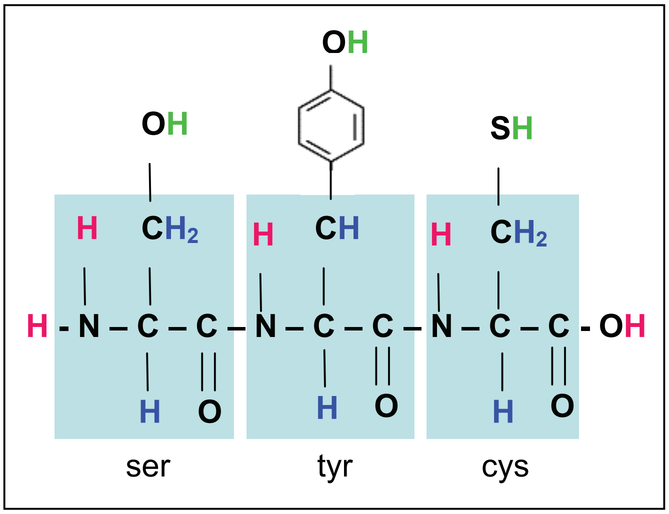

Figure 4.1 Timescale of exchange of protons. Amide protons (pink) exchange within a timescale which is amenable to analysis. The side chain protons (green) and the carbonyl protons (blue) exchange at rates which are too fast and too slow respectively for analysis.

The intrinsic exchange rate (k_{int}) of an amide hydrogen is the rate at which it exchanges if freely exposed to solvent. This rate is sensitive to pH (242), as it is catalyzed by both acids and bases as described:

$$k_{\text{int}} = k_w + k_{acid}\left[H^+\right] + k_{base}\left[OH^-\right]$$ **Equation 4.1**

where k_w is the water catalyzed, k_{acid} the acid catalyzed and k_{base} the base catalyzed second-order rate constants. In addition to being pH-dependent, k_{int} is also dependent upon temperature, with rates changing by a factor of 10 per 22 ºC (243).

The intrinsic exchange rate of an amide proton is sequence specific as bulky amino acid side chain can sterically block exchange, or conversely neighbouring polar amino acids can increase exchange (242). Bai and colleagues have quantified the effects of neighbouring amino acids on exchange for all amino acids and thus using these values, k_{int} can be calculated both individually for each amino acid in a sequence, and also for the protein as a whole (244).

In folded proteins, exchange involves a two-state transition from a closed state (C) not accessible to exchange, to an open accessible state (O) which is described as:

$$C^{H} \underset{k_{cl}}{\overset{k_{op}}{\rightleftarrows}} O^{H} \xrightarrow[\mathbf{D_2O}]{k_{\text{int}}} O^{D} \underset{k_{op}}{\overset{k_{cl}}{\rightleftarrows}} C^{D}$$

Equation 4.2

where C^H and O^H represent amide protons which are in closed or open conformations either locally or globally, C^D and O^D are the exchanged or deuterated amides in a closed or open conformation and k_{op} and k_{cl} are the rates of opening and closing respectively. In a folded protein, the mechanism of exchange is dependent upon the rate of unfolding in addition to the intrinsic rate of exchange. Therefore according to Eq. 4.2, the exchange rate of a proton (k_{ex}) becomes:

$$k_{ex} = \frac{k_{op} k_{\text{int}}}{k_{op} + k_{cl} + k_{\text{int}}}$$

Equation 4.3

Under native conditions, generally $k_{cl} >> k_{op}$, and therefore Eq. 4.3 can be simplified to:

Equation 4.4

$$k_{ex} = \frac{k_{op} k_{\text{int}}}{k_{cl} + k_{\text{int}}}$$

There are two extreme limits of Eq. 4.4, which are termed EX1 and EX2. EX2 is most commonly observed under physiological conditions and occurs when $k_{cl} >> k_{int}$, such that:

$$k_{ex} = \frac{k_{op} k_{\text{int}}}{k_{cl}} = K_o k_{\text{int}} \qquad \text{where} \qquad K_o = \frac{k_{op}}{k_{cl}}$$

Equation 4.5

Thus under an EX2 mechanism a protein will undergo random rapid visits to a conformation where exchange is possible, however the probability of exchange each time is low. As k_{ex} is dependent upon K_o, the equilibrium constant between a closed and open conformation, the apparent free energy of exchange (ΔG_{ex}^{app}) can be determined where R is the gas constant and T the absolute temperature:

$$\Delta G_{ex}^{app} = - \text{RT} \ln \left[\frac{k_{obs}}{k_{\text{int}}} \right]$$ **Equation 4.6**

EX1 is the other limit that can be observed, and occurs where $k_{int} >> k_{cl}$. Less common under native conditions, this corresponds to a situation where proteins rarely visit a conformation in which exchange can occur, however upon visiting a conformation amenable to exchange then complete exchange will occur. Therefore under this regime Eq. 4.4 is simplified to:

$$k_{ex} = k_{op}$$ **Equation 4.7**

The EX1 and EX2 mechanisms of exchange are easily distinguished when HX is analyzed using MS (240). EX1 results in a significant increase in mass to the fully deuterated mass and then an increase in intensity of this mass over time as more molecules visit an open conformation. In comparison, EX2 exchange results in a gradual increase in mass over time, as the protein frequently visits an open conformation yet only a small amount of exchange occurs each time.

In this study a MS approach is used to investigate the conformation of Josephin under both native and denaturing conditions, and show that multiple conformations of Josephin are populated in solution under native conditions. Using HX these conformations are demonstrated to be in equilibrium, thus highlighting the highly dynamic nature of Josephin.

4.2 RESULTS

4.2.1 Josephin MS under Native Conditions

Electrospray mass spectroscopy (ESI-MS) is a technique which under native conditions can be used to determine the number of protein conformations which exist in solution, as the more compact the structure, the fewer charges that can be accommodated on its surface (245). Initially, the characteristic mass spectrum displayed by the Josephin domain of ataxin-3 (Fig 4.2) under native conditions was investigated.

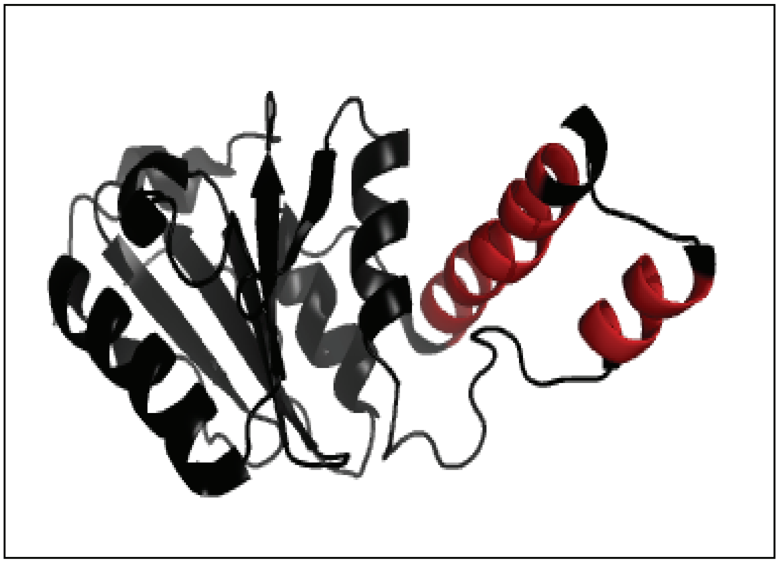

Figure 4.2 Josephin NMR structure.
Ribbon representation of the Josephin domain of ataxin-3 with the flexible helical hairpin highlighted in red (PDB: 1YZB) (166).

The three volatile buffers predominantly used in combination for native state MS are ammonium acetate, ammonium bicarbonate and ammonium formate. When buffered in ammonium formate, Josephin immediately precipitated, and thus this buffer was not used. The use of an ammonium acetate buffer resulted in a stronger signal than ammonium bicarbonate, however this buffer did not buffer as well at pH 7.4 over time. Thus a buffer containing both ammonium acetate and ammonium bicarbonate was chosen for all native MS experiments as it resulted in clean spectra with sufficient intensity (Fig 4.3).

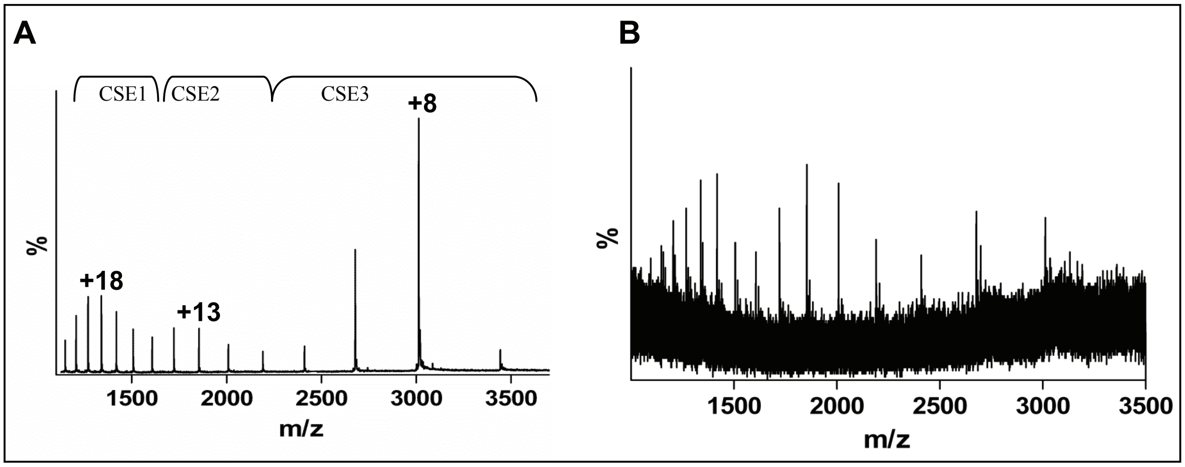

Figure 4.3 Josephin mass spectra under native conditions. (A) The mass spectra of Josephin under native conditions obtained using nanoESI-MS shows multiple charge state envelopes (CSE) centered about n = +8, +13 and +18. The spectra was obtained using a low ionic strength buffer. (B) The mass spectra of Josephin in a high ionic strength buffer shows a loss of signal due to noise.

Both a low and high ionic strength buffer were tested in order to determine which resulted in the cleanest spectra with the highest intensity (Fig 4.3). A 50 mM ammonium acetate, 50 mM ammonium bicarbonate pH 7.4 buffer resulted in a significantly greater signal intensity than a 90 mM ammonium acetate, 90 mM ammonium bicarbonate pH 7.4 buffer which had a great deal of noise, and thus the former buffer was used for all native condition MS experiments.

Unlike other spectroscopic techniques such as CD and NMR where the signal represents an average of the conformations which exist in solution, if native and non-native conformations co-exist in solution, then a bimodal distribution is observed using ESI-MS (246). Therefore under native conditions, the number of charge state envelopes in ESI-MS corresponds to the number of protein conformations in solution.

Despite the well defined NMR structure of the Josephin domain (247), the mass spectra shows a larger charge distribution (n = +22 to +7) than would be expected for a folded protein, in addition to multiple charge state envelopes (Fig 4.3). The first distribution centres on the charge state n = +8, and corresponds to approximately 60 % of the molecules, as calculated from summing the area under the peaks in each distribution. With the ability to bind the least amount of charge, this population is the most folded in solution (246). The second and third populations centre around n = +13 and n = +18, together corresponding to approximately 40 % of molecules in solution. These two charge state envelopes correspond to molecules which exist in solution in a partially unfolded conformation.

4.2.2 Josephin Exists in Multiple Conformations in Solution

4.2.2.1 Multiple charge state envelopes are not linked to parameters on the MS

A series of control experiments were performed to ensure these conformations were not merely an artifact of the mass spectrometer. The cone voltage and ionization source temperature were systematically altered, as was the sample temperature. Increasing the cone voltage can shift unfolded conformations to a higher m/z and thus lower charge state, due to a ‘charge stripping’ effect (248,249). The cone voltage was increased from 50 V to 110 V, however changing it had no effect on the ratio of molecules in each population (Fig 4.4A). Increasing the ionization source temperature can unfold proteins at high temperatures during the ionization process (248). The effect of having a temperature of 50 ºC to 100 ºC was investigated, and similarly did not change the proportion of each charge state envelope (Fig 4.4B). Therefore a standard cone voltage of 70 V and ionization source temperature of 50 ºC was used for all experiments.

The effect of changing the sample temperature on the multiple charge state envelopes was also determined. A sample temperature of between 4 ºC and 42 ºC did not affect the Josephin mass spectra (Fig 4.4C). In addition, using two different ESI-MS instruments (Waters and Bruker), and two expression constructs of Josephin all resulted in Josephin mass spectra with multiple charge state envelopes (Tomé, Radford and Macedo-Ribeiro, personal communication). This suggests that the presence of multiple charge state envelopes is not an artifact of the ionization process of ESI-MS.

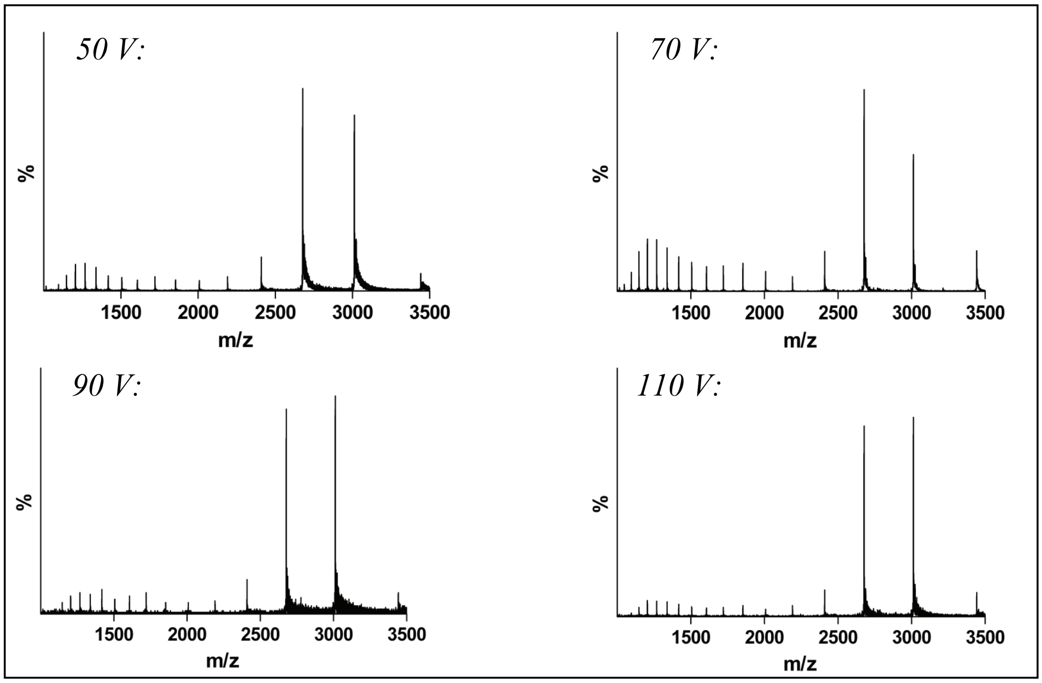

Figure 4.4 (A) Effects of changing the cone voltage on the Josephin mass spectra. Changing the cone voltage from 50 – 110 V does not significantly affect the proportions of the multiple charge state envelopes.

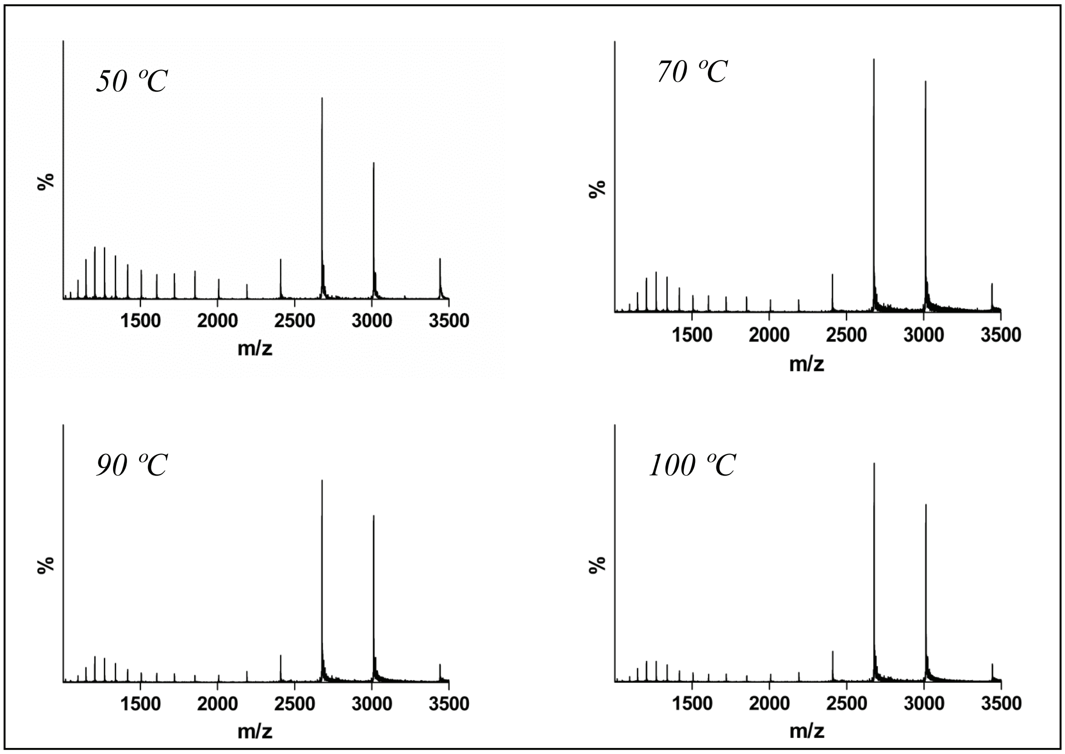

Figure 4.4 (B) Effects of changing the ionization source temperature on the Josephin mass spectra. Changing the ionization source temperature from 50 – 100 ºC does not significantly affect the proportions of the multiple charge state envelopes.

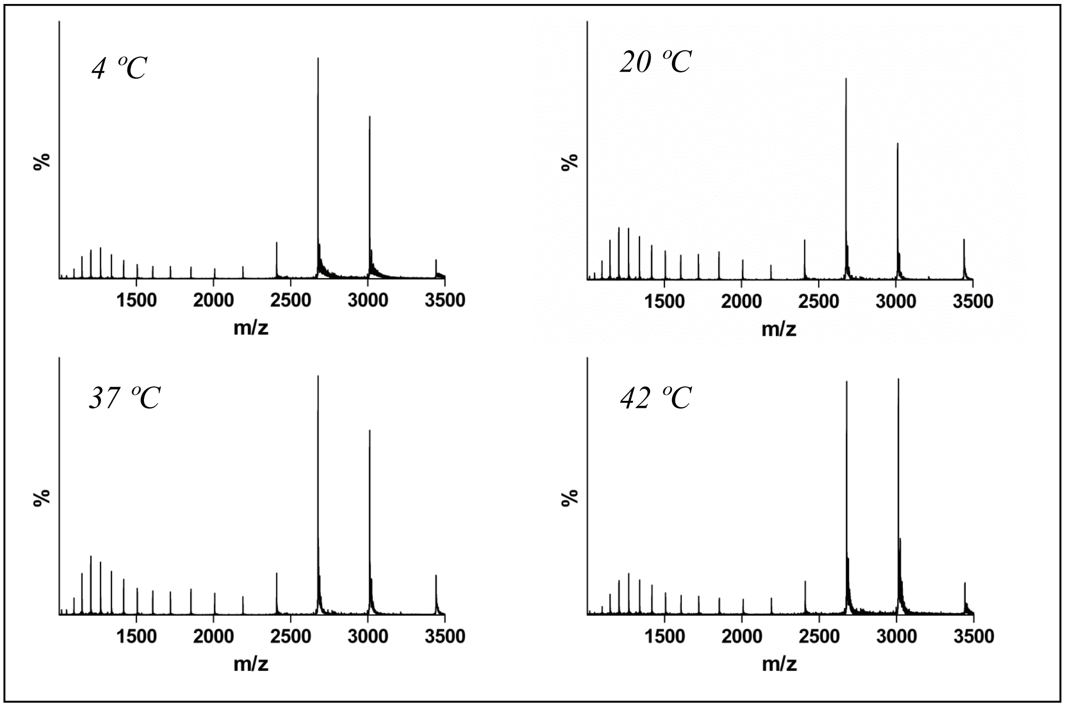

Figure 4.4 (C) Effects of changing the sample temperature on the Josephin mass spectra. Changing the sample temperature from 4 – 42 ºC does not significantly affect the proportions of the multiple charge state envelopes.

4.2.2.2 Denaturing Conditions Shift the Charge State Envelope

The mass spectrum of Josephin under ‘denaturing’ conditions (50 % (v/v) acetonitrile, 1 % (v/v) TFA, pH 2.0) showed a single charge state envelope from n = +22 to +8, which was centered around n = +18 (Fig 4.5A). This is similar to the partially unfolded conformation seen under native conditions which centers on n = +18. The overlap suggests that either the partially unfolded conformation is similar in conformation to the denatured state, or it has partially unfolded in such a way that a similar amount of charge is able to bind during the ionization process.

The far-UV CD spectrum of Josephin has previously been well characterized (206,208). Far-UV CD was used to confirm that the conformations seen in the mass spectra were not due to effects of the atypical buffers affecting Josephin structure (Fig 4.5B). The volatile ammonium acetate/ammonium bicarbonate pH 7.4 buffer used for native conditions, and the low pH acetonitrile buffer are quite different to the strong tris or phosphate buffered salines typically used to buffer Josephin. However, in all of these conditions, the secondary structure of Josephin is clearly unchanged. Spectral analysis using CONTIN indicated that Josephin has approximately 39 % α-helix, 26 % random coil and 34 % β-sheet and turn structure which is identical to that previously reported. Although widely used to measure protein structure in solution, CD is a measure of the average structure of a protein, and thus does not detect multiple conformations which co-exist in solution.

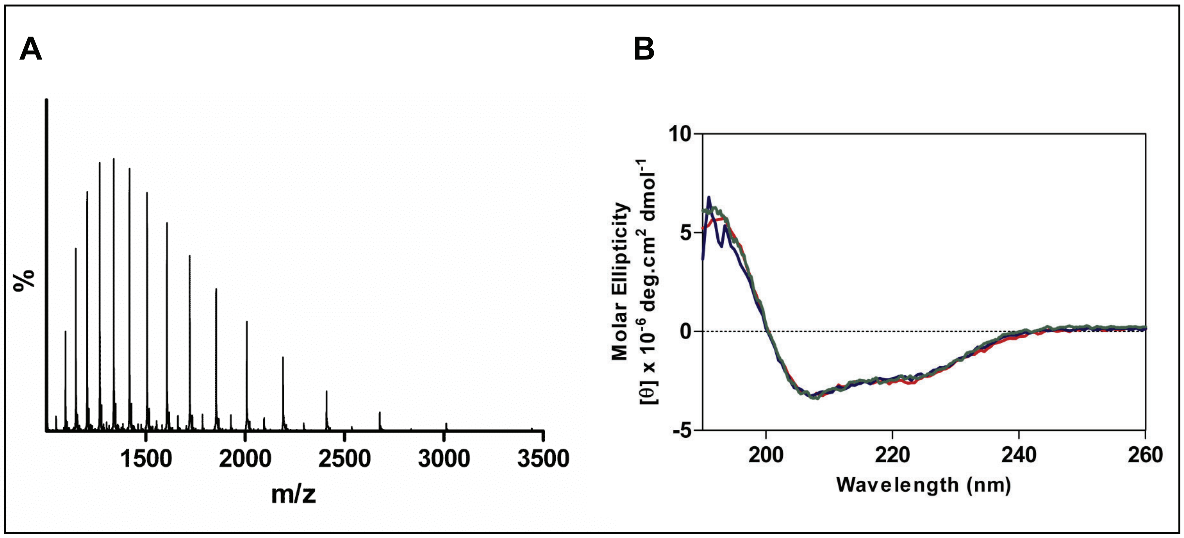

Figure 4.5 Josephin displays one conformation under denaturing conditions. (A) The ESI-MS of Josephin in 50 % (v/v) acetonitrile, 1 % (v/v) TFA, pH 2.0 shows a single charge state envelope centered on n = +18. (B) Far-UV CD spectra of Josephin in 50 % (v/v) acetonitrile, 1 % TFA (v/v), pH 2.0 (red), 100 mM Tris, 80 mM NaCl, 10 % (v/v) Glycerol, pH 7.4 (blue) and 50 mM ammonium acetate, 50 mM ammonium bicarbonate, pH 7.4 (green). The spectra were obtained at 20 ºC at a protein concentration of 30 µM.

4.2.2.3 The Partially Unfolded Conformations are Not Linked to Aggregation

The intrinsic ability of Josephin to aggregate (233,234) led to the question: are the partially unfolded conformations linked to the aggregation pathway? In order to investigate this, two mutants of Josephin which have altered thermodynamic stability and aggregation kinetics were used. Josephin L169H and Josephin R103G S81A respectively have midpoints of aggregation of 19 fold faster and 2.5 fold slower than Josephin (Ch 3). Analysis of the peak area in each charge state envelope show similar proportions of the folded and unfolded conformations for both the mutants and wildtype Josephin (Fig 4.6), and thus the partially unfolded conformations cannot be directly linked to the aggregation pathway.

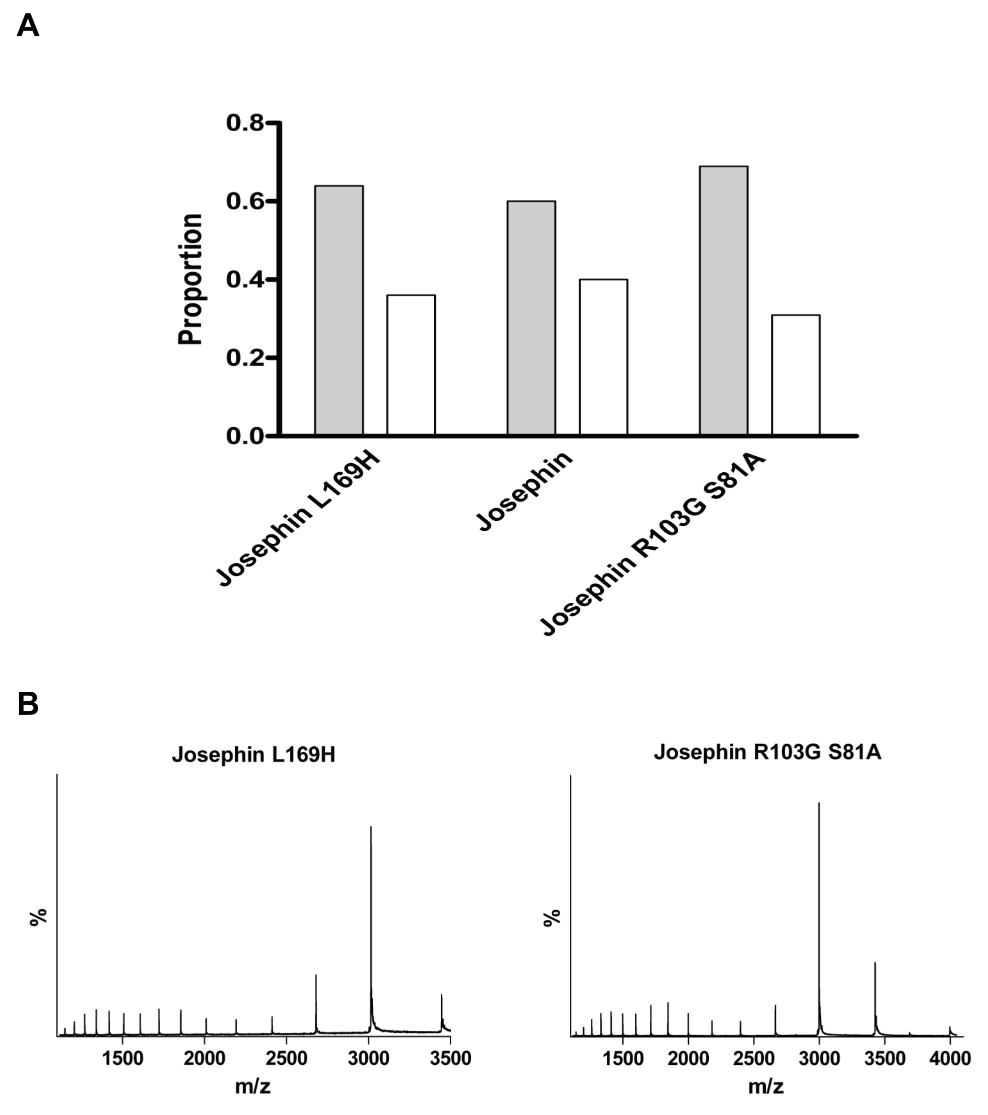

Fig 4.6 The multiple conformations are unaffected by amyloidogenic mutation or Josephin binding partners. (A) The proportion of the folded conformation (grey bar) to the partially unfolded conformations (white bar) was calculated from the area under each charge state envelope from Josephin, the stabilizing mutant Josephin R103G S81A and the destabilizing mutant Josephin L169H. (B) The mass spectra of Josephin L169H and Josephin R103G S81A under native conditions obtained using nanoESI-MS show multiple charge state envelopes similar to wildtype Josephin.

The effect of known protein interactors of Josephin on the proportions of the conformations were also investigated. Josephin was incubated with HHR23A, HHR23B and α-B-crystallin, which all impact the aggregation of Josephin *in vitro* (Ellisdon &

Bottomley, personal communication)(App 1) and in each case the proportions of the charge state envelopes in the Josephin mass spectra were unchanged (data not shown).

Ubiquitin was incubated with Josephin at a ratio of 2:1 Ubiquitin:Josephin, as it has been demonstrated previously that Ubiquitin binds Josephin in this ratio (169). Although the ubiquitin signal is significantly stronger than that of Josephin due to its higher concentration, multiple charge state envelopes are still observed from Josephin, suggesting that the binding of Ubiquitin does not change the presence of the partially unfolded forms (PUF) (Fig 4.7).

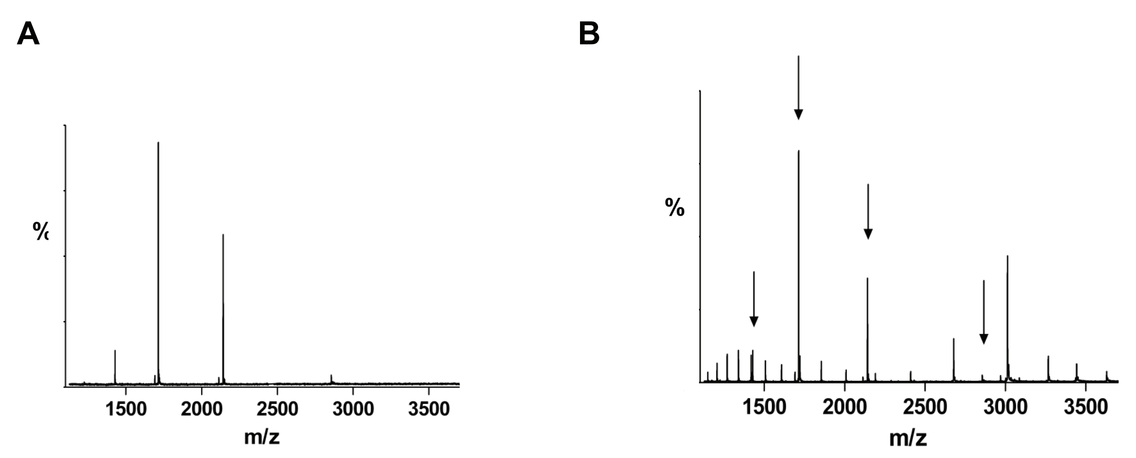

Figure 4.7 Ubiquitin does not change the Josephin spectra. (A) The mass spectra of ubiquitin alone. (B) The mass spectra of Josephin with 2:1 Ubiquitin:Josephin. The peaks corresponding to ubiquitin are indicated using arrows.

4.2.3 Josephin HX MS

4.2.3.1 Deuteration of Josephin

Josephin has a molecular mass of 24,093 Da, and has 366 exchangeable protons which thus gives a theoretical deuterated mass of 24,459 Da (Table 4.2). For some proteins, such as lysozyme, there is a protected region within the protein which does not undergo deuteration (75). Therefore we initially investigated whether Josephin reaches the theoretical deuterated mass under experimental exchange conditions.

H→D exchange was initially completed using an enclosed electrospray source to eliminate back exchange from the atmosphere, and showed that Josephin has little protection from exchange. 325 protons were exchanged within the first time point of 2 min and the theoretical end point mass of 24,444 Da in a 96 % deuterated solvent was reached after 3.25 hr (Fig 4.8).

Table 4.2 Calculation of Theoretical Deuterated Mass of Josephin

Amino Acid	Number of Amino Acids	Increase in Mass	Deuterated Mass
Ala	10	1	720.80
Arg	8	4	1281.52
Asn	10	3	1170.90
Asp	9	2	1053.81
Cys	4	2	420.56
Gln	15	3	1966.95
Glu	18	2	2359.98
Gly	13	1	754.65
His	10	2	1391.40
Ile	12	1	1369.92
Leu	26	1	2968.16
Lys	8	3	1049.36
Met	6	1	793.20
Phe	13	1	1926.34
Pro	6	-	582.72
Ser	16	2	1425.28
Thr	6	2	618.60
Trp	3	2	564.63
Tyr	8	2	1321.36
Val	7	1	700.91
Plus N-H_2 & -OH on ends			20
Theoretical Deuterated Mass:			**24461.05**

Although hydrogen exchange can be analyzed using ESI-MS, the lower signal due to the electrospray source in addition to the decrease in signal which occurs due to deuteration resulted in only the folded charge state envelope being observed (Fig 4.8). Therefore to try to improve the quality of the spectra, we investigated whether the nanoESI source could be used to follow Josephin HX. As the nanoESI source is open to the atmosphere, analyzing D→H exchange is preferable in order to eliminate the effects of back exchange during ionization.

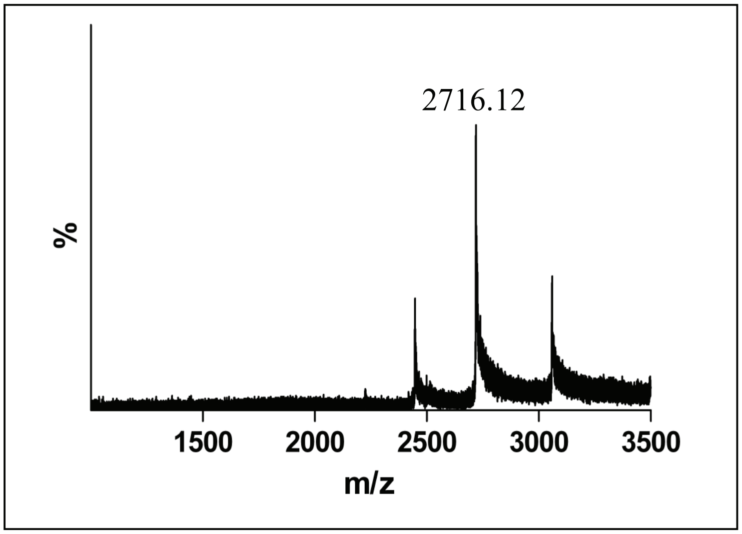

Figure 4.8 Complete deuteration of Josephin. Josephin is fully deuterated after 3.25hr at 37 °C with a +9 charge state of 2716.12. Using an electrospray source, the partially unfolded forms were not observed after deuteration.

4.2.3.2 D→H Exchange

To complete D→H exchange, the protein must be fully deuterated prior to initiating exchange. A number of techniques were used to buffer exchange Josephin into a deuterated buffer due to problems with Josephin aggregating during either the deuteration process or soon after the initiation of exchange. Buffer exchange was attempted using a number of chromatography columns (Superdex75, NAP5 and Desalting HiTrap), dilution using a centrifugal concentrator and dialysis (Fig 4.9). Except for dialysis, which was incubated at 37 ºC during exchange, Josephin was then incubated at 37 ºC for 3.5 hrs to allow full deuteration to occur.

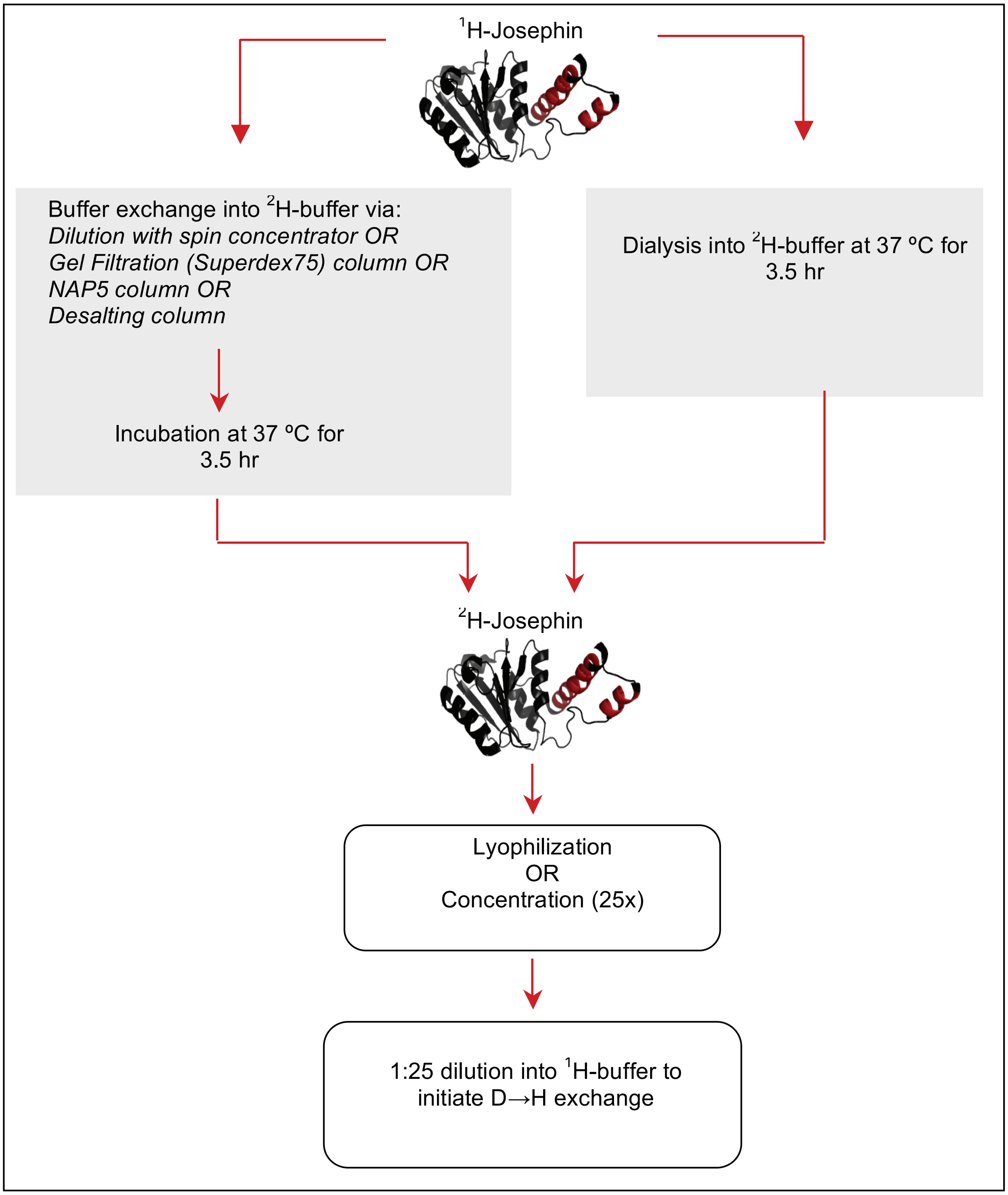

^{1}H-Josephin
Buffer exchange into ^{2}H-buffer via:
Dilution with spin concentrator OR
Gel Filtration (Superdex75) column OR
NAP5 column OR
Desalting column
Incubation at 37 ºC for 3.5 hr
Dialysis into ^{2}H-buffer at 37 ºC for 3.5 hr
^{2}H-Josephin
Lyophilization OR Concentration (25x)
1:25 dilution into ^{1}H-buffer to initiate D→H exchange

Figure 4.9 Techniques used to achieve deuteration of Josephin for D→H exchange.

Josephin was incubated at a dilute concentration in order to prevent aggregation. Following incubation, the deuterated Josephin then needed to be concentrated as the HX reaction is initiated via a 1:20 dilution into protonated buffer. Concentration was completed using either lyophilization or a centrifugal concentrator. Regardless of which technique was used to deuterate and concentrate Josephin, aggregation occurred within 1 hr of initiation of HX, resulting in no signal on the MS (data not shown).

4.2.3.3 H→D Exchange Using NanoESI-MS Demonstrates the Multiple Conformations of Josephin Exist in Equilibrium

Initially, there was a concern that nanoESI-MS could not be used for H→D exchange, due to the back exchange which occurs during the ionization process with an open air source. However using β_2-microglobulin, a protein for which the HX rate has been previously established (250), it has been determined that although back exchange prevents the theoretical end mass being reached, the kinetics of exchange are unchanged (Hodkinson & Radford, personal communication). Therefore in order to firstly eliminate the extra deuteration step needed for D→H exchange and to secondly observe the exchange rates of the partially unfolded conformations, H→D exchange of Josephin was followed using a nanoESI source.

Josephin HX was initiated by diluting Josephin 25 fold into deuterated buffer, pH 7.4 (corrected) and analyzing time points using nanoESI-MS. HX is dependent on temperature, and as at 37 ºC Josephin was fully deuterated in 3.25 hr, 20 ºC was used for kinetic analysis as it resulted in slower and thus more reproducible kinetics.

Therefore following H→D exchange using nanoESI-MS under native conditions at 20 ºC, there is a gradual shift in the n = +8 charge state to a higher m/z over time (Fig 4.10A). This is indicative of an EX2 mechanism of exchange which is characterized by small rapid fluctuations in the protein that gradually allow the incorporation of deuterons (240). The smaller peak in Figure 4.10A is due to Cu^{2+} adducts.

The incorporation of deuterium was plotted as a change in mass over time for all three conformations (Fig 4.10B), and the observed rate of exchange (k_{obs}) of 0.028 ± 0.01 min^{-1} was the same for all three conformations. This confirms that the conformations are present in an equilibrium, and must be rapidly interconverting at a rate faster than that of exchange, as has been seen previously in apomyoglobin (251).

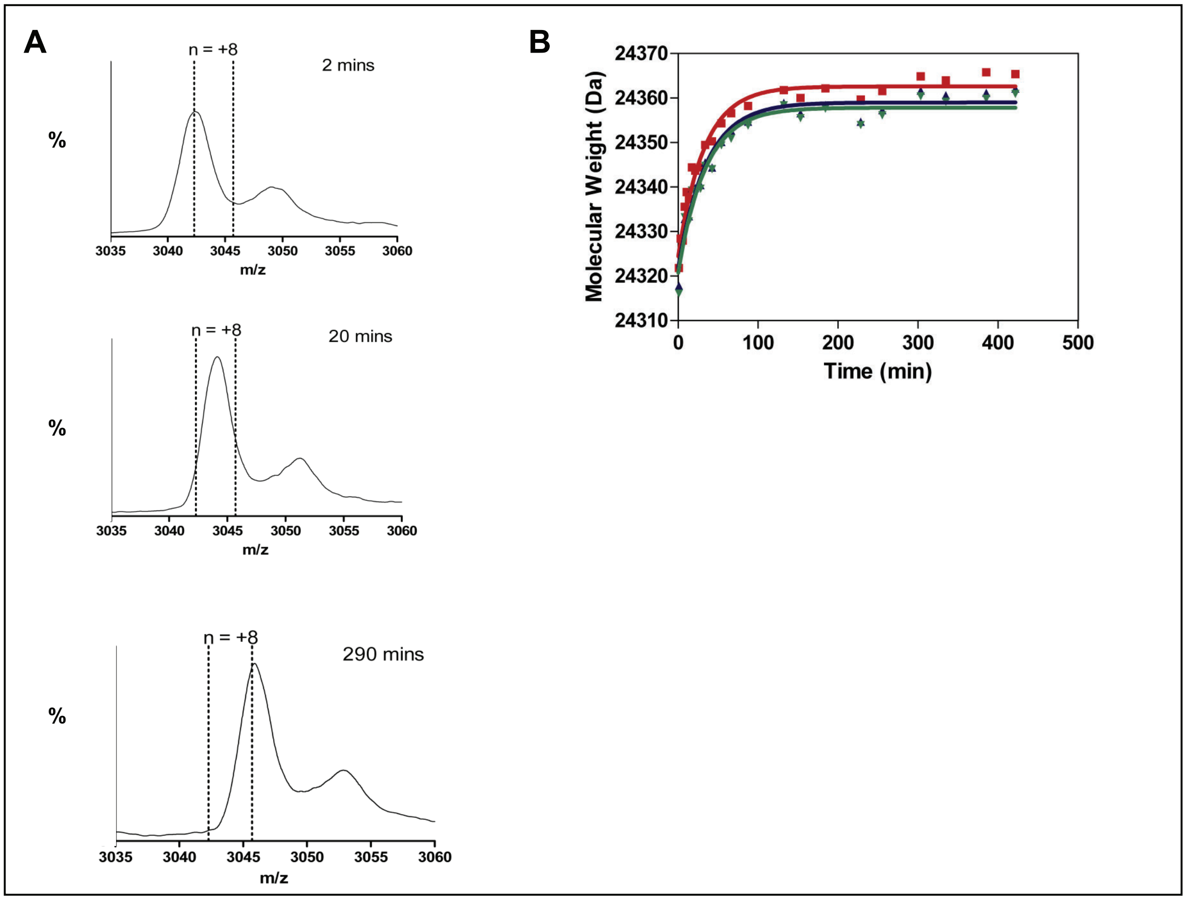

Figure 4.10 Josephin HX confirms multiple conformations are in equilibrium. (A) H→D HX of the Josephin domain at 20 ºC, pH 7.4 monitored using nanoESI-MS. The increase in the n = +8 charge state is shown at 2 min, 20 mins and 290 mins. (B) The increase in molecular weight over time was plotted for each charge state envelope: the folded conformation centered around n = +8 (—■—), the first PUF centered around n = +13 (—▲—) and the second PUF centered around n = +18 (—▼—). The data were fit to a single exponential function.

4.2.3.4 Analysis of Josephin HX Kinetics

The contribution of structure to the HX rate of a particular sequence can be considered by comparing it to the intrinsic exchange rate of the sequence if it were in a random coil structure (244,252). Using model peptides, Bai *et al.* have investigated the contribution of sequence to the intrinsic exchange rate of unprotected amino acids to determine the overall exchange rate for each amino acid in an unfolded sequence (244).

Using these data to determine the rate of exchange of Josephin if it were in a random coil structure under the conditions used in this study, the intrinsic rate of exchange or k_{int} is 3700 events min^{-1}. The difference between these two rates thus fits with the high level of structure known to be present in Josephin. Based on these rates of exchange occurring under an EX2 mechanism, the apparent free energy of hydrogen exchange (ΔG_{ex}^{app}) for Josephin was calculated to be 0.69 ± 0.06 kcal mol^{-1}.

For comparison, the equilibrium unfolding curve for Josephin under the conditions used for hydrogen exchange was determined using the denaturant GdnHCl and following the change in secondary structure at 222 nm using far-UV CD (Fig 4.11). The data were fit to a two-state unfolding mechanism, and the midpoint of the transition occured at 2.47 M GdnHCl. Similar to results previously published for Josephin (234), this suggests that the volatile buffer does not significantly impact upon the thermodynamic stability of the protein. From the equilibrium unfolding data, the free energy of unfolding (ΔG) was calculated to be 1.7 ± 0.3 kcal mol^{-1}.

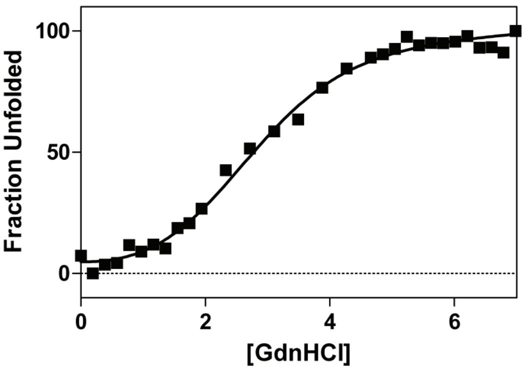

Figure 4.11 Josephin equilibrium unfolding is unaffected by a volatile buffer. Equilibrium unfolding curve for Josephin performed in the conditions used for HX (50 mM ammonium acetate, 50 mM ammonium bicarbonate, pH 7.4 at 20 ºC), using the denaturant GdnHCl. The data were fit to a two-state unfolding curve.

The analysis of the HX data relies upon the assumption that the protein remains monomeric throughout the timescale of the experiment. As Josephin is prone to aggregation, we used size exclusion chromatography (SEC) and thioflavin T (thioT) fluorescence to confirm that the protein remained monomeric during the experiments (Fig 4.12). Josephin was incubated under the same conditions used for hydrogen exchange, and at specific time points aliquots were removed and analyzed using SEC and thioT. Both thioT and SEC showed no change over time, thus suggesting that there are no multimeric species present and Josephin has remained monomeric throughout the timescale of the HX experiments.

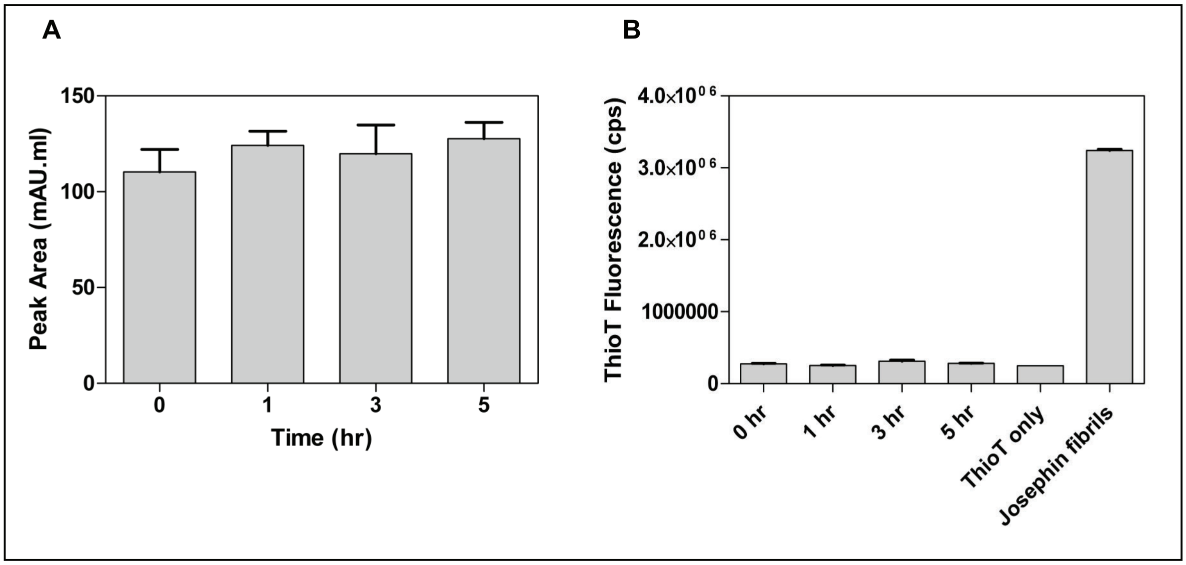

Figure 4.12 Josephin remains monomeric throughout the timescale of HX. (A) Size exclusion chromatography of Josephin incubated in the conditions used for HX. The area under the monomer peak at 19 mL was calculated and is shown at timepoints across the length of the HX experiment. No loss of monomer occurred during this timescale. (B) ThioT fluorescence also demonstrates there is no formation of fibrillar species over 5 hrs at 20 ºC, as there is no increase in thioT fluorescence in comparison to the thioT only negative control. A positive control using Josephin endpoint fibrils is also shown.

4.3 DISCUSSION

4.3.1 Implications of the Conformational Heterogeneity of Josephin

The ESI-MS data provides new insight into the conformational heterogeneity of the Josephin domain. Techniques such as CD, NMR and intrinsic fluorescence have previously suggested that Josephin is in a stable, highly structured conformation (166,233,234). The mass spectra under native conditions instead shows that Josephin co-populates a number of conformations in solution (Fig 4.3). Although the spectra of most proteins show a single charge state envelope, there have been a number of proteins reported which also co-populate several conformations under native conditions and correspondingly have multiple charge state envelopes (248,251,253). More commonly, multiple conformations can be induced using denaturing conditions and used to identify partially unfolded intermediates which may exist either on or off the folding pathway (254).

The multiple charge state envelopes were however present under native conditions for Josephin. The HX data (Fig 4.10) suggest that the multiple conformations are rapidly interconverting in equilibrium, as if a fixed population in an unfolded conformation existed then different rates of HX within each charge state envelope would be obtained. The most folded population binds the least number of charges (245), and thus in the Josephin mass spectra the folded conformation is represented by the charge state envelope centred around n = +8 (Fig 4.3A). In addition to this, there were two charge state envelopes with lower m/z ratios which thus corresponded to PUF (255). Based on the peak area under each charge state envelope, 40% of the population was calculated to be unfolded. However previous studies show that non-native polypeptides have a higher signal relative to native, with up to two fold difference between the ion distribution and the distribution actually in solution (256). Thus based on ESI-MS alone, we cannot definitively estimate the proportion of partially unfolded Josephin molecules in solution, and a complementary technique such as single molecule fluorescence is needed to determine this.

The increase in charge which binds to unfolded proteins during positive ESI-MS is generally attributed to an increase in surface area and thus an increased steric accessibility of possible protonation sites (257,258). The extent of unfolding in the PUF of Josephin is not clear. A clue to this is provided by the mass spectra of Josephin in acetonitrile, whereby only the most unfolded charge state envelope remains (Fig 4.5 A). Although there is a significant difference in the mass spectra between acetonitrile and native conditions, the CD spectra under both conditions are identical (Fig 4.5 B), therefore suggesting that the secondary structure is unchanged and thus the PUF are not significantly unfolded. NMR dynamics studies of Josephin have shown that the helical hairpin, which contains the α_2 and α_3 helices (Fig 4.2), is significantly more dynamic than the rest of the protein (166). Therefore one possibility is that the flexibility of the helical hairpin region allows for the binding of additional charge in some conformations and thus the multiple charge state envelopes seen in the mass spectra. Alternatively, the conformations could be due to the unfolding of another region that has not been identified as dynamic in the NMR spectra due to the timescale of exchange.

The intrinsic aggregation propensity of Josephin means these PUF are of particular interest, however the proportion of each conformation was unchanged in several mutants with differing amyloidogenicity (Fig 4.6). This suggests that the partially unfolded conformations are not linked to the aggregation pathway. For some proteins which populate multiple conformations in solution, one conformation can be stabilized via the interactions of a binding partner (248,259-261). This was not however the case for Josephin as known protein interactors ubiquitin, HHR23A or B, and α-Bcrystallin all did not affect the proportions of the conformations. Although the role of the PUF could not be identified within this study, the conformational heterogeneity could be linked to the unusual DUB activity displayed by Josephin (168).

The folding pathway of Josephin has been previously characterized (233,234), and it is important to consider how the PUF may fit into this pathway. A scheme is proposed in Fig. 4.13 whereby the partially unfolded conformations are in equilibrium with the native state. Evidence for this comes from the Josephin stability mutants (Fig 4.6) which have thermodynamic stabilities that are either increased (Josephin R103G S81A) or decreased (Josephin L169H) from wild type. Although the changed stability of these mutants affect the N↔I equilibrium, they do not change the relative proportions of N and the PUF, and this suggests that the PUF are not directly linked to the intermediate states on the folding pathway.

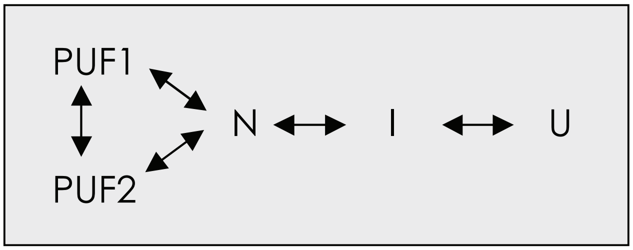

Figure 4.13 Proposed model of the Josephin folding pathway. A proposed scheme suggests that both of the PUF exist in equilibrium with the native state in the folding pathway of Josephin.

4.3.2 The Dynamic Nature of the Josephin Domain

This study found that Josephin exists in an equilibrium between multiple conformations, however although ESI-MS of Josephin has also been completed by another group, the multiple conformations were not previously observed (234). This may be attributed to nanoESI-MS being used in this study, as it results in cleaner signals and thus allows the characterization of the less populated PUF during HX. The HX rate could not be compared with the previous study as key information such as the temperature used for exchange was not disclosed.

The HX kinetics of Josephin demonstrates that it is a highly dynamic protein in comparison to other amyloidogenic proteins, which may explain its high propensity to form fibrils *in vitro* under native conditions. For example β_2-microglobulin, a protein which readily forms fibrils under low pH conditions, has a similar HX rate reported to Josephin, however the experiments were completed at 37 ºC which is 17 ºC higher than the temperature Josephin HX was completed under. Given the temperature dependence of HX (262), this suggests that Josephin is significantly more dynamic. This dynamic nature potentially links to the unique ability of Josephin to cleave multi-linked ubiquitin chains (168).

In this study a system was set up to determine the conformational dynamics of the Josephin domain in order to provide insights into the normal function and early misfolding events of ataxin-3. Future experiments to determine the impact of full length ataxin-3 both with and without an expanded polyQ tract upon the dynamics of this domain may provide insight into the increased aggregation kinetics observed with increased polyQ tract length (191).

CHAPTER 5

AGGREGATION OF ATAXIN-3 IN SDS: EVIDENCE FOR ALTERNATIVE AGGREGATION PATHWAYS

PREFACE

The focus on characterizing aggregation *in vitro* in this thesis allows the conformational changes of ataxin-3 which occur during aggregation to be determined. The limitation of this approach is that ataxin-3 containing any length polyQ tract has been demonstrated to aggregate *in vitro*, which does not mirror disease. This therefore implicates the role of other cellular components in ataxin-3 pathogenesis. Cellular membranes are one such factor which have been demonstrated to affect the aggregation of a number of amyloid proteins (263-266). Within the polyQ proteins, Kegel and colleagues have completed several studies that demonstrate that huntingtin interacts with phospholipids at the plasma membrane within the cell, and an expanded polyQ tract increases this interaction (116-118). The question remains as to whether the interactions observed between huntingtin and phospholipids are common to all polyQ proteins.

There are a number of studies that suggest ataxin-3 may be involved with lipids as part of its normal cellular function. Firstly, ataxin-3 has been demonstrated to transiently associate with the ER membrane through its interaction with binding partner VCP (267). In addition to this, monomeric ataxin-3 has been isolated from mitochondrial membranes (268). Although it has been demonstrated that ataxin-3 with an expanded polyQ tract results in disrupted electrophysiological properties in a cell model, the impact of lipids on aggregation has not been investigated for ataxin-3. Therefore the last part of this thesis investigates the effects of the membrane mimic SDS on the *in vitro* ataxin-3 aggregation pathway, in addition to determining the ability of ataxin-3 to bind to various phospholipids.

Conformational Behavior and Aggregation of Ataxin-3 in SDS

Helen Saunders*, Andrew M. Ellisdon*, Roberto Cappai‡ and Stephen P. Bottomley*

*Department of Biochemistry and Molecular Biology, Monash University, Clayton, Victoria 3800, Australia.

‡ Department of Pathology and Bio21 Molecular Science & Biotechnology Institute, The University of Melbourne, Parkville, Victoria 3010, Australia.

Correspondence should be addressed to: Stephen P. Bottomley, Department of Biochemistry and Molecular Biology, Monash University, Clayton, VIC 3800, Australia. Tel: 61-3-99029362; Fax. 61-3-99029500; Email: steve.bottomley@monash.edu

Running title: Aggregation and conformation of ataxin-3 in SDS

Abstract

Spinocerebellar ataxia type 3 (SCA3) is one of nine polyglutamine (polyQ) diseases all characterized by the presence of intraneuronal inclusions which contain aggregated protein. Aggregation of ataxin-3, the causative protein of SCA3, has been well characterized *in vitro*, with both pathogenic and non-pathogenic length ataxin-3 undergoing fibrillogenesis. However, only ataxin-3 containing an expanded polyQ tract leads to SCA3. Therefore other cellular factors, not present in previous *in vitro* studies, may modulate aggregation during disease. The interactions between fibrillar species and cell membranes have been characterized in a number of amyloid diseases, including the polyQ disease Huntington Disease, and these interactions affect aggregation and toxicity. We have characterized the effects of the membrane mimetic sodium dodecyl sulfate (SDS) on ataxin-3 structure and aggregation, to show that both micellar and non-micellar SDS have differing effects on the two stages of ataxin-3 aggregation. We also demonstrate that fibrillar ataxin-3 binds phospholipids, in particular phosphorylated phosphotidylinositols. These results highlight the mitigating effect of intracellular factors on the ataxin-3 misfolding landscape and implications of these data in SCA3 and polyQ diseases in general are discussed.

Introduction

Ataxin-3 misfolding and its subsequent aggregation underlies the autosomal dominant neurodegenerative disease Spinocerebellar ataxia type 3 (SCA3). This disease is characterized by progressive neuronal dysfunction and the presence of neuronal nuclear inclusions which contain aggregated ataxin-3. The polyglutamine (polyQ) protein ataxin-3 functions as a de-ubiquitinating enzyme, and consists of an N-terminal catalytic Josephin domain which has structural homology to papain-like cysteine proteases, and a comparatively unordered C-terminal region containing two ubiquitin interaction motifs and the polyQ tract[1; 2; 3; 4]. Expansion of this polyQ tract to greater than 45 residues results in protein aggregation and disease, with the age of onset inversely correlated with repeat length[5; 6].

Knowledge of the kinetic and structural changes involved in ataxin-3 misfolding and aggregation will help us to understand the molecular events and disease progression involved in SCA3. The structural changes and kinetics involved with the *in vitro* aggregation mechanism of ataxin-3 has been characterized. These data indicate that ataxin-3 aggregation involves a two-stage aggregation pathway with interactions facilitated initially by the Josephin domain and subsequently by the polyQ tract[7; 8; 9]. Despite both the Josephin domain as well as the non-pathogenic length ataxin-3 forming the first stage fibrils *in vitro*[9; 10; 11; 12], contradicting data exists regarding the presence of non-pathogenic length ataxin-3 aggregates in cells[13; 14; 15]. However, evidence from various polyQ proteins[16; 17] and model systems[18] increasingly suggests that this multi-stage mechanism is not unique to ataxin-3, and that the flanking regions of the polyQ tract impact upon polyQ aggregation (see review[7]).

The intrinsic fibrillogenic nature of both pathogenic and non-pathogenic length ataxin-3 implicates other cellular factors in disease pathogenesis. As a significant proportion of the cellular environment, membranes of varying compositions influence the aggregation of amyloid proteins such as amyloid β-peptide, α-synuclein and prion protein[19; 20; 21]. Of the polyQ proteins, huntingtin binds various cellular membranes with some evidence that it forms ion channels within bilayer membranes[22; 23; 24]. Aggregates formed from polyQ peptides are internalized by mammalian cells and cross the cell membrane to gain access to the cytoplasmic compartment[25]. Ataxin-3 has been proposed to associate with cellular membranes in several ways. Within the cell ataxin-3 transiently associates with membranes via its binding partner VCP[26], in addition to directly binding mitochondrial membranes[27]. Interestingly, both huntingtin and ataxin-3 perturb the structure of synthetic lipid bilayers when oligomeric in structure[28; 29], however the impact of membranes and specific lipids on ataxin-3 structure and aggregation is unknown.

Acidic phospholipids, which are present in a number of intracellular membranes, accelerate the aggregation of numerous fibrillogenic proteins including huntingtin[30; 31; 32]. The concentration of positively charged phospholipids within the membrane creates a local environment with an acidic pH, which in turn accelerates aggregation[33]. The detergent Sodium Dodecyl Sulfate (SDS) is a membrane mimetic at micellar concentrations and at low non-micellar concentrations mimics anionic phospholipids due to its positively charged head group and long tail. SDS has the ability to induce changes in secondary structure and it can be used to probe the conformational change events occurring during aggregation[34; 35]. The impact of SDS on the aggregation kinetics of amyloidogenic proteins such as β_2-

microglobulin, amyloid-β and α-synuclein has been determined[35; 36; 37]; however the effects of SDS on polyQ proteins have not been investigated to date.

Using biophysical techniques, we demonstrate that in the presence of SDS, ataxin-3 is able to form aggregates via a number of alternate pathways. We investigate the effects of both micellar and sub-micellar concentrations of SDS on ataxin-3 and show that there are differential effects of SDS at different points of the multi-stage ataxin-3 aggregation pathway. Finally, we show that oligomeric and fibrillar ataxin-3 binds acidic phospholipids, in particular phosphotidylinositols, with different specificities.

Results

SDS induces an α-helical conformation in ataxin-3

SDS forms micelles at concentrations above the critical micelle concentration (CMC) and in the buffer conditions used within this study the CMC of SDS was determined to be 1.2 mM (data not shown)[35; 38]. SDS has previously been demonstrated to induce helical secondary structure in a range of proteins at concentrations above the CMC[34; 35; 36]. In this study, the effects of SDS on pathogenic length ataxin-3(Q64), non-pathogenic length ataxin-3(Q15) and the Josephin domain were investigated. Changes in the secondary structure of the ataxin-3 variants with the addition of up to 10 mM SDS were analyzed using far-UV CD spectroscopy (Fig. 1). Consistent with previous reports, all ataxin-3 variants in the absence of SDS displayed spectra with minima at 208 nm and 222 nm, indicative of predominantly α-helical secondary structure[12; 39]. Only minor changes in secondary structure were observed when SDS was added. In the presence of 1 mM SDS, no significant change in structure occurred for any of the proteins, whereas above 5 mM SDS there was an average increase in α-helical structure of 5 % for all proteins (Table 1). The magnitude of the structural changes induced by SDS in ataxin-3(Q64) (Fig. 1A), ataxin-3(Q15) (Fig. 1B) and the isolated Josephin domain (Fig. 1C) were similar, thus suggesting that the changes in secondary structure occur predominantly within the Josephin domain.

SDS modulates SDS-soluble aggregation of ataxin-3

Ataxin-3 aggregation occurs via a two-stage mechanism. The first stage involves the formation of SDS-soluble curvilinear protofibrils and is common to all ataxin-3 variants. In the second stage of aggregation, only pathogenic length ataxin-3 forms SDS-insoluble fibrils which have a straighter morphology[9]. Formation of the first stage SDS-soluble fibrils was monitored by following changes in thioflavin T (thioT) fluorescence as previously described[9]. Without SDS, all ataxin-3 variants show a sigmoidal aggregation curve indicative of a nucleation-dependent process, with a lag phase followed by exponential growth which then plateaus. The overall aggregation kinetics vary such that the isolated Josephin domain has the slowest aggregation rate and ataxin-3(Q64) the fastest (Fig. 2). The presence of 1 mM SDS eliminated the lag phase of all the ataxin-3 variants, resulting in an immediate exponential growth phase with a rate independent of polyQ length.

The midpoint of aggregation decreased to two hours for all proteins with 1 mM SDS present, suggesting that the small conformational change induced by SDS is similar for all proteins and results in a highly amyloidogenic species. In addition, 1 mM SDS also resulted in hyperfluorescence of thioT (Fig. 2) which may be related to the greater number of short fibrils being formed, as visualized using transmission electron microscopy (TEM) (Fig. 5), thereby creating more binding sites. In contrast, at both 5 mM and 10 mM SDS, there is no increase in thioT fluorescence for any of the ataxin-3 variants, thus suggesting that fibril formation is suppressed at these micellar SDS concentrations. These results, in which a specific range of SDS concentrations around the CMC modulate thioT detected fibrillogenesis, are consistent with those previously reported for a range of other non-polyQ amyloid proteins [34; 35; 36].

SDS-insoluble aggregation of pathogenic length ataxin-3 is affected by SDS

Having demonstrated that the effects of SDS on the formation of SDS-soluble stage 1 fibrils are similar to those previously reported for other amyloid proteins, we then investigated the effects of SDS on the second stage of the multi-stage ataxin-3 aggregation pathway. The formation of stage 2 aggregates can be monitored using a membrane filter trap assay in which after boiling in 2 % (w/v) SDS, only SDS-insoluble fibrils are retained upon the filter. It should be noted that the concentration of SDS used to solubilize the fibrils (2 % (w/v) SDS) is six times greater than the concentrations around the CMC which impact upon fibrillogenesis (0.03 % - 0.29 %). It can clearly be seen that in the absence of SDS ataxin-3(Q64) forms SDS-insoluble aggregates following 51 hrs of incubation (Fig. 3A). With 0–10 mM SDS, both non-pathogenic length ataxin-3(Q15) and the Josephin domain did not form SDS-insoluble aggregates when incubated up to 200 hours (data not shown).

Although it was anticipated that due to the sequential nature of the aggregation pathway modulation of stage 1 aggregation would mediate similar kinetic effects on stage 2 aggregation, quite different results were obtained. Despite 1 mM SDS significantly accelerating the rate of SDS-soluble fibril formation as detected by thioT fluorescence (Fig. 2A), the formation of SDS-insoluble fibrils by ataxin-3(Q64) with 1 mM SDS is slower and has a midpoint 24 hours later than in the absence of SDS (Table 2). In contrast, ataxin-3(Q64) with 5 mM SDS shows no increase in thioT fluorescence over 100 hours (Fig. 2A) yet the formation of SDS-insoluble aggregates appear in the filter trap assay from 51 hours (Fig. 3A), suggesting that the aggregates are forming on an alternative aggregation pathway. Addition of the polyQ-binding peptide QBP1 eliminated the formation of SDS-insoluble aggregates formed by ataxin-3(Q64) with 5 mM SDS.

In a strongly micellar environment (10 mM SDS), ataxin-3(Q64) does not show the formation of either SDS-soluble (Fig. 2A) or SDS-insoluble aggregates (Fig. 3). Several studies have reported distinct effects of micellar and non-micellar SDS concentrations, with micellar concentrations inhibiting aggregation, and non-micellar concentrations accelerating aggregation[34; 35; 36]. However with the complexity of the two-stage ataxin-3 aggregation mechanism, there is not such a clear distinction. Only the highly micellar 10 mM SDS inhibits both stages of the pathway, and the other SDS concentrations differentially affect the first and second stages of aggregation.

SDS modulates the change to β-sheet secondary structure typical of aggregation

With the intriguing formation of thioT unreactive fibrils by 5 mM SDS, we then went on to characterize the changes in secondary structure occurring during aggregation. SDS induces an increase in α-helical structure at concentrations above the CMC (Fig. 1), however a key event in fibrillogenesis is the gain of β-sheet structure, and hence far-UV CD was used to follow the impact of SDS upon this structural transition.

As previously reported, we observed that in the absence of SDS ataxin-3(Q64) converts to a β-sheet rich fibrillar species (Fig. 4A). The loss in signal observed over time has been previously suggested to reflect an increase in light scatter[9]. Incubation in 1 mM SDS (Fig. 4B) accelerates the kinetics of aggregation such that by four hours there has been substantial loss of helical structure and a conversion to β-sheet structure which continues over time with a loss of signal similar to that seen in the absence of SDS at 100 hours (Fig. 4A).

Incubation of ataxin-3(Q64) in both 5 mM and 10 mM SDS leads to a retention of α-helical structure over 100 hours, and for 10 mM SDS there is a small increase in the minima at 208 nm and 222 nm (Fig. 4D). This is consistent with the lack of aggregation detected with 10 mM SDS throughout this study and suggests that SDS has stabilized the α-helical structure to the extent that the conversion to β-sheet is prevented. With 5 mM SDS present, the retention of α-helical structure over time concurs with the lack of thioT fluorescence observed (Fig. 2) and thus suggests that the SDS-insoluble fibrils being formed (Fig. 3) are more similar to amorphous aggregates than the β-sheet rich amyloid-like fibrils typically formed by ataxin-3. Interestingly, these aggregates are still formed via interactions of the polyQ tract, as addition of QBP1 inhibits their formation (Fig. 3A). The same effects of SDS on the change in secondary structure over time were also observed for ataxin-3(Q15) and the Josephin domain (Fig. S1).

SDS addition results in changed morphology of fibrils

The formation of SDS insoluble fibrils which are not thioT reactive suggests that ataxin-3 is forming these fibrils via an atypical pathway. In order to investigate this further, TEM was used to visualize the morphology of the aggregates being formed with 0, 1, 5 and 10 mM SDS present (Fig. 5, Fig. S2). As expected, ataxin-3(Q64) in the presence of 10 mM SDS did not form fibrils (data not shown). In contrast, with 5 mM SDS ataxin-3(Q64) forms amorphous aggregates with a diameter of 20 – 30 nm which although SDS-insoluble, do not have a fibrillar morphology but appear clumped together to form large amorphous aggregates of up to 0.5 µm in length (Fig. 5C and F).

The fibrils formed by ataxin-3(Q64) in the presence of 1 mM SDS (Fig. 5B) had lengths of 23 - 29 nm and a diameter of 5 nm. These fibrils were initially shorter and smaller in diameter than the curvilinear fibrils formed in the absence of SDS which showed diameters of 12 - 15 nm and lengths of hundreds of nanometers (Fig. 5A) as observed previously[9]. Further incubation resulted in the formation of larger, more rigid SDS-insoluble fibrils which were 40 - 50 nm in width and up to 1 µm in length (Fig. 5D and E).

PolyQ oligomers interact with acidic phospholipids

As SDS is a mimetic of acidic phospholipids we then decided to investigate whether ataxin-3 shows a specificity of binding to acidic phospholipids. To test a variety of lipids, we incubated ataxin-3(Q64) from specific stages of the aggregation pathway in a protein-lipid overlay assay. Monomeric ataxin-3(Q64) and the Josephin domain both showed no binding to any of the lipids (data not shown). When a heterogeneous solution taken from the plateau stage of the thioT curve was incubated with the PIP strips, binding to phosphorylated phosphotidylinositols (PtdIns) was observed for both ataxin-3(Q64) and the Josephin domain. Interestingly, there tended to be an additional subset of lipids which bound to the endpoint fibrils of both the Josephin domain and ataxin-3(Q64) (Fig. 6A i - iv), with the endpoint fibrils binding to essentially the same subset of lipids. Ataxin-3(Q64) incubated with QBP1, an inhibitor of polyQ mediated aggregation, showed the same binding pattern as ataxin-3(Q64) thus suggesting that the lipids are predominantly binding to the misfolded Josephin domain (data not shown).

In order to help confirm that the polyQ tract was not involved, we used the model system Staphylococcus protein A (SpA) with an attached polyQ tract of 52 glutamines (SpA(Q52))[40]. SpA is a membrane-anchored protein and thus native SpA was used as a control. SpA and SpA(Q52) demonstrated similar binding patterns, further suggesting that the polyQ tract is not involved in lipid binding (Fig. 6 v and vi).

Discussion

Effects of SDS on ataxin-3 conformation and aggregation

SDS appears to interact in a common fashion with monomeric fibril-forming proteins, inducing α-helical structure irrespective of the protein's initial structure[34; 35; 36; 41]. It is interesting that this can lead to rapid aggregation, considering the key structural change required for aggregation is the conversion to β-sheet dominated structure. A large number of aggregating proteins, including both disease-causing proteins and the fibril-forming peptide SRC3 show this accelerated aggregation at sub-micellar SDS concentrations, and slowed or inhibited aggregation at SDS concentrations well above the CMC[34; 35; 36; 37; 42]. The inhibition of aggregation may be due to the highly α-helical structure stabilized by micellar SDS concentrations (Fig. 1) preventing the transition to β-sheet structure which occurs during aggregation. For ataxin-3 at sub-micellar concentrations, there was significant acceleration of SDS-soluble aggregation, similar to other fibrillogenic proteins, in addition to a significant increase in thioT fluorescence intensity. Pertinhez *et al.* also show that fibrils in sub-micellar concentrations are shorter than normal, perhaps providing evidence that in this early stage of aggregation SDS directs monomeric protein down similar pathways [34].

An interesting result in this study was the differing effects of SDS upon formation of SDS-insoluble ataxin-3 fibrils as opposed to the more commonly observed effects of SDS on SDS-soluble fibril formation. With 1 mM SDS, the lack of an observable lag phase suggests either the lag phase has been accelerated to the extent that it cannot be observed or that ataxin-3 is following an alternate mechanism not involving nucleated elongation. Although the subsequent formation of SDS-insoluble aggregates is slower, the morphology of the end point aggregates remains unchanged. Thus it appears that with sub-micellar SDS present, the protein is proceeding through the typical aggregation pathway, with differing rates of stage 1 and stage 2 aggregation (Fig. 7).

In contrast to 1 mM SDS, the morphology of the aggregates is not fibrillar in the presence of 5 mM SDS, thus demonstrating that ataxin-3 has the ability to undertake alternate aggregation pathways to form a range of fibril types (Fig. 7). This is supported by the lack of both thioT binding and conversion to β-sheet structure. At this micellar concentration, although there is no formation of thioT reactive SDS-soluble aggregates, SDS-insoluble aggregates are still formed. These aggregates have a substantially different morphology, appearing amorphous in structure, however they are still formed via interactions of the polyQ tract, as formation of these aggregates is inhibited QBP1 (Fig. 3A). The formation of different aggregate morphologies is not unprecedented as environmental conditions affect the type of aggregate formed by a number of proteins *in vitro*[43; 44]. Within the cell such changes in the intracellular environment could be achieved by conditions of stress such as elevated temperature or decreased pH in localized environments caused by specific lipids being clustered in membranes[31; 45].

Ataxin-3 oligomers and fibrils displayed a specificity in binding to PtdIns with varying degrees of phosphorylation. PtdIns are generally located on the cytoplasmic side of the plasma membrane and are present in specific membranes depending on phosphorylation, with a higher abundance of these lipids (10 %) in brain tissue[46]. Although monomeric huntingtin also bound similar phospholipids[30], it appears that this is not a common polyQ specific effect as only fibrillar species of ataxin-3 showed binding. Furthermore, when the polyQ-binding peptide QBP1 was added there was no change to the binding pattern which suggests that binding occurs through the Josephin domain. This is similarly seen in the SDS experiments in this study, where the effect of SDS on the Josephin domain is identical to that on ataxin-3, and unaffected by QBP1.

Phospholipids have been demonstrated to affect aggregating proteins by creating regions which have a local environment with a decreased pH, and through electrostatic interactions which can increase the local concentration of protein at the membrane and induce partial unfolding of proteins[47; 48; 49]. It is interesting that oligomers and fibrillar ataxin-3 bound to the lipid overlay with different specificities as several studies show that oligomers have a generic ability to permeabilize cell membranes by creating pores or single channels within membranes[50; 51; 52].

Overall, our findings demonstrate the sensitivity of ataxin-3 fibril formation to solution conditions and suggest a possible role for lipid molecules in the development of SCA3. The specificity of binding with only fibrillar species associating with phosphorylated phospholipids provides a link between ataxin-3 and the growing evidence that soluble oligomers disrupt membranes as part of the mechanism of toxicity within amyloidoses[41; 53; 54].

Materials and Methods

Materials - Phenylmethylsulfonyl fluoride, β-mercaptoethanol and thioT were all obtained from Sigma.

Expression and Purification of Ataxin-3 Variants - All ataxin-3 variants were expressed and purified as previously described[55], and the proteins were stored at -80 °C. Following purification the deubiquitinating activity of the proteins was measured[10] and before use all were analyzed using gel filtration to ensure that no multimeric species were present.

Circular Dichroism - Far-UV CD spectra were measured on a Jasco-810 spectropolarimeter at 37 ºC using a path length of 0.1 mm. Scans of monomeric protein in the presence of different concentrations of SDS were carried out. For time course assays, protein aliquots were diluted 1:1 with TBSG (100 mM Tris, 80 mM NaCl, 10 % (v/v) glycerol, pH 7.4), to a final concentration of 30 µM protein. In all scans, spectra were measured from 190 to 260 nm with a scanning speed of 50 nm/min. The CD spectra were analyzed by spectral deconvolution using the CONTINLL algorithm[56].

Calculation of the CMC of SDS – To calculate the CMC, the fluorescent probe ANS was used as previously described[35]. The fluorescence intensity was measured at 475 nm, with an excitation wavelength of 385 nm using a PerkinElmer Life Sciences LS50B spectrofluorometer with a thermostatted cuvette holder and a 1 cm pathlength quartz cuvette. The reaction mix contained 10 µM ANS with 0 – 10 mM SDS in TBSG, pH 7.4 at 37 ºC. Two straight lines were fit to the data points with the intersection determining the CMC.

Fibrillogenesis Time Course Assays - Ataxin-3 variants (30 µM) were incubated in TBSG containing 5 mM EDTA, 15 mM β-mercaptoethanol and 2 mM phenylmethylsulfonyl fluoride, with the addition of 0 – 10 mM SDS as required. Samples were incubated without shaking at 37 ºC in air-tight containers to prevent evaporation.

Thioflavin T Fluorescence - ThioT fluorescence measurements were recorded on a Gemini platereader, using the buffering conditions described previously with the addition of 30 μM ThT and 0 - 10 mM SDS. Excitation and emission wavelengths of 430 nm and 480 nm with a cut off filter of 455 nm were used, and both excitation and emission were read from the underneath of a black clear bottom plate. All reactions were completed at 37 ºC with no shaking.

Membrane Filter Trap Assay - Aliquots containing 7.4 μg of protein were taken from the fibrillogenesis reaction, diluted 1:1 with a 4 % (w/v) SDS / 100 mM DTT solution and then boiled for 5 min at 100 ºC. 200 μL of 2 % (w/v) SDS was then added to each of the samples, and 5 μg of protein were filtered through a 0.2 μm cellulose acetate membrane (Schleicher and Schuell) using a Bio-Rad Bio-Dot SF microfiltration unit. The membrane was then washed twice by filtering 200 μL of 0.1 % (w/v) SDS, and blotted with a hexahistidine (His6) antibody (Serotec). Densitometry was completed using the program Phoretix 1D Quantifier.

Transmission Electron Microscopy - TEM images were obtained using a Hitatchi H7500 transmission electron microscope with an accelerating voltage of 80 kV. The samples were adsorbed onto a carbon-coated grid and stained with 1 % (w/v) uranyl acetate.

Protein-Lipid Overlay – The protein-lipid overlay assay was performed using fibrillar protein stopped at various timepoints. The protein was incubated with the phospholipids (PIP Strips, Molecular Probes) overnight at 4 ºC. Each lipid dot contained 100 pmol of phospholipids. The membrane was then blotted using His6 primary antibody (Serotec) and peroxidase-conjugated secondary antibody as described[57].

Acknowledgements

SPB and RC are Senior Research Fellows of the NHMRC and the work was supported by both the ARC and NHMRC of Australia.

References

1. Burnett, B., Li, F. & Pittman, R. N. (2003). The polyglutamine neurodegenerative protein ataxin-3 binds polyubiquitylated proteins and has ubiquitin protease activity. *Hum Mol Genet* **12**, 3195-205.
2. Nicastro, G., Menon, R. P., Masino, L., Knowles, P. P., McDonald, N. Q. & Pastore, A. (2005). The solution structure of the Josephin domain of ataxin-3: structural determinants for molecular recognition. *Proc Natl Acad Sci U S A* **102**, 10493-8.
3. Winborn, B. J., Travis, S. M., Todi, S. V., Scaglione, K. M., Xu, P., Williams, A. J., Cohen, R. E., Peng, J. & Paulson, H. L. (2008). The deubiquitinating enzyme ataxin-3, a polyglutamine disease protein, edits Lys63 linkages in mixed linkage ubiquitin chains. *J Biol Chem* **283**, 26436-43.
4. Masino, L., Musi, V., Menon, R. P., Fusi, P., Kelly, G., Frenkiel, T. A., Trottier, Y. & Pastore, A. (2003). Domain architecture of the polyglutamine protein ataxin-3: a globular domain followed by a flexible tail. *FEBS Lett* **549**, 21-5.
5. Kawaguchi, Y., Okamoto, T., Taniwaki, M., Aizawa, M., Inoue, M., Katayama, S., Kawakami, H., Nakamura, S., Nishimura, M., Akiguchi, I. & et al. (1994). CAG expansions in a novel gene for Machado-Joseph disease at chromosome 14q32.1. *Nat Genet* **8**, 221-8.
6. Padiath, Q. S., Srivastava, A. K., Roy, S., Jain, S. & Brahmachari, S. K. (2005). Identification of a novel 45 repeat unstable allele associated with a disease phenotype at the MJD1/SCA3 locus. *Am J Med Genet B Neuropsychiatr Genet* **133**, 124-6.
7. Saunders, H. M. & Bottomley, S. P. (2009). Multi-domain misfolding: understanding the aggregation pathway of polyglutamine proteins. *Protein Eng Des Sel* **22**, 447-51.
8. Ellisdon, A. M., Pearce, M. C. & Bottomley, S. P. (2007). Mechanisms of ataxin-3 misfolding and fibril formation: Kinetic analysis of a disease-associated polyglutamine protein. *Journal of Molecular Biology* **368**, 595-605.
9. Ellisdon, A. M., Thomas, B. & Bottomley, S. P. (2006). The two-stage pathway of ataxin-3 fibrillogenesis involves a polyglutamine-independent step. *J Biol Chem* **281**, 16888-96.
10. Chow, M. K., Mackay, J. P., Whisstock, J. C., Scanlon, M. J. & Bottomley, S. P. (2004). Structural and functional analysis of the Josephin domain of the polyglutamine protein ataxin-3. *Biochem Biophys Res Commun* **322**, 387-94.
11. Gales, L., Cortes, L., Almeida, C., Melo, C. V., do Carmo Costa, M., Maciel, P., Clarke, D. T., Damas, A. M. & Macedo-Ribeiro, S. (2005). Towards a structural understanding of the fibrillization pathway in Machado-Joseph's disease: trapping early oligomers of non-expanded ataxin-3. *J Mol Biol* **353**, 642-54.
12. Masino, L., Nicastro, G., Menon, R. P., Dal Piaz, F., Calder, L. & Pastore, A. (2004). Characterization of the structure and the amyloidogenic properties of the Josephin domain of the polyglutamine-containing protein ataxin-3. *J Mol Biol* **344**, 1021-35.

13. Menon, R. P. & Pastore, A. (2006). Expansion of amino acid homo-sequences in proteins: insights into the role of amino acid homo-polymers and of the protein context in aggregation. *Cell Mol Life Sci* **63**, 1677-85.
14. Chai, Y., Wu, L., Griffin, J. D. & Paulson, H. L. (2001). The role of protein composition in specifying nuclear inclusion formation in polyglutamine disease. *J Biol Chem* **276**, 44889-97.
15. Haacke, A., Broadley, S. A., Boteva, R., Tzvetkov, N., Hartl, F. U. & Breuer, P. (2006). Proteolytic cleavage of polyglutamine-expanded ataxin-3 is critical for aggregation and sequestration of non-expanded ataxin-3. *Hum Mol Genet* **15**, 555-68.
16. de Chiara, C., Menon, R. P., Dal Piaz, F., Calder, L. & Pastore, A. (2005). Polyglutamine is not all: the functional role of the AXH domain in the ataxin-1 protein. *J Mol Biol* **354**, 883-93.
17. Thakur, A. K., Jayaraman, M., Mishra, R., Thakur, M., Chellgren, V. M., IJ, L. B., Anjum, D. H., Kodali, R., Creamer, T. P., Conway, J. F., A, M. G. & Wetzel, R. (2009). Polyglutamine disruption of the huntingtin exon 1 N terminus triggers a complex aggregation mechanism. *Nat Struct Mol Biol* **16**, 380-389.
18. Ignatova, Z., Thakur, A. K., Wetzel, R. & Gierasch, L. M. (2007). In-cell aggregation of a polyglutamine-containing chimera is a multistep process initiated by the flanking sequence. *J Biol Chem* **282**, 36736-43.
19. Kazlauskaite, J., Sanghera, N., Sylvester, I., Venien-Bryan, C. & Pinheiro, T. J. (2003). Structural changes of the prion protein in lipid membranes leading to aggregation and fibrillization. *Biochemistry* **42**, 3295-304.
20. Terzi, E., Holzemann, G. & Seelig, J. (1997). Interaction of Alzheimer beta-amyloid peptide(1-40) with lipid membranes. *Biochemistry* **36**, 14845-52.
21. Zhu, M. & Fink, A. L. (2003). Lipid binding inhibits alpha-synuclein fibril formation. *J Biol Chem* **278**, 16873-7.
22. Hirakura, Y., Azimov, R., Azimova, R. & Kagan, B. L. (2000). Polyglutamine-induced ion channels: a possible mechanism for the neurotoxicity of Huntington and other CAG repeat diseases. *J Neurosci Res* **60**, 490-4.
23. Kagan, B. L., Hirakura, Y., Azimov, R. & Azimova, R. (2001). The channel hypothesis of Huntington's disease. *Brain Res Bull* **56**, 281-4.
24. Monoi, H., Futaki, S., Kugimiya, S., Minakata, H. & Yoshihara, K. (2000). Poly-L-glutamine forms cation channels: relevance to the pathogenesis of the polyglutamine diseases. *Biophys J* **78**, 2892-9.
25. Ren, P. H., Lauckner, J. E., Kachirskaia, I., Heuser, J. E., Melki, R. & Kopito, R. R. (2009). Cytoplasmic penetration and persistent infection of mammalian cells by polyglutamine aggregates. *Nat Cell Biol* **11**, 219-25.
26. Wang, Q., Li, L. & Ye, Y. (2006). Regulation of retrotranslocation by p97-associated deubiquitinating enzyme ataxin-3. *J Cell Biol* **174**, 963-71.
27. Pozzi C., V. M., Tedeschi G., Galbusera E., Pastori V., Bigi A., Nonnis S., Grassi E. and Fusi P. (2008). Study of subcellular localization and proteolysis of ataxin-3. *Neurobiol Dis* **30**, 190-200.
28. Ricchelli, F., Fusi, P., Tortora, P., Valtorta, M., Riva, M., Tognon, G., Chieregato, K., Bolognin, S. & Zatta, P. (2007). Destabilization of non-pathological variants of

ataxin-3 by metal ions results in aggregation/fibrillogenesis. *Int J Biochem Cell Biol* **39**, 966-77.

29. Suopanki, J., Gotz, C., Lutsch, G., Schiller, J., Harjes, P., Herrmann, A. & Wanker, E. E. (2006). Interaction of huntingtin fragments with brain membranes--clues to early dysfunction in Huntington's disease. *J Neurochem* **96**, 870-84.
30. Kegel, K. B., Sapp, E., Yoder, J., Cuiffo, B., Sobin, L., Kim, Y. J., Qin, Z. H., Hayden, M. R., Aronin, N., Scott, D. L., Isenberg, G., Goldmann, W. H. & DiFiglia, M. (2005). Huntingtin associates with acidic phospholipids at the plasma membrane. *J Biol Chem* **280**, 36464-73.
31. Zhao, H., Tuominen, E. K. & Kinnunen, P. K. (2004). Formation of amyloid fibers triggered by phosphatidylserine-containing membranes. *Biochemistry* **43**, 10302-7.
32. Kegel, K. B., Sapp, E., Alexander, J., Valencia, A., Reeves, P., Li, X., Masso, N., Sobin, L., Aronin, N. & DiFiglia, M. (2009). Polyglutamine expansion in huntingtin alters its interaction with phospholipids. *J Neurochem* **110**, 1585-97.
33. Kraayenhof, R., Sterk, G. J. & Sang, H. W. (1993). Probing biomembrane interfacial potential and pH profiles with a new type of float-like fluorophores positioned at varying distance from the membrane surface. *Biochemistry* **32**, 10057-66.
34. Pertinhez, T. A., Bouchard, M., Smith, R. A., Dobson, C. M. & Smith, L. J. (2002). Stimulation and inhibition of fibril formation by a peptide in the presence of different concentrations of SDS. *FEBS Lett* **529**, 193-7.
35. Yamamoto, S., Hasegawa, K., Yamaguchi, I., Tsutsumi, S., Kardos, J., Goto, Y., Gejyo, F. & Naiki, H. (2004). Low concentrations of sodium dodecyl sulfate induce the extension of beta 2-microglobulin-related amyloid fibrils at a neutral pH. *Biochemistry* **43**, 11075-82.
36. Ahmad, M. F., Ramakrishna, T., Raman, B. & Rao Ch, M. (2006). Fibrillogenic and non-fibrillogenic ensembles of SDS-bound human alpha-synuclein. *J Mol Biol* **364**, 1061-72.
37. Rangachari, V., Moore, B. D., Reed, D. K., Sonoda, L. K., Bridges, A. W., Conboy, E., Hartigan, D. & Rosenberry, T. L. (2007). Amyloid-beta(1-42) rapidly forms protofibrils and oligomers by distinct pathways in low concentrations of sodium dodecylsulfate. *Biochemistry* **46**, 12451-62.
38. Helenius, A., McCaslin, D. R., Fries, E. & Tanford, C. (1979). Properties of detergents. *Methods Enzymol* **56**, 734-49.
39. Chow, M. K., Ellisdon, A. M., Cabrita, L. D. & Bottomley, S. P. (2004). Polyglutamine expansion in ataxin-3 does not affect protein stability: implications for misfolding and disease. *J Biol Chem* **279**, 47643-51.
40. Robertson, A. L., Horne, J., Ellisdon, A. M., Thomas, B., Scanlon, M. J. & Bottomley, S. P. (2008). The structural impact of a polyglutamine tract is location-dependent. *Biophys J* **95**, 5922-30.
41. Tew, D. J., Bottomley, S. P., Smith, D. P., Ciccotosto, G. D., Babon, J., Hinds, M. G., Masters, C. L., Cappai, R. & Barnham, K. J. (2008). Stabilization of neurotoxic soluble beta-sheet-rich conformations of the Alzheimer's disease amyloid-beta peptide. *Biophys J* **94**, 2752-66.

42. Rangachari, V., Reed, D. K., Moore, B. D. & Rosenberry, T. L. (2006). Secondary structure and interfacial aggregation of amyloid-beta(1-40) on sodium dodecyl sulfate micelles. *Biochemistry* **45**, 8639-48.
43. Stine, W. B., Jr., Dahlgren, K. N., Krafft, G. A. & LaDu, M. J. (2003). In vitro characterization of conditions for amyloid-beta peptide oligomerization and fibrillogenesis. *J Biol Chem* **278**, 11612-22.
44. Marchal, S., Shehi, E., Harricane, M. C., Fusi, P., Heitz, F., Tortora, P. & Lange, R. (2003). Structural instability and fibrillar aggregation of non-expanded human ataxin-3 revealed under high pressure and temperature. *J Biol Chem* **278**, 31554-63.
45. Lindquist, S. (1986). The heat-shock response. *Annu Rev Biochem* **55**, 1151-91.
46. Thompson, W. & MacDonald, G. (1976). Cytidine diphosphate diglyceride of bovine brain. Positional distribution of fatty acids and analysis of major molecular species. *Eur J Biochem* **65**, 107-11.
47. Davis, C. H. & Berkowitz, M. L. (2009). Interaction between amyloid-beta (1-42) peptide and phospholipid bilayers: a molecular dynamics study. *Biophys J* **96**, 785-97.
48. Gorbenko, G. P. & Kinnunen, P. K. (2006). The role of lipid-protein interactions in amyloid-type protein fibril formation. *Chem Phys Lipids* **141**, 72-82.
49. Zhu, M., Li, J. & Fink, A. L. (2003). The association of alpha-synuclein with membranes affects bilayer structure, stability, and fibril formation. *J Biol Chem* **278**, 40186-97.
50. Quist, A., Doudevski, I., Lin, H., Azimova, R., Ng, D., Frangione, B., Kagan, B., Ghiso, J. & Lal, R. (2005). Amyloid ion channels: a common structural link for protein-misfolding disease. *Proc Natl Acad Sci U S A* **102**, 10427-32.
51. Bucciantini, M., Calloni, G., Chiti, F., Formigli, L., Nosi, D., Dobson, C. M. & Stefani, M. (2004). Prefibrillar amyloid protein aggregates share common features of cytotoxicity. *J Biol Chem* **279**, 31374-82.
52. Demuro, A., Mina, E., Kayed, R., Milton, S. C., Parker, I. & Glabe, C. G. (2005). Calcium dysregulation and membrane disruption as a ubiquitous neurotoxic mechanism of soluble amyloid oligomers. *J Biol Chem* **280**, 17294-300.
53. Baglioni, S., Casamenti, F., Bucciantini, M., Luheshi, L. M., Taddei, N., Chiti, F., Dobson, C. M. & Stefani, M. (2006). Prefibrillar amyloid aggregates could be generic toxins in higher organisms. *J Neurosci* **26**, 8160-7.
54. Kayed, R., Head, E., Thompson, J. L., McIntire, T. M., Milton, S. C., Cotman, C. W. & Glabe, C. G. (2003). Common structure of soluble amyloid oligomers implies common mechanism of pathogenesis. *Science* **300**, 486-9.
55. Chow, M. K., Paulson, H. L. & Bottomley, S. P. (2004). Destabilization of a non-pathological variant of ataxin-3 results in fibrillogenesis via a partially folded intermediate: a model for misfolding in polyglutamine disease. *J Mol Biol* **335**, 333-41.
56. Van Stokkum, I. H. M., Spoelder, H. J. W., Bloemendal, M., Van Grondelle, R. & Groen, F. C. A. (1990). Estimation of protein secondary structure and error analysis from CD spectra. . *Anal. Biochem* **191**, 110-118.
57. Stevenson, J. M., Perera, I. Y. & Boss, W. F. (1998). A phosphatidylinositol 4-kinase pleckstrin homology domain that binds phosphatidylinositol 4-monophosphate. *J Biol Chem* **273**, 22761-7.

Tables

Table 1 Percentage of α-helical content of monomeric protein with SDS present.

[SDS] mM	Ataxin-3(64)		Ataxin-3(Q15)		Josephin	
	% α- helix	Standard Error	% α- helix	Standard Error	% α- helix	Standard Error
0	27.5	2.3	30.3	2.6	30.8	3.5
1	28.7	2.7	30.4	2.0	29.5	1.3
5	32.0	1.9	37.5	2.0	36.4	2.4
10	32.0	1.8	39.1	2.9	35.4	3.3

Table 2 Midpoints of ataxin-3(Q64) aggregation

	SDS-Soluble Aggregation		SDS-Insoluble Aggregation	
[SDS] mM	Midpoint (hrs)	Standard Error (hrs)	Midpoint (hrs)	Standard Error (hrs)
0	11.50	1.65	44.7	2.7
1	2	0.5	69.0	2.6
5	-	-	79.9	3.0
10	-	-	-	-

Figure Legends

Figure 1 Far-UV CD spectra of ataxin-3 variants in increasing concentrations of SDS. The far-UV CD spectra for each ataxin-3 variant was determined at 37 ºC with increasing concentrations of SDS; 0 mM SDS (*black solid line*), 1 mM SDS (*black dotted line*), 5 mM SDS (*grey solid line)* or 10 mM SDS (*grey dashed line*). The final protein concentration was 30 μM and the spectra measured with a path length of 0.1 mm.

Figure 2 Aggregation of ataxin-3 in the presence of SDS monitored by ThioT. Aggregation of ataxin-3 (30 μM) at pH 7.4 and 37 ºC in the presence of a range of SDS concentrations was monitored by thioT. ThioT fluorescence values were read at 480 nm (λ_{ex} = 430 nm) every 30 minutes using a fluorescence plate reader. (A) Ataxin-3(Q64), (B) ataxin-3(Q15) and (C) Josephin domain are shown with the addition of 0 mM SDS (*black solid line*), 1 mM SDS (*dashed line*), 5 mM SDS (*grey solid line*) and 10 mM SDS (*dotted and dashed line*).

Figure 3 Aggregation of ataxin-3 in the presence of SDS monitored by SDS-insolubility. Formation of SDS-insoluble fibrils was followed by taking aliquots from a 30 μM ataxin-3(Q64) timecourse assay at 37 ºC, pH 7.4. (A) A representative filter-trap membrane of ataxin-3(Q64) with 0 – 10 mM SDS is shown. QBP1 was added to a ataxin-3(Q64) containing 5 mM SDS as indicated. (B) Analysis of the filter trap membrane by densitometry. Ataxin-3(Q64) is shown with the addition of 0 mM SDS(-■-), 1 mM SDS(-▲-), 5 mM SDS (-♦-), 5 mM SDS with QBP1 (-◇-) and 10 mM SDS (-●-). Results from three independent experiments were fit to an exponential curve.

Figure 4 Far–UV CD spectra of ataxin-3(Q64) during aggregation in the presence of SDS. Aliquots of ataxin-3(Q64) were taken from a fibrillogenesis time course assay (see Materials and Methods) and their far-UV CD spectra determined. For each indicated SDS concentration aliquots were taken at times of 0 (*black*), 4 (*green*), 46 (*red*) and 100 (*blue*) hours.

Figure 5 Morphology of fibrils formed by ataxin-3(Q64) with SDS. Transmission Electron Microscopy of ataxin-3(Q64) with 0 mM SDS at 30 hr (A) and 50 hr (D), 1 mM SDS at 5 hr (B) and 30 hr (E) and 5 mM SDS at 30 hr (C) and 50 hr (F). Time course samples from 5 hr, 30 hr or 50 hr were negatively stained using 1 % (w/v) uranyl acetate. Scale bars represent 200 nm.

Figure 6 Binding of polyglutamine proteins to phospholipids.

(A) Protein-lipid overlays of ataxin-3(Q64) at 24 hrs (i) and 200 hrs (ii), Josephin domain at 70 hrs (iii) and 200 hrs (iv), and monomeric SpA (v) and SpA(Q52) (vi). A representative membrane is shown. (B) A summary of three independent experiments, with a fully shaded square representing strong binding in all experiments, and a triangle representing weak binding in one or two membranes only. Spot 16 is not included as it is a blank dot.

Figure 7 Summary of effects of SDS on ataxin-3 aggregation

Schematic summarizing the effects of micellar and non-micellar SDS on both stages of ataxin-3 aggregation.

Figure S1. Far-UV CD spectra of ataxin-3(Q15) and the Josephin domain during aggregation in the presence of SDS. Protein aliquots were taken from a fibrillogenesis time course assay and the far-UV CD spectra determined. For each indicated SDS concentration aliquots were taken at times of 0 hr (black), 4 hr (green), 46 hr (red) and 100 hr (blue).

Figure S2. Morphology of fibrils formed by ataxin-3(Q15) and Josephin with SDS. Transmission Electron Microscopy of ataxin-3(Q15) with 0 mM (A), 1 mM (B) and 5 mM SDS (C), and Josephin domain with 0 mM (D), 1 mM (E) and 5 mM (F) SDS. Samples after 100 hr incubation were negatively stained using 1 % (w/v) uranyl acetate. Scale bars represent 200 nm.

Figure 1

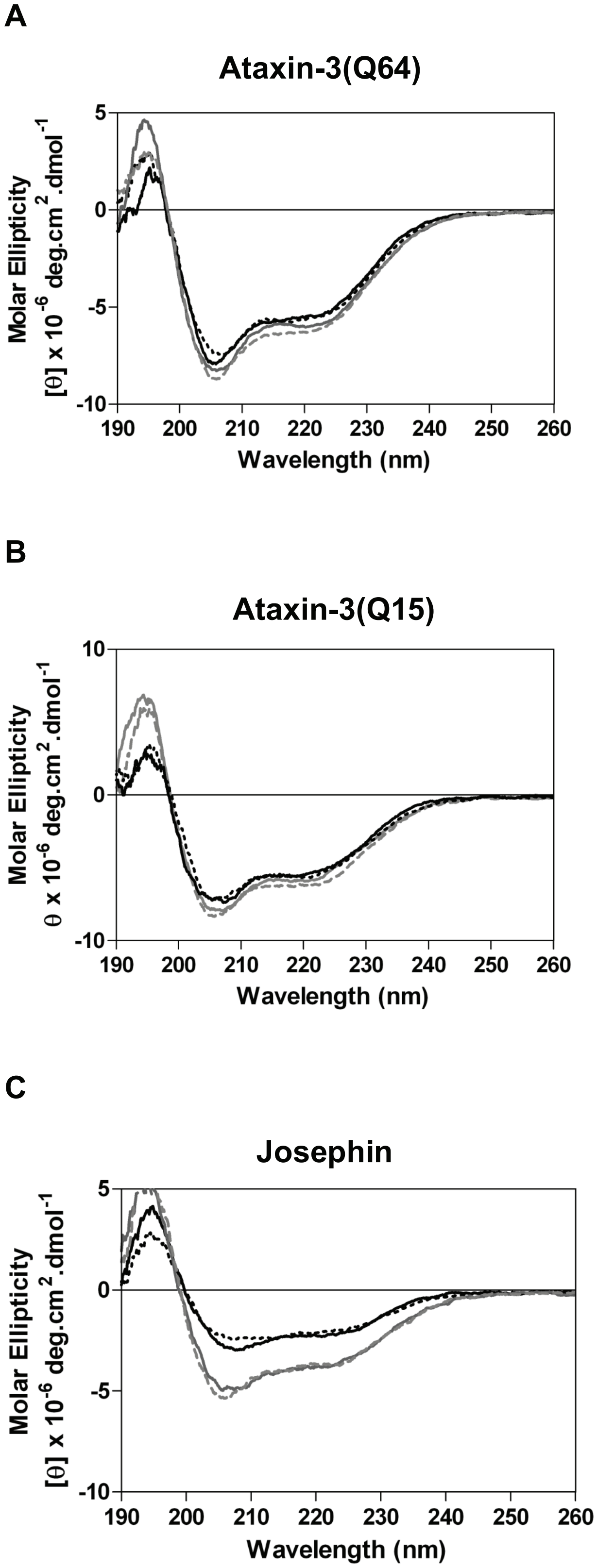
A
Ataxin-3(Q64)
Molar Ellipticity
[θ] x 10^{-6} deg.cm^{2}.dmol^{-1}
5
0
-5
-10
190
200
210
220
230
240
250
260
Wavelength (nm)
B
Ataxin-3(Q15)
Molar Ellipticity
θ x 10^{-6} deg.cm^{2}.dmol^{-1}
10
0
-10
190
200
210
220
230
240
250
260
Wavelength (nm)
C
Josephin
Molar Ellipticity
[θ] x 10^{-6} deg.cm^{2}.dmol^{-1}
5
0
-5
-10
190
200
210
220
230
240
250
260
Wavelength (nm)

Figure 2

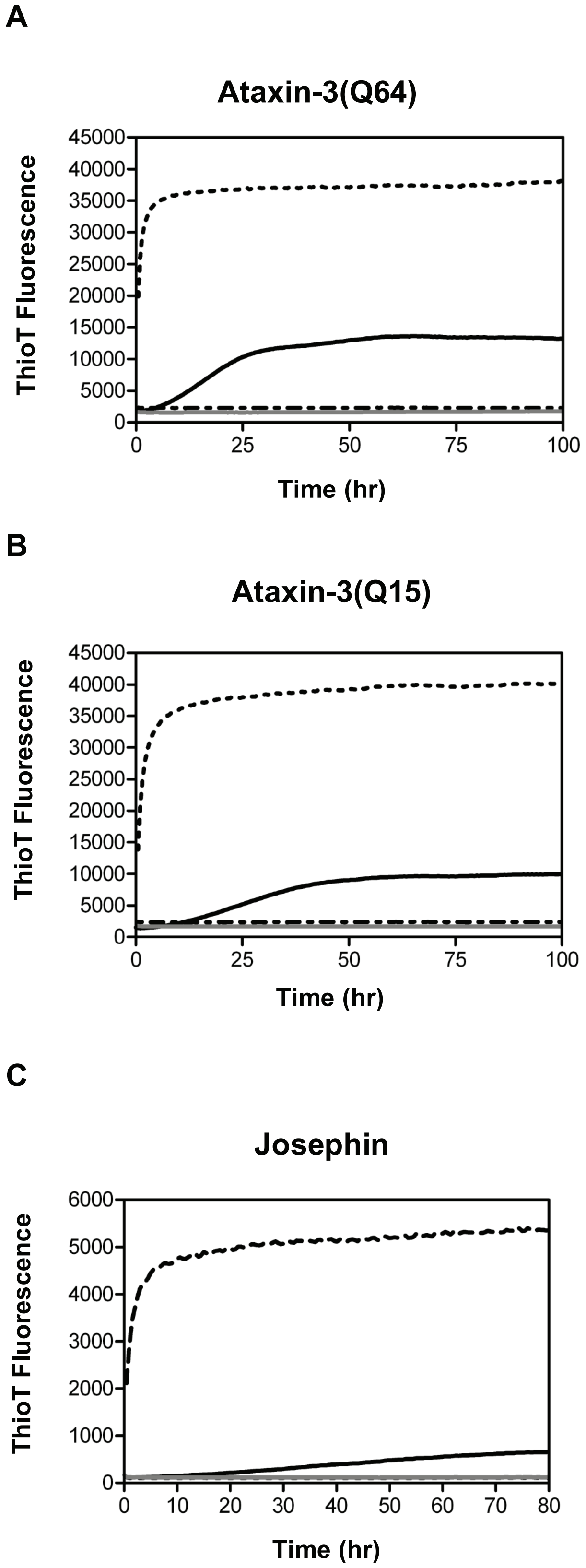
A
Ataxin-3(Q64)
ThioT Fluorescence
45000
40000
35000
30000
25000
20000
15000
10000
5000
0
0
25
50
75
100
Time (hr)
B
Ataxin-3(Q15)
ThioT Fluorescence
45000
40000
35000
30000
25000
20000
15000
10000
5000
0
0
25
50
75
100
Time (hr)
C
Josephin
ThioT Fluorescence
6000
5000
4000
3000
2000
1000
0
0
10
20
30
40
50
60
70
80
Time (hr)

Figure 3

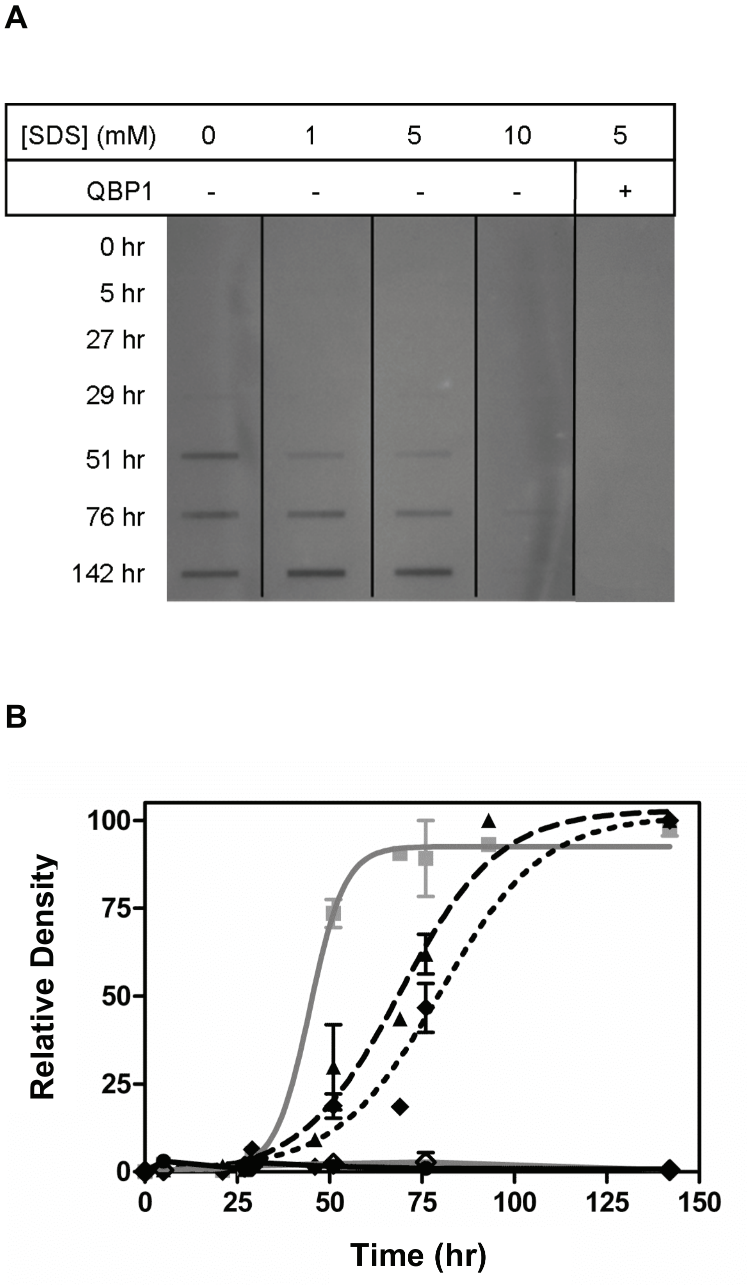
A
[SDS] (mM) 0 1 5 10 5
QBP1 - - - - +
0 hr
5 hr
27 hr
29 hr
51 hr
76 hr
142 hr
B
Relative Density
0
25
50
75
100
Time (hr)
0
25
50
75
100
125
150

Figure 4

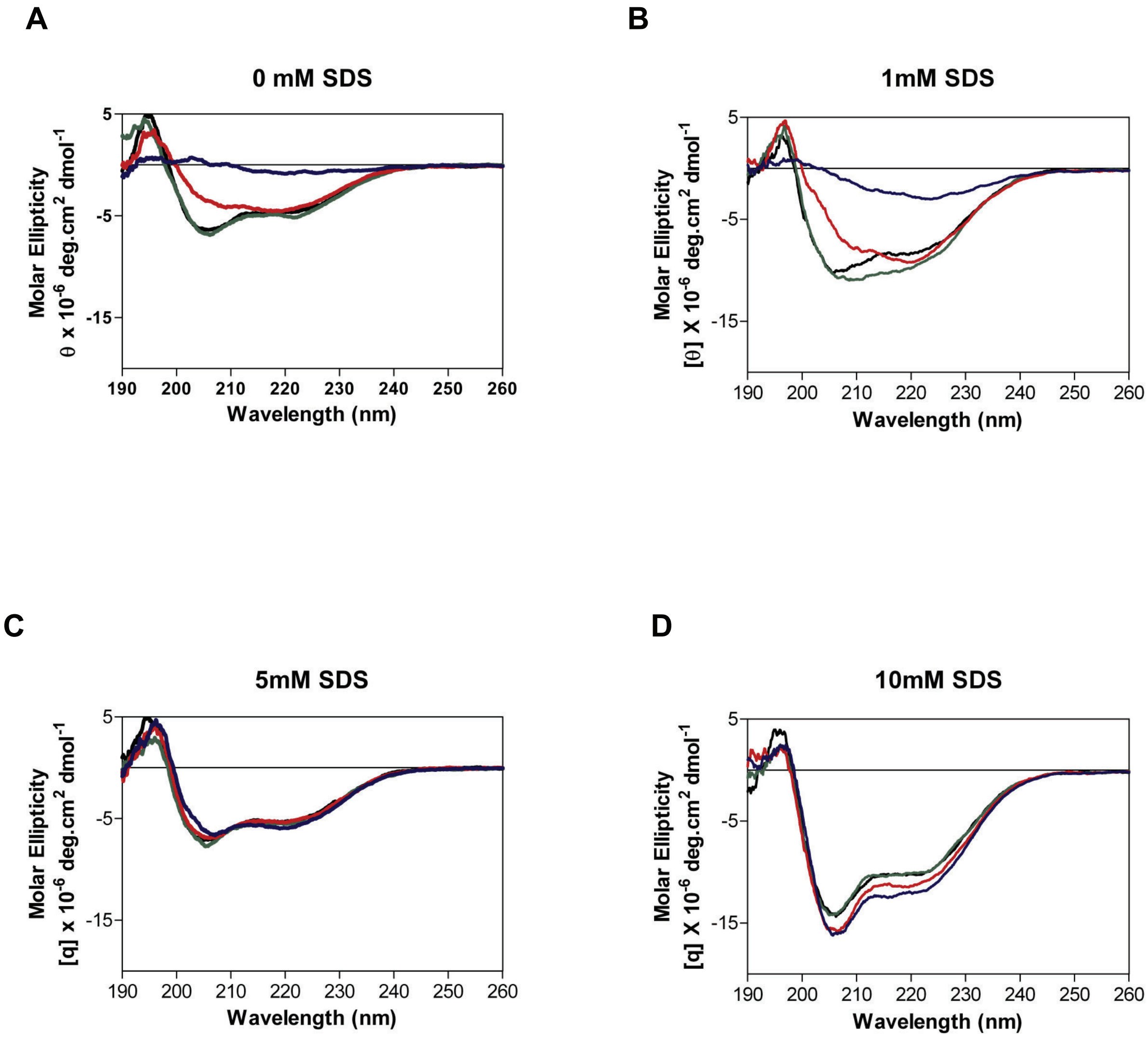
A
0 mM SDS
Molar Ellipticity
θ x 10-6 deg.cm2 dmol-1
5
-5
-15
190 200 210 220 230 240 250 260
Wavelength (nm)
B
1mM SDS
Molar Ellipticity
[θ] X 10-6 deg.cm2 dmol-1
5
-5
-15
190 200 210 220 230 240 250 260
Wavelength (nm)
C
5mM SDS
Molar Ellipticity
[q] x 10-6 deg.cm2 dmol-1
5
-5
-15
190 200 210 220 230 240 250 260
Wavelength (nm)
D
10mM SDS
Molar Ellipticity
[q] X 10-6 deg.cm2 dmol-1
5
-5
-15
190 200 210 220 230 240 250 260
Wavelength (nm)

Figure 5

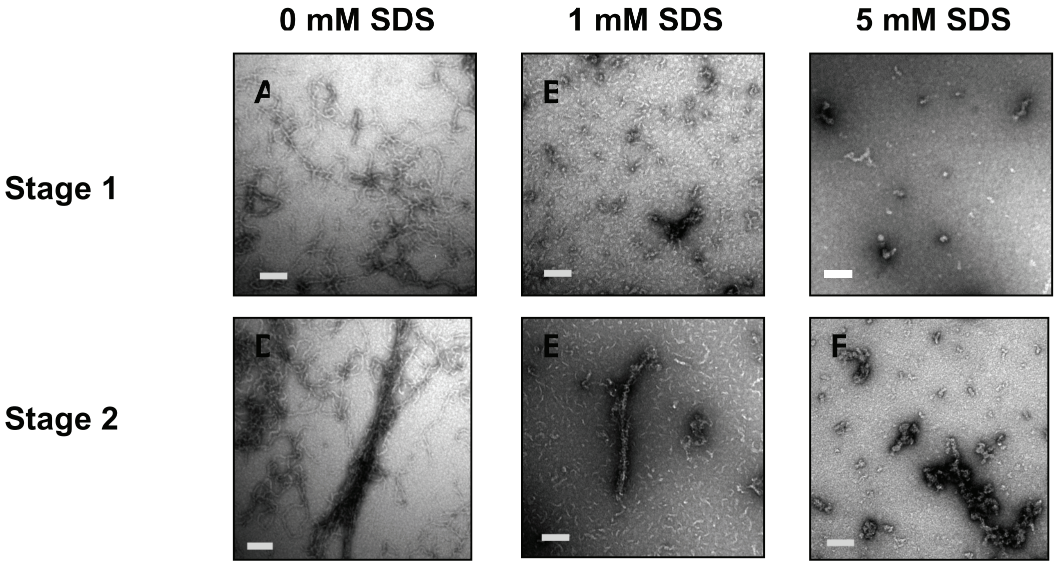
0 mM SDS
1 mM SDS
5 mM SDS
Stage 1
Stage 2
A
D
E
F

Figure 6

A

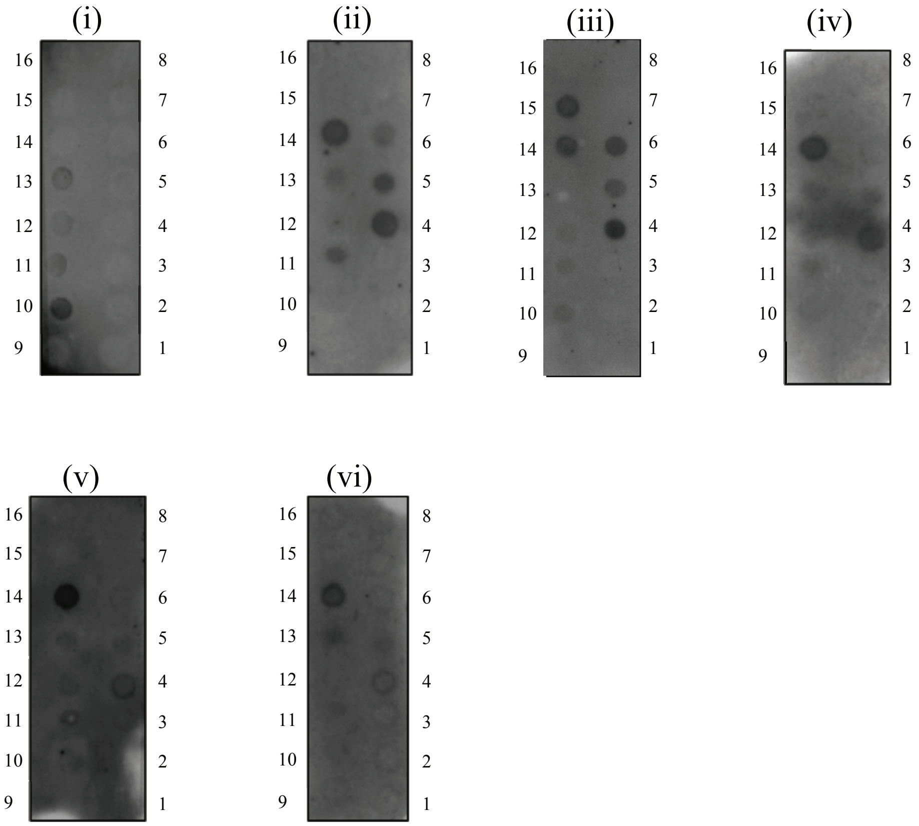
(i)
(ii)
(iii)
(iv)
(v)
(vi)
16
15
14
13
12
11
10
9
8
7
6
5
4
3
2
1

B

		LPA	LPC	PI	PI(3)P	PI(4)P	PI(5)P	PE	PC	S1P	PI(3,4)P2	PI(3,5)P2	PI(4,5)P2	PI(3,4,5)P3	PA	PS
Protein	**Sample Type**	**1**	**2**	**3**	**4**	**5**	**6**	**7**	**8**	**9**	**10**	**11**	**12**	**13**	**14**	**15**
Ataxin-3(Q64)	24 hr Incubation										■	■	■	■	■	
Ataxin-3(Q64)	Endpoint Fibril				■	■	◣					◣	◣	■	■	
Josephin	70 hr Incubation				■	■	■								■	◣
Josephin	Endpoint Fibril				■	■						◣	◣	◣	■	
SpA	Monomer				■	■	◣					◣	◣	◣	■	
SpA(Q52)	Endpoint Fibril				■	■								◣	■	

Figure 7

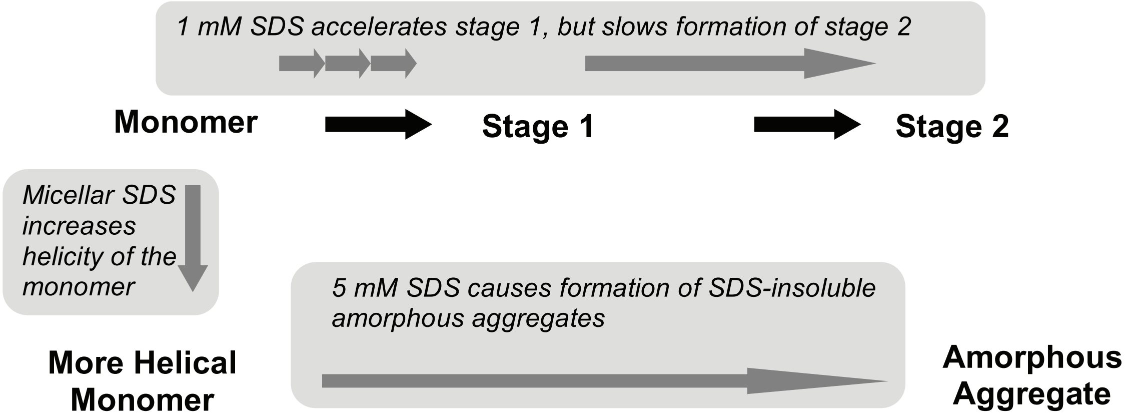
1 mM SDS accelerates stage 1, but slows formation of stage 2
Monomer
Stage 1
Stage 2
Micellar SDS increases helicity of the monomer
More Helical Monomer
5 mM SDS causes formation of SDS-insoluble amorphous aggregates
Amorphous Aggregate

Supplementary Data

Figure S1

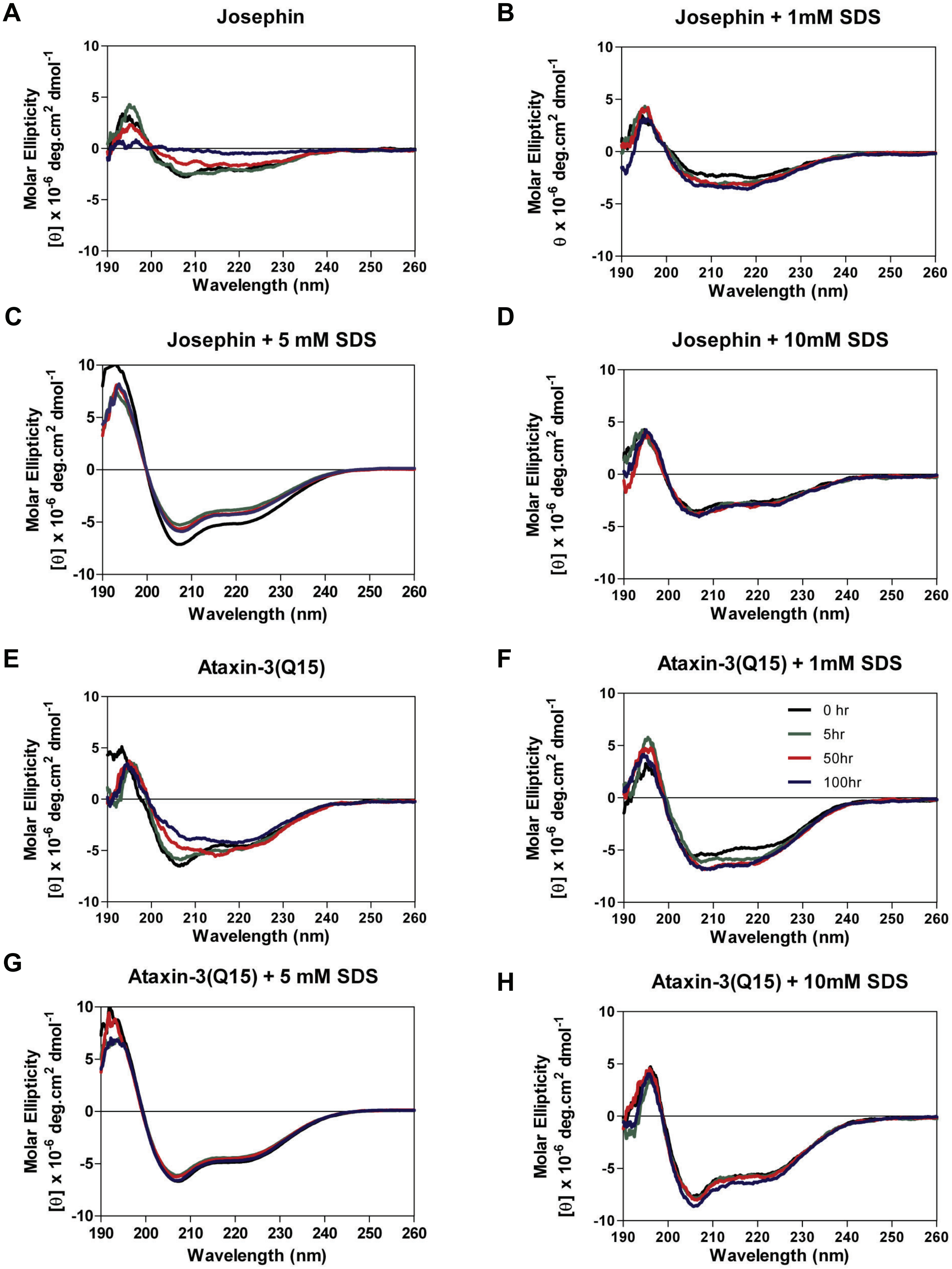

Figure S2

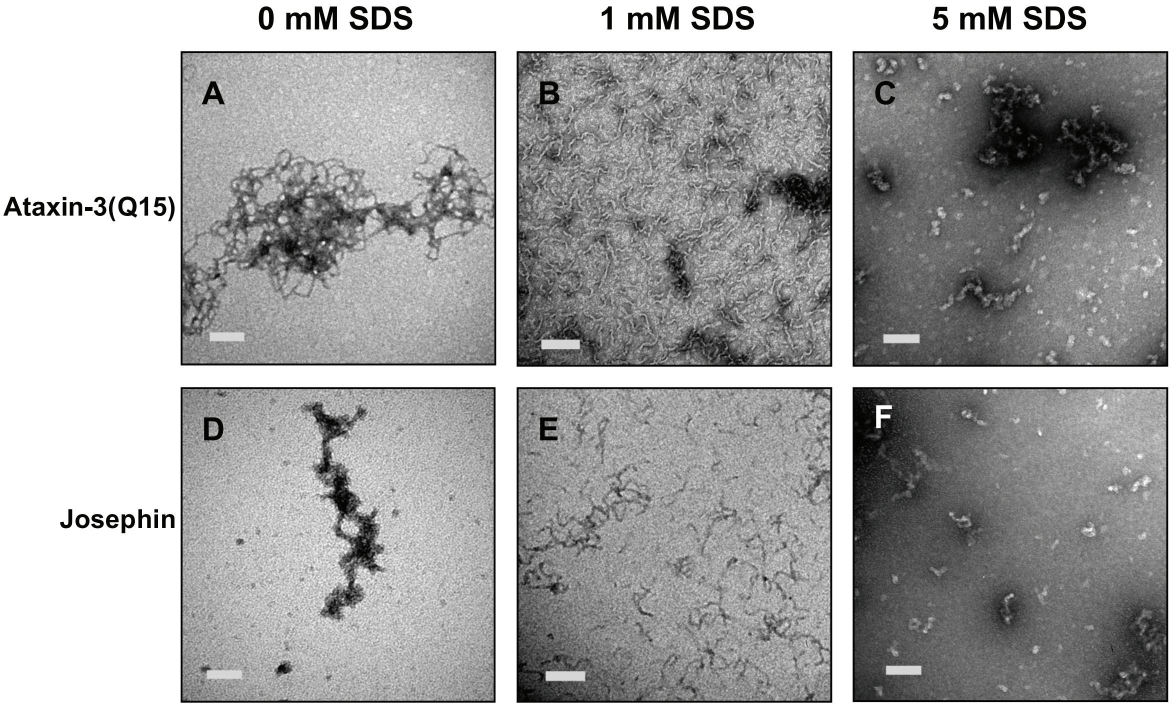
0 mM SDS
1 mM SDS
5 mM SDS
Ataxin-3(Q15)
Josephin
A
B
C
D
E
F

CHAPTER 6

GENERAL DISCUSSION & CONCLUSIONS

6.1 Role of Flanking Domains in PolyQ Aggregation

The mechanism of toxicity within the amyloid diseases has increasingly been linked to intermediate species formed along the aggregation pathway. Thus there is great interest in the characterization of conformational changes which occur during aggregation. The amyloid diseases are often associated with an amyloidogenic mutation, as exemplified by the polyQ diseases which have a strong correlation between polyQ tract length and disease pathology (269). The only sequence homology between the nine polyQ proteins is the presence of an expanded polyQ tract. Consequently, the host protein dictates factors which vary between polyQ diseases such as the localization of protein deposits and neurodegeneration, in addition to modulating disease progression (179,196,270,271).

Increasingly, domains which flank the polyQ tract have been demonstrated to modulate the aggregation of numerous polyQ proteins (164,191,193,194,196), yet the mechanism via which these flanking domains act remains poorly understood.

A new model was proposed at the commencement of my study whereby the aggregation of pathogenic length ataxin-3 occurs via a multi-stage mechanism involving both the flanking Josephin domain as well as the polyQ tract (191). However Ellisdon *et al.* did not conclusively demonstrate whether it was the Josephin domain or the C-terminal region surrounding the polyQ tract involved within the first stage of aggregation (192). This thesis has focused to a large degree on the characterization of the conformational changes occurring in the Josephin domain both when isolated and when in the context of the full length protein.

Decreased thermodynamic stability of amyloidogenic proteins is often linked to increased aggregation rates and vice versa (73,77,272,273). This link was exploited in the first part of this study to confirm that the initial stage of the ataxin-3 aggregation pathway is mediated by interactions of the Josephin domain (Ch 3). This study substantiated the role of the Josephin domain within the two-stage aggregation mechanism for ataxin-3, as initially suggested (191). The involvement of the flanking domain in ataxin-3 aggregation is not unique within the polyQ proteins. Concurrent to this study, multi-domain aggregation mechanisms have also been identified for huntingtin exon-1, and the model polyQ protein CRABP I-htt exon-1 (8,204). A multi-domain aggregation mechanism has also been demonstrated for a number of non-polyQ proteins (210-212). Taken together, these studies highlight the importance of characterizing the flanking domains of polyQ proteins, and determining their influence on polyQ protein aggregation.

Different types of fibrils are formed along the multi-stage aggregation pathway of ataxin-3 (191). The conformational transition from stage 1 fibrils to stage 2 fibrils has not been characterized, and it appears that under different conditions there are a number of alternative pathways via which ataxin-3 forms end-stage morphologically-similar fibrils (Fig 6.1). With 1 mM SDS present, ataxin-3 showed an increase in the rate of stage 1 fibril formation yet a decrease in the rate of stage 2 fibril formation (Ch 5). In an alternate pathway, the stabilized ataxin-3(Q64) R103G S81A mutant showed a similar midpoint for both stage 1 and stage 2 fibril formation (Ch 3). Both these results suggest that whilst linked, the formation of stage 2 fibrils is not solely dependent upon the rate of stage 1 fibril formation. In both these pathways however, in order to transition from fibrils mediated via Josephin domain interactions to fibrils formed through polyQ interactions a structural rearrangement must occur within the fibril. This is not unprecedented, with structural rearrangements within a fibril reported for other amyloidogenic proteins (274-276).

A third pathway was characterized in the presence of a stoichiometric excess of αB-crystallin, where stage 2 ataxin-3 fibrils formed without significant formation of stage 1 fibrils, albeit at a slower rate (App 1). The formation of morphologically similar fibrils under these conditions suggests that the Josephin domain is not involved in the core of the stage 2 fibril. Indeed, the presence of flanking domains along the fibril may explain the atypical morphology of the endpoint fibrils formed by polyQ proteins in comparison to most amyloid fibrils (Ch 5)(11,191). It is possible the core fibril structure involves just the polyQ tract, as structural studies using polyQ peptides demonstrate a core cross-β fibril structure can be formed by the polyQ tract alone (32). Proteolysis studies to determine the core of both the stage 1 and stage 2 type fibrils will provide great insight into how the Josephin domain fits within the architecture of the fibril.

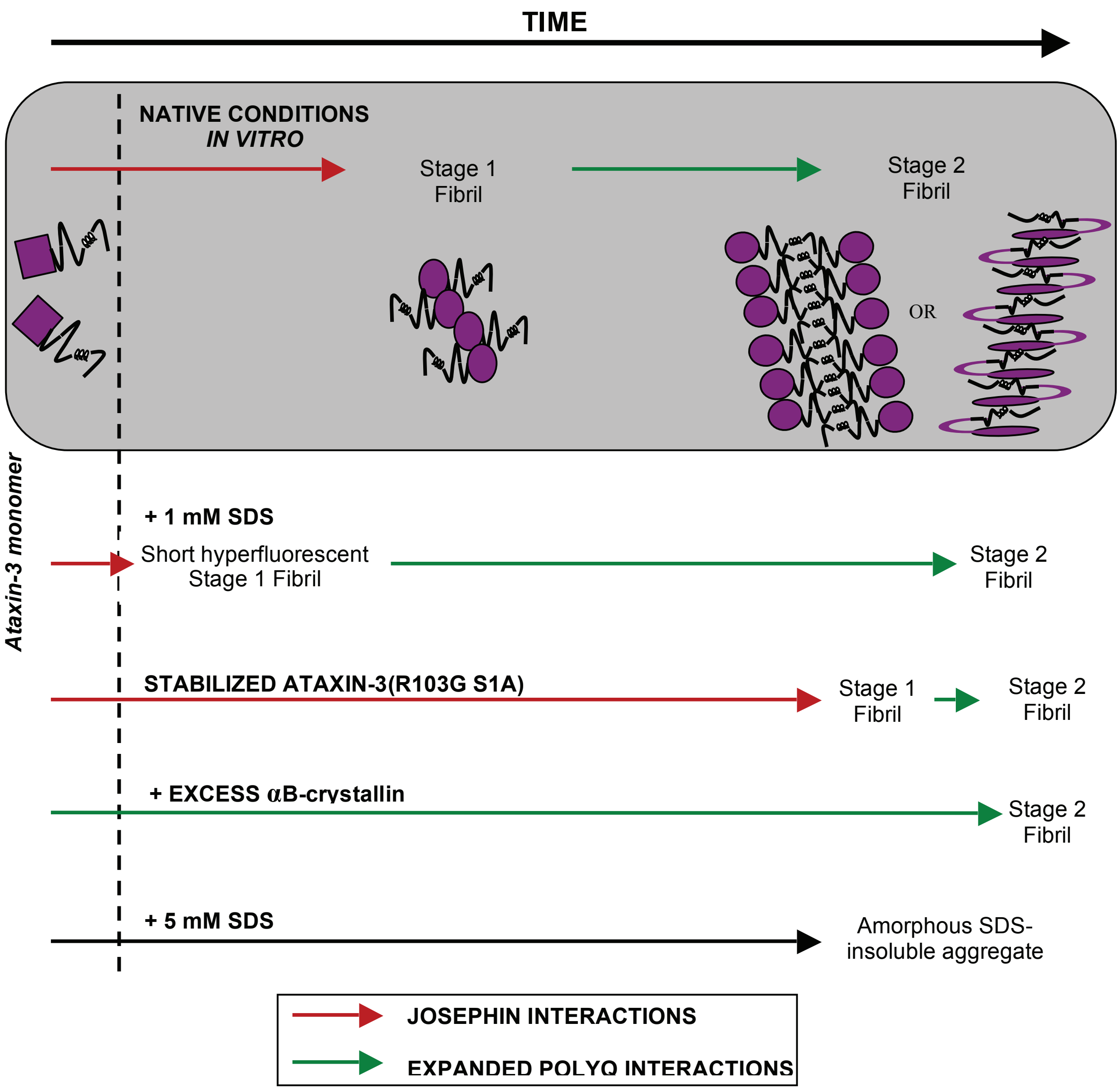
TIME
NATIVE CONDITIONS
IN VITRO
Stage 1
Fibril
Stage 2
Fibril
OR
Ataxin-3 monomer
+ 1 mM SDS
Short hyperfluorescent
Stage 1 Fibril
Stage 2
Fibril
STABILIZED ATAXIN-3(R103G S1A)
Stage 1
Fibril
Stage 2
Fibril
+ EXCESS αB-crystallin
Stage 2
Fibril
+ 5 mM SDS
Amorphous SDS-
insoluble aggregate
JOSEPHIN INTERACTIONS
EXPANDED POLYQ INTERACTIONS

Figure 6.1 Alternative Aggregation Pathways of Ataxin-3. Under native conditions *in vitro,* ataxin-3 shows the sequential formation of stage 1 then stage 2 fibrils mediated via interactions of the Josephin domain (red arrows) and polyQ tract (green arrows) respectively. Potential arrangements of the Josephin domain and polyQ tract within these fibrils are shown in the grey box. Stage 2 fibrils may involve either just the polyQ tract or the polyQ tract and part of the Josephin domain within the core cross-β structure of the fibril. The alternative pathways do not all show the sequential nature of formation of stage 1 and 2 fibrils seen under native conditions *in vitro,* whilst the addition of 5 mM SDS demonstrates that ataxin-3 is also able to form aggregates of a non-fibrillar nature.

6.2 Relationship Between the Folding and Aggregation Pathways of Ataxin-3

The folding and aggregation pathways are intrinsically linked, and the relationship between them differs for amyloidogenic proteins. A natively folded protein typically must unfold in order to form an amyloidogenic partially folded intermediate and there have been two models proposed for this mechanism for ataxin-3 (Fig 6.2). Initially, it was considered that ataxin-3 follows the conformational change hypothesis and aggregates via an intermediate along the unfolding pathway (163,201). However a later study proposed that the amyloidogenic intermediate is formed from the native state, separate to the folding pathway (69). This present study has distinguished between these two previously proposed mechanisms and supported the conformational change model whereby the initial misfolding event in ataxin-3 aggregation occurs from a partially unfolded intermediate along the folding pathway (Ch 3).

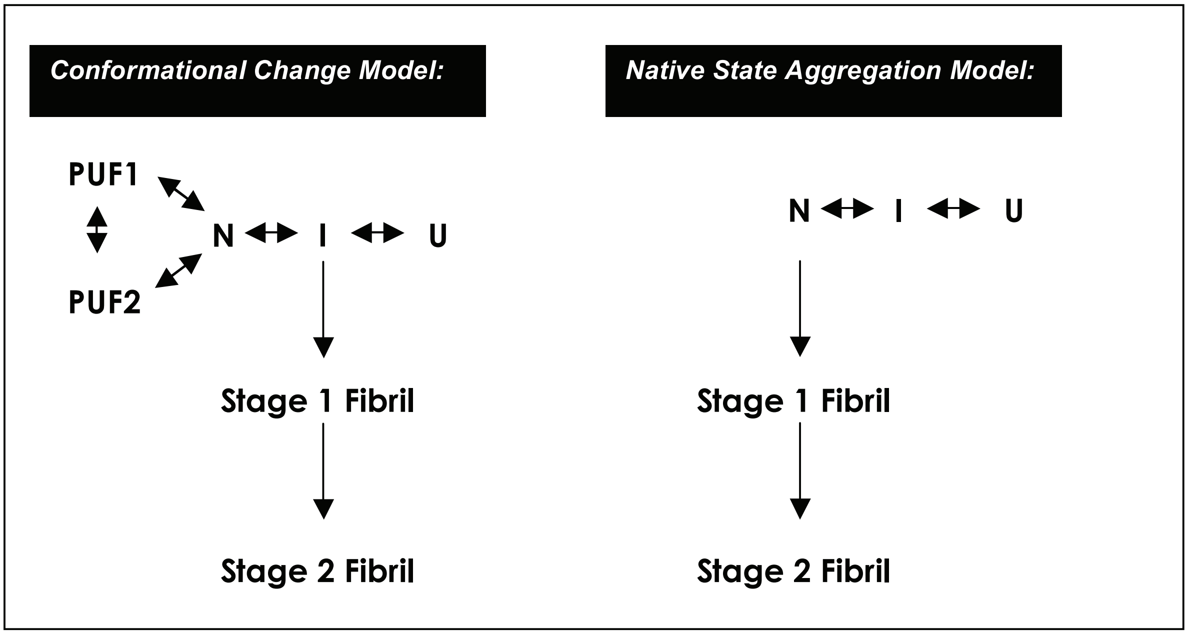

Figure 6.2 The Folding and Aggregation Pathways of Ataxin-3. The two models which have been proposed for ataxin-3 aggregation are depicted. This study has demonstrated that ataxin-3 aggregates according to the conformational change model of aggregation.

Within the family of natively folded amyloid proteins both mechanisms of initial conformational change have been observed. A number of proteins such as transthyretin and lysozyme aggregate according to the conformational change hypothesis of aggregation (68,277), however a growing number of proteins including acylphosphatase, HypF-N and insulin aggregate from an off-pathway intermediate (40,70,278). In addition, studies on the prion protein have shown that different mutations can result in both models of aggregation (279-281). This highlights the importance of using mutations which are spread throughout the tertiary structure of the protein as was done in this study (Ch 3) and thus less likely to push a protein down a specific pathway due to changing other characteristics of the protein.

In a conformational change aggregation model, to increase the propensity of a folded protein to form a partially unfolded intermediate there is typically a change in protein stability or dynamics (74). Previous studies have demonstrated that an expanded polyQ tract does not change the stability of ataxin-3 (69), which thus implicates a potential role for dynamics in initiation of aggregation. The complexity of ataxin-3 aggregation is again highlighted when it is considered that of the two amyloidogenic domains in ataxin-3, the Josephin domain is natively folded whilst the polyQ tract is predominantly unordered (282). Therefore a complete analysis of the early events of ataxin-3 misfolding requires the study of the dynamics of both the Josephin domain and the polyQ tract.

The Josephin domain has been demonstrated to be highly dynamic using hydrogen exchange mass spectrometry (Ch 4). This is consistent with the high amyloidogenicity of this domain under native conditions (206,208). Molecular dynamics simulations have been completed on Josephin in the context of ubiquitin binding (169). These studies correlate with previous NMR dynamics experiments proposing that the helical hairpin of Josephin is more dynamic than the rest of the domain (166,169). It is yet to be determined which regions of Josephin are important in mediating aggregation, and thus whether the dynamic motion of the helical hairpin may play a role.

The Josephin dynamics study found that native Josephin exists in solution in equilibrium with multiple partially unfolded forms (PUF) (Ch 4, Fig 6.2). These PUF appear to be only slightly unfolded, and interconverting on a timescale which means they are not amenable to detection by NMR spectroscopy. Despite identification of this structural heterogeneity of the folded Josephin domain, connections between these conformations and function or aggregation could not be identified in this study. The presence of PUF in equilibrium with their native state has been identified in a number of proteins, and in some cases, for example the GroEL apical domain, is linked to protein function (248,251,253). To further investigate the specific conformations of the PUF in both Josephin and ataxin-3, single-molecule fluorescence studies could be completed as it is another technique with the capacity to detect multiple conformations in solution.

Having developed a system to determine the hydrogen exchange kinetics of Josephin, future studies can now determine the dynamics of the full length protein and the impact of an expanded polyQ tract. A number of previous studies have focused on the dynamics of an isolated polyQ tract, and found the polyQ tract exists as a heterogeneous ensemble of fluctuating conformations which are in a collapsed state (213,267,283-286). In addition, crystal structures of huntingtin exon-1 suggested that the conformation of the polyQ tract is influenced by flanking regions (285). Taken together, this suggests that for polyQ proteins, determining the impact of flanking domains on polyQ dynamics may provide some insight into the initial conformational change events involved in aggregation.

6.3 Multi-domain Misfolding and PolyQ Disease

The mechanism of toxicity is currently considered to be linked to the formation of prefibrillar oligomers for both polyQ and other amyloid diseases (42,53,139). Together with the strong link between polyQ tract length and toxicity, this suggests there must be a difference in the oligomers formed by pathogenic and non-pathogenic length ataxin-3, regardless of both involving Josephin domain interactions. The structure of oligomers formed by a polyQ protein containing pathogenic and non-pathogenic length polyQ tracts has not been determined. Aggregates have not been detected within animal or cell models with overexpression of non-pathogenic length polyQ proteins (141,207,287). This suggests that either there is no formation of aggregates *in vivo* with non-pathogenic length polyQ proteins, or alternatively non-toxic aggregates form which are cleared from cells.

An assumption of the multi-domain misfolding mechanism is that there is no cleavage of ataxin-3 before aggregation. Conflicting evidence exists as to the presence of ataxin-3 fragments in disease inclusions (141,174-176). However in a study where fragments were detected in diseased brain, there was still an equal proportion of full length ataxin-3 (141). Thus an unsolved question is whether it is the fragment or the full length ataxin-3 responsible for initiation of aggregation and subsequent fibril formation in disease. Yet even if full length ataxin-3 is involved in aggregation, the Josephin domain may not be directly involved in aggregation *in vivo* due to its interaction with other cellular components. Recently, it was demonstrated that non-polyQ domains were involved in nuclear localization of ataxin-3 after a heat shock or oxidative stress was applied (288). With inclusions targeted to the nucleus resulting in increased toxicity for a number of polyQ proteins (104-108), this is an example of an indirect mechanism via which Josephin may contribute to toxicity.

Despite the currently poor understanding of the structural species forming within the cell, a well characterized *in vitro* aggregation mechanism provides many opportunities to characterize the interaction between cellular components and aggregation. For example, characterization of the effects of αB-crystallin on aggregation *in vitro* found that the inhibition of aggregation by this small heat shock protein occurred solely through an interaction with the Josephin domain (App 1). In addition, ataxin-3 with either a pathogenic or non-pathogenic length polyQ tract was found to interact with phospholipids only when fibrillar in structure (Ch 5). *In vitro* techniques also provide the tools to investigate effects of potential inhibitors of polyQ aggregation such as the polyphenol (-)-epi-gallocatechine gallate (EGCG), which inhibits aggregation of a number of amyloid proteins (289,290). Thus characterization of the *in vitro* aggregation mechanism provides a platform to both investigate the details of cellular interactions, and determine the effects of potential aggregation inhibitors.

6.4 General Conclusions

The aggregation pathway of multiple polyQ proteins has been demonstrated to be modulated by flanking domains both in cell models and *in vitro* (8,164,191,193,196). Whilst there is an overriding correlation between disease severity and polyQ tract length, the conformational changes and mechanisms of toxicity *in vivo* remains unclear for the nine polyQ diseases. There is a trend towards the flanking domain of the polyQ proteins being intrinsically fibrillogenic, as observed in the three polyQ proteins characterized *in vitro*

(8,191,206-208). Thus investigation of the involvement of flanking domains in both *in vitro* and *in vivo* aggregation is important to determine their role in modulating disease progression.

This study has contributed to this area by the further characterization of the multi-stage aggregation pathway of ataxin-3, in particular the involvement of the flanking Josephin domain. The folding and fibrillogenic pathways and link between them has been described in more detail, with the identification of partially unfolded conformations of Josephin which exist in equilibrium with the natively folded states. In addition, this study has determined that ataxin-3 follows the conformational change hypothesis with aggregation initiating from a partially unfolded intermediate which is on the folding pathway, and then the first stage of aggregation occurring via interactions of the Josephin domain. Analysis across the polyQ disease proteins in the future will allow identification of factors which dictate the characteristics of each disease.

The ability of ataxin-3 to aggregate via alternate pathways under conditions which may be encountered within the cell has also been highlighted by this study. Identification of the conformational space accessible to the polyQ proteins provides insight into the structural changes which occur *in vivo* under both physiological and stress conditions. Futhermore, characterization of the structural changes *in vitro* therefore provides the opportunity to screen inhibitors targeting the specific conformational change events of aggregation.

Chapter 7

REFERENCE LIST

1. Gething, M. J., and Sambrook, J. (1992) Protein folding in the cell *Nature* **355**, 33-45
2. Carrell, R. W., and Lomas, D. A. (1997) Conformational disease *Lancet* **350**, 134-138
3. Westermark, P., Benson, M. D., Buxbaum, J. N., Cohen, A. S., Frangione, B., Ikeda, S., Masters, C. L., Merlini, G., Saraiva, M. J., Sipe, J. D., and Nomenclature Committee of the International Society of, A. (2005) Amyloid: toward terminology clarification. Report from the Nomenclature Committee of the International Society of Amyloidosis *Amyloid* **12**, 1-4
4. Fujigasaki, H., Uchihara, T., Koyano, S., Iwabuchi, K., Yagishita, S., Makifuchi, T., Nakamura, A., Ishida, K., Toru, S., Hirai, S., Ishikawa, K., Tanabe, T., and Mizusawa, H. (2000) Ataxin-3 is translocated into the nucleus for the formation of intranuclear inclusions in normal and Machado-Joseph disease brains *Exp Neurol* **165**, 248-256
5. Sumner Makin, O., and Serpell, L. C. (2004) Structural characterisation of islet amyloid polypeptide fibrils *J Mol Biol* **335**, 1279-1288
6. Petkova, A. T., Ishii, Y., Balbach, J. J., Antzutkin, O. N., Leapman, R. D., Delaglio, F., and Tycko, R. (2002) A structural model for Alzheimer's beta -amyloid fibrils based on experimental constraints from solid state NMR *Proc Natl Acad Sci U S A* **99**, 16742-16747
7. Conway, K. A., Harper, J. D., and Lansbury, P. T. (1998) Accelerated in vitro fibril formation by a mutant alpha-synuclein linked to early-onset Parkinson disease *Nat Med* **4**, 1318-1320
8. Thakur, A. K., Jayaraman, M., Mishra, R., Thakur, M., Chellgren, V. M., IJ, L. B., Anjum, D. H., Kodali, R., Creamer, T. P., Conway, J. F., A, M. G., and Wetzel, R. (2009) Polyglutamine disruption of the huntingtin exon 1 N terminus triggers a complex aggregation mechanism *Nat Struct Mol Biol* **16**, 380-389

9. Soto, C. (2003) Unfolding the role of protein misfolding in neurodegenerative diseases *Nat Rev Neurosci* **4**, 49-60
10. Westermark, P., Benson, M. D., Buxbaum, J. N., Cohen, A. S., Frangione, B., Ikeda, S., Masters, C. L., Merlini, G., Saraiva, M. J., and Sipe, J. D. (2007) A primer of amyloid nomenclature *Amyloid* **14**, 179-183
11. Serpell, L. C., Sunde, M., Benson, M. D., Tennent, G. A., Pepys, M. B., and Fraser, P. E. (2000) The protofilament substructure of amyloid fibrils *J Mol Biol* **300**, 1033-1039
12. Groenning, M. (2009) Binding mode of Thioflavin T and other molecular probes in the context of amyloid fibrils-current status *J Chem Biol* **3**, 1-18
13. Jimenez, J. L., Nettleton, E. J., Bouchard, M., Robinson, C. V., Dobson, C. M., and Saibil, H. R. (2002) The protofilament structure of insulin amyloid fibrils *Proc Natl Acad Sci U S A* **99**, 9196-9201
14. Sunde, M., and Blake, C. (1997) The structure of amyloid fibrils by electron microscopy and X-ray diffraction *Adv Prot Chem* **50**, 123-159
15. Sunde, M., Serpell, L. C., Bartlam, M., Fraser, P. E., Pepys, M. B., and Blake, C. C. (1997) Common core structure of amyloid fibrils by synchrotron X-ray diffraction *J Mol Biol* **273**, 729-739
16. Dobson, C. M. (1999) Protein misfolding, evolution and disease *Trends Biochem Sci* **24**, 329-332
17. Fändrich, M., Fletcher, M. A., and Dobson, C. M. (2001) Amyloid fibrils from muscle myoglobin *Nature* **410**, 165-166
18. Wetzel, R. (2002) Ideas of order for amyloid fibril structure *Structure* **10**, 1031-1036
19. Jaroniec, C. P., MacPhee, C. E., Bajaj, V. S., McMahon, M. T., Dobson, C. M., and Griffin, R. G. (2004) High-resolution molecular structure of a peptide in an amyloid fibril determined by magic angle spinning NMR spectroscopy *Proc Natl Acad Sci U S A* **101**, 711-716
20. Ritter, C., Maddelein, M. L., Siemer, A. B., Luhrs, T., Ernst, M., Meier, B. H., Saupe, S. J., and Riek, R. (2005) Correlation of structural elements and infectivity of the HET-s prion *Nature* **435**, 844-848
21. Vilar, M., Chou, H. T., Luhrs, T., Maji, S. K., Riek-Loher, D., Verel, R., Manning, G., Stahlberg, H., and Riek, R. (2008) The fold of alpha-synuclein fibrils *Proc Natl Acad Sci U S A* **105**, 8637-8642
22. Balbach, J. J., Petkova, A. T., Oyler, N. A., Antzutkin, O. N., Gordon, D. J., Meredith, S. C., and Tycko, R. (2002) Supramolecular structure in full-length Alzheimer's beta-amyloid fibrils: evidence for a parallel beta-sheet organization from solid-state nuclear magnetic resonance *Biophys J* **83**, 1205-1216
23. Bu, Z., Shi, Y., Callaway, D. J., and Tycko, R. (2007) Molecular alignment within beta-sheets in Abeta(14-23) fibrils: solid-state NMR experiments and theoretical predictions *Biophys J* **92**, 594-602
24. Lansbury, P. T., Jr., Costa, P. R., Griffiths, J. M., Simon, E. J., Auger, M., Halverson, K. J., Kocisko, D. A., Hendsch, Z. S., Ashburn, T. T., Spencer, R. G., and et al. (1995) Structural model for the beta-amyloid fibril based on interstrand alignment of an antiparallel-sheet comprising a C-terminal peptide *Nat Struct Biol* **2**, 990-998

25. Makin, O. S., Atkins, E., Sikorski, P., Johansson, J., and Serpell, L. C. (2005) Molecular basis for amyloid fibril formation and stability *Proc Natl Acad Sci U S A* **102**, 315-320
26. Nelson, R., Sawaya, M. R., Balbirnie, M., Madsen, A. O., Riekel, C., Grothe, R., and Eisenberg, D. (2005) Structure of the cross-beta spine of amyloid-like fibrils *Nature* **435**, 773-778
27. Sawaya, M. R., Sambashivan, S., Nelson, R., Ivanova, M. I., Sievers, S. A., Apostol, M. I., Thompson, M. J., Balbirnie, M., Wiltzius, J. J., McFarlane, H. T., Madsen, A. O., Riekel, C., and Eisenberg, D. (2007) Atomic structures of amyloid cross-beta spines reveal varied steric zippers *Nature* **447**, 453-457
28. Jenkins, J., and Pickersgill, R. (2001) The architecture of parallel beta-helices and related folds *Prog Biophys Mol Biol* **77**, 111-175
29. Hoshino, M., Katou, H., Hagihara, Y., Hasegawa, K., Naiki, H., and Goto, Y. (2002) Mapping the core of the beta(2)-microglobulin amyloid fibril by H/D exchange *Nat Struct Biol* **9**, 332-336
30. Kunes, K. C., Clark, S. C., Cox, D. L., and Singh, R. R. (2008) Left handed beta helix models for mammalian prion fibrils *Prion* **2**, 81-90
31. Perutz, M. F., Finch, J. T., Berriman, J., and Lesk, A. (2002) Amyloid fibers are water-filled nanotubes *Proc Natl Acad Sci U S A* **99**, 5591-5595
32. Sikorski, P., and Atkins, E. (2005) New model for crystalline polyglutamine assemblies and their connection with amyloid fibrils *Biomacromolecules* **6**, 425-432
33. Jahn, T. R., Makin, O. S., Morris, K. L., Marshall, K. E., Tian, P., Sikorski, P., and Serpell, L. C. (2009) The common architecture of cross-beta amyloid *J Mol Biol*
34. Fandrich, M., and Dobson, C. M. (2002) The behaviour of polyamino acids reveals an inverse side chain effect in amyloid structure formation *Embo J* **21**, 5682-5690
35. Margittai, M., and Langen, R. (2008) Fibrils with parallel in-register structure constitute a major class of amyloid fibrils: molecular insights from electron paramagnetic resonance spectroscopy *Q Rev Biophys* **41**, 265-297
36. Gutekunst, C. A., Li, S. H., Yi, H., Mulroy, J. S., Kuemmerle, S., Jones, R., Rye, D., Ferrante, R. J., Hersch, S. M., and Li, X. J. (1999) Nuclear and neuropil aggregates in Huntington's disease: relationship to neuropathology *J Neurosci* **19**, 2522-2534
37. Terry, R. D., Masliah, E., Salmon, D. P., Butters, N., DeTeresa, R., Hill, R., Hansen, L. A., and Katzman, R. (1991) Physical basis of cognitive alterations in Alzheimer's disease: synapse loss is the major correlate of cognitive impairment *Ann Neurol* **30**, 572-580
38. Chiti, F., and Dobson, C. (2006) Protein misfolding, functional amyloid, and human disease. *Annu Rev Biochem* **75**, 333-366
39. Bitan, G., Kirkitadze, M. D., Lomakin, A., Vollers, S. S., Benedek, G. B., and Teplow, D. B. (2003) Amyloid ß-protein (Aß) assembly: Aß40 and Aß42 oligomerize through distinct pathways. *Proc Natl Acad Sci U S A* **100**, 330-335
40. Bouchard, M., Zurdo, J., Nettleton, E. J., Dobson, C. M., and Robinson, C. V. (2000) Formation of insulin amyloid fibrils followed by FTIR simultaneously with CD and electron microscopy *Protein Sci* **9**, 1960-1967

41. Bousset, L., Redeker, V., Decottignies, P., Dubois, S., Le Marechal, P., and Melki, R. (2004) Structural characterization of the fibrillar form of the yeast Saccharomyces cerevisiae prion Ure2p *Biochemistry* **43**, 5022-5032
42. Kayed, R., Head, E., Thompson, J. L., McIntire, T. M., Milton, S. C., Cotman, C. W., and Glabe, C. G. (2003) Common structure of soluble amyloid oligomers implies common mechanism of pathogenesis *Science* **300**, 486-489
43. Caughey, B., and Lansbury, P. T., Jr. (2003) Protofibrils, Pores, Fibrils, and Neurodegeneration: Separating the Responsible Protein Aggregates from the Innocent Bystanders *Ann Rev Neurosci* **26**, 267-298
44. Harper, J. D., Wong, S. S., Lieber, C. M., and Lansbury, P. T. (1997) Observation of metastable Abeta amyloid protofibrils by atomic force microscopy *Chem Biol* **4**, 119-125
45. Poirier, M. A., Li, H., Macosko, J., Cai, S., Amzel, M., and Ross, C. A. (2002) Huntingtin spheroids and protofibrils as precursors in polyglutamine fibrilization *J Biol Chem* **277**, 41032-41037
46. Uversky, V. N., and Fink, A. L. (2004) Conformational constraints for amyloid fibrillation: the importance of being unfolded *Biochim Biophys Acta* **1698**, 131-153
47. Petty, S. A., and Decatur, S. M. (2005) Intersheet rearrangement of polypeptides during nucleation of {beta}-sheet aggregates *Proc Natl Acad Sci U S A* **102**, 14272-14277
48. Crowther, D. C., Kinghorn, K. J., Miranda, E., Page, R., Curry, J. A., Duthie, F. A., Gubb, D. C., and Lomas, D. A. (2005) Intraneuronal Abeta, non-amyloid aggregates and neurodegeneration in a Drosophila model of Alzheimer's disease *Neuroscience* **132**, 123-135
49. Moechars, D., Dewachter, I., Lorent, K., Reverse, D., Baekelandt, V., Naidu, A., Tesseur, I., Spittaels, K., Haute, C. V., Checler, F., Godaux, E., Cordell, B., and Van Leuven, F. (1999) Early phenotypic changes in transgenic mice that overexpress different mutants of amyloid precursor protein in brain *J Biol Chem* **274**, 6483-6492
50. Reixach, N., Deechongkit, S., Jiang, X., Kelly, J. W., and Buxbaum, J. N. (2004) Tissue damage in the amyloidoses: Transthyretin monomers and nonnative oligomers are the major cytotoxic species in tissue culture *Proc Natl Acad Sci U S A* **101**, 2817-2822
51. Kitada, T., Asakawa, S., Hattori, N., Matsumine, H., Yamamura, Y., Minoshima, S., Yokochi, M., Mizuno, Y., and Shimizu, N. (1998) Mutations in the parkin gene cause autosomal recessive juvenile parkinsonism *Nature* **392**, 605-608
52. Spillantini, M. G., Schmidt, M. L., Lee, V. M., Trojanowski, J. Q., Jakes, R., and Goedert, M. (1997) Alpha-synuclein in Lewy bodies *Nature* **388**, 839-840
53. Bucciantini, M., Giannoni, E., Chiti, F., Baroni, F., Formigli, L., Zurdo, J., Taddel, N., Ramponi, G., Dobson, C. M., and Stefani, M. (2002) Inherent toxicity of aggregates implies a common mechanism for protein misfolding diseases *Nature* **416**, 507-511
54. Malisauskas, M., Ostman, J., Darinskas, A., Zamotin, V., Liutkevicius, E., Lundgren, E., and Morozova-Roche, L. A. (2005) Does the cytotoxic effect of transient amyloid oligomers from common equine lysozyme in vitro imply innate amyloid toxicity? *J Biol Chem* **280**, 6269-6275

55. Harper, J. D., and Lansbury, P. T., Jr. (1997) Models of amyloid seeding in Alzheimer's disease and scrapie: Mechanistic Truths and Physiological Consequences of the Time-Dependent Solubility of Amyloid Proteins *Ann Rev Biochem* **66**, 385-407
56. Chen, S., Ferrone, F. A., and Wetzel, R. (2002) Huntington's disease age-of-onset linked to polyglutamine aggregation nucleation *Proc Natl Acad Sci U S A* **99**, 11884-11889
57. Xue, W. F., Homans, S. W., and Radford, S. E. (2008) Systematic analysis of nucleation-dependent polymerization reveals new insights into the mechanism of amyloid self-assembly *Proc Natl Acad Sci U S A* **105**, 8926-8931
58. Collins, S. R., Douglass, A., Vale, R. D., and Weissman, J. S. (2004) Mechanism of prion propagation: amyloid growth occurs by monomer addition *PLoS Biol* **2**, e321
59. Serio, T. R., Cashikar, A. G., Kowal, A. S., Sawicki, G. J., Moslehi, J. J., Serpell, L., Arnsdorf, M. F., and Lindquist, S. L. (2000) Nucleated conformational conversion and the replication of conformational information by a prion determinant *Science* **289**, 1317-1321
60. Ferrone, F. (1999) Analysis of protein aggregation kinetics *Methods Enzymol* **309**, 256-274
61. Krebs, M. R., Morozova-Roche, L. A., Daniel, K., Robinson, C. V., and Dobson, C. M. (2004) Observation of sequence specificity in the seeding of protein amyloid fibrils *Protein Sci* **13**, 1933-1938
62. Tanaka, M., Chien, P., Yonekura, K., and Weissman, J. S. (2005) Mechanism of cross-species prion transmission: an infectious conformation compatible with two highly divergent yeast prion proteins *Cell* **121**, 49-62
63. Wright, C. F., Teichmann, S. A., Clarke, J., and Dobson, C. M. (2005) The importance of sequence diversity in the aggregation and evolution of proteins *Nature* **438**, 878-881
64. Wolynes, P. G. (2005) Energy landscapes and solved protein-folding problems *Philos Transact A Math Phys Eng Sci* **363**, 453-464; discussion 464-457
65. Anfinsen, C. B. (1973) Principles that govern the folding of protein chains *Science* **181**, 223-230
66. Dinner, A. R., Sali, A., Smith, L. J., Dobson, C. M., and Karplus, M. (2000) Understanding protein folding via free-energy surfaces from theory and experiment *Trends Biochem Sci* **25**, 331-339
67. Uversky, V. N. (2008) Amyloidogenesis of natively unfolded proteins *Curr Alzheimer Res* **5**, 260-287
68. Kelly, J. W. (1998) The alternative conformations of amyloidogenic proteins and their multi-step assembly pathways *Curr Opin Struct Biol* **8**, 101-106
69. Chow, M. K., Ellisdon, A. M., Cabrita, L. D., and Bottomley, S. P. (2004) Polyglutamine expansion in ataxin-3 does not affect protein stability: implications for misfolding and disease *J Biol Chem* **279**, 47643-47651
70. Plakoutsi, G., Taddei, N., Stefani, M., and Chiti, F. (2004) Aggregation of the Acylphosphatase from Sulfolobus solfataricus: the folded and partially unfolded states can both be precursors for amyloid formation *J Biol Chem* **279**, 14111-14119

71. Chiti, F., Taddei, N., Baroni, F., Capanni, C., Stefani, M., Ramponi, G., and Dobson, C. M. (2002) Kinetic partitioning of protein folding and aggregation *Nat Struct Biol* **9**, 137-143
72. Tartaglia, G. G., Pawar, A. P., Campioni, S., Dobson, C. M., Chiti, F., and Vendruscolo, M. (2008) Prediction of aggregation-prone regions in structured proteins *J Mol Biol* **380**, 425-436
73. Bertoncini, C. W., Fernandez, C. O., Griesinger, C., Jovin, T. M., and Zweckstetter, M. (2005) Familial mutants of alpha-synuclein with increased neurotoxicity have a destabilized conformation *J Biol Chem* **280**, 30649-30652
74. Chiti, F., and Dobson, C. M. (2009) Amyloid formation by globular proteins under native conditions *Nat Chem Biol* **5**, 15-22
75. Booth, D. R., Sunde, M., Bellotti, V., Robinson, C. V., Hutchinson, W. L., Fraser, P. E., Hawkins, P. N., Dobson, C. M., Radford, S. E., Blake, C. C., and Pepys, M. B. (1997) Instability, unfolding and aggregation of human lysozyme variants underlying amyloid fibrillogenesis *Nature* **385**, 787-793
76. Liu, K., Kelly, J. W., and Wemmer, D. E. (2002) Native state hydrogen exchange study of suppressor and pathogenic variants of transthyretin *Journal of Molecular Biology* **320**, 821-832
77. Takano, K., Funahashi, J., and Yutani, K. (2001) The stability and folding process of amyloidogenic mutant human lysozymes *Eur J Biochem* **268**, 155-159
78. Diaz-Hernandez, M., Moreno-Herrero, F., Gomez-Ramos, P., Moran, M. A., Ferrer, I., Baro, A. M., Avila, J., Hernandez, F., and Lucas, J. J. (2004) Biochemical, ultrastructural, and reversibility studies on huntingtin filaments isolated from mouse and human brain *J Neurosci* **24**, 9361-9371
79. Takahashi, T., Kikuchi, S., Katada, S., Nagai, Y., Nishizawa, M., and Onodera, O. (2008) Soluble polyglutamine oligomers formed prior to inclusion body formation are cytotoxic *Hum. Mol. Genet.* **17**, 345-356
80. Chai, Y., Koppenhafer, S. L., Bonini, N. M., and Paulson, H. L. (1999) Analysis of the role of heat shock protein (Hsp) molecular chaperones in polyglutamine disease *J Neurosci* **19**, 10338-10347
81. Chai, Y., Koppenhafer, S. L., Shoesmith, S. J., Perez, M. K., and Paulson, H. L. (1999) Evidence for proteasome involvement in polyglutamine disease: localization to nuclear inclusions in SCA3/MJD and suppression of polyglutamine aggregation in vitro *Hum Mol Genet* **8**, 673-682
82. Stenoien, D. L., Mielke, M., and Mancini, M. A. (2002) Intranuclear ataxin1 inclusions contain both fast- and slow-exchanging components *Nat Cell Biol* **4**, 806-810
83. Klockgether, T., Wullner, U., Spauschus, A., and Evert, B. (2000) The molecular biology of the autosomal-dominant cerebellar ataxias *Mov Disord* **15**, 604-612
84. Gusella, J. F., and MacDonald, M. E. (2000) Molecular Genetics: Unmasking polyglutamine triggers in neurodegenerative disease *Nat Rev Neurosci* **1**, 109 -115
85. Chung, M. Y., Ranum, L. P., Duvick, L. A., Servadio, A., Zoghbi, H. Y., and Orr, H. T. (1993) Evidence for a mechanism predisposing to intergenerational CAG repeat instability in spinocerebellar ataxia type I *Nat Genet* **5**, 254-258

86. Lahiri, M., Gustafson, T. L., Majors, E. R., and Freudenreich, C. H. (2004) Expanded CAG repeats activate the DNA damage checkpoint pathway *Mol Cell* **15**, 287-293
87. Trottier, Y., Biancalana, V., and Mandel, J. L. (1994) Instability of CAG repeats in Huntington's disease: relation to parental transmission and age of onset *J Med Genet* **31**, 377-382
88. Paulson, H. L. (1999) Protein fate in neurodegenerative proteinopathies: polyglutamine diseases join the (mis)fold *Am J Hum Genet* **64**, 339-345
89. Nahhas, F. A., Garbern, J., Krajewski, K. M., Roa, B. B., and Feldman, G. L. (2005) Juvenile onset Huntington disease resulting from a very large maternal expansion *Am J Med Genet A* **137A**, 328-331
90. Group, T. H. s. D. C. R. (1993) A novel gene containing a trinucleotide repeat that is expanded and unstable on Huntington's disease chromosomes. *Cell* **72**, 971-983
91. Matilla, T., Volpini, V., Genis, D., Rosell, J., Corral, J., Davalos, A., Molins, A., and Estivill, X. (1993) Presymptomatic analysis of spinocerebellar ataxia type 1 (SCA1) via the expansion of the SCA1 CAG-repeat in a large pedigree displaying anticipation and parental male bias *Hum Mol Genet* **2**, 2123-2128
92. Ranum, L. P., Chung, M. Y., Banfi, S., Bryer, A., Schut, L. J., Ramesar, R., Duvick, L. A., McCall, A., Subramony, S. H., Goldfarb, L., and et al. (1994) Molecular and clinical correlations in spinocerebellar ataxia type I: evidence for familial effects on the age at onset *Am J Hum Genet* **55**, 244-252
93. Pulst, S. M., Santos, N., Wang, D., Yang, H., Huynh, D., Velazquez, L., and Figueroa, K. P. (2005) Spinocerebellar ataxia type 2: polyQ repeat variation in the CACNA1A calcium channel modifies age of onset *Brain* **128**, 2297-2303
94. Kawaguchi, Y., Okamoto, T., Taniwaki, M., Aizawa, M., Inoue, M., Katayama, S., Kawakami, H., Nakamura, S., Nishimura, M., Akiguchi, I., Kimura, J., Narumiya, S., and Kakizuka, A. (1994) CAG expansions in a novel gene for Machado-Joseph disease at chromosome 14q32.1 *Nat Genet* **8**, 221-228
95. Padiath, Q. S., Srivastava, A. K., Roy, S., Jain, S., and Brahmachari, S. K. (2005) Identification of a novel 45 repeat unstable allele associated with a disease phenotype at the MJD1/SCA3 locus *Am J Med Genet B Neuropsychiatr Genet* **133**, 124-126
96. Zhuchenko, O., Bailey, J., Bonnen, P., Ashizawa, T., Stockton, D. W., Amos, C., Dobyns, W. B., Subramony, S. H., Zoghbi, H. Y., and Lee, C. C. (1997) Autosomal dominant cerebellar ataxia (SCA6) associated with small polyglutamine expansions in the alpha 1A-voltage-dependent calcium channel *Nat Genet* **15**, 62-69
97. Benton, C. S., de Silva, R., Rutledge, S. L., Bohlega, S., Ashizawa, T., and Zoghbi, H. Y. (1998) Molecular and clinical studies in SCA-7 define a broad clinical spectrum and the infantile phenotype *Neurology* **51**, 1081-1086
98. David, G., Abbas, N., Stevanin, G., Durr, A., Yvert, G., Cancel, G., Weber, C., Imbert, G., Saudou, F., Antoniou, E., Drabkin, H., Gemmill, R., Giunti, P., Benomar, A., Wood, N., Ruberg, M., Agid, Y., Mandel, J. L., and Brice, A. (1997) Cloning of the SCA7 gene reveals a highly unstable CAG repeat expansion *Nat Genet* **17**, 65-70
99. Koide, R., Kobayashi, S., Shimohata, T., Ikeuchi, T., Maruyama, M., Saito, M., Yamada, M., Takahashi, H., and Tsuji, S. (1999) A neurological disease caused by

an expanded CAG trinucleotide repeat in the TATA-binding protein gene: a new polyglutamine disease? *Hum Mol Genet* **8**, 2047-2053

100. Nakamura, K., Jeong, S. Y., Uchihara, T., Anno, M., Nagashima, K., Nagashima, T., Ikeda, S., Tsuji, S., and Kanazawa, I. (2001) SCA17, a novel autosomal dominant cerebellar ataxia caused by an expanded polyglutamine in TATA-binding protein *Hum Mol Genet* **10**, 1441-1448
101. Komure, O., Sano, A., Nishino, N., Yamauchi, N., Ueno, S., Kondoh, K., Sano, N., Takahashi, M., Murayama, N., Kondo, I., and et al. (1995) DNA analysis in hereditary dentatorubral-pallidoluysian atrophy: correlation between CAG repeat length and phenotypic variation and the molecular basis of anticipation *Neurology* **45**, 143-149
102. La Spada, A. R., Wilson, E. M., Lubahn, D. B., Harding, A. E., and Fischbeck, K. H. (1991) Androgen receptor gene mutations in X-linked spinal and bulbar muscular atrophy *Nature* **352**, 77-79
103. Katsuno, M., Adachi, H., Doyu, M., Minamiyama, M., Sang, C., Kobayashi, Y., Inukai, A., and Sobue, G. (2003) Leuprorelin rescues polyglutamine-dependent phenotypes in a transgenic mouse model of spinal and bulbar muscular atrophy *Nat Med* **9**, 768-775
104. Bichelmeier, U., Schmidt, T., Hubener, J., Boy, J., Ruttiger, L., Habig, K., Poths, S., Bonin, M., Knipper, M., Schmidt, W. J., Wilbertz, J., Wolburg, H., Laccone, F., and Riess, O. (2007) Nuclear localization of ataxin-3 is required for the manifestation of symptoms in SCA3: in vivo evidence *J Neurosci* **27**, 7418-7428
105. Klement, I. A., Skinner, P. J., Kaytor, M. D., Yi, H., Hersch, S. M., Clark, H. B., Zoghbi, H. Y., and Orr, H. T. (1998) Ataxin-1 nuclear localization and aggregation: Role in polyglutamine-induced disease in SCA1 transgenic mice *Cell* **95**, 41-53
106. Peters, M. F., Nucifora, F. C., Jr., Kushi, J., Seaman, H. C., Cooper, J. K., Herring, W. J., Dawson, V. L., Dawson, T. M., and Ross, C. A. (1999) Nuclear targeting of mutant Huntingtin increases toxicity *Mol Cell Neurosci* **14**, 121-128
107. Schilling, G., Savonenko, A. V., Klevytska, A., Morton, J. L., Tucker, S. M., Poirier, M., Gale, A., Chan, N., Gonzales, V., Slunt, H. H., Coonfield, M. L., Jenkins, N. A., Copeland, N. G., Ross, C. A., and Borchelt, D. R. (2004) Nuclear-targeting of mutant huntingtin fragments produces Huntington's disease-like phenotypes in transgenic mice *Hum Mol Genet* **13**, 1599-1610
108. Toyoshima, I., Sugawara, M., Kato, K., Wada, C., Shimohata, T., Koide, R., Onodera, O., and Tsuji, S. (2002) Time course of polyglutamine aggregate body formation and cell death: enhanced growth in nucleus and an interval for cell death *J Neurosci Res* **68**, 442-448
109. Li, M., Chevalier-Larsen, E. S., Merry, D. E., and Diamond, M. I. (2007) Soluble androgen receptor oligomers underlie pathology in a mouse model of SBMA *J Biol Chem* **282** 3157-3164
110. Menon, R. P., and Pastore, A. (2006) Expansion of amino acid homo-sequences in proteins: insights into the role of amino acid homo-polymers and of the protein context in aggregation *Cell Mol Life Sci* **63**, 1677-1685
111. Lee, W. C., Yoshihara, M., and Littleton, J. T. (2004) Cytoplasmic aggregates trap polyglutamine-containing proteins and block axonal transport in a Drosophila model of Huntington's disease *Proc Natl Acad Sci U S A* **101**, 3224-3229

112. Iwata, A., Christianson, J. C., Bucci, M., Ellerby, L. M., Nukina, N., Forno, L. S., and Kopito, R. R. (2005) Increased susceptibility of cytoplasmic over nuclear polyglutamine aggregates to autophagic degradation *Proc Natl Acad Sci U S A* **102**, 13135-13140
113. Menzies, F. M., Huebener, J., Renna, M., Bonin, M., Riess, O., and Rubinsztein, D. C. (2010) Autophagy induction reduces mutant ataxin-3 levels and toxicity in a mouse model of spinocerebellar ataxia type 3 *Brain* **133**, 93-104
114. Montie, H. L., and Merry, D. E. (2009) Autophagy and access: understanding the role of androgen receptor subcellular localization in SBMA *Autophagy* **5**, 1194-1197
115. Williams, A., Jahreiss, L., Sarkar, S., Saiki, S., Menzies, F. M., Ravikumar, B., and Rubinsztein, D. C. (2006) Aggregate-prone proteins are cleared from the cytosol by autophagy: therapeutic implications *Curr Top Dev Biol* **76**, 89-101
116. Kegel, K. B., Sapp, E., Alexander, J., Valencia, A., Reeves, P., Li, X., Masso, N., Sobin, L., Aronin, N., and DiFiglia, M. (2009) Polyglutamine expansion in huntingtin alters its interaction with phospholipids *J Neurochem* **110**, 1585-1597
117. Kegel, K. B., Sapp, E., Yoder, J., Cuiffo, B., Sobin, L., Kim, Y. J., Qin, Z. H., Hayden, M. R., Aronin, N., Scott, D. L., Isenberg, G., Goldmann, W. H., and DiFiglia, M. (2005) Huntingtin associates with acidic phospholipids at the plasma membrane *J Biol Chem* **280**, 36464-36473
118. Kegel, K. B., Schewkunow, V., Sapp, E., Masso, N., Wanker, E. E., DiFiglia, M., and Goldmann, W. H. (2009) Polyglutamine expansion in huntingtin increases its insertion into lipid bilayers *Biochem Biophys Res Commun* **387**, 472-475
119. Hirakura, Y., Azimov, R., Azimova, R., and Kagan, B. L. (2000) Polyglutamine-induced ion channels: a possible mechanism for the neurotoxicity of Huntington and other CAG repeat diseases *J Neurosci Res* **60**, 490-494
120. Kagan, B. L., Hirakura, Y., Azimov, R., and Azimova, R. (2001) The channel hypothesis of Huntington's disease *Brain Res Bull* **56**, 281-284
121. Jeub, M., Herbst, M., Spauschus, A., Fleischer, H., Klockgether, T., Wuellner, U., and Evert, B. O. (2006) Potassium channel dysfunction and depolarized resting membrane potential in a cell model of SCA3 *Exp Neurol* **201**, 182-192
122. Johansson, J., Forsgren, L., Sandgren, O., Brice, A., Holmgren, G., and Holmberg, M. (1998) Expanded CAG repeats in Swedish spinocerebellar ataxia type 7 (SCA7) patients: effect of CAG repeat length on the clinical manifestation *Hum Mol Genet* **7**, 171-176
123. Goldberg, Y. P., Nicholson, D. W., Rasper, D. M., Kalchman, M. A., Koide, H. B., Graham, R. K., Bromm, M., Kazemi-Esfarjani, P., Thornberry, N. A., Vaillancourt, J. P., and Hayden, M. R. (1996) Cleavage of huntingtin by apopain, a proapoptotic cysteine protease, is modulated by the polyglutamine tract *Nat Genet* **13**, 442-449
124. Haacke, A., Broadley, S. A., Boteva, R., Tzvetkov, N., Hartl, F. U., and Breuer, P. (2006) Proteolytic cleavage of polyglutamine-expanded ataxin-3 is critical for aggregation and sequestration of non-expanded ataxin-3 *Hum Mol Genet* **15**, 555-568
125. Orr, H. T., and Zoghbi, H. Y. (2007) Trinucleotide repeat disorders *Annu Rev Neurosci* **30**, 575-621

126. Yang, W., Dunlap, J. R., Andrews, R. B., and Wetzel, R. (2002) Aggregated polyglutamine peptides delivered to nuclei are toxic to mammalian cells *Hum Mol Genet* **11**, 2905-2917
127. Chen, S., Berthelier, V., Hamilton, J. B., O'Nuallain, B., and Wetzel, R. (2002) Amyloid-like features of polyglutamine aggregates and their assembly kinetics *Biochemistry* **41**, 7391-7399
128. Becher, M. W., Kotzuk, J. A., Sharp, A. H., Davies, S. W., Bates, G. P., Price, D. L., and Ross, C. A. (1998) Intranuclear neuronal inclusions in Huntington's disease and Dentatorubral and Pallidoluysian atrophy: Correlation between the density of Inclusions and triplet repeat length *Neurobiology of Disease* **4**, 387-397
129. DiFiglia, M., Sapp, E., Chase, K. O., Davies, S. W., Bates, G. P., Vonsattel, J. P., and Aronin, N. (1997) Aggregation of Huntingtin in neuronal intranuclear inclusions and dystrophic neurites in brain *Science* **277**, 1990-1993
130. Lunkes, A., and Mandel, J. L. (1998) A cellular model that recapitulates major pathogenic steps of Huntington's disease *Hum Mol Genet* **7**, 1355-1361
131. Mangiarini, L., Sathasivam, K., Seller, M., Cozens, B., Harper, A., Hetherington, C., Lawton, M., Trottier, Y., Lehrach, H., Davies, S. W., and Bates, G. P. (1996) Exon 1 of the HD Gene with an Expanded CAG Repeat Is Sufficient to Cause a Progressive Neurological Phenotype in Transgenic Mice *Cell* **87**, 493-506
132. Wellington, C. L., Ellerby, L. M., Hackam, A. S., Margolis, R. L., Trifiro, M. A., Singaraja, R., McCutcheon, K., Salvesen, G. S., Propp, S. S., Bromm, M., Rowland, K. J., Zhang, T., Rasper, D., Roy, S., Thornberry, N., Pinsky, L., Kakizuka, A., Ross, C. A., Nicholson, D. W., Bredesen, D. E., and Hayden, M. R. (1998) Caspase cleavage of gene products associated with triplet expansion disorders generates truncated fragments containing the polyglutamine tract *J Biol Chem* **273**, 9158-9167
133. Gafni, J., Hermel, E., Young, J. E., Wellington, C. L., Hayden, M. R., and Ellerby, L. M. (2004) Inhibition of calpain cleavage of huntingtin reduces toxicity: accumulation of calpain/caspase fragments in the nucleus *J Biol Chem* **279**, 20211-20220
134. Bowman, A. B., Yoo, S. Y., Dantuma, N. P., and Zoghbi, H. Y. (2005) Neuronal dysfunction in a polyglutamine disease model occurs in the absence of ubiquitin-proteasome system impairment and inversely correlates with the degree of nuclear inclusion formation *Hum Mol Genet* **14**, 679-691
135. Evert, B. O., Schelhaas, J., Fleischer, H., de Vos, R. A., Brunt, E. R., Stenzel, W., Klockgether, T., and Wullner, U. (2006) Neuronal intranuclear inclusions, dysregulation of cytokine expression and cell death in spinocerebellar ataxia type 3 *Clin Neuropathol* **25**, 272-281
136. Rub, U., de Vos, R. A., Brunt, E. R., Sebesteny, T., Schols, L., Auburger, G., Bohl, J., Ghebremedhin, E., Gierga, K., Seidel, K., den Dunnen, W., Heinsen, H., Paulson, H., and Deller, T. (2006) Spinocerebellar ataxia type 3 (SCA3): thalamic neurodegeneration occurs independently from thalamic ataxin-3 immunopositive neuronal intranuclear inclusions *Brain Pathol* **16**, 218-227
137. Taylor, J., Grote, S. K., Xia, J., Vandelft, M., Graczyk, J., Ellerby, L. M., La Spada, A. R., and Truant, R. (2006) Ataxin-7 can export from the nucleus via a conserved exportin-dependent signal *J Biol Chem* **281**, 2730-2739

138. Yoshizawa, T., Yoshida, H., and Shoji, S. (2001) Differential susceptibility of cultured cell lines to aggregate formation and cell death produced by the truncated Machado-Joseph disease gene product with an expanded polyglutamine stretch *Brain Res Bull* **56**, 349-352
139. Arrasate, M., Mitra, S., Schweitzer, E. S., Segal, M. R., and Finkbeiner, S. (2004) Inclusion body formation reduces levels of mutant huntingtin and the risk of neuronal death *Nature* **431**, 805-810
140. Nagai, Y. (2008) Toxic conformer of the polyglutamine protein *Tanpakushitsu Kakusan Koso* **53**, 235-241
141. Goti, D., Katzen, S. M., Mez, J., Kurtis, N., Kiluk, J., Ben-Haiem, L., Jenkins, N. A., Copeland, N. G., Kakizuka, A., Sharp, A. H., Ross, C. A., Mouton, P. R., and Colomer, V. (2004) A mutant ataxin-3 putative-cleavage fragment in brains of Machado-Joseph disease patients and transgenic mice is cytotoxic above a critical concentration *J Neurosci* **24**, 10266-10279
142. Li, S. H., and Li, X. J. (1998) Aggregation of N-terminal huntingtin is dependent on the length of its glutamine repeats *Hum. Mol. Genet.* **7**, 777-782
143. Merry, D. E., Kobayashi, Y., Bailey, C. K., Taye, A. A., and Fischbeck, K. H. (1998) Cleavage, aggregation and toxicity of the expanded androgen receptor in spinal and bulbar muscular atrophy *Hum Mol Genet* **7**, 693-701
144. Reddy, P. H., Williams, M., Charles, V., Garrett, L., Pike-Buchanan, L., Whetsell, W. O., Jr., Miller, G., and Tagle, D. A. (1998) Behavioural abnormalities and selective neuronal loss in HD transgenic mice expressing mutated full-length HD cDNA *Nat Genet* **20**, 198-202
145. Schöls, L., Amoiridis, G., Büttner, T., Przuntek, H., Epplen, J. T., and Riess, O. (1997) Autosomal dominant cerebellar ataxia: Phenotypic differences in genetically defined subtypes? *Annals of Neurology* **42**, 924-932
146. Schols, L., Amoiridis, G., Langkafel, M., Buttner, T., Przuntek, H., Riess, O., Vieira-Saecker, A. M., and Epplen, J. T. (1995) Machado-Joseph disease mutations as the genetic basis of most spinocerebellar ataxias in Germany *J Neurol Neurosurg Psychiatry* **59**, 449-450
147. Silveira, I., Coutinho, P., Maciel, P., Gaspar, C., Hayes, S., Dias, A., Guimaraes, J., Loureiro, L., Sequeiros, J., and Rouleau, G. A. (1998) Analysis of SCA1, DRPLA, MJD, SCA2, and SCA6 CAG repeats in 48 Portuguese ataxia families *Am J Med Genet* **81**, 134-138
148. Nakano, K. K., Dawson, D. M., and Spence, A. (1972) Machado disease: A hereditary ataxia in Portuguese emigrants to Massachusetts *Neurology* **22**, 49-55
149. Woods, B. T., and Schaumburg, H. H. (1972) Nigro-spino-dentatal degeneration with nuclear ophthalmoplegia *J Neurosci* **17**, 149-166
150. Burt, T., Currie, B., Kilburn, C., Lethlean, A. K., Dempsey, K., Blair, I., Cohen, A., and Nicholson, G. (1996) Machado-Joseph disease in east Arnhem Land, Australia: chromosome 14q32.1 expanded repeat confirmed in four families *Neurology* **46**, 1118-1122
151. Gaspar, C., Lopes-Cendes, I., Hayes, S., Goto, J., Arvidsson, K., Dias, A., Silveira, I., Maciel, P., Coutinho, P., Lima, M., Zhou, Y. X., Soong, B. W., Watanabe, M., Giunti, P., Stevanin, G., Riess, O., Sasaki, H., Hsieh, M., Nicholson, G. A., Brunt, E., Higgins, J. J., Lauritzen, M., Tranebjaerg, L., Volpini, V., Wood, N., Ranum, L.,

Tsuji, S., Brice, A., Sequeiros, J., and Rouleau, G. A. (2001) Ancestral origins of the Machado-Joseph disease mutation: a worldwide haplotype study *Am J Hum Genet* **68**, 523-528

152. Vale, J., Bugalho, P., Silveira, I., Sequeiros, J., Guimaraes, J., and Coutinho, P. (2009) Autosomal dominant cerebellar ataxia: frequency analysis and clinical characterization of 45 families from Portugal *Eur J Neurol*
153. Iughetti, P., Zatz, M., Bueno, M. R., and Marie, S. K. (1996) Different origins of mutations at the Machado-Joseph locus (MJD1) *J Med Genet* **33**, 439
154. Stevanin, G., Cancel, G., Didierjean, O., Durr, A., Abbas, N., Cassa, E., Feingold, J., Agid, Y., and Brice, A. (1995) Linkage disequilibrium at the Machado-Joseph disease/spinal cerebellar ataxia 3 locus: evidence for a common founder effect in French and Portuguese-Brazilian families as well as a second ancestral Portuguese-Azorean mutation *Am J Hum Genet* **57**, 1247-1250
155. Burk, K., Abele, M., Fetter, M., Dichgans, J., Skalej, M., Laccone, F., Didierjean, O., Brice, A., and Klockgether, T. (1996) Autosomal dominant cerebellar ataxia type I clinical features and MRI in families with SCA1, SCA2 and SCA3 *Brain* **119 (Pt 5)**, 1497-1505
156. Kawaguchi, Y., Okamoto, T., Taniwaki, M., Aizawa, M., Inoue, M., Katayama, S., Kawakami, H., Nakamura, S., Nishimura, M., Akiguchi, I., and et al. (1994) CAG expansions in a novel gene for Machado-Joseph disease at chromosome 14q32.1 *Nat Genet* **8**, 221-228
157. Takiyama, Y., Nishzawa, M., Tanaka, H., Kawashima, S., Sakamoto, H., Karube, Y., Shimazaki, H., Soutome, M., ENdo, K., Ohta, S., Kagawa, Y., Kanazawa, I., Mizuno, Y., Yoshida, M., Yuasa, T., Horikawa, Y., Oyanagi, K., Nagai, H., Kondo, T., Inuzuka, T., Onodera, O., and Tsuji, S. (1993) The gene for Machado-Joseph disease maps to human chromosome 14q. *Nat Genet* **4**, 300-304
158. Carvalho, D. R., La Rocque-Ferreira, A., Rizzo, I. M., Imamura, E. U., and Speck-Martins, C. E. (2008) Homozygosity enhances severity in spinocerebellar ataxia type 3 *Pediatr Neurol* **38**, 296-299
159. Rosenberg, R. N. (1992) Machado-Joseph disease: an autosomal dominant motor system degeneration *Mov Disord* **7**, 193-203
160. Rub, U., Brunt, E. R., and Deller, T. (2008) New insights into the pathoanatomy of spinocerebellar ataxia type 3 (Machado-Joseph disease) *Curr Opin Neurol* **21**, 111-116
161. Schmidt, T., Landwehrmeyer, G. B., Schmitt, I., Trottier, Y., Auburger, G., Laccone, F., Klockgether, T., Volpel, M., Epplen, J. T., Schols, L., and Riess, O. (1998) An isoform of ataxin-3 accumulates in the nucleus of neuronal cells in affected brain regions of SCA3 patients *Brain Pathol* **8**, 669-679
162. Berke, S. J., Chai, Y., Marrs, G. L., Wen, H., and Paulson, H. L. (2005) Defining the role of ubiquitin-interacting motifs in the polyglutamine disease protein, ataxin-3 *J Biol Chem* **280**, 32026-32034
163. Chow, M. K., Paulson, H. L., and Bottomley, S. P. (2004) Destabilization of a non-pathological variant of ataxin-3 results in fibrillogenesis via a partially folded intermediate: a model for misfolding in polyglutamine disease *J Mol Biol* **335**, 333-341

164. Gales, L., Cortes, L., Almeida, C., Melo, C. V., do Carmo Costa, M., Maciel, P., Clarke, D. T., Damas, A. M., and Macedo-Ribeiro, S. (2005) Towards a structural understanding of the fibrillization pathway in Machado-Joseph's disease: trapping early oligomers of non-expanded ataxin-3 *J Mol Biol* **353**, 642-654
165. Mao, Y., Senic-Matuglia, F., Di Fiore, P. P., Polo, S., Hodsdon, M. E., and De Camilli, P. (2005) Deubiquitinating function of ataxin-3: insights from the solution structure of the Josephin domain *Proc Natl Acad Sci U S A* **102**, 12700-12705
166. Nicastro, G., Menon, R. P., Masino, L., Knowles, P. P., McDonald, N. Q., and Pastore, A. (2005) The solution structure of the Josephin domain of ataxin-3: structural determinants for molecular recognition *Proc Natl Acad Sci U S A* **102**, 10493-10498
167. Chai, Y., Berke, S. S., Cohen, R. E., and Paulson, H. L. (2004) Poly-ubiquitin binding by the polyglutamine disease protein ataxin-3 links its normal function to protein surveillance pathways *J Biol Chem* **279**, 3605-3611
168. Winborn, B. J., Travis, S. M., Todi, S. V., Scaglione, K. M., Xu, P., Williams, A. J., Cohen, R. E., Peng, J., and Paulson, H. L. (2008) The deubiquitinating enzyme ataxin-3, a polyglutamine disease protein, edits Lys63 linkages in mixed linkage ubiquitin chains *J Biol Chem* **283**, 26436-26443
169. Nicastro, G., Masino, L., Esposito, V., Menon, R. P., De Simone, A., Fraternali, F., and Pastore, A. (2009) Josephin domain of ataxin-3 contains two distinct ubiquitin-binding sites *Biopolymers* **91**, 1203-1214
170. Warrick, J. M., Morabito, L. M., Bilen, J., Gordesky-Gold, B., Faust, L. Z., Paulson, H. L., and Bonini, N. M. (2005) Ataxin-3 suppresses polyglutamine neurodegeneration in Drosophila by a ubiquitin-associated mechanism *Mol Cell* **18**, 37-48
171. Wang, G., Sawai, N., Kotliarova, S., Kanazawa, I., and Nukina, N. (2000) Ataxin-3, the MJD1 gene product, interacts with the two human homologs of yeast DNA repair protein RAD23, HHR23A and HHR23B *Hum Mol Genet* **9**, 1795-1803
172. Boeddrich, A., Gaumer, S., Haacke, A., Tzvetkov, N., Albrecht, M., Evert, B. O., Muller, E. C., Lurz, R., Breuer, P., Schugardt, N., Plassmann, S., Xu, K., Warrick, J. M., Suopanki, J., Wullner, U., Frank, R., Hartl, U. F., Bonini, N. M., and Wanker, E. E. (2006) An arginine/lysine-rich motif is crucial for VCP/p97-mediated modulation of ataxin-3 fibrillogenesis *Embo J* **25**, 1547-1558
173. Zhong, X., and Pittman, R. N. (2006) Ataxin-3 binds VCP/p97 and regulates retrotranslocation of ERAD substrates *Hum Mol Genet* **15**, 2409-2420
174. Berke, S. J., Schmied, F. A., Brunt, E. R., Ellerby, L. M., and Paulson, H. L. (2004) Caspase-mediated proteolysis of the polyglutamine disease protein ataxin-3 *J Neurochem* **89**, 908-918
175. Cemal, C. K., Carroll, C. J., Lawrence, L., Lowrie, M. B., Ruddle, P., Al-Mahdawi, S., King, R. H. M., Pook, M. A., Huxley, C., and Chamberlain, S. (2002) YAC transgenic mice carrying pathological alleles of the MJD1 locus exhibit a mild and slowly progressive cerebellar deficit *Hum Mol Genet* **11**, 1075-1094
176. Paulson, H. L., Das, S. S., Crino, P. B., Perez, M. K., Patel, S. C., Gotsdiner, D., Fischbeck, K. H., and Pittman, R. N. (1997) Machado-Joseph disease gene product is a cytoplasmic protein widely expressed in brain *Ann Neurol* **41**, 453-462

177. Haacke, A., Hartl, F. U., and Breuer, P. (2007) Calpain inhibition is sufficient to suppress aggregation of polyglutamine-expanded ataxin-3 *J Biol Chem* **282**, 18851-18856
178. Paulson, H. L., Perez, M. K., Trottier, Y., Trojanowski, J. Q., Subramony, S. H., Das, S. S., Vig, P., Mandel, J. L., Fischbeck, K. H., and Pittman, R. N. (1997) Intranuclear inclusions of expanded polyglutamine protein in spinocerebellar ataxia type 3 *Neuron* **19**, 333-344
179. Chai, Y., Wu, L., Griffin, J. D., and Paulson, H. L. (2001) The role of protein composition in specifying nuclear inclusion formation in polyglutamine disease *J Biol Chem* **276**, 44889-44897
180. Warrick, J. M., Chan, H. Y., Gray-Board, G. L., Chai, Y., Paulson, H. L., and Bonini, N. M. (1999) Suppression of polyglutamine-mediated neurodegeneration in Drosophila by the molecular chaperone HSP70 *Nat Genet* **23**, 425-428
181. Yamada, M., Hayashi, S., Tsuji, S., and Takahashi, H. (2001) Involvement of the cerebral cortex and autonomic ganglia in Machado-Joseph disease *Acta Neuropathol* **101**, 140-144
182. Chai, Y., Shao, J., Miller, V. M., Williams, A., and Paulson, H. L. (2002) Live-cell imaging reveals divergent intracellular dynamics of polyglutamine disease proteins and supports a sequestration model of pathogenesis *Proc Natl Acad Sci U S A* **99**, 9310-9315
183. Ciechanover, A., Orian, A., and Schwartz, A. L. (2000) Ubiquitin-mediated proteolysis: biological regulation via destruction *Bioessays* **22**, 442-451
184. Bence, N. F., Sampat, R. M., and Kopito, R. R. (2001) Impairment of the Ubiquitin-proteasome system by protein aggregation *Science* **292**, 1552-1555
185. Bhutani, N., Venkatraman, P., and Goldberg, A. L. (2007) Puromycin-sensitive aminopeptidase is the major peptidase responsible for digesting polyglutamine sequences released by proteasomes during protein degradation *Embo J* **26**, 1385-1396
186. Pratt, G., and Rechsteiner, M. (2008) Proteasomes cleave at multiple sites within polyglutamine tracts: activation by PA28gamma(K188E) *J Biol Chem* **283**, 12919-12925
187. Riley, B. E., and Orr, H. T. (2006) Polyglutamine neurodegenerative diseases and regulation of transcription: assembling the puzzle *Genes Dev* **20**, 2183-2192
188. Chen, S., Ferrone, F. A., and Wetzel, R. (2002) Huntington's disease age-of-onset linked to polyglutamine aggregation nucleation *Proc Natl Acad Sci U S A* **99**, 11884-11889
189. Thakur, A. K., Jayaraman, M., Mishra, R., Thakur, M., Chellgren, V. M., IJ, L. B., Anjum, D. H., Kodali, R., Creamer, T. P., Conway, J. F., A, M. G., and Wetzel, R. (2009) Polyglutamine disruption of the huntingtin exon 1 N terminus triggers a complex aggregation mechanism *Nat Struct Mol Biol* **16**, 380 - 389
190. Li, M., Chevalier-Larsen, E. S., Merry, D. E., and Diamond, M. I. (2007) Soluble androgen receptor oligomers underlie pathology in a mouse model of SBMA *J Biol Chem* **282** 3157-3164
191. Ellisdon, A. M., Thomas, B., and Bottomley, S. P. (2006) The two-stage pathway of ataxin-3 fibrillogenesis involves a polyglutamine-independent step *J Biol Chem* **281**, 16888-16896

192. Ellisdon, A. M., Pearce, M. C., and Bottomley, S. P. (2007) Mechanisms of ataxin-3 misfolding and fibril formation: Kinetic analysis of a disease-associated polyglutamine protein *J Mol Biol* **368**, 595-605

193. Nozaki, K., Onodera, O., Takano, H., and Tsuji, S. (2001) Amino acid sequences flanking polyglutamine stretches influence their potential for aggregate formation *Neuroreport* **12**, 3357-3364

194. Bhattacharyya, A., Thakur, A. K., Chellgren, V. M., Thiagarajan, G., Williams, A. D., Chellgren, B. W., Creamer, T. P., and Wetzel, R. (2006) Oligoproline effects on polyglutamine conformation and aggregation *J Mol Biol* **355**, 524-535

195. Darnell, G., Orgel, J. P., Pahl, R., and Meredith, S. C. (2007) Flanking Polyproline Sequences Inhibit beta-Sheet Structure in Polyglutamine Segments by Inducing PPII-like Helix Structure *J Mol Biol* **374**, 688-704

196. Duennwald, M. L., Jagadish, S., Muchowski, P. J., and Lindquist, S. (2006) Flanking sequences profoundly alter polyglutamine toxicity in yeast *Proc Natl Acad Sci USA* **103**, 11045-11050

197. Chiti, F., Stefani, M., Taddei, N., Ramponi, G., and Dobson, C. M. (2003) Rationalization of the effects of mutations on peptide and protein aggregation rates *Nature* **424**, 805-808

198. Monsellier, E., and Chiti, F. (2007) Prevention of amyloid-like aggregation as a driving force of protein evolution *EMBO Rep* **8**, 737-742

199. Rousseau, F., Serranob, L., and Schymkowitz, J. W. H. (2006) How Evolutionary Pressure Against Protein Aggregation Shaped Chaperone Specificity *J Mol Biol* **355**, 1037-1047

200. Kaltenbach, L. S., Romero, E., Becklin, R. R., Chettier, R., Bell, R., Phansalkar, A., Strand, A., Torcassi, C., Savage, J., Hurlburt, A., Cha, G. H., Ukani, L., Chepanoske, C. L., Zhen, Y., Sahasrabudhe, S., Olson, J., Kurschner, C., Ellerby, L. M., Peltier, J. M., Botas, J., and Hughes, R. E. (2007) Huntingtin interacting proteins are genetic modifiers of neurodegeneration *PLoS Genet* **3**, e82

201. Bevivino, A. E., and Loll, P. J. (2001) An expanded glutamine repeat destabilizes native ataxin-3 structure and mediates formation of parallel beta -fibrils *Proc Natl Acad Sci U S A* **98**, 11955-11960

202. Robertson, A. L., Horne, J., Ellisdon, A. M., Thomas, B., Scanlon, M. J., and Bottomley, S. P. (2008) The structural impact of a polyglutamine tract is location-dependent *Biophys. J.* **95**, 5922-5930

203. Masino, L., Kelly, G., Leonard, K., Trottier, Y., and Pastore, A. (2002) Solution structure of polyglutamine tracts in GST-polyglutamine fusion proteins *FEBS Letters* **513**, 267-272

204. Ignatova, Z., Thakur, A. K., Wetzel, R., and Gierasch, L. M. (2007) In-cell aggregation of a polyglutamine-containing chimera is a multistep process initiated by the flanking sequence *J Biol Chem* **282**, 36736-36743

205. Nagai, Y., Tucker, T., Ren, H., Kenan, D. J., Henderson, B. S., Keene, J. D., Strittmatter, W. J., and Burke, J. R. (2000) Inhibition of polyglutamine protein aggregation and cell death by novel peptides identified by phage display screening *J Biol Chem* **275**, 10437-10442

206. Chow, M. K., Mackay, J. P., Whisstock, J. C., Scanlon, M. J., and Bottomley, S. P. (2004) Structural and functional analysis of the Josephin domain of the polyglutamine protein ataxin-3 *Biochem Biophys Res Commun* **322**, 387-394
207. de Chiara, C., Menon, R. P., Dal Piaz, F., Calder, L., and Pastore, A. (2005) Polyglutamine is not all: the functional role of the AXH domain in the ataxin-1 protein *J Mol Biol* **354**, 883-893
208. Masino, L., Nicastro, G., Menon, R. P., Dal Piaz, F., Calder, L., and Pastore, A. (2004) Characterization of the structure and the amyloidogenic properties of the Josephin domain of the polyglutamine-containing protein ataxin-3 *J Mol Biol* **344**, 1021-1035
209. Williamson, T. E., Vitalis, A., Crick, S. L., and Pappu, R. V. (2009) Modulation of Polyglutamine Conformations and Dimer Formation by the N-Terminus of Huntingtin *J Mol Biol* **396**, 1295-1309
210. Klein, A. F., Ebihara, M., Alexander, C., Dicaire, M. J., Sasseville, A. M., Langelier, Y., Rouleau, G. A., and Brais, B. (2008) PABPN1 polyalanine tract deletion and long expansions modify its aggregation pattern and expression *Exp Cell Res* **314**, 1652-1666
211. Thual, C., Komar, A. A., Bousset, L., Fernandez-Bellot, E., Cullin, C., and Melki, R. (1999) Structural characterization of Saccharomyces cerevisiae prion-like protein Ure2 *J Biol Chem* **274**, 13666-13674
212. Thual, C., Bousset, L., Komar, A. A., Walter, S., Buchner, J., Cullin, C., and Melki, R. (2001) Stability, folding, dimerization, and assembly properties of the yeast prion Ure2p *Biochemistry* **40**, 1764-1773
213. Vitalis, A., Wang, X., and Pappu, R. V. (2008) Atomistic Simulations of the Effects of Polyglutamine Chain Length and Solvent Quality on Conformational Equilibria and Spontaneous Homodimerization *J Mol Biol* **384**, 279-297
214. Walters, R. H., and Murphy, R. M. (2009) Examining polyglutamine peptide length: a connection between collapsed conformations and increased aggregation *J Mol Biol* **393**, 978-992
215. Leitgeb, B., Kerenyi, A., Bogar, F., Paragi, G., Penke, B., and Rakhely, G. (2007) Studying the structural properties of polyalanine and polyglutamine peptides *J Mol Model* **13**, 1141-1150
216. Ogawa, H., Nakano, M., Watanabe, H., Starikov, E. B., Rothstein, S. M., and Tanaka, S. (2008) Molecular dynamics simulation study on the structural stabilities of polyglutamine peptides *Comput Biol Chem* **32**, 102-110
217. Hanahan, D. (1983) Studies on transformation of Escherichia coli with plasmids *J Mol Biol* **166**, 557-580
218. Wang, A., and Bolen, D. W. (1997) A Naturally Occurring Protective System in Urea-Rich Cells: Mechanism of Osmolyte Protection of Proteins against Urea Denaturation *Biochemistry* **36**, 9101-9108
219. Holowaty, M. N., Sheng, Y., Nguyen, T., Arrowsmith, C., and Frappier, L. (2003) Protein interaction domains of the ubiquitin-specific protease, USP7/HAUSP *J Biol Chem* **278**, 47753-47761
220. Provencher, S. W., and Glockner, J. (1981) Estimation of globular protein secondary structure from circular dichroism *Biochemistry* **20**, 33-37

221. Van Stokkum, I. H. M., Spoelder, H. J. W., Bloemendal, M., Van Grondelle, R., and Groen, F. C. A. (1990) Estimation of protein secondary structure and error analysis from CD spectra. *Anal. Biochem* **191**, 110-118

222. Whitmore, L., and Wallace, B. A. (2004) DICHROWEB, an online server for protein secondary structure analyses from circular dichroism spectroscopic data *Nucl Acid Res* **32**, 668-673

223. Whitmore, L., and Wallace, B. A. (2008) Protein secondary structure analyses from circular dichroism spectroscopy: Methods and reference databases *Biopolymers* **89**, 392-400

224. Bolen, D. W., and Santoro, M. M. (1988) Unfolding free energy changes determined by the linear extrapolation method. 2. Incorporation of delta G degrees N-U values in a thermodynamic cycle *Biochemistry* **27**, 8069-8074

225. Stevenson, J. M., Perera, I. Y., and Boss, W. F. (1998) A phosphatidylinositol 4-kinase pleckstrin homology domain that binds phosphatidylinositol 4-monophosphate *J Biol Chem* **273**, 22761-22767

226. Horwich, A. (2002) Protein aggregation in disease: a role for folding intermediates forming specific multimeric interactions *J Clin Invest* **110**, 1221-1232

227. Cho, M. K., Nodet, G., Kim, H. Y., Jensen, M. R., Bernado, P., Fernandez, C. O., Becker, S., Blackledge, M., and Zweckstetter, M. (2009) Structural characterization of alpha-synuclein in an aggregation prone state *Protein Sci* **18**, 1840-1846

228. Platt, G. W., McParland, V. J., Kalverda, A. P., Homans, S. W., and Radford, S. E. (2005) Dynamics in the unfolded state of beta2-microglobulin studied by NMR *J Mol Biol* **346**, 279-294

229. Calloni, G., Lendel, C., Campioni, S., Giannini, S., Gliozzi, A., Relini, A., Vendruscolo, M., Dobson, C. M., Salvatella, X., and Chiti, F. (2008) Structure and dynamics of a partially folded protein are decoupled from its mechanism of aggregation *J Am Chem Soc* **130**, 13040-13050

230. Hurle, M. R., Helms, L. R., Li, L., Chan, W., and Wetzel, R. (1994) A role for destabilizing amino acid replacements in light-chain amyloidosis *Proc Natl Acad Sci U S A* **91**, 5446-5450

231. Hammarstrom, P., Jiang, X., Hurshman, A. R., Powers, E. T., and Kelly, J. W. (2002) Sequence-dependent denaturation energetics: A major determinant in amyloid disease diversity *Proc Natl Acad Sci U S A* **99 Suppl 4**, 16427-16432

232. Wu, K. P., Kim, S., Fela, D. A., and Baum, J. (2008) Characterization of conformational and dynamic properties of natively unfolded human and mouse alpha-synuclein ensembles by NMR: implication for aggregation *J Mol Biol* **378**, 1104-1115

233. Chow, M. K., Ellisdon, A. M., Cabrita, L. D., and Bottomley, S. P. (2004) Polyglutamine expansion in ataxin3 does not affect protein stability *J Biol Chem* **279**, 47643-47651

234. Masino, L., Nicastro, G., Menon, R. P., Piaz, F. D., Calder, L., and Pastore, A. (2004) Characterization of the structure and the amyloidogenic properties of the Josephin domain of the polyglutamine-containing protein ataxin-3 *J Mol Biol* **344**, 1021-1035

235. de Chiara, C., Menon, R. P., Adinolfi, S., de Boer, J., Ktistaki, E., Kelly, G., Calder, L., Kioussis, D., and Pastore, A. (2005) The AXH domain adopts alternative folds the solution structure of HBP1 AXH *Structure* **13**, 743-753
236. Gusella, J. F., and MacDonald, M. E. (2000) Molecular Genetics: Unmasking polyglutamine triggers in neurodegenerative disease *Nat Rev Neurosci* **1**, 109 -115
237. Ignatova, Z., and Gierasch, L. M. (2006) Extended polyglutamine tracts cause aggregation and structural perturbation of an adjacent beta barrel protein *J Biol Chem* **281**, 12959-12967
238. Robertson, A. L., Horne, J., Ellisdon, A. M., Thomas, B., Scanlon, M. J., and Bottomley, S. P. (2008) The structural impact of a polyglutamine tract is location-dependent *Biophys J* **95**, 5922-5930
239. Kheterpal, I., Cook, K. D., and Wetzel, R. (2006) Hydrogen/deuterium exchange mass spectrometry analysis of protein aggregates *Methods Enzymol* **413**, 140-166
240. Miranker, A., Robinson, C. V., Radford, S. E., and Dobson, C. M. (1996) Investigation of protein folding by mass spectrometry *FASEB J* **10**, 93-101
241. Clarke, J., Itzhaki, L. S., and Fersht, A. R. (1997) Hydrogen exchange at equilibrium: a short cut for analysing protein-folding pathways? *Trends Biochem Sci* **22**, 284-287
242. Hoshino, M., Katou, H., Yamaguchi, K., and Goto, Y. (2007) Dimethylsulfoxide-quenched hydrogen/deuterium exchange method to study amyloid fibril structure *Biochim Biophys Acta* **1768**, 1886-1899
243. Englander, S. W. (2006) Hydrogen exchange and mass spectrometry: A historical perspective *J Am Soc Mass Spectrom* **17**, 1481-1489
244. Bai, Y., Milne, J. S., Mayne, L., and Englander, S. W. (1993) Primary structure effects on peptide group hydrogen exchange *Proteins* **17**, 75-86
245. Konermann, L., and Douglas, D. J. (1998) Equilibrium unfolding of proteins monitored by electrospray ionization mass spectrometry: distinguishing two-state from multi-state transitions *Rapid Commun Mass Spectrom* **12**, 435-442
246. Kaltashov, I. A., and Abzalimov, R. R. (2008) Do ionic charges in ESI MS provide useful information on macromolecular structure? *J Am Soc Mass Spectrom* **19**, 1239-1246
247. Mao, Y., Senic-Matugilia, F., Di Fiore, P. P., Polo, S., Hodsdon, M. E., and De Camilli, P. (2005) Deubiquitinating function of ataxin-3: Insights from the solution structure of Josephin domain *Proc Natl Acad Sci U S A* **102**, 12700-12705
248. Ashcroft, A. E., Brinker, A., Coyle, J. E., Weber, F., Kaiser, M., Moroder, L., Parsons, M. R., Jager, J., Hartl, U. F., Hayer-Hartl, M., and Radford, S. E. (2002) Structural plasticity and noncovalent substrate binding in the GroEL apical domain. A study using electrospay ionization mass spectrometry and fluorescence binding studies *J Biol Chem* **277**, 33115-33126
249. Raftery, M. J., and Geczy, C. L. (1998) Identification of noncovalent dimeric complexes of the recombinant murine S100 protein CP10 by electrospray ionization mass spectrometry and chemical cross-linking *J Am Soc Mass Spectrom* **9**, 533-539
250. Hodkinson, J. P., Jahn, T. R., Radford, S. E., and Ashcroft, A. E. (2009) HDX-ESI-MS reveals enhanced conformational dynamics of the amyloidogenic protein beta(2)-microglobulin upon release from the MHC-1 *J Am Soc Mass Spectrom* **20**, 278-286

251. Wang, F., and Tang, X. (1996) Conformational heterogeneity of stability of apomyoglobin studied by hydrogen/deuterium exchange and electrospray ionization mass spectrometry *Biochemistry* **35**, 4069-4078
252. Molday, R. S., Englander, S. W., and Kallen, R. G. (1972) Primary structure effects on peptide group hydrogen exchange *Biochemistry* **11**, 150-158
253. Takei, J., Pei, W., Vu, D., and Bai, Y. (2002) Populating partially unfolded forms by hydrogen exchange-directed protein engineering *Biochemistry* **41**, 12308-12312
254. Konermann, L., and Douglas, D. J. (1997) Acid-induced unfolding of cytochrome c at different methanol concentrations: electrospray ionization mass spectrometry specifically monitors changes in the tertiary structure *Biochemistry* **36**, 12296-12302
255. Chowdhury, S. K., Katta, V., and Chait, B. T. (1990) Probing Conformational Changes in Proteins by Mass Spectrometry *J Am Chem Soc* **112**, 9012-9013
256. Kuprowski, M. C., and Konermann, L. (2007) Signal response of coexisting protein conformers in electrospray mass spectrometry *Anal Chem* **79**, 2499-2506
257. Fenn, J. B. (1993) Ion Formaton from Charged Droplets: Roles of Geometry, Energy and Time *J Am Soc Mass Spectrom* **4**, 524-535
258. Katta, V., and Chait, B. T. (1991) Conformational changes in proteins probed by hydrogen-exchange electrospray-ionization mass spectrometry *Rapid Commun Mass Spectrom* **5**, 214-217
259. Gumerov, D. R., and Kaltashov, I. A. (2001) Dynamics of iron release from transferrin N-lobe studied by electrospray ionization mass spectrometry *Anal Chem* **73**, 2565-2570
260. Low, L. Y., Hernandez, H., Robinson, C. V., O'Brien, R., Grossmann, J. G., Ladbury, J. E., and Luisi, B. (2002) Metal-dependent folding and stability of nuclear hormone receptor DNA-binding domains *J Mol Biol* **319**, 87-106
261. van den Bremer, E. T., Jiskoot, W., James, R., Moore, G. R., Kleanthous, C., Heck, A. J., and Maier, C. S. (2002) Probing metal ion binding and conformational properties of the colicin E9 endonuclease by electrospray ionization time-of-flight mass spectrometry *Protein Sci* **11**, 1738-1752
262. Englander, S. W., Mayne, L., and Krishna, M. M. (2007) Protein folding and misfolding: mechanism and principles *Q Rev Biophys* **40**, 287-326
263. Davis, C. H., and Berkowitz, M. L. (2009) Interaction between amyloid-beta (1-42) peptide and phospholipid bilayers: a molecular dynamics study *Biophys J* **96**, 785-797
264. Hatters, D. M., Lawrence, L. J., and Howlett, G. J. (2001) Sub-micellar phospholipid accelerates amyloid formation by apolipoprotein C-II *FEBS Lett* **494**, 220-224
265. Kazlauskaite, J., Sanghera, N., Sylvester, I., Venien-Bryan, C., and Pinheiro, T. J. (2003) Structural changes of the prion protein in lipid membranes leading to aggregation and fibrillization *Biochemistry* **42**, 3295-3304
266. Zhu, M., and Fink, A. L. (2003) Lipid binding inhibits alpha-synuclein fibril formation *J Biol Chem* **278**, 16873-16877
267. Wang, Q., Li, L., and Ye, Y. (2006) Regulation of retrotranslocation by p97-associated deubiquitinating enzyme ataxin-3 *J Cell Biol* **174**, 963-971

268. Pozzi, C., Valtorta, M., Tedeschi, G., Galbusera, E., Pastori, V., Bigi, A., Nonnis, S., Grassi, E., and Fusi, P. (2008) Study of subcellular localization and proteolysis of ataxin-3 *Neurobiol Dis* **30**, 190-200
269. Gusella, J. F., and MacDonald, M. E. (2000) Molecular Genetics: Unmasking polyglutamine triggers in neurodegenerative disease *Nat Rev Neurosci* **1**, 109 -115
270. Atwal, R. S., Xia, J., Pinchev, D., Taylor, J., Epand, R. M., and Truant, R. (2007) Huntingtin has a membrane association signal that can modulate huntingtin aggregation, nuclear entry and toxicity *Hum Mol Genet* **16**, 2600-2615
271. Rockabrand, E., Slepko, N., Pantalone, A., Nukala, V. N., Kazantsev, A., Marsh, J. L., Sullivan, P. G., Steffan, J. S., Sensi, S. L., and Thompson, L. M. (2007) The first 17 amino acids of Huntingtin modulate its sub-cellular localization, aggregation and effects on calcium homeostasis *Hum Mol Genet* **16**, 61-77
272. Canet, D., Last, A. M., Tito, P., Sunde, M., Spencer, A., Archer, D. B., Redfield, C., Robinson, C. V., and Dobson, C. M. (2002) Local cooperativity in the unfolding of an amyloidogenic variant of human lysozyme *Nat Struct Biol* **9**, 308-315
273. Lindberg, M. J., Tibell, L., and Oliveberg, M. (2002) Common denominator of Cu/Zn superoxide dismutase mutants associated with amyotrophic lateral sclerosis: decreased stability of the apo state *Proc Natl Acad Sci U S A* **99**, 16607-16612
274. Bemporad, F., and Chiti, F. (2009) "Native-like aggregation" of the acylphosphatase from Sulfolobus solfataricus and its biological implications *FEBS Lett* **583**, 2630-2638
275. Leonil, J., Henry, G., Jouanneau, D., Delage, M. M., Forge, V., and Putaux, J. L. (2008) Kinetics of fibril formation of bovine kappa-casein indicate a conformational rearrangement as a critical step in the process *J Mol Biol* **381**, 1267-1280
276. Souillac, P. O., Uversky, V. N., and Fink, A. L. (2003) Structural transformations of oligomeric intermediates in the fibrillation of the immunoglobulin light chain LEN *Biochemistry* **42**, 8094-8104
277. Rochet, J. C., and Lansbury, P. T., Jr. (2000) Amyloid fibrillogenesis: themes and variations *Curr Opin Struct Biol* **10**, 60-68
278. Marcon, G., Plakoutsi, G., Canale, C., Relini, A., Taddei, N., Dobson, C. M., Ramponi, G., and Chiti, F. (2005) Amyloid formation from HypF-N under conditions in which the protein is initially in its native state *J Mol Biol* **347**, 323-335
279. Liemann, S., and Glockshuber, R. (1999) Influence of amino acid substitutions related to inherited human prion diseases on the thermodynamic stability of the cellular prion protein *Biochemistry* **38**, 3258-3267
280. Swietnicki, W., Petersen, R. B., Gambetti, P., and Surewicz, W. K. (1998) Familial mutations and the thermodynamic stability of the recombinant human prion protein *J Biol Chem* **273**, 31048-31052
281. Huang, Z., Gabriel, J. M., Baldwin, M. A., Fletterick, R. J., Prusiner, S. B., and Cohen, F. E. (1994) Proposed three-dimensional structure for the cellular prion protein *Proc Natl Acad Sci U S A* **91**, 7139-7143
282. Masino, L., Musi, V., Menon, R. P., Fusi, P., Kelly, G., Frenkiel, T. A., Trottier, Y., and Pastore, A. (2003) Domain architecture of the polyglutamine protein ataxin-3: a globular domain followed by a flexible tail *FEBS Lett* **549**, 21-25
283. Crick, S. L., Jayaraman, M., Frieden, C., Wetzel, R., and Pappu, R. V. (2006) Fluorescence correlation spectroscopy shows that monomeric polyglutamine

molecules form collapsed structures in aqueous solutions *Proc Natl Acad Sci U S A* **103**, 16764-16769

284. Dougan, L., Li, J., Badilla, C. L., Berne, B. J., and Fernandez, J. M. (2009) Single homopolypeptide chains collapse into mechanically rigid conformations *Proc Natl Acad Sci U S A* **106**, 12605-12610
285. Kim, M. W., Chelliah, Y., Kim, S. W., Otwinowski, Z., and Bezprozvanny, I. (2009) Secondary structure of Huntingtin amino-terminal region *Structure* **17**, 1205-1212
286. Legleiter, J., Lotz, G. P., Miller, J., Ko, J., Ng, C., Williams, G. L., Finkbeiner, S., Patterson, P. H., and Muchowski, P. J. (2009) Monoclonal antibodies recognize distinct conformational epitopes formed by polyglutamine in a mutant huntingtin fragment *J Biol Chem* **284**, 21647-21658
287. Olshina, M. A., Angley, L. M., Ramdzan, Y. M., Tang, J., Bailey, M. F., Hill, A. F., and Hatters, D. M. (2010) Tracking mutant huntingtin aggregation kinetics in cells reveals three major populations including an invariant oligomer pool *The Journal of biological chemistry* **(In Press)**
288. Reina, C. P., Zhong, X., and Pittman, R. N. (2010) Proteotoxic stress increases nuclear localization of ataxin-3 *Hum Mol Genet* **19**, 235-249
289. Bieschke, J., Russ, J., Friedrich, R. P., Ehrnhoefer, D. E., Wobst, H., Neugebauer, K., and Wanker, E. E. (2010) EGCG remodels mature alpha-synuclein and amyloid-beta fibrils and reduces cellular toxicity *Proc Natl Acad Sci U S A* **107**, 7710-7715
290. Ferreira, N., Cardoso, I., Domingues, M. R., Vitorino, R., Bastos, M., Bai, G., Saraiva, M. J., and Almeida, M. R. (2009) Binding of epigallocatechin-3-gallate to transthyretin modulates its amyloidogenicity *FEBS Lett* **583**, 3569-3576

APPENDICES

Appendix 1:

Small heat shock proteins interact with a flanking domain to suppress polyglutamine aggregation

Appendix 2:

Multi-domain misfolding: understanding the aggregation pathway of polyglutamine proteins

Small heat-shock proteins interact with a flanking domain to suppress polyglutamine aggregation

Amy L. Robertson[a], Stephen J. Headey[b], Helen M. Saunders[a], Heath Ecroyd[c], Martin J. Scanlon[b], John A. Carver[d], and Stephen P. Bottomley[a,1]

[a]Department of Biochemistry and Molecular Biology, Monash University, Clayton, Victoria, 3800, Australia; [b]Medicinal Chemistry and Drug Action, Monash Institute of Pharmaceutical Sciences, Monash University, Parkville, Victoria, 3052, Australia; [c]School of Biological Sciences, University of Wollongong, Wollongong, New South Wales, 2522, Australia; and [d]School of Chemistry and Physics, The University of Adelaide, Adelaide, South Australia, 5005, Australia

Edited by George H. Lorimer, University of Maryland, College Park, MD, and approved April 15, 2010 (received for review December 20, 2009)

Small heat-shock proteins (sHsps) are molecular chaperones that play an important protective role against cellular protein misfolding by interacting with partially unfolded proteins on their off-folding pathway, preventing their aggregation. Polyglutamine (polyQ) repeat expansion leads to the formation of fibrillar protein aggregates and neuronal cell death in nine diseases, including Huntington disease and the spinocerebellar ataxias (SCAs). There is evidence that sHsps have a role in suppression of polyQ-induced neurodegeneration; for example, the sHsp alphaB-crystallin (αB-c) has been identified as a suppressor of SCA3 toxicity in a *Drosophila* model. However, the molecular mechanism for this suppression is unknown. In this study we tested the ability of αB-c to suppress the aggregation of a polyQ protein. We found that αB-c does not inhibit the formation of SDS-insoluble polyQ fibrils. We further tested the effect of αB-c on the aggregation of ataxin-3, a polyQ protein that aggregates via a two-stage aggregation mechanism. The first stage involves association of the N-terminal Josephin domain followed by polyQ-mediated interactions and the formation of SDS-resistant mature fibrils. Our data show that αB-c potently inhibits the first stage of ataxin-3 aggregation; however, the second polyQ-dependent stage can still proceed. By using NMR spectroscopy, we have determined that αB-c interacts with an extensive region on the surface of the Josephin domain. These data provide an example of a domain/region flanking an amyloidogenic sequence that has a critical role in modulating aggregation of a polypeptide and plays a role in the interaction with molecular chaperones to prevent this aggregation.

fibrillogenesis | α-crystallin

Small heat-shock proteins (sHsps) are important in the maintenance of cellular homeostasis. sHsps are induced under stress conditions and interact with partially unfolded proteins on their off-folding pathways, thereby providing a protective mechanism against protein misfolding and aggregation (1). They are present in many species, and 10 have been identified in the human proteome (see reviews in refs. 1 and 2). Alpha-crystallin (α-crystallin) is the most well characterized sHsp. The two isoforms of α-crystallin, αA-crystallin (αA-c) and αB-crystallin (αB-c), are a large component of the human eye lens, and αB-c is expressed in many other cell types including neurons (3, 4). Monomeric αB-c is approximately 20 kDa in mass, and under native conditions it forms a heterogeneous array of multimeric complexes ranging from 160 to 1,000 kDa in mass (2). The activity of αB-c is thought to involve hydrophobic interactions between αB-c and the partially folded protein. Under stress conditions, such as elevated temperature, the activity of αB-c is enhanced because of a conformational change within the multimeric complex (5, 6). Cellular stress is induced in several neurodegenerative diseases, such as Alzheimer's disease (7), prion diseases (8), Parkinson disease (4), and Huntington disease (HD) (4), and there is evidence of increased αB-c activity (4). In addition, αB-c reduces neurotoxicity in a number of disease models (9, 10). In vitro the interaction between αB-c and a number of aggregating proteins has been characterized. Most substrates aggregate through a nucleation-dependent kinetic mechanism; however, the mode of interaction with αB-c appears to be dependent upon the specific target protein and the type of aggregation—i.e., amorphous or fibrillar (11–13). Complex stability is influenced by properties of the target protein, for example, the fibril-forming proteins apolipoprotein-CII (11) and amyloid-β (14) transiently interact with αB-c whereas α-synuclein (6) and κ-casein (15) form stable noncovalent complexes. Determining the mechanism by which αB-c interacts with specific aggregation-prone substrates is therefore important and may provide insight into the misfolding pathways leading to toxicity.

Polyglutamine (polyQ) expansion leads to the formation of fibrillar protein aggregates and neuronal cell death in nine diseases, including HD and the spinocerebellar ataxias (SCAs) 1, 2, 3, 6, 7, and 17. PolyQ peptides and proteins form fibrillar aggregates by a nucleation-dependent mechanism that is initiated by a monomeric nucleus (16–18). Recent evidence suggests that polyQ protein misfolding involves not only the polyQ tract but other aggregation-prone regions within the polyQ proteins (19–21). There is experimental evidence that the proteins ataxin-3 (in SCA3), ataxin-1 (in SCA1), and huntingtin (in HD) form fibrillar aggregates by a multidomain misfolding mechanism in which non-polyQ regions of the protein self-associate before the polyQ tract (19, 20, 22). Our laboratory has previously shown that ataxin-3 has a minimal two-stage aggregation mechanism (19). The first stage involves aggregation of the globular N-terminal Josephin domain that precedes the self-association of expanded polyQ segments (19).

sHsp overexpression decreases neuronal toxicity in HD by nonchaperone mechanisms, including suppression of reactive oxygen species (23) and stimulation of autophagy (24). In disease models overexpression of αB-c modulates toxicity in a context-dependent manner. αB-c did not alter the HD phenotype in a *Drosophila* model (25); however, it suppressed SCA3 toxicity in a *Drosophila* model (9). Enhanced suppression was observed when αB-c was coexpressed with full-length ataxin-3 in comparison with a C-terminal fragment not containing the Josephin domain (9). These data suggest that non-polyQ protein regions influence sHsp chaperone activity.

In this study we tested the chaperone ability of αB-c for a polyQ protein (SpAcQ52) that forms fibrillar aggregates by a mechanism involving only the polyQ region. We found that

---

Author contributions: A.L.R., J.A.C., and S.P.B. designed research; A.L.R., S.J.H., H.M.S., and M.J.S. performed research; H.E. contributed new reagents/analytic tools; A.L.R., S.J.H., H.M.S., M.J.S., J.A.C., and S.P.B. analyzed data; and A.L.R., S.J.H., H.E., M.J.S., J.A.C., and S.P.B. wrote the paper.

The authors declare no conflict of interest.

This article is a PNAS Direct Submission.

[1]To whom correspondence should be addressed. E-mail: steve.bottomley@med.monash.edu.au.

This article contains supporting information online at www.pnas.org/lookup/suppl/doi:10.1073/pnas.0914773107/-/DCSupplemental.

αB-c does not inhibit fibrillogenesis in this system. We then tested the effect of αB-c on the aggregation of ataxin-3 harboring a pathological length polyQ tract [at3(Q64)] and a truncated variant comprising only the Josephin domain. Our data show that αB-c potently inhibits the initial Josephin-dependent stage of ataxin-3 aggregation. By using NMR spectroscopy, we determined that αB-c interacts with specific regions of Josephin. These data provide an example and characterization of a domain/region flanking an amyloidogenic sequence that has a critical role in modulation of aggregation by interacting with molecular chaperones.

Results

αB-c Does Not Inhibit PolyQ-Mediated Aggregation. We first tested whether αB-c can prevent polyQ tract-mediated aggregation. We coincubated αB-c with a polyQ protein (SpAcQ52), which forms SDS-insoluble aggregates by a mechanism involving only the polyQ tract (26). The rate at which SpAcQ52 forms ThT-reactive aggregates does not change when incubated with increasing concentrations of αB-c (Fig. 1*A*). It has been previously shown that molecular chaperones can redirect the aggregation pathway of a protein from amyloid to amorphous aggregation (27, 28). Amorphous aggregates can be differentiated from amyloid by their sensitivity to SDS and appearance when visualized by transmission electron microscopy (TEM). So we tested whether SpAcQ52 incubated with αB-c forms SDS-insoluble aggregates by using a membrane filter-trap assay (29). These data demonstrate that the aggregates formed in the presence or absence of αB-c are insoluble in SDS (Fig. 1*B*). In addition, TEM analysis of the aggregates indicated that αB-c does not affect their fibrillar morphology. Fibrils ranging from 15 to 8 nm in width and 300 to 400 nm in length were observed in both the presence and absence of αB-c (Fig. 1*C*). Together, these data demonstrate that αB-c does not inhibit or modify the fibrillar aggregation of SpAcQ52.

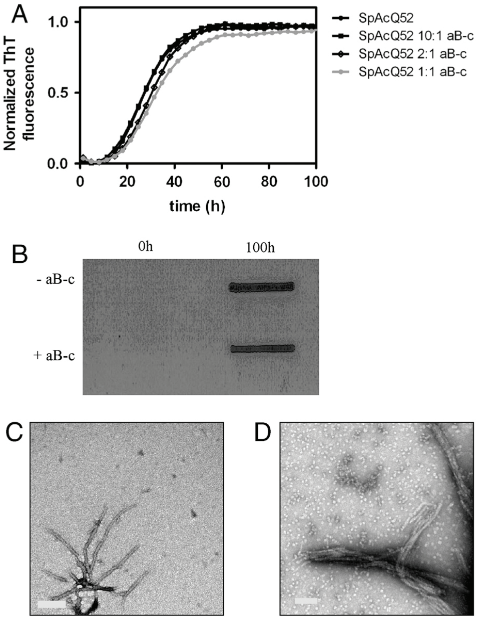

Fig. 1. The effect of αB-c on poly(Q) aggregation. (*A*) SpAcQ52 aggregation in the presence of increasing concentrations of αB-c monitored by ThT fluorescence. (*B*) Analysis of the SDS solubility of endpoint aggregates (100 h) in the presence and absence of αB-c. (*C* and *D*) TEM analysis of SpAcQ52 aggregates in the absence (*C*) and presence of αB-c. Ratios of SpAcQ52:αB-c are given on a molar basis.

αB-c Inhibits the Josephin-Dependent Stage of the Two-Stage Ataxin-3 Aggregation Pathway. We have previously reported that full-length ataxin-3 forms aggregates by a two-stage mechanism (18). The aggregates formed in both stages are ThT-reactive, and in the absence of glycerol the two stages are characterized by a biphasic time course (Fig. 2*A*). The first stage is dominated by interactions of the N-terminal Josephin domain, which is an independently aggregation-prone domain (30). Aggregates formed during the first stage appear as short curvilinear structures and can be solubilized by SDS (19). These aggregates are stabilized in the second stage by interactions of the polyQ regions. Stage-two aggregates can be distinguished from stage-one aggregates because they are SDS-insoluble and morphologically appear as larger fibrillar structures. We determined the effect of αB-c on the two-stage aggregation pathway of at3(Q64). αB-c significantly slows the formation of ThT-reactive at3(Q64) aggregates in a concentration-dependent manner (Fig. 2*A* and Table 1).

The Josephin domain forms short aggregates with a ribbon-like morphology (30); however, the aggregation kinetics have not been described. Isolated Josephin forms ThT-reactive aggregates at a much slower rate than at3(Q64) (Fig. 2*B* and Table 1). The half-life of the first ThT-reactive phase of at3(Q64) aggregation represents the formation of Josephin-dependent fibrils (19). The half-life shifts from approximately 9 h in the full-length protein to around 60 h for the isolated Josephin domain (Table 1). These data indicate that the C-terminal polyQ tail in the context of the full-length protein accelerates Josephin domain aggregation.

αB-c has potent inhibitory activity on the aggregation of Josephin (Fig. 2*B* and Table 1), compared to the full-length at3(Q64) variant. Thus, an equimolar concentration of αB-c completely suppresses Josephin aggregation, but at3(Q64) still forms some ThT-reactive aggregates, even when αB-c is present in a 2:1 molar excess. The reaction time course is too long to determine if the biphasic ThT pattern is altered at stoichiometric concentrations of αB-c. The potent inhibitory effect of αB-c on Josephin aggregation, combined with the data in Fig. 1 showing that αB-c does not inhibit polyQ-dependent aggregation, suggests that the slow ThT phase in the presence of high αB-c concentrations is dominated by polyQ intermolecular interactions.

We analyzed the Josephin and at3(Q64) fibrils by TEM (Fig. 3*A*). Josephin forms short curvilinear fibrils, 5–10 nm in width and 10–100 nm long, when incubated alone. However,

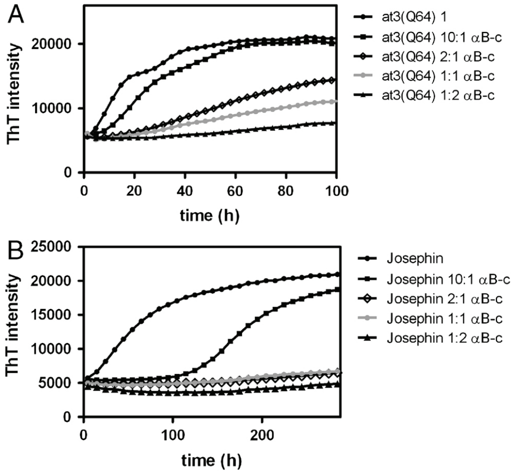

Fig. 2. The effect of αB-c on at3 aggregation. (*A*) At3(Q64) and (*B*) Josephin aggregation in the presence of increasing concentrations of αB-c monitored by ThT-fluorescence. Ratios of at3 variant:αB-c are given on a molar basis.

Table 1. Half-lives (in hours) of Ataxin-3(Q64) aggregation followed by ThT and SDS insolubility in the presence and absence of αB-c

	ThT		SDS insolubility
	Stage 1	*Stage 2*	
Ataxin-3(Q64)	9.3 ± 0.2	31.7 ± 0.9	25.5 ± 1.1
Ataxin-3(Q64) 10∶1 αB-c	19.7 ± 0.6	49 ± 4	45.1 ± 1.3
Ataxin-3(Q64) 1∶1 αB-c	*	*	*
Josephin	59.1 ± 3	†	†
Josephin 10∶1 αB-c	174 ± 0.3	†	†
Josephin 1∶1 αB-c	‡	†	†

*Aggregation incomplete after 300 h; therefore, data could not be fitted.

†Josephin does not undergo stage 2 of the ataxin-3 aggregation pathway and therefore does not form SDS-insoluble fibrils.

‡An equimolar amount of αB-c completely inhibited Josephin aggregation over 300 h.

no fibrils were observed in samples incubated with equimolar concentrations of αB-c. Small, spherical aggregates characteristic of oligomeric αB-c are observed (Fig. 3*A*). After 7 h of incubation, curvilinear worm-like aggregates, 5–15 nm in width, consistent with the previously described morphology of stage-one aggregates (19), were observed in samples of at3(Q64) incubated alone. In the presence of αB-c, there were very few small aggregates present after 7 h. After 24 h, at3(Q64) was beginning to form larger fibrillar structures, ranging from 200 to 300 nm in length and 12 to 30 nm in width. These are consistent with the morphology of stage-two/endpoint fibrils. There were very few stage-two fibrils present in the samples incubated with αB-c.

At3(Q64) Forms SDS-Insoluble Fibrils at a Rate Modulated by Increasing αB-c Concentrations. We tested the effect of αB-c on the formation of SDS-resistant at3(Q64) fibrils by using the filter-trap assay. Analysis of the membranes by densitometry showed that αB-c retards the formation of SDS-insoluble fibrils, as demonstrated by a twofold increase in half-life for at3(Q64) aggregation occurring in the presence of substoichiometric concentrations of αB-c [at3(Q64) 10∶1 αB-c] (Fig. 3*B* and Table 1). The inhibitory effect of αB-c is more pronounced at stoichiometric concentrations where SDS-insoluble fibrils were still formed but at much lower amounts relative to at3(Q64) incubated alone. The equimolar data could not be fit to the classic nucleation-dependent model because aggregation is incomplete over the 300-h time scale.

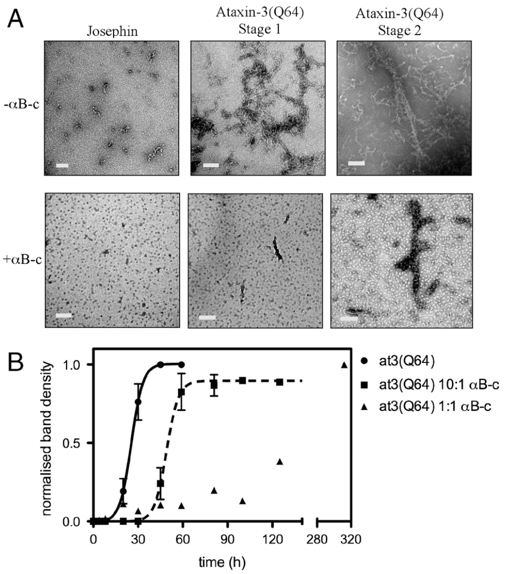

Fig. 3. The effect of αB-c on the formation of at3(Q64) SDS-insoluble fibrils. (*A*) TEM analysis of Josephin and ataxin-3 fibrils. (*B*) The poly(Q)-dependent stage of At3(Q64) aggregation was monitored by detection of SDS-insoluble fibrils using the membrane filter-trap assay. Membranes were analyzed by densitometry and data normalized.

The Presence of αB-c Retains Ataxin-3 in a Monomeric Conformation. αB-c exists as a dynamic oligomeric complex (2). Depending on the target protein, it can irreversibly or transiently bind to target proteins, thereby inhibiting aggregation. To determine the stability of the αB-c:at3 association we performed size-exclusion chromatography (SEC) of Josephin and at3(Q64) incubated with equimolar concentrations of αB-c (Fig. 4).

Monomeric Josephin eluted from a Superose 6 column at approximately 18.9 mL. After 24-h incubation, Josephin formed insoluble aggregates that were removed by centrifugation prior to injection onto the column; therefore, the monomeric protein peak eluting at 18.9 mL was diminished (Fig. 4, *Top Left*). αB-c displayed a broad peak centered around 14 mL, consistent with αB-c being present as a polydisperse oligomer. In the presence of αB-c, most of the Josephin is retained in a monomeric conformation at 49 h, with some recruited into the αB-c complex, observed by a distinct shift and broadening of the αB-c peak (Fig. 4, *Top Right*). We performed SDS-PAGE to examine the composition of the peaks eluting at various times in the SEC experiments (Fig. S1*A*). A small amount of Josephin coelutes with the multimeric αB-c complex after a 48-h incubation period, and this is consistent with the shift and broadening of the peak corresponding to multimeric αB-c (Fig. 4).

At3(Q64) eluted as a single peak with a retention volume of approximately 17.8 mL. After 8 h, most of the at3(Q64) had aggregated, indicated by the presence of a large peak in the void volume (approximately 8 mL) of the Superose 6 column (Fig. 4, *Bottom Left*). After 8 h in the presence of αB-c, most of the at3(Q64) is retained in a monomeric conformation, with little change in the elution profile after this time (Fig. 4, *Bottom Right*). No at3(Q64) coeluted with the multimeric αB-c (Fig. S1*B*), consistent with the observation that the αB-c peak did not shift in the experiments with at3(Q64) (Fig. 4). The SEC data suggest that αB-c does not form a stable complex with at3(Q64)/Josephin maintaining the proteins in a monomeric conformation.

Addition of αB-c Affects Josephin/at3(Q64) Fibril Propagation. The observation that αB-c retains Josephin and at3(Q64) in a monomeric conformation suggests that αB-c inhibits the conformational changes involved in nucleation of aggregation. αB-c has also been shown to inhibit fibril propagation in a number of systems (6, 11, 14, 27). We tested the effect of αB-c on Josephin and at3(Q64) fibril propagation by adding αB-c at various intervals after the commencement of aggregation.

When αB-c was added to isolated Josephin at 48 and 96 h, there was no further increase in ThT intensity, suggesting that αB-c prevents the further propagation of Josephin fibrils (Fig. S2*A*). Similar behavior is observed when αB-c is added at time points along the aggregation pathway of α-synuclein (6). When αB-c was added to the at3(Q64) reactions at various intervals, there was a flattening of the curve for a period of time and then a second slower aggregation phase (Fig. S2*B*). Because of the absence of this phase in the isolated Josephin reactions, we predict that the second phase is because of polyQ-dependent aggregation. Interestingly, the length of the flattened period was longer when αB-c was added at earlier time points in comparison to later time points, supporting the hypothesis that the rate at which poly(Q) interactions occurs is accelerated by the initial formation of stage-one Josephin-dependent fibrils.

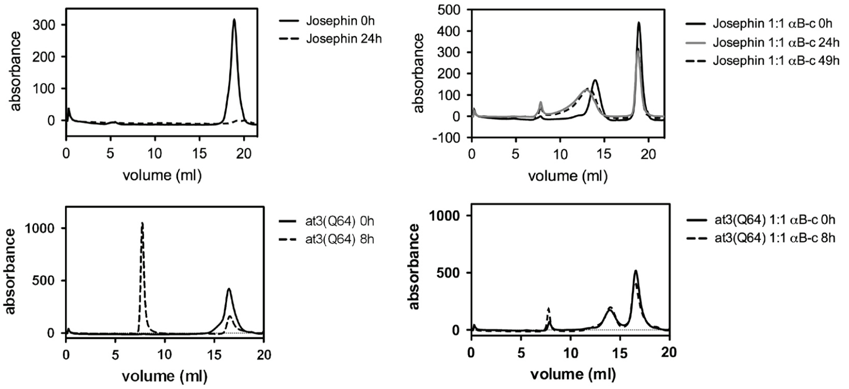

Fig. 4. Ataxin-3 aggregation in the presence and absence of αB-c monitored by SEC. Samples of Josephin and At3(Q64) incubated in the presence and absence of αB-c were removed at indicated time points and analyzed by SEC using a Superose 6 column. In the samples containing αB-c, equimolar amounts of substrate: αB-c were used.

αB-c Interacts with an Extensive Region of Josephin. The ability of αB-c to inhibit ataxin-3 aggregation appears to be derived from inhibition of the Josephin-dependent stage (stage one) of the multi-domain aggregation pathway. We used NMR spectroscopy to probe the molecular details of the Josephin:αB-c interaction surface.

The NMR data show that αB-c interacts with an extensive region of Josephin (Fig. 5). A number of backbone amide cross-peaks in the ^{15}N-HSQC (heteronuclear single quantum coherence) spectrum of Josephin were significantly broadened upon titration of αB-c up to a fivefold stoichiometric excess (Fig. S3). The broadening is consistent with exchange between the free and αB-c bound states of Josephin. Exchange broadening occurs when the time scale of the interaction is commensurate with the difference in NMR frequencies between the bound and free states, which is consistent with the transient interaction mechanism observed by SEC (Fig. 4). The Josephin residues perturbed to the largest degree were Q16, L19, N21, E26, S29, S35, I36, I77, W87, Q100, C114, V123, G127, F131, S135, L137, T138, L148, L155,Q156, E158, I162, Q176, and R182. These residues are confined to the globular subdomain of Josephin and include the active site residue C114.

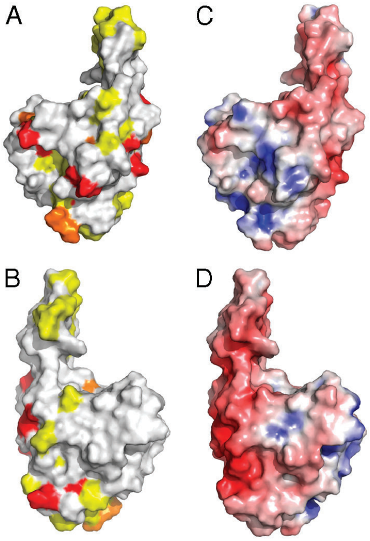

Fig. 5. αB-c interacts with specific regions of Josephin. (*A* and *B*) The residues perturbed upon addition of αB-c were mapped onto the Josephin domain (Protein Data Bank ID code 1YZB). Residues in intermediate exchange in the presence of αB-c (*Red*), residues shielded from broadening by Gd (DTPA-BMA) in the presence of αB-c (*Yellow*), and orange shows the overlapping residues. *A* and *B* show opposing faces of the Josephin structure. (*C* and *D*) The electrostatic surface of Josephin. Blue represents positive charge and red indicates negatively charged regions. *C* and *D* show opposing faces of the Josephin structure.

Because chemical shift perturbations can arise through indirect mechanisms (rather than a direct interaction between αB-c and Josephin), we used the paramagnetic relaxation agent Gd-diethylenetriamine pentaacetic acid-bismethylamide [Gd (DTPA-BMA)] to independently confirm the interaction surface (31, 32). The presence of Gd(DTPA-BMA) in solution causes paramagnetic relaxation enhancement, broadening the protein resonances. By performing these ^{15}N-HSQC experiments in the presence and absence of αB-c, we could determine the αB-c interaction surface of Josephin, because the regions that interact with αB-c were partially shielded from paramagnetic relaxation (Fig. S4). Josephin residues that had >20% stronger signals in the presence of Gd(DTPA-BMA) and a twofold excess of αB-c were S3, G11, L13, Q24, F28, A49, E50, G51, G52, T54, E56, D57, R59, T60, F61, S66, D71, G73, F75, S76, E90, N115, K128, N132, G139, L142, F151, G159, D168, E173, L178, M180, and I181. The identity of these residues correlates well with those broadened in the αB-c-bound state of Josephin (see above, Fig. 5). When mapped to the Josephin structure all of the residues that appeared to be most shielded from the paramagnetic probe by the presence of αB-c were found to be surface-exposed, validating these regions as the αB-c binding interface.

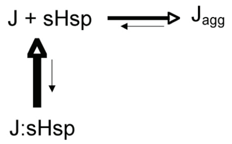

Fig. 6. A schematic model describing the effect of αB-c on at3 aggregation. Multimeric αB-c (a sHsp) transiently binds to at3 molecules in which Josephin is in an aggregation-prone conformation (J$_{agg}$). The J:sHsp complex is unstable, and monomeric Josephin is released from the sHsp.

Discussion

sHsps Do Not Inhibit PolyQ Aggregation. sHsps have a critical role in cellular homeostasis and can provide a barrier to the aggregation of partially unfolded proteins that are central to many neurodegenerative diseases. We investigated the effect of αB-c on the aggregation of a polyQ-containing model protein, finding that αB-c does not affect the formation of SDS-resistant polyQ fibrils when fibril formation is entirely polyQ-dependent (Fig. 1). Typically, sHsps (along with many other molecular chaperones) interact with exposed hydrophobic patches on target proteins. Glutamine is a hydrophilic amino acid; therefore, the surface hydrophobicity of polyQ would not increase during early aggregation stages. In addition, the polyQ region is thought to be in a condensed disordered state in the native ensemble (33, 34), therefore decreasing the accessibility of the side chains to sHsp interactions (35). In a manner akin to our findings with sHsps, molecular chaperones from other classes, e.g., Hsp70 and the chaperonin TRiC, which recognize surface hydrophobic patches of amyloidogenic intermediates, only weakly associate with polyQ proteins (28, 36). Therefore, the physiochemical properties of the polyQ tract may lead to its evasion by some chaperone protective mechanisms.

αB-c Inhibits the Josephin-Dependent Stage of Ataxin-3 Aggregation. Pathological polyQ tracts are located within specific host proteins, and properties of the host protein are known to modulate aggregation and cellular toxicity (37, 38). Although molecular chaperones do not alter the misfolding of pure polyQ, genetic screens in *Drosophila* and *Caenorhabditis elegans* have identified several chaperones that modulate toxicity induced by ataxin-3, ataxin-1, and Htt exon 1, proteins that contain well-structured domain(s) coupled to a polyQ repeat (9, 39). As a result, we hypothesize that non-polyQ aggregation mechanisms play a role in pathogenesis. A previous study from our group has described a two-stage aggregation mechanism for pathological variants of ataxin-3 (19). Our data show that αB-c inhibits nucleation of the Josephin-dependent stage of ataxin-3 aggregation, subsequently having an indirect effect on the rate of poly(Q) intermolecular interactions. The chaperonin TRiC was recently shown to have a similar effect on the aggregation of Htt exon 1; TRiC suppresses aggregation by binding to the N-terminal domain adjacent to the polyQ tract (40).

αB-c had a more potent inhibitory effect on the aggregation of Josephin alone compared with at3(Q64). The Josephin aggregation stage is enhanced when this domain is part of at3(Q64), suggesting that the presence of the polyQ-containing C-terminal tail increases the rate of Josephin aggregation. The presence of the C-terminal polyQ tail leads to a slight decrease in the thermodynamic stability of Josephin (41), and we speculate that the tail alters the dynamic properties of the core domain enhancing the rate of conformational rearrangements on the aggregation pathway. The observation that αB-c has a greater inhibitory effect on the aggregation of isolated Josephin can be rationalized by a previous study demonstrating that larger target proteins require more αB-c (on a molar basis) for complete suppression of aggregation (42). The altered potency is also consistent with data showing that αB-c has a preference for target proteins that aggregate more slowly (43).

For the full-length protein, the interaction of αB-c with Josephin significantly slows the subsequent poly(Q)-dependent aggregation (Fig. 1 and Table 1). These data suggest that Josephin self-interactions lower the kinetic barrier to poly(Q)-dependent aggregation. The multidomain aggregation mechanisms described for ataxin-3 and Htt exon 1 suggest that a pool of small stage-one species can enhance the rate of polyQ-dependent aggregation by increasing the local polyQ concentration (19, 20). This suggestion is consistent with our data (Fig. S2*B*), which demonstrated that the formation of small Josephin fibrils is necessary for efficient formation of poly(Q)-dependent SDS-insoluble fibrils.

The significant effect of αB-c on ataxin-3 aggregation is consistent with a *Drosophila* model in which overexpression of αB-c decreased SCA3-induced toxicity (9), suggesting that inhibition of aggregation by chaperones is relevant in vivo. Another *Drosophila* study demonstrated that chaperone-induced retention of ataxin-3 in a monomeric conformation suppresses toxicity (44). Conversely, αB-c overexpression had no effect on the HD phenotype (25). Htt exon 1 has been proposed to have a similar two-stage aggregation mechanism compared to ataxin-3 (20). The alternative effects of αB-c in the ataxin-3 and Htt systems demonstrate how specific differences in multidomain misfolding pathways could lead to variable cellular responses.

αB-c Transiently Interacts with Monomeric Josephin. The aggregation data clearly show that αB-c suppresses aggregation by associating with species on the Josephin aggregation pathway. Our SEC and NMR data show that inhibition mechanistically occurs by transient association of αB-c with a defined region on the Josephin surface that is partially coincident with the ubiquitin and HHR23B interacting surfaces (45–47). Interestingly, the perturbed residues are not all hydrophobic in character, and it is possible that some surface polar residues appear perturbed in our NMR studies because their amide groups are neighboring interacting hydrophobic groups. Whereas hydrophobic interactions are clearly important for chaperone action, it is also being increasingly recognized that substrate specificity is not purely driven by hydrophobic contacts (48–50).

The SEC data show that the proteins are retained in a monomeric conformation in the presence of αB-c (Fig. 4). These data suggest that the rate at which αB-c interacts with Josephin is more rapid than the rate of misfolding. The NMR data indicate that this is a low affinity interaction; therefore, during this interaction, most of the Josephin is in a monomeric uncomplexed state. These data are consistent with a mechanism whereby αB-c binds and sequesters the free pool of monomeric proteins, thereby preventing fibril growth (Fig. 6).

The interaction between αB-c and monomeric Josephin, encompassing a large region of the target protein, is also observed, in the interaction of αB-c with the fibril-forming proteins α-synuclein (27) and *κ*-casein (6).

Conclusions

Our data demonstrate that inhibition of a non-polyQ aggregation stage by a chaperone can significantly impede protein aggregation involved in polyQ diseases. These data support the two-stage model as a plausible scheme for ataxin-3 aggregation in vitro. Therapeutic up-regulation of chaperone activity may be beneficial in SCA3 and other polyQ diseases that have a multidomain aggregation mechanism.

Experimental Procedures

Preparation of Proteins. SpAcQ52 and the ataxin-3 variants used in this study were expressed and purified as previously described (26, 51). αB-c was expressed and purified as described in ref. 52.

Protein Aggregation Assays. Aggregation assays were performed for SpAcQ52 and ataxin-3 variants at a protein concentration of 20 μM in Tris-buffered saline (TBS) (100 mM Tris, 80 mM NaCl, pH 7.4) containing 2 mM PMSF, 5 mM EDTA, and 15 mM ß-mercaptoethanol. Variable concentrations of αB-c were added to the samples, ranging from 2 to 40 μM. Samples were incubated at 37 °C.

ThT Measurements, Membrane Filter-Trap Assay, and TEM. ThT measurements, the membrane filter-trap assay, and TEM analysis were performed as described in refs. 19 and 26.

SEC. SEC of at3(Q64) and Josephin in the presence and absence of equimolar concentrations of αB-c was performed on an Akta-

FPLC equipped with a Superose 6 10/300 GL column (Pharmacia). Prior to injection onto the column, samples were centrifuged for 5 min at 13,000 rpm to remove insoluble aggregated material. The absorbance at 214 nm was measured as proteins were eluted in TBS buffer at a constant flow rate of 0.5 mL/ min.

NMR Spectroscopy. NMR methods are described in *SI Text*.

ACKNOWLEDGMENTS. This work was supported by the Australian Research Council and the National Health and Medical Research Council (NHMRC). S.P.B. is a NHMRC Research Fellow. H.E. was a NHMRC Peter Doherty Fellow.

1. Haslbeck M, Franzmann T, Weinfurtner D, Buchner J (2005) Some like it hot: The structure and function of small heat-shock proteins. *Nat Struct Mol Biol* 12(10):842–846.
2. Ecroyd H, Carver JA (2009) Crystallin proteins and amyloid fibrils. *Cell Mol Life Sci* 66(1):62–81.
3. Horwitz J (2003) Alpha-crystallin. *Exp Eye Res* 76(2):145–153.
4. Iwaki T, et al. (1992) Accumulation of alpha B-crystallin in central nervous system glia and neurons in pathologic conditions. *Am J Pathol* 140(2):345–356.
5. Das KP, Surewicz WK (1995) Temperature-induced exposure of hydrophobic surfaces and its effect on the chaperone activity of alpha-crystallin. *FEBS Lett* 369(2–3):321–325.
6. Rekas A, Jankova L, Thorn DC, Cappai R, Carver JA (2007) Monitoring the prevention of amyloid fibril formation by alpha-crystallin. Temperature dependence and the nature of the aggregating species. *FEBS J* 274(24):6290–6304.
7. Lowe J, et al. (1992) alpha B crystallin expression in non-lenticular tissues and selective presence in ubiquitinated inclusion bodies in human disease. *J Pathol* 166(1):61–68.
8. Renkawek K, et al. (1992) alpha B-crystallin is present in reactive glia in Creutzfeldt-Jakob disease. *Acta Neuropathol* 83(3):324–327.
9. Bilen J, Bonini NM (2007) Genome-wide screen for modifiers of ataxin-3 neurodegeneration in Drosophila. *PLoS Genet* 3(10):1950–1964.
10. Wilhelmus MM, et al. (2006) Small heat shock proteins inhibit amyloid-beta protein aggregation and cerebrovascular amyloid-beta protein toxicity. *Brain Res* 1089(1):67–78.
11. Hatters DM, Lindner RA, Carver JA, Howlett GJ (2001) The molecular chaperone, alpha-crystallin, inhibits amyloid formation by apolipoprotein C-II. *J Biol Chem* 276(36):33755–33761.
12. Carver JA, et al. (2002) The interaction of the molecular chaperone alpha-crystallin with unfolding alpha-lactalbumin: A structural and kinetic spectroscopic study. *J Mol Biol* 318(3):815–827.
13. Devlin GL, Carver JA, Bottomley SP (2003) The selective inhibition of serpin aggregation by the molecular chaperone, alpha-crystallin, indicates a nucleation-dependent specificity. *J Biol Chem* 278(49):48644–48650.
14. Raman B, et al. (2005) AlphaB-crystallin, a small heat-shock protein, prevents the amyloid fibril growth of an amyloid beta-peptide and beta2-microglobulin. *Biochem J* 392(Pt 3):573–581.
15. Ecroyd H, et al. (2007) Mimicking phosphorylation of alphaB-crystallin affects its chaperone activity. *Biochem J* 401(1):129–141.
16. Chen S, Ferrone FA, Wetzel R (2002) Huntington's disease age-of-onset linked to polyglutamine aggregation nucleation. *Proc Natl Acad Sci USA* 99(18):11884–11889.
17. Ignatova Z, Gierasch LM (2006) Extended polyglutamine tracts cause aggregation and structural perturbation of an adjacent beta barrel protein. *J Biol Chem* 281(18):12959–12967.
18. Ellisdon AM, Pearce MC, Bottomley SP (2007) Mechanisms of ataxin-3 misfolding and fibril formation: Kinetic analysis of a disease-associated polyglutamine protein. *J Mol Biol* 368(2):595–605.
19. Ellisdon AM, Thomas B, Bottomley SP (2006) The two-stage pathway of ataxin-3 fibrillogenesis involves a polyglutamine-independent step. *J Biol Chem* 281(25): 16888–16896.
20. Thakur AK, et al. (2009) Polyglutamine disruption of the huntingtin exon 1 N terminus triggers a complex aggregation mechanism. *Nat Struct Mol Biol* 16(4):380–389.
21. Bulone D, Masino L, Thomas DJ, San Biagio PL, Pastore A (2006) The interplay between PolyQ and protein context delays aggregation by forming a reservoir of protofibrils. *PLoS ONE* 1:e111.
22. de Chiara C, et al. (2005) The AXH domain adopts alternative folds the solution structure of HBP1 AXH. *Structure* 13(5):743–753.
23. Wyttenbach A, et al. (2002) Heat shock protein 27 prevents cellular polyglutamine toxicity and suppresses the increase of reactive oxygen species caused by huntingtin. *Hum Mol Genet* 11(9):1137–1151.
24. Carra S, Brunsting JF, Lambert H, Landry J, Kampinga HH (2009) HspB8 participates in protein quality control by a non-chaperone-like mechanism that requires eIF2{alpha} phosphorylation. *J Biol Chem* 284(9):5523–5532.
25. Carra S, Sivilotti M, Chavez Zobel AT, Lambert H, Landry J (2005) HspB8, a small heat shock protein mutated in human neuromuscular disorders, has in vivo chaperone activity in cultured cells. *Hum Mol Genet* 14(12):1659–1669.
26. Robertson AL, et al. (2008) The structural impact of a polyglutamine tract is location-dependent. *Biophys J* 95(12):5922–5930.
27. Rekas A, et al. (2004) Interaction of the molecular chaperone alphaB-crystallin with alpha-synuclein: Effects on amyloid fibril formation and chaperone activity. *J Mol Biol* 340(5):1167–1183.
28. Muchowski PJ, et al. (2000) Hsp70 and hsp40 chaperones can inhibit self-assembly of polyglutamine proteins into amyloid-like fibrils. *Proc Natl Acad Sci USA* 97(14): 7841–7846.
29. Scherzinger E, et al. (1997) Huntingtin-encoded polyglutamine expansions form amyloid-like protein aggregates in vitro and in vivo. *Cell* 90(3):549–558.
30. Masino L, et al. (2004) Characterization of the structure and the amyloidogenic properties of the Josephin domain of the polyglutamine-containing protein ataxin-3. *J Mol Biol* 344(4):1021–1035.
31. Liepinsh E, et al. (2001) Thioredoxin fold as homodimerization module in the putative chaperone ERp29: NMR structures of the domains and experimental model of the 51 kDa dimer. *Structure* 9(6):457–471.
32. Pintacuda G, Otting G (2002) Identification of protein surfaces by NMR measurements with a pramagnetic Gd(III) chelate. *J Am Chem Soc* 124(3):372–373.
33. Dougan L, Li J, Badilla CL, Berne BJ, Fernandez JM (2009) Single homopolypeptide chains collapse into mechanically rigid conformations. *Proc Natl Acad Sci USA* 106(31): 12605–12610.
34. Crick SL, Jayaraman M, Frieden C, Wetzel R, Pappu RV (2006) Fluorescence correlation spectroscopy shows that monomeric polyglutamine molecules form collapsed structures in aqueous solutions. *Proc Natl Acad Sci USA* 103(45):16764–16769.
35. Klein FA, et al. (2007) Pathogenic and non-pathogenic polyglutamine tracts have similar structural properties: Towards a length-dependent toxicity gradient. *J Mol Biol* 371(1):235–244.
36. Behrends C, et al. (2006) Chaperonin TRiC promotes the assembly of polyQ expansion proteins into nontoxic oligomers. *Mol Cell* 23(6):887–897.
37. Nozaki K, Onodera O, Takano H, Tsuji S (2001) Amino acid sequences flanking polyglutamine stretches influence their potential for aggregate formation. *Neuroreport* 12(15):3357–3364.
38. Duennwald ML, Jagadish S, Muchowski PJ, Lindquist S (2006) Flanking sequences profoundly alter polyglutamine toxicity in yeast. *Proc Natl Acad Sci USA* 103(29): 11045–11050.
39. Branco J, et al. (2008) Comparative analysis of genetic modifiers in Drosophila points to common and distinct mechanisms of pathogenesis among polyglutamine diseases. *Hum Mol Genet* 17(3):376–390.
40. Tam S, et al. (2009) The chaperonin TRiC blocks a huntingtin sequence element that promotes the conformational switch to aggregation. *Nat Struct Mol Biol* 16(12): 1279–1285.
41. Chow MK, Mackay JP, Whisstock JC, Scanlon MJ, Bottomley SP (2004) Structural and functional analysis of the Josephin domain of the polyglutamine protein ataxin-3. *Biochem Biophys Res Commun* 322(2):387–394.
42. Lindner RA, Kapur A, Mariani M, Titmuss SJ, Carver JA (1998) Structural alterations of alpha-crystallin during its chaperone action. *Eur J Biochem* 258(1):170–183.
43. Lindner RA, Kapur A, Carver JA (1997) The interaction of the molecular chaperone, alpha-crystallin, with molten globule states of bovine alpha-lactalbumin. *J Biol Chem* 272(44):27722–27729.
44. Chan HY, Warrick JM, Gray-Board GL, Paulson HL, Bonini NM (2000) Mechanisms of chaperone suppression of polyglutamine disease: Selectivity, synergy and modulation of protein solubility in Drosophila. *Hum Mol Genet* 9(19):2811–2820.
45. Nicastro G, Habeck M, Masino L, Svergun DI, Pastore A (2006) Structure validation of the Josephin domain of ataxin-3: Conclusive evidence for an open conformation. *J Biomol NMR* 36(4):267–277.
46. Nicastro G, et al. (2009) Josephin domain of ataxin-3 contains two distinct ubiquitin binding sites. *Biopolymers* 91(12):1204–1214.
47. Nicastro G, et al. (2005) The solution structure of the Josephin domain of ataxin-3: structural determinants for molecular recognition. *Proc Natl Acad Sci USA* 102(30): 10493–10498.
48. Plater ML, Goode D, Crabbe MJ (1996) Effects of site-directed mutations on the chaperone-like activity of alphaB-crystallin. *J Biol Chem* 271(45):28558–28566.
49. Aquilina JA, Watt SJ (2007) The N-terminal domain of alphaB-crystallin is protected from proteolysis by bound substrate. *Biochem Biophys Res Commun* 353(4): 1115–1120.
50. Jaya N, Garcia V, Vierling E (2009) Substrate binding site flexibility of the small heat shock protein molecular chaperones. *Proc Natl Acad Sci USA* 106(37):15604–15609.
51. Chow MK, Ellisdon AM, Cabrita LD, Bottomley SP (2004) Polyglutamine expansion in ataxin-3 does not affect protein stability: Implications for misfolding and disease. *J Biol Chem* 279(46):47643–47651.
52. Horwitz J, Huang QL, Ding L, Bova MP (1998) Lens alpha-crystallin: Chaperone-like properties. *Methods Enzymol* 290:365–383.

Protein Engineering, Design & Selection vol. 22 no. 8 pp. 447–451, 2009

Published online July 9, 2009 doi:10.1093/protein/gzp033

REVIEW

Multi-domain misfolding: understanding the aggregation pathway of polyglutamine proteins

Helen M. Saunders and Stephen P. Bottomley[1]

Department of Biochemistry and Molecular Biology, Monash University, Clayton, VIC 3800, Australia

[1]To whom correspondence should be addressed.
E-mail: steve.bottomley@med.monash.edu.au

The polyglutamine (polyQ) diseases consist of nine neurodegenerative diseases in which a polyQ tract expansion leads to protein misfolding and subsequent aggregation. Even when the causative proteins have the same length polyQ tract, there are differences in the severity and age of disease onset which implicate the polyQ flanking sequences as modulators of disease. Recent studies on the polyQ proteins ataxin-1, ataxin-3 and huntingtin exon-1 have shown that the flanking domains have an intrinsic ability to aggregate. This complex behavior leads to a multi-stage aggregation mechanism which we have termed multi-domain misfolding. In multi-domain misfolding, a flanking domain to the polyQ tract plays an early role in aggregation, before the contribution of the polyQ tract. A number of factors including the stability, dynamics and amyloidogenicity of the flanking domain modulate the impact on polyQ tract aggregation as well as any protein–protein interactions it undertakes. In this review, we examine the recent data in support of this novel mechanism of protein aggregation.

Keywords: aggregation/ataxin-3/polyglutamine repeat/protein misfolding

PolyQ aggregation and protein context

The polyglutamine (polyQ) diseases are a group of nine inherited diseases (Table I) whereby mutation, in the form of a CAG repeat expansion, results in neurodegenerative disease. An inverse exponential correlation exists between glutamine repeat length and age of disease onset and severity (Gusella and MacDonald, 2000). The same polyQ expansion in different contexts results in varying toxicity and disease pathology, and thus many studies have investigated the role that protein context plays in modulating the extrinsic toxicity of the polyQ sequence. Recently, the flanking domains of three polyQ proteins ataxin-1, ataxin-3 and huntingtin (Fig. 1) have been shown, *in vitro*, to have intrinsic aggregation propensities which modulate the aggregation of the full-length proteins. In this review, we will focus on the aggregation of these proteins and discuss multi-domain misfolding events which result in their multi-stage aggregation mechanisms.

The ability of polyQ flanking sequences to modulate aggregation was clearly demonstrated by Nozaki *et al.* (2001) who saw differing aggregation rates when the surrounding 17 amino acids of ataxin-2, ataxin-3, huntingtin and atrophin were added to the same length polyQ tract. In addition to this, they found that mutating four hydrophobic residues in the upstream flanking sequence of ataxin-2 to charged amino acids decreased the aggregation rate, further highlighting the impact of sequence specificity upon aggregation.

Subsequently, a number of studies have investigated the flanking regions to the polyQ tract within huntingtin exon-1. Through the use of peptide studies, the poly proline (polyP) region immediately C-terminal to the polyQ tract in huntingtin (Fig. 1) has been shown to slow aggregation and decrease the stability of aggregates compared with a polyQ peptide alone (Bhattacharyya *et al.*, 2006). This study also found that the protective effects of the polyP region are directional, having no impact on aggregation when N-terminal to the polyQ tract. The mechanism of inhibition was investigated by Darnell *et al.* (2007) who show that the polyP region exists as a PPII helix (proline type II helix), inducing a PPII-like structure in the polyQ tract that opposed the aggregation-prone β-sheet conformation formed by this region. In addition to the *in vitro* study using polyQ peptides, it was shown that the polyP sequence decreases toxicity in a yeast huntingtin exon-1 model system (Duennwald *et al.*, 2006). Duennwald *et al.* also investigated the impact of two commonly used tags and show that the soluble GST domain prevents toxicity whereas the negatively charged FLAG tag increases toxicity. Therefore, the polyQ surrounding sequence within huntingtin exon-1 has a significant modulating effect on huntingtin exon-1 aggregation kinetics.

The flanking domain also plays a role in determining the molecular species formed during aggregation (Fig. 2). Although pathogenic length pure polyQ peptides only form two species during aggregation, monomer and fibril (Fig. 2) (Chen *et al.*, 2002), in the context of the disease, protein intermediate species such as spherical oligomers and curvilinear protofibrils are also formed (Gales *et al.*, 2005; Thakur *et al.*, 2009). Similar to a number of other amyloidogenic proteins, polyQ oligomers have also been shown to be toxic (Bucciantini *et al.*, 2002; Li *et al.*, 2007; Takahashi *et al.*, 2008), showing the importance of flanking domains in controlling the species formed during fibrillogenesis.

The sequence-specific effects of the flanking domain are unsurprising, given that primary protein sequences vary in their amyloidogenicity. Aggregation is known to depend on factors determined by the primary sequence such as hydrophobicity, charge and propensity to form secondary structure (Chiti *et al.*, 2003), with certain amino acids having specific effects upon aggregation propensity. In keeping with its inhibitory effect on huntingtin exon-1 aggregation, proline is considered to be a ‘β-breaker’ as it is structurally incompatible with β-sheet formation (Monsellier and Chiti, 2007). There is also a group of ‘gatekeeper’ residues which are

© The Author 2009. Published by Oxford University Press. All rights reserved.
For Permissions, please e-mail: journals.permissions@oxfordjournals.org

Table I. Characteristics of PolyQ disease proteins

Disease	Protein	PolyQ tract location (Black) and relative size 0 1000 2000 3145 aa	Pathogenic Q length	Refs
HD	Huntingtin	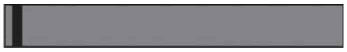	36–121	Group (1993), Nahhas *et al.* (2005)
SCA1	Ataxin-1	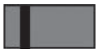	40–83	Matilla *et al.* (1993), Ranum *et al.* (1994)
SCA3	Ataxin-3	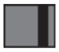	45–84	Kawaguchi *et al.* (1994) Padiath *et al.* (2005)
SCA2	Ataxin-2	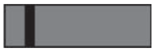	35–59	Pulst *et al.* (2005)
SCA6	CACNA1A	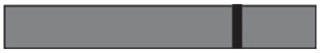	21–29	Zhuchenko *et al.* (1997)
SCA7	Ataxin-7	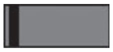	37–306	Benton *et al.* (1998), David *et al.* (1997)
SCA17	TBP	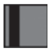	47–63	Koide *et al.* (1999), Nakamura *et al.* (2001)
DRPLA	Atrophin 1	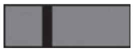	49–88	Komure *et al.* (1995)
SBMA	Androgen receptor	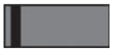	40–62	La Spada *et al.* (1991)

DRPLA, dentatorubral and pallidoluysian atrophy; HD, Huntington's disease; SCA, spinocerebellar ataxia; SBMA, spinal and bulbar muscular atrophy; CACNA1A-alpha. 1A-voltage-dependent calcium channel; TBP, TATA-box-binding protein.

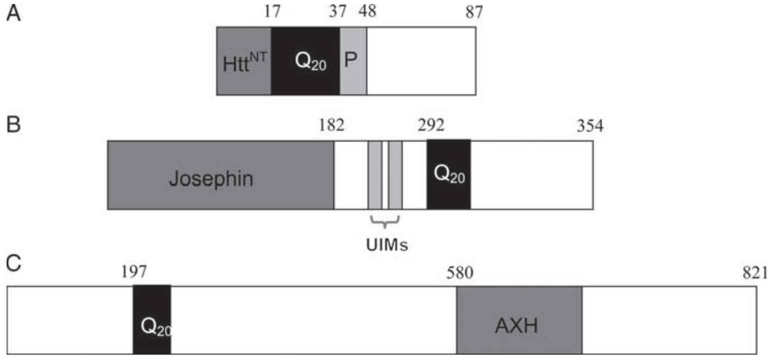

Fig. 1. Domain architecture of huntingtin exon-1, ataxin-3 and ataxin-1. The three polyQ proteins huntingtin exon-1 (**A**), ataxin-3 (**B**) and ataxin-1 (**C**) are shown with an arbitrarily chosen polyQ tract length of 20 glutamines. Huntingtin exon-1 consists of the $\mathrm{Htt}^{\mathrm{NT}}$ domain which comprises the first 17 amino acids of the protein, the polyQ tract (Q_{20}) and the polyP region (P). Ataxin-3 contains the Josephin domain, the polyQ tract and ubiquitin interacting motifs. Ataxin-1 contains the AXH domain and the polyQ tract. The proteins are not illustrated to scale.

commonly found flanking aggregation-prone regions. These include proline, lysine, arginine, glutamate and aspartate, and all have low hydrophobicity, are charged and show a low propensity to form β-sheet structure (Rousseau *et al.*, 2006), as demonstrated in the mutagenesis study on ataxin-2 (Nozaki *et al.*, 2001).

Analysis of primary sequence can be very informative for unstructured proteins; however, for the natively structured polyQ proteins, an extra level of complexity exists. Evolution selects for burial of hydrophobic amyloidogenic regions, and so predicted amyloidogenic regions may be buried in a stable fold and shielded from forming the interactions required for aggregation. Thus, local destabilization of the native protein fold or increased dynamics is needed before aggregation can occur (Tartaglia *et al.*, 2008). The role of dynamics in the initial misfolding events of polyQ aggregation has not been well characterized. We speculate that as for a number of other amyloid proteins (Wu *et al.*, 2008; Hodkinson *et al.*, 2009), the more dynamic the native state polyQ protein is, the more frequently it will sample amyloidogenic-prone conformations. The question remains as to whether mutation, such as the polyQ expansion in polyQ proteins, can change the protein dynamics and subsequently affect aggregation.

In addition to having a direct impact upon the polyQ tract, the flanking sequences allow for varying protein–protein interactions which also modulate aggregation. Ubiquitin is one protein present in the neuronal intranuclear inclusions (NIIs) of most polyQ diseases; however, typically the subset

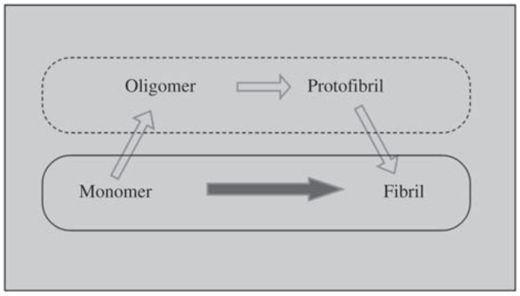

Fig. 2. Structural species in pathological polyQ aggregation. The structural species which are formed during aggregation of pathological length polyQ proteins with the dotted region indicating species mediated by the flanking domains, and the solid region indicating species specifically formed as a result of the pathogenic length polyQ tract.

of proteins sequestered within the NIIs is specific to each disease. The importance of the flanking domain in determining interactions is seen in ataxin-3, where differences between components of NIIs have been shown between full length versus truncated ataxin-3 (Chai *et al*., 2001). In addition to this, huntingtin has over 100 interaction partners within the cell, all of which could potentially affect aggregation (Kaltenbach *et al*., 2007). Therefore, flanking sequences and domains, although not the key cause of toxicity in polyQ proteins, can have a modifying effect on polyQ aggregation through their interactions partners.

Characterization of multi-domain misfolding and aggregation

It has long been known that protein domains can fold independently, and recently, it has been shown that within a protein, multiple domains are able to misfold in separate steps. Owing to the technical difficulties involved in producing these proteins *in vitro*, the aggregation kinetics and pathways of only three of the nine polyQ proteins have been characterized. Ataxin-1, ataxin-3 and huntingtin exon-1 all contain a flanking region which is able to aggregate independently of the polyQ tract, albeit with slower kinetics. A key tool in the identification of these polyQ-independent aggregation regions has been the polyQ binding peptide QBP1, which inhibits aggregation by the polyQ tract (Nagai *et al*., 2000). The ability of flanking regions to independently aggregate accounts for the aggregation seen by non-expanded ataxin-1 and ataxin-3 *in vitro* (Chow *et al*., 2004a; Masino *et al*., 2004; de Chiara *et al*., 2005a, 2005b; Gales *et al*., 2005).

The aggregation pathway of ataxin-3 has been well defined *in vitro* and it has been shown that the folded 24 kDa Josephin domain of ataxin-3 aggregates when isolated (Chow *et al*., 2004c; Masino *et al*., 2004). Our group has shown that full-length ataxin-3 aggregates with a two-stage mechanism (Ellisdon *et al*., 2006, 2007). The first stage of aggregation involving interactions of the Josephin domain results in formation of morphologically similar soluble protofibrils by ataxin-3 with any length glutamine tract. The key evidence these fibrils are formed along the same aggregation pathway is their ability to cross-seed each other (Ellisdon *et al*., 2006). We know from the addition of QBP1 that the polyQ tract is not directly involved in the first step; however, the expanded ataxin-3 has the fastest aggregation kinetics, suggesting that it still impacts the Josephin domain in some way. The second stage in the polyQ aggregation mechanism involves a subsequent misfolding event, whereby interaction of the polyQ tract results in formation of SDS-insoluble fibrils. Thus, the two domains in ataxin-3, with an intrinsic ability to misfold, aggregate sequentially (Fig. 3).

Although a complete kinetic analysis has not been completed for ataxin-1 due to the limitations caused by its size, the AXH domain of ataxin-1 has similarly been found to aggregate when isolated (de Chiara *et al*., 2005a, 2005b). Within the context of ataxin-1, the AXH domain has a pro-aggregation effect, as replacement with a homologous non-aggregation-prone sequence decreases the formation of nuclear inclusions within a cell model (de Chiara *et al*., 2005a, 2005b). The formation of detergent insoluble aggregates, commonly attributed to polyQ tract aggregation, has not been investigated, nor has the use of QBP1 to ascertain whether the polyQ tract misfolds and aggregates subsequently to the AXH domain.

A recent study by the Wetzel group has shown that huntingtin exon-1 also undergoes multi-domain misfolding during aggregation (Thakur *et al*., 2009). They found the 17 amino acids N-terminal of the polyQ tract accelerated aggregation, whether N- or C-terminal to the polyQ tract. This differs from ataxin-1 and ataxin-3, in that the 17 amino acids are not a globular structured domain, but instead exists in a collapsed state, which an expanded polyQ tract induces into a more aggregation competent extended conformation.

Intriguingly, a kinetic analysis of the huntingtin peptide with the N-terminal sequence resulted in a critical nucleus of minus one, which suggests there is no kinetic barrier to aggregation, and spontaneous aggregation of oligomers occurs in a 'downhill' fashion (Thakur *et al*., 2009). They also found that amorphous aggregates formed in the initial step of aggregation had an exposed polyQ tract that could still bind antibodies, whereas later aggregates masked the polyQ epitope, thus suggesting an additional misfolding event and conformational rearrangement of the polyQ tract to become involved in the fibrils (Thakur *et al*., 2009). Thus,

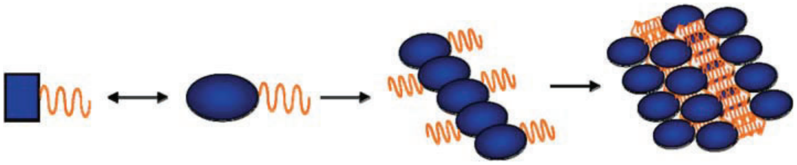

Fig. 3. PolyQ multi-domain aggregation mechanism. This is a schematic representation of the multi-stage polyQ aggregation mechanism. In this pathway, an initial misfolding event occurs in the polyQ flanking folded domain (square), followed by the formation of soluble species mediated by flanking domain interactions. There is then a conformational rearrangement of the polyQ tract (orange) which results in formation of end stage SDS-insoluble fibrils.

huntingtin exon-1 involves two different misfolding events which each result in formation of different species along the pathway.

With the presence of an amyloidogenic flanking domain being common to polyQ disease proteins, model polyQ protein containing flanking domains with an intrinsic ability to aggregate provide the most representative insight into the aggregation mechanism of polyQ proteins. One model polyQ system involving the cellular retinoic acid binding protein I (CRABP I) domain fused to huntingtin exon-1 has proved to have an aggregation pathway which is analogous to ataxin-3. The CRABP I domain has been demonstrated to aggregate independently and when fused to huntingtin exon-1, the aggregation pathway is characterized by an initial step involving CRABP I followed by a second step mediated by polyQ tract interactions (Ignatova *et al*., 2007). Using proteolysis, this study also observed the two-stage aggregation pathway in an *Escherichia coli* cell model, which is the first evidence of the multi-domain mechanism within the cell. The recent huntingtin exon-1 aggregation study by the Wetzel group highlights the importance of detecting aggregation by a number of techniques *in vitro*, and thus it would be interesting to investigate whether the additional aggregation step due to the flanking 17 amino acids could also be identified within the context of the CRABP I model, with the possibility of three independently aggregating domains within the one protein.

Therefore, the three characterized polyQ proteins all show domain independent misfolding which translates into multi-step aggregation pathways, whereby the different domains aggregate sequentially. Common to all three cases is the role of non-polyQ containing domain in forming the initial interactions, thus suggesting a mechanism where these domains initially self-associate, thus increasing the local concentration of the polyQ tract before the polyQ tract plays a significant role in fibril formation. As additional polyQ disease proteins are characterized *in vitro*, it will be interestingly to observe whether this emerging trend continues.

The interplay between the polyQ domain and the stability of adjacent regions

The interplay between the polyQ tract and flanking domains clearly depends upon the characteristics of the domains. The stability of the flanking domain is known to play an important modulatory role in aggregation. In accordance with the general amyloid aggregation theory, an early hypothesis proposed that the expanded polyQ tract destabilized the protein, leading to an increased propensity to aggregate (Bevivino and Loll, 2001). Ataxin-3 is the only disease protein for which kinetic and thermodynamic stability has been determined, and contrary to the initial hypothesis, our lab has shown that the addition of a non-pathogenic length polyQ tract leads to a destabilization of the protein in comparison with the Josephin domain alone, yet expanding the polyQ tract into the pathogenic length has no further effect on stability (Chow *et al*., 2004a, 2004b). As the aggregation kinetics of expanded ataxin-3 is accelerated in comparison with non-expanded ataxin-3, this suggests that because there is no further global destabilization, the expanded polyQ tract is modulating local stability or conformational dynamics.

The complexity of the effect of the polyQ tract on protein stability is demonstrated by a number of polyQ model systems. On the one hand, the addition and subsequent expansion of a polyQ tract did not result in a change in the thermodynamic stability of a *Staphylococcus aureus* protein A domain (Robertson *et al*., 2008). However, this domain is one of the most stable of the model proteins used, so it is unsurprising that the addition of a pathogenic length polyQ tract was not sufficient to disrupt the fold. The CRABP I domain has a similar stability to the Josephin domain of ataxin-3; however, the addition of a non-expanded polyQ tract does not impact upon stability, and it is only when the polyQ tract is expanded that there is a corresponding decrease in the stability of the protein. Furthermore, although in a GST-polyQ model, the stability was not determined, aggregation could only be induced above 50ºC, suggesting the stability and/or solubility of the GST domain overrides any effects of the polyQ tract at physiological temperatures (Masino *et al*., 2002). Therefore, these model systems demonstrate the complexity of the relationship between the polyQ tract and the flanking domains and show that although in some situations, a polyQ tract can decrease the global stability of a protein, it is not necessary in order to induce aggregation.

Effects of flanking domains on aggregation of non-polyQ proteins

Multi-domain misfolding is not exclusive to polyQ proteins, being also seen in several other aggregating proteins such as the poly alanine (polyA) protein Poly A Binding Protein Nuclear 1 (PABPN1) and the yeast prion protein Ure2p. Expansion of the polyA tract occurs at the N-terminal of PABPN1, with an increase from 10 to 17 alanines leading to disease. Similar to ataxin-1 and ataxin-3, aggregation still occurs in the absence of the homo-sequence domain, resulting in aggregates which are smaller and more numerous than full-length PABPN1 (Klein *et al*., 2008). A second example, Ure2p, consists of a highly amyloidogenic unstructured N-terminal domain which is responsible for the prion phenotype, and a compactly folded C-terminal catalytic domain (Thual *et al*., 1999). Dimerization of the protein occurs through the C-terminal domain, which is also able to aggregate independently, forming high molecular weight insoluble oligomers, which do not progress to fibrillar aggregates (Thual *et al*., 2001). Interestingly, the presence of the amyloidogenic N-terminal domain has no impact upon the stability of the full-length protein (Thual *et al*., 2001).

Conclusions

The aggregation pathways of polyQ proteins characterized to date have involved multiple domains. With the variation seen between polyQ diseases, it is unsurprising that their specific flanking domains, although not the primary cause of aggregation, have the ability to independently misfold and modulate the fibrillogenic mechanism within the context of the full-length protein *in vitro*. In these studies, the importance of using a number of complementary techniques to follow the multiple aggregation steps has been highlighted. The mechanism via which an expanded polyQ tract results in accelerated aggregation remains unknown, with no clear relationship between the effects of the expanded polyQ tract and global stability of the protein. Further investigation into polyQ protein dynamics and the effects of the expanded polyQ tract upon local stability will therefore be important for determining the early aggregation events.

Funding

This work was funded by a Program grant from the National Health and Medical Research Council of Australia (NHMRC). SPB is a Senior Research Fellow of the NHMRC.

References

Benton,C.S., de Silva,R., Rutledge,S.L., Bohlega,S., Ashizawa,T. and Zoghbi,H.Y. (1998) *Neurology*, **51**, 1081–1086.

Bevivino,A.E. and Loll,P.J. (2001) *Proc. Natl Acad. Sci. USA*, **98**, 11955–11960.

Bhattacharyya,A., Thakur,A.K., Chellgren,V.M., Thiagarajan,G., Williams,A.D., Chellgren,B.W., Creamer,T.P. and Wetzel,R. (2006) *J. Mol. Biol.*, **355**, 524–535.

Bucciantini,M., Giannoni,E., Chiti,F., Baroni,F., Formigli,L., Zurdo,J., Taddel,N., Ramponi,G., Dobson,C.M. and Stefani,M. (2002) *Nature*, **416**, 507–511.

Chai,Y., Wu,L., Griffin,J.D. and Paulson,H.L. (2001) *J. Biol. Chem.*, **276**, 44889–44897.

Chen,S., Ferrone,F.A. and Wetzel,R. (2002) *Proc. Natl Acad. Sci. USA*, **99**, 11884–11889.

Chiti,F., Stefani,M., Taddei,N., Ramponi,G. and Dobson,C.M. (2003) *Nature*, **424**, 805–808.

Chow,M.K., Ellisdon,A.M., Cabrita,L.D. and Bottomley,S.P. (2004a) *J. Biol. Chem.*, **279**, 47643–47651.

Chow,M.K., Mackay,J.P., Whisstock,J.C., Scanlon,M.J. and Bottomley,S.P. (2004b) *Biochem. Biophys. Res. Commun.*, **322**, 387–394.

Chow,M.K., Paulson,H.L. and Bottomley,S.P. (2004c) *J. Mol. Biol.*, **335**, 333–341.

Darnell,G., Orgel,J.P., Pahl,R. and Meredith,S.C. (2007) *J. Mol. Biol.*, **374**, 688–704.

David,G., *et al.* (1997) *Nat. Genet.*, **17**, 65–70.

de Chiara,C., Menon,R.P., Adinolfi,S., de Boer,J., Ktistaki,E., Kelly,G., Calder,L., Kioussis,D. and Pastore,A. (2005a) *Structure*, **13**, 743–753.

de Chiara,C., Menon,R.P., Dal Piaz,F., Calder,L. and Pastore,A. (2005b) *J. Mol. Biol.*, **354**, 883–893.

Duennwald,M.L., Jagadish,S., Muchowski,P.J. and Lindquist,S. (2006) *Proc. Natl Acad. Sci. USA*, **103**, 11045–11050.

Ellisdon,A.M., Thomas,B. and Bottomley,S.P. (2006) *J. Biol. Chem.*, **281**, 16888–16896.

Ellisdon,A.M., Pearce,M.C. and Bottomley,S.P. (2007) *J. Mol. Biol.*, **368**, 595–605.

Gales,L., Cortes,L., Almeida,C., Melo,C.V., do Carmo Costa,M., Maciel,P., Clarke,D.T., Damas,A.M. and Macedo-Ribeiro,S. (2005) *J. Mol. Biol.*, **353**, 642–654.

Group T.H.s.D.C.R (1993) *Cell*, **72**, 971–983.

Gusella,J.F. and MacDonald,M.E. (2000) *Nat. Rev. Neurosci.*, **1**, 109–115.

Hodkinson,J.P., Jahn,T.R., Radford,S.E. and Ashcroft,A.E. (2009) *J. Am. Soc. Mass Spectrom.*, **20**, 278–286.

Ignatova,Z., Thakur,A.K., Wetzel,R. and Gierasch,L.M. (2007) *J. Biol. Chem.*, **282**, 36736–36743.

Kaltenbach,L.S., *et al.* (2007) *PLoS Genet.*, **3**, e82.

Kawaguchi,Y., *et al.* (1994) *Nat. Genet.*, **8**, 221–228.

Klein,A.F., Ebihara,M., Alexander,C., Dicaire,M.J., Sasseville,A.M., Langelier,Y., Rouleau,G.A. and Brais,B. (2008) *Exp. Cell Res.*, **314**, 1652–1666.

Koide,R., Kobayashi,S., Shimohata,T., Ikeuchi,T., Maruyama,M., Saito,M., Yamada,M., Takahashi,H. and Tsuji,S. (1999) *Hum. Mol. Genet.*, **8**, 2047–2053.

Komure,O., *et al.* (1995) *Neurology*, **45**, 143–149.

La Spada,A.R., Wilson,E.M., Lubahn,D.B., Harding,A.E. and Fischbeck,K.H. (1991) *Nature*, **352**, 77–79.

Li,M., Chevalier-Larsen,E.S., Merry,D.E. and Diamond,M.I. (2007) *J. Biol. Chem.*, **282**, 3157–3164.

Masino,L., Kelly,G., Leonard,K., Trottier,Y. and Pastore,A. (2002) *FEBS Lett.*, **513**, 267–272.

Masino,L., Nicastro,G., Menon,R.P., Dal Piaz,F., Calder,L. and Pastore,A. (2004) *J. Mol. Biol.*, **344**, 1021–1035.

Matilla,T., Volpini,V., Genis,D., Rosell,J., Corral,J., Davalos,A., Molins,A. and Estivill,X. (1993) *Hum. Mol. Genet.*, **2**, 2123–2128.

Monsellier,E. and Chiti,F. (2007) *EMBO Rep.*, **8**, 737–742.

Nagai,Y., Tucker,T., Ren,H., Kenan,D.J., Henderson,B.S., Keene,J.D., Strittmatter,W.J. and Burke,J.R. (2000) *J. Biol. Chem.*, **275**, 10437–10442.

Nahhas,F.A., Garbern,J., Krajewski,K.M., Roa,B.B. and Feldman,G.L. (2005) *Am. J. Med. Genet. A*, **137A**, 328–331.

Nakamura,K., Jeong,S.Y., Uchihara,T., Anno,M., Nagashima,K., Nagashima,T., Ikeda,S., Tsuji,S. and Kanazawa,I. (2001) *Hum. Mol. Genet.*, **10**, 1441–1448.

Nozaki,K., Onodera,O., Takano,H. and Tsuji,S. (2001) *Neuroreport*, **12**, 3357–3364.

Padiath,Q.S., Srivastava,A.K., Roy,S., Jain,S. and Brahmachari,S.K. (2005) *Am. J. Med. Genet. B Neuropsychiatr. Genet.*, **133**, 124–126.

Pulst,S.M., Santos,N., Wang,D., Yang,H., Huynh,D., Velazquez,L. and Figueroa,K.P. (2005) *Brain*, **128**, 2297–2303.

Ranum,L.P., *et al.* (1994) *Am. J. Hum. Genet.*, **55**, 244–252.

Robertson,A.L., Horne,J., Ellisdon,A.M., Thomas,B., Scanlon,M.J. and Bottomley,S.P. (2008) *Biophys. J.*, **95**, 5922–5930.

Rousseau,F., Serranob,L. and Schymkowitz,J.W.H. (2006) *J. Mol. Biol.*, **355**, 1037–1047.

Takahashi,T., Kikuchi,S., Katada,S., Nagai,Y., Nishizawa,M. and Onodera,O. (2008) *Hum. Mol. Genet.*, **17**, 345–356.

Tartaglia,G.G., Pawar,A.P., Campioni,S., Dobson,C.M., Chiti,F. and Vendruscolo,M. (2008) *J. Mol. Biol.*, **380**, 425–436.

Thakur,A.K., *et al.* (2009) *Nat. Struct. Mol. Biol.*, **16**, 380–389.

Thual,C., Komar,A.A., Bousset,L., Fernandez-Bellot,E., Cullin,C. and Melki,R. (1999) *J. Biol. Chem.*, **274**, 13666–13674.

Thual,C., Bousset,L., Komar,A.A., Walter,S., Buchner,J., Cullin,C. and Melki,R. (2001) *Biochemistry*, **40**, 1764–1773.

Wu,K.P., Kim,S., Fela,D.A. and Baum,J. (2008) *J. Mol. Biol.*, **378**, 1104–1115.

Zhuchenko,O., Bailey,J., Bonnen,P., Ashizawa,T., Stockton,D.W., Amos,C., Dobyns,W.B., Subramony,S.H., Zoghbi,H.Y. and Lee,C.C. (1997) *Nat. Genet.*, **15**, 62–69.

Received June 4, 2009; revised June 4, 2009;
accepted June 7, 2009

Edited by Sheena Radford